ISSN 0910-2531
Suwa用

Eighth Preliminary Report of African Studies Nagoya University

(Earth Sciences 5)

March 1983

Association for African Studies, Nagoya University
c/o Department of Earth Sciences, Faculty of Science,
Nagoya University, Chikusa, Nagoya 464, JAPAN

Information to Readers

Since 1975, the following eight volumes of the Preliminary Report of African Studies, Nagoya University have been published:

First Preliminary Report in 1975. This report is Earth Sciences 1.

Second Preliminary Report (Earth Sciences 2) in 1977.

Third Preliminary Report (Archaeology 1) in 1977.

Fourth Preliminary Report (Earth Sciences 3) in 1979.

Fifth Preliminary Report (Archaeology 2) in 1980.

Sixth Preliminary Report (Earth Sciences 4) in 1981.

Seventh Preliminary Report (Archaeology 3) in 1982.

Eighth Preliminary Report (Earth Sciences 5) in 1983.

K. Suwa

Eighth Preliminary Report (Earth Sciences 5)

Editor: Kanenori Suwa March 1983

Association for African Studies, Nagoya University
c/o Department of Earth Sciences
Faculty of Science
Nagoya University

This Preliminary Report is published by the Association for African Studies, Nagoya University, with the financial support of the Grant-in-Aid for Scientific Research (Overseas Scientific Survey) of the Japanese Ministry of Education, Science and Culture.

The papers printed in the Preliminary Reports are generally résumés, while the publication of the full texts is left to the respective authors' choice.

Any reference to this report in a formal list should read:
8th Prelim. Rept. Afr. Studies, Nagoya Univ. (Earth Sciences 5)

Contents

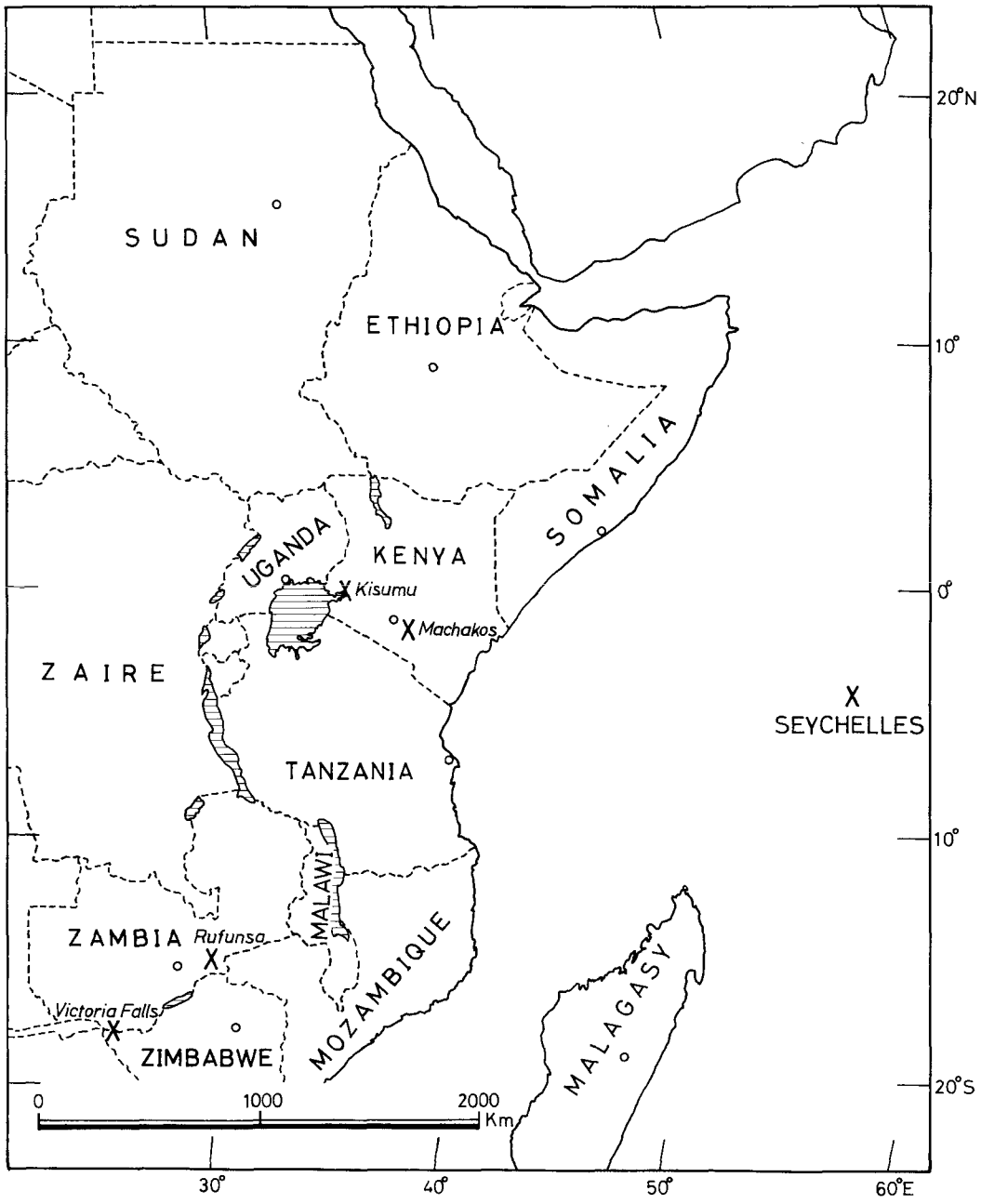

Index map for the 8th Preliminary Report of African Studies, Nagoya University (Earth Sciences 5) in 1983.

The Preliminary Report of African Studies, Nagoya University

Introduction

This report covers work done in Africa from the Association for African Studies, Nagoya University and some related work done from the Department of Earth Sciences, Nagoya University during the periods 1981 and 1982.

During the periods 1981 and 1982, some geologists of Nagoya University have done continuously their field surveys in East Africa as follows.

1981 ----- K. Suwa, T. Yanagi, K. Tokieda, H. Umemura, M. Asami and M. Hoshino (Kenya, Zambia and Seychelles); H. Shiozaki (Kenya)

1982 ----- H. Shiozaki (Kenya)

In this report, Prof. Suwa and his co-workers presented a basic evidence for the idea of continental disruption by reporting petrographical and petrochemical characteristics of Precambrian granitic rocks in the Mahe and adjoining islets, Seychelles. Dr. Yanagi gave the ages of 713 Ma for gneissose granodiorite and 683 Ma for porphyritic granite in the Mahe island with his colleagues. Mr. Tokieda gave the results that the stable paleomagnetic remanence of the Precambrian granites in the Seychelles falls to a northerly mean direction with declination of 348.5° and inclination of 48.7° with his colleagues. Mr. Hoshino gave and discussed the mineralogical data on amphiboles including Fe^{2+}-poor and Fe^{2+}-rich hornblende, ferroedenite, ferrorichterite and riebeckite in the Precambrian granites, Seychelles with his colleague. Mr. Agata gave and discussed the mineralogical data on opaque minerals including magnetite and ilmenite in the Precambrian granites, Seychelles with his colleague.

Mr. Miyake divided into ten groups of pelitic and psammitic gneisses in the Uvete area, central Kenya. Phase relation among the metamorphic minerals indicates that the rocks in the Uvete area were metamorphosed under narrow ranges of pressure–temperature conditions of the kyanite-zone. Dr. Asami found chloritoid in a paragonite-chlorite-kyanite-staurolite-garnet-muscovite-albite-quartz gneiss near Kilungu, central Kenya. This rock shows some retrograde replacement texture of kyanite, staurolite and garnet by paragonite, chloritoid and chlorite. Dr. Asami and his co-workers described and discussed the geological structure of the Mozambique metamorphic belt in the Kilungu area, central Kenya. Mr. Shiozaki carried out measurements of magnetic susceptibility of the granites, granitoid gneisses and paragneisses in the Mozambique belt of Kenya and he described and discussed the measurement data. Dr. Suzuki and his co-wokers synthesized glass from the powder of olivine-nephelinite to investigate the melt structure. The AlKβ peak of the olivine-nephelinite glass is found between the peak positions of corundum and the $An_{35}Di_{65}$ glass.

Mr. Hoshino and his co-workers described and discussed the geological structure of the Archaean greenstone belt in Kisumu area, west Kenya. Archaean granite-greenstone terrane of the Kisumu area consists mainly of Nyanzian System, Kavirondian System and post-Kavirondian granites. The Nyanzian System occurs as a thick pile of volcanic rocks, in which basaltic rocks are predominant in the lower unit, andesitic rocks in the middle unit and rhyolitic rocks in the upper unit. The Kavirondian System deposited unconformably on the Nyanzian rocks is composed of conglomerate, sandstone and mudstone. The Nyanzian and the Kavirondian rocks exhibit folded structures. The general trend of the axial traces of the folds is ENE-WSW to E-W. Post-Kavirondian granites occur in concordant with the general trend of the fold. Dr. Kagami and his co-workers performed Rb-Sr isochron dating on Maragori granite belonging to the post-Kavirondian granites and gave the age of 2,595 Ma. Mr. Shiozaki carried out measurement of magnetic susceptibility of granitic bodies in the Tanzania craton of west Kenya and he described and discussed the measurement data. Mr. Ito and his co-workers described the kimberlite and its xenoliths of harzburgite, fine-grained melanocratic rocks, leucocratic rocks and gabbroic rocks from western part of the Kisumu area, west Kenya and discussed their petrogenesis.

Dr. Umemura described and discussed pseudoconglomerate in the Rufunsa quartzites of the Kibaran metamorphic belt, Zambia with his colleague. Kibaran metamorphic rocks suffer, at least, four phases of deformation. Two types of pseudoconglomerates are found in the quartzites, one is lenticular type and the other is brecciated type. Double boudinage structure sometimes is found in the pseudoconglomerates. Mr. Tokieda performed paleomagnetic studies on the Karroo basalt from the Victoria Falls, Zambia with his colleague.

Field works were much facilitated by the Office of the President, Kenya; the Mines and Geological Department, Ministry of Natural Resources, Kenya; the Department of Geology, University of Nairobi, Kenya; the Ministry of Mines, Zambia; the Geological Survey Department, Ministry of Mines, Zambia; the National Research and Development Council, Ministry of Planning and Development, Seychelles; the Ministry of Education and Information, Seychelles. To all of them I express my sincere thanks for the most esteemed and invaluable assistance.

Field and laboratory works were supported by the Grant-in-Aid for Overseas Scientific Survey of the Ministry of Education, Science and Culture of Japanese Government, to which I would like to record my sincere thanks.

This report has been edited by Prof. Kanenori Suwa.

ISAO MATSUZAWA
Director
March, 1983

Geology and petrology of the Seychelles Islands

Kanenori SUWA*, Takeru YANAGI**, Katsuyasu TOKIEDA***,
Hayao UMEMURA****, Masao ASAMI***** and Mitsuo HOSHINO******

* Department of Earth Sciences, Faculty of Science, Nagoya University
** Department of Geology, Faculty of Science, Kyushu University
*** Department of Physics, Faculty of Science, Shimane University
**** Department of Geology, Faculty of Science, Kochi University
***** Department of Geological Sciences, College of Liberal Arts, Okayama University
****** Laboratory of Geology, College of General Education, Nagoya University

Abstract

The geology of Mahe and adjoining islets, Seychelles consists of three types of Precambrian granitic rock-series: (1) gneissose granodiorite – gneissose tonalite and amphibilite – leucogranite series, (2) grey granite – gneissose grey granite series, and (3) porphyritic granite – pink granite series. All these granitic rocks are cut by dykes of doleritic compositions, mostly with a WNW-ESE trend.

Rb-Sr radiometric analyses yielded the ages of 713 Ma for the gneissose granodiorite (1) and of 683 Ma for the porphyritic granite (3). The stable paleomagnetic remanence of the Precambrian granites in the Seychelles fell to a northerly mean direction with declination of 348.5° and inclination of 48.7°.

Silhouette and North islands consist of syenitic and dioritic rocks of early Tertiary in age. Radiometric age of 60 Ma was given on the diorite of North island.

The petrographical, mineralogical, petrochemical, geochronological and paleomagnetic studies on the Precambrian granitic rocks show that the Precambrian granitic rocks of the Seychelles are well correlated to the Precambrian granitic rocks occurring in the areas along the Red sea and Gulf of Aden (north-eastern Sudan and northern Somalia). The separation of Seychelles occurred probably from the areas of NE Sudan and northern Somalia in the African continent.

Introduction

The Seychelles Archipelago in the western Indian Ocean consists of a large number of islands. The Mahe-Praslin group of islands, the principal islands of the archipelago, are situated approximately 1,600 km east of Mombasa, and have been known to be composed largely of Precambrian granitic rocks. The Mahe-Praslin group consists of 24 inhabited islands totalling some 200 square kilometers in area, which rise from the central part of the Seychelles Bank. A submarine Seychelles Bank is generally less than 60 m below sea-level, which covers approximately 41,000

8th Prelim. Rept. Afr. Studies, Nagoya Univ., 3-21, 1983.

square kilometers. The Seychelles Bank is the northern extremity of the Mascarene Plateau linking the Seychelles, Reunion and Mauritius. The Mascarene Plateau extends as a faulted composite arc for 2,300 km, from the Precambrian granitic microcontinent of the Seychelles Bank southward through the coral-reef capped, volcanic structures of Saya de Malha, Nazareth, and Cargados Carajos banks to the faulted Tertiary-Quaternary oceanic volcanic island of Mauritius.

The dominating feature of the Indian Ocean is the seismically active mid-ocean ridges such as Carlsberg ridge, central Indian ridge, south-east Indian ridge and south-west Indian ridge. Another characteristic of the Indian Ocean is the abundance of relatively shallow ridges and plateaus that are free from earthquake activity. These aseismic features have been grouped together under collective names such as "microcontinents" and "oceanic ridges". The majority of the aseismic ridges and plateaus (Seamount chain southeast of Socotra, North part of Mascarene Plateau, Mozambique Ridge, Madagascar Ridge, Agulhas Plateau, Naturaliste Plateau and others) can well be called "microcontinents" as was done by Heezen and Tharp (1965), but this term does not apply to the Chagos-Laccadive Ridge and South part of Mascarene Plateau designated as Linear volcanic features, or to the Ninety-east Ridge designated as Uplifted oceanic crust (Laughton *et al.*, 1970).

According to the seismic refraction experiments carried out on the Seychelles Bank, the following five layers have been recognized: Superficial layer with 0.3 km in thickness, the 5.72 km/s layer (Sp.Gr., 2.71), the 6.26 km/s layer (Sp.Gr., 2.83), the 6.78 km/s layer (Sp.Gr., 2.99) and the 8.1 km/s layer (Sp.Gr., 3.4). The interface between the 5.72 km/s layer and the 6.26 km/s layer is found at depth of about 4 km. The velocities 5.72 and 6.26 km/s are typical of granitic rocks. The interface between the 6.26 km/s layer and the 6.78 km/s layer, found at a depth of about 15 km, corresponds to the postulated Conrad discontinuity under the continents. The depth of 33 km to the interface between the 6.78 km/s layer and the 8.1 km/s layer which it is interpreted as the Mohorovičić discontinuity is determined. The granitic rocks extend to a depth of about 15 km in the Seychelles Bank and the crust there has both a continental character and a continental thickness (Davies and Francis, 1964; Francis *et al.*, 1966; Matthews and Davis, 1966).

The comprehensive geological survey of almost all islands of the Seychelles Archipelago was made first by Baker (1963). He recognized three main types of Precambrian granite, i.e., the grey Mahe granite, the grey faintly gneissose granite and the reddish Praslin – La Digue granite. The first two are main geological units found in Mahe and nearby islets, and the last composes Praslin – La Digue islands. He also recognized minor amounts of porphyritic granite and doleritic rocks. The porphyritic granite occurring along the west coast of Mahe was regarded as a facies of the grey Mahe granite. A swarm of doleritic dykes are also found in all three types of granite in Mahe and Praslin, but no such dyke swarm was found in Silhouette and North islands, which consist of syenitic and dioritic rocks of early Tertiary in age.

Radiometric dating was done on whole rock samples and rock-forming minerals

(biotite and hornblende) in Seychelles by Miller and Mudie (1961), Wasserburg *et al.* (1963) and Baker and Miller (1963). Their results showed that the emplacement of the Seychelles granitic rocks is in late Precambrian and the emplacement of the syenite and diorite is in early Tertiary.

Paleomagnetic study was done by Matthews and Reilly (1964). No meaningful result was obtained by them because of their treatment without demagnetizing technique.

Petrographical and petrochemical studies were done by Baker (1963) and Frankel and Kent (1964). From the Mahe island, grey granite, hornblende microgranite, grey mottled adamellite, salmon-pink adamellite, quartz microdiorite, aplite, xenolithic inclusions and plagioclase-quartz hornfels were described. From Long island, slightly gneissic grey granite was described. From Praslin island, red granite was described. From Cerf island, andalusite-muscovite-quartz hornfels was described. These studies showed that the granites of the Seychelles Islands are essentially hornblende-bearing and alkalic and that the hornblende is probably somewhat sodic and that the main feldspar of the Seychelles granites is usually a perthite with a minimum amount of albite-oligoclase as discrete grains.

During September and October in 1981, the geological team from Nagoya University has been sent to investigate the Mahe and nearby islands. The team has been constructed by the present six authors.

Radiometric dating was done on whole rock samples and rock-forming minerals by Yanagi *et al.* (1983). They gave the ages of 713±19 Ma for the gneissose granodiorite and of 683±16 Ma for the porphyritic granite in the Mahe island. They also gave the age of 60±4 Ma for the diorite at the North island and showed an evidence of igneous acticity occurred after the continental disruption.

Paleomagnetic study was done by Tokieda *et al.* (1983). They gave the results that the stable paleomagnetic remanence of the Precambrian granites falls to a northerly mean direction with declination of 348.5° and inclination of 48.7° and that the stable remanences of the dolerite fall to a similar direction with the Precambrian granites and to a southerly mean direction with declination of 192.4° and inclination of 67.7°.

Petrographical and mineralogical studies on the rock-forming minerals were done by Hoshino and Suwa (1983) and Agata and Suwa (1983). Hoshino and Suwa (1983) gave the mineralogical data on amphiboles including Fe^{2+}-poor and Fe^{2+}-rich hornblende, ferroedenite, ferrorichterite and riebeckite and discussed how the amphiboles change their properties with differentiation of host granitic magma. Agata and Suwa (1983) gave the mineralogical data on opaque minerals including magnetite and ilmenite and discussed how the MnO contents in ilmenite vary with differentiation in host granitic magma.

The Seychelles Islands are believed to be continental fragments left behind as a result of the disruption of Gondwanaland and the succeeding opening of the Indian

Ocean.

The object of this paper is to present a basic evidence for this idea by reporting petrographical and petrochemical characteristics of Precambrian granitic rocks in the Mahe and adjoining islets. This paper is also to present another evidence of an igneous activity occurred after the continental disruption, which resulted in the emplacement of syenite and diorite in the Silhouette and North islands of the Seychelles.

Geological Setting

The geological team from Nagoya University revised the geological map of the Mahe island and its adjoining islets as shown in Fig. 1.

The geology of Mahe consists of three types of Precambrian granitic rock-series, namely (1) gneissose granodiorite – gneissose tonalite and amphibolite – leucogranite series, (2) grey granite – gneissose grey granite series, and (3) porphyritic granite – pink granite series. All these granitic rocks are cut by dykes of doleritic compositions, mostly with a WNW-ESE trend.

(1) *Gneissose granodiorite – gneissose tonalite and amphibolite – leucogranite series:* This rock series occurs mainly in the northern part of Mahe island. Amphibolite occurs also in such small islets lying east of Port Victoria as Cerf island. Radiometric age of gneissose granodiorite is 713±19 Ma (Yanagi *et al.*, 1983).

The gneissose granodiorite, grey in colour, is petrographically heterogeneous with many ellipsoidal and angular basic xenoliths.

The gneissose tonalite, grey in colour, occurs near the boundary between the gneissose granodiorite and amphibolite, and is considered to be a contamination facies of amphibolite by gneissose granodiorite. They have parallel banding and foliation, though these are faint. They are coarse-grained in some places and fine-grained in other places. Rock facies with different grain sizes are distributed complicatedly in this mass. This ellipsoidal and angular basic xenoliths, 5 to 20 cm across, are arranged in parallel to the foliation. The foliation has a NNE trend and a steep dip to SE (N20°E and 75°SE dip).

Along the west coast of north Mahe the gneissose granodiorite, gneissose tonalite and amphibolite are penetrated discordantly by the leucogranite and these rocks are crushed into angular blocks and are agmatitic in appearance (Plate II-1, Plate V-1 and 2, and Plate VI-1).

The leucogranite, white-grey in colour, occurs along the west coast and northwest coast of north Mahe and is petrographically homogeneous in majority and becomes heterogeneous near the boundary between the leucogranite and the gneissose granodiorite-gneissose tonalite-amphibolite. From the field occurrence, the leucogranite is considered to be a post-kinematic intrusive body after the emplacement of gneissose granodiorite, gneissose tonalite and amphibolite.

(2) *Grey granite – gneissose grey granite series:* Grey granite occurs in the main part of Mahe island and gneissose grey granite occurs in such small islets lying east

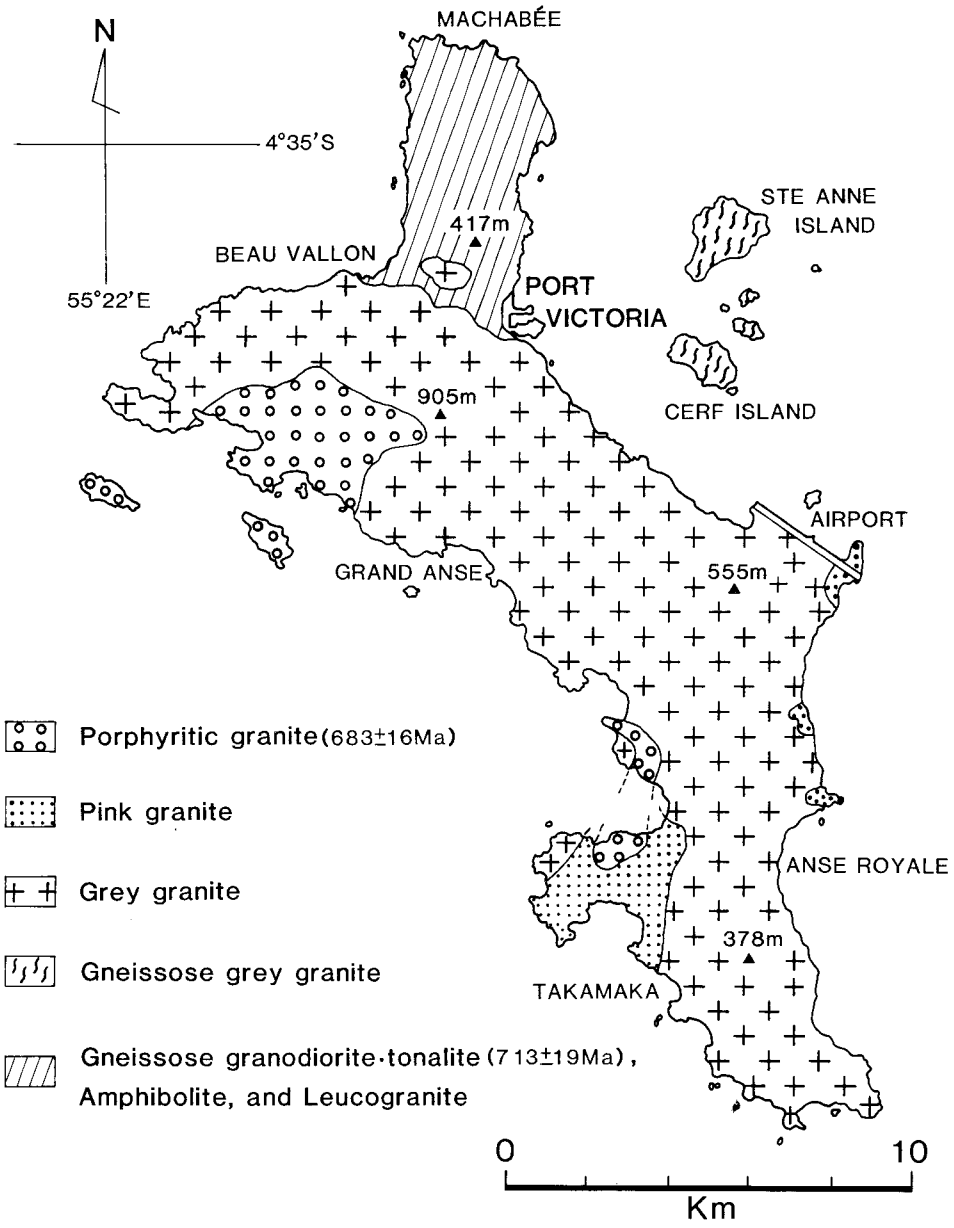

Fig. 1: Geological map of the Mahe islands, Seychelles.

of Port Victoria as Cerf island.

The grey granite, grey to greenish grey in colour, is coarse-grained equigranular plutonic rock and is massive with no foliation. Mafic xenoliths are rather small and few in this rock. These petrographic characters are uniformly constant throughout the body. The grey granite body in a stock-like form is found to the northwest of Port Victoria and this body seems to have been emplaced discordantly in the gneissose granodiorite. On the west coast of Mahe, however, the boundary between

the grey granite and the gneissose granodiorite is not so sharp. The gneissose granodiorite may grade into the coarse-grained grey granite across the boundary zone.

The gneissose grey granite, grey to white grey in colour, is apparently similar to the gneissose granodiorite occurring in the northern part of Mahe island. In the beginning of 1982, the present authors preliminarily made their geological map, in which gneissose grey granite and gneissose granodiorite were designated together as gneissose granite. Petrographically the gneissose grey granite must be discriminated from the gneissose granodiorite owing to its quite different character, and the gneissose grey granite petrographically resembles to the grey granite. The nature of this faintly gneissose structure suggests that it is due to primary flow banding, possibly emphasized by movement at a late stage of crystallization.

(3) *Porphyritic granite – pink granite series:* Porphyritic granite occurs along west coast of Mahe island. The radiometric age of the porphyritic granite is 683±16 Ma (Yanagi *et al.*, 1983). Pink granite occurs sporadically as small bodies along the east coast between Airport and Anse Royale and occurs at the southwest coast of Mahe island.

The porphyritic granite is characterized by its porphyritic texture with phenocrysts of feldspar. Majority of feldspar phenocrysts is microcline perthite mantled by albite fringe, and minority is antiperthite mantled by microcline fringe. The porphyritic granite in the north crops out between Port Launary Estate and Grand Anse. The rock near the northwestern contact with the grey granite represents a chilled facies of the intrusion. This rock consists of very fine-grained crystals of groundmass and a lesser amount of phenocrysts. Although the intrusive body is massive and homogeneous, in some places phenocrysts of feldspars segregate to form pegmatitic parts with molybdenite. The porphyritic granite in the south crops out between Anse Boileau and Baie Lazare Village. This rock is intruded both the grey granite and the pink granite as a small stock. It is interesting that its northern half portion lying in the grey granite is grey in colour and the southern half portion in the pink granite is reddish brown to orange in colour.

The pink granite, salmon-pink to brownish pink in colour, is coarse-grained equigranular plutonic rock and is distributed as small masses in the grey granite. Among these masses of the pink granite, the one body occurring in the Baie Lazare Village (north of Takamaka) is the largest with a surface extention of about 6 Km^2. The pink granite is similar to porphyritic granite in petrography with exception its non-porphyritic texture.

These granitic rocks are intruded by a number of parallel doleritic dykes with thickness of 0.2 to 10 m. The emplacement of parallel dykes of dolerites is the last event of magmatic activity recorded in Mahe island.

The Mahe-Praslin group of islands, the principal islands of Seychelles Archipelago, have been known to be composed largely of Precambrian granitic rocks. Geological sketch map of the Mahe-Praslin group is shown in Fig. 2. As shown in Fig. 2, the gneissose granodiorite (A) is mainly distributed in the northern Mahe island. The majority of the Mahe-Praslin group of islands is occupied by the grey granite and

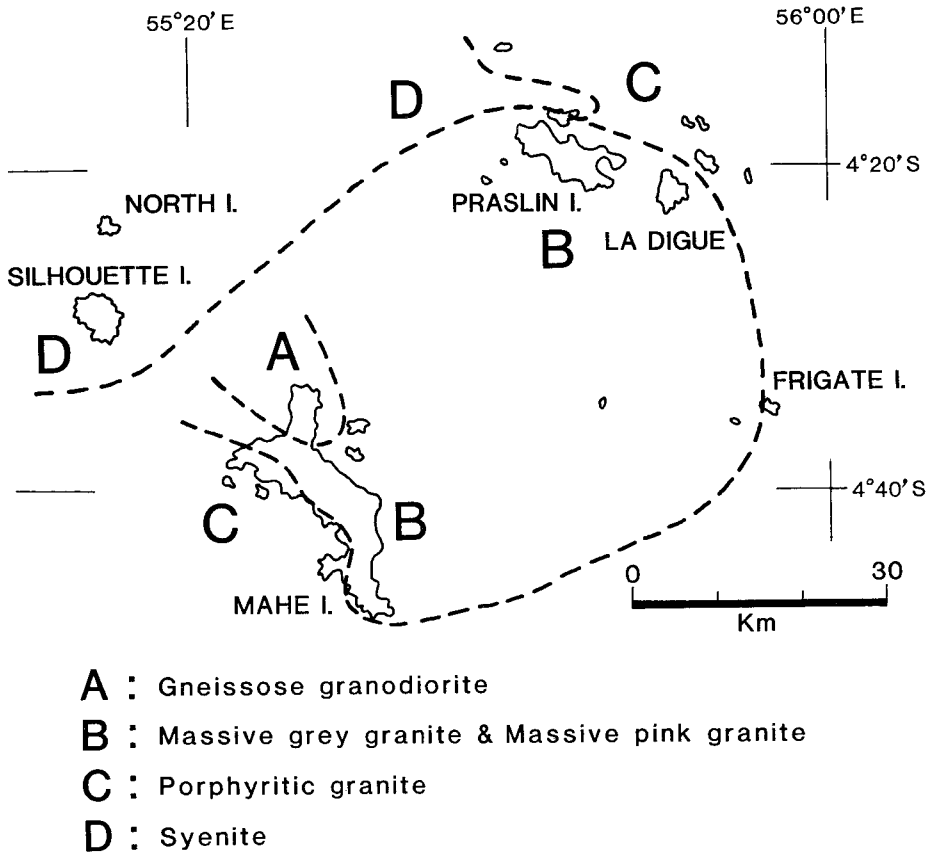

Fig. 2 Geological sketch map of the Mahe-Praslin group of islands, Seychelles.

pink granite (B). The grey granite and pink granite are considered to be main mass of the Precambrian granitic rock body and are considered to occupy the core part of the body. The porphyritic granite (C) is considered to be a marginal facies of the Precambrian granitic rock body and is distributed encircling the main mass of the body. Syenitic and dioritic rocks (D) of early Tertiary age (60 Ma) are distributed around the Silhouette and North islands and these young intrusives are considered to occupy the northwestern margin of the Mahe-Praslin group of islands.

Petrography of Precambrian granitic rocks

Three types of the Precambrian granitic rock-series are recognized in the Mahe island and its adjoining islets. Petrography of the rocks will be given on each rock-series.

(1) *Gneissose granodiorite – gneissose tonalite and amphibolite – leucogranite series:*

The gneissose granodiorite consists mainly of oligoclase, quartz and microcline with minorly of biotite, hornblende, sphene, zircon, apatite, magnetite and ilmenite.

Groundmass is equigranular granoblastic and is composed of quartz, microcline, plagioclase and others with a grain size of 0.2 to 2 mm. The groundmass is studded with phenocrystic crystals with a grain size of 2.5 to 7 mm. Phenocrystic oligoclase crystals are polysynthetically twinned and normally zoned with core (An 25) and rim (An 19), and sometimes show antiperthitic texture. Phenocrystic microcline crystals are of pure K-feldspar with composition of $Or_{96-97}Ab_{4-3}$ and show mainly microperthitic and rarely cryptoperthitic texture. Myrmekite is rarely found. Quartz crystals unexceptionally display a recrystallization texture, which is very distinctive from those in other intrusions. It is considered that the quartz crystals had once been as large as associated phenocrystic oligoclase and microcline crystals and then the quartz crystals became an aggregate of small grains with a granoblastic texture. Biotite shows Z-axial colour of green brown. Hornblende is of Fe-poor and alkali-poor common hornblende with Z-axial colour of blue green or yellow green and is long prismatic of 2.5 mm in maximum. Opaque minerals are associated with ferromagnesian silicate minerals such as biotite, hornblende and sphene. Magnetite is ubiquitously intergrown with ilmenite. Magnetite and ilmenite also occur as discrete grains. Magnetite is partly replaced by haematite and ilmenite is mostly replaced by sphene. MnO contents in ilmenite intergrown with magnetite and in discrete ilmenite attain up to 19 wt.% and 11 wt.% respectively.

The gneissose tonalite consists mainly of plagioclase, quartz and hornblende with minorly of biotite, sphene, apatite, zircon, magnetite and ilmenite. Secondary minerals such as chlorite, sericite, epidote, haematite, sphene and pyrite are found. Coarse-grained plagioclase and hornblende measure 2 to 5 mm in size and fine-grained granoblastic plagioclase and hornblende measure 0.4 to 1 mm in size. Magnetite is intergrown with ilmenite and this grain measures 2 mm in size.

The amphibolite consists mainly of hornblende and plagioclase with minorly of biotite, sphene, apatite and pyrite. Secondary minerals such as chlorite and epidote are found. This rock is equigranular and granoblastic with 0.1 to 0.3 mm in size. Hornblende with Z-axial colour of brown green attains 1.8 mm in maximum. Plagioclase is twinned and weakly zoned. Sometimes the amphibolite is studded with plagioclase-zoisite clots with 3 to 5 mm in size. This clot consists of plagioclase, zoisite and ilmenite with minorly of muscovite.

Mafic xenolith occurs in a rounded and/or angular shape in the gneissose granodiorite, gneissose tonalite and leucogranite. The mafic xenolith consists mainly of sodic plagioclase, quartz, hornblende, biotite and microcline with minorly of apatite, sphene, zircon, magnetite and ilmenite. Epidote is found as secondary mineral. Three types of plagioclase crystal are recognized, i.e., (a) relict phenocryst of 2 to 5 mm in size is normally zoned with core (An 23) and rim (An 9) and is polysynthetically twinned, (b) antiperthite of 0.5 to 1 mm in size, and (c) equigranular granoblastic plagioclase of 0.2 to 0.4 mm in size. Anhedral porphyritic microcline crystal up to 3 mm in size and equigranular granoblastic microcline of 0.3 to 0.4 mm in size are found. Myrmekite is found between granoblastic plagioclase and microcline grains. Hornblende is of Fe-poor and alkali-poor common hornblende with

Z-axial colour of green and is sometimes twinned. Biotite shows Z-axial colour of deep brown green. Mafic clot up to 3 mm in size consists of hornblende, biotite, sphene, apatite and opaque minerals. Opaque minerals are very similar to those in the gneissose granodiorite. In addition, blastoporphyritic biotite-hornblende fine-grained tonalite to granodiorite is found as mafic xenolith.

The leucogranite consists mainly of microcline, plagioclase, quartz and biotite with minorly of hornblende, sphene, apatite, zircon, allanite, magnetite and ilmenite. Secondary minerals such as biotite, epidote and chlorite are found. This rock is totally coarse-grained, and equigranular granoblastic groundmass of 0.5 to 1 mm in grain-size is studded with phenocrystic crystals of 3 to 6 mm in size. Phenocrystic microcline is twinned after Carlsbad law and is mesoperthitic and perthitic. Phenocrystic albite is polysynthetically twinned. Myrmekite is found. Equigranular granoblastic groundmass consists of microcline, sodic plagioclase and quartz. Opaque minerals are very similar to those in the gneissose granodiorite. MnO contents in ilmenite intergrown with magnetite and in discrete ilmenite attain up to 32 wt.% and 26 wt.%, respectively. Intergrown ilmenite is dramatically Mn-rich and it suggests that the leucogranite is late crystallization-differentiation product of granite magma.

(2) *Grey granite – gneissose grey granite series:*

The grey granite consists mainly of microcline, quartz, ferrorichterite and riebeckite with minorly of biotite, ferroactinolite, hedenbergite, allanite, apatite, zircon, fluorite, magnetite and ilmenite. This rock is equigranular and coarse-grained with a grain size of 2 to 9 mm. Microcline occurs as anhedral or subhedral mesoperthite, in which the volume of exsolution lamellae of microcline (Or_{97-99}) and albite (Ab_{99-100}) is same. Along the boundaries between microcline grains, thin band of albite and quartz with 0.1 mm in width are developed. Quartz grains show undulatory extinction. Ferrorichterite with (–) 2V = 45° occurs as subhedral and short prismatic crystals with a strong pleochroism (X = light greenish yellow, Z = deep yellowish green to deep green) and an abnormal interference colour. Riebeckite occurs ubiquitously in the grey granite as minute minerals overgrown around the ferrorichterite. Riebeckite with (±) 2V = 90° exhibits a strong pleochroism (X = deep blue, Z = light greenish yellow) and an abnormal interference colour. Ferroactinolite with (–) 2V = 23° rarely occurs at the core of the ferrorichterite and shows Z-axial colour of bluish green. Small flakes of biotite occur around the ferrorichterite, along the grain boundaries between microcline mesoperthite and along the grain boundaries between microcline mesoperthite and quartz grains. Opaque mineral occupies only 0.2% in volume and its mode of occurrence is similar to that in the gneissose granodiorite. MnO contents in ilmenite intergrown with magnetite and in discrete ilmenite attain up to 4 wt.% and 6 wt.%, respectively.

The gneissose grey granite consists mainly of microcline, quartz, ferrorichterite and riebeckite with minorly of biotite, apatite, sphene, zircon and ilmenite. This rock is equigranular and medium-grained of 0.5 to 3 mm in size. Microcline occurs

as mesoperthite, in which the compositions of microcline (Or_{98}) and albite (Ab_{100}) are close in pure composition. This band of quartz is developed along the boundaries between microcline grains. Quartz grains show slightly undulatory extinction. Ferrorichterite is strongly pleochroic (X = light brownish yellow, Z = deep brownish green) and shows abnormal interference colour. It is (−) 2V = 46° and 56° with optical dispersion r<v. Riebeckite occurs as an aggregate of small flakes overgrown around the ferrorichterite and occurs as an aggregate of acicular crystals developed along the grain boundaries. Riebeckite with (−) 2V = 76° exhibits a strong pleochroism (X = deep violet blue, Z = light greenish yellow). Biotite shows Z-axial colour of reddish brown. Opaque mineral occupies only 0.1 - 0.2% in volume and its mode of occurrence is very similar to that in the grey granite. MnO content in ilmenite intergrown with magnetite (now replaced by haematite) attains only 1.6 wt.%.

(3) *Porphyritic granite – pink granite series:*

The porphyritic granite consists mainly of microcline, albite, quartz, hornblende and biotite with minorly of allanite, sphene, zircon, apatite, fluorite, topaz (?), clinopyroxene, magnetite and ilmenite. Phenocrystic crystals are euhedral or subhedral and measure 2 to 7 mm in size. Microcline phenocryst is mesoperthitic and/or perthitic and is mantled by albite fringe. In mesoperthite the compositions of microcline (Or_{98}) and albite (Ab_{98}) are close in pure composition. It sometimes is twinned after Carlsbad law. Antiperthite phenocryst is sometimes found and is mantled by microcline fringe. Quartz phenocryst shows corroded form. Groundmass is composed of microcline, albite (Ab_{93-98}), quartz, hornblende and biotite. Groundmass minerals measure 0.2 to 1 mm in size. Groundmass exhibits monzonitic texture, in which microcline fills grain boundaries between other constituent minerals. Myrmekite is found. Hornblende is subhedral and prismatic and is strongly pleochroic (X = light greenish yellow, Z = bluish green). Hornblende is of Fe-rich common hornblende and its rim is edenitic. Clinopyroxene is sometimes mantled with hornblende. Biotite with Z-axial colour of brown occurs as a stout crystal and its rim is sometimes greenish. Ilmenite intergrown magnetite and discrete ilmenite are mostly replaced by sphene. MnO content in ilmenite intergrown with magnetite attains 6 wt.%.

The pink granite consists mainly of microcline, quartz, albite, ferroedenite and biotite with minorly of allanite, apatite, sphene, zircon, fluorite, eudialyte (?), magnetite and ilmenite. This rock is equigranular and coarse-grained of 2 to 10 mm in size. Many varieties of feldspars are observed under the microscope. Microcline crystals occur as mesoperthite and perthite, in which the compositions of microcline (Or_{97}) and albite (Ab_{98}) are close in pure composition. Antiperthite crystal is sometimes found and is sometimes mantled by microcline fringe. Albite crystal (Ab_{90-93}) shows polysynthetic twin and weak zoning and is mantled by perthite fringe. A heterogeneous crystal consisting of albitic, mesoperthitic and perthitic parts is also observed. Ferroedenite with (−) 2V = 45° is subhedral and short prismatic with a strong pleochroism (X = light yellowish green, Z = deep bluish green).

It shows sometimes sieve texture containing feldspar and quartz inclusions. Biotite flakes with Z-axial colour of dark brown commonly make an intergrowth with the ferroedenite. Magnetite is partly replaced by haematite and pyrite. MnO content in discrete ilmenite attains 11 wt.%.

Petrochemistry of Precambrian granitic rocks

Chemical compositions and C.I.P.W. norms of the Precambrian granitic rocks from the Mahe-Praslin group of islands, Seychelles are shown in Table 1. Average chemical composition of the Precambrian granitic rocks is also shown in Table 1. The differentiation index (normative Q + Qr + Ab) of the average granitic rock is 92.8. Normative albite is more than normative orthoclase.

Major linear structure and dolerite-basalt dykes in the Mahe island

Major linear structure in the Mahe island is shown in Fig. 3. This figure was constructed from an air photograph. Two directions of NW-SE and ENE-WSW are most recognizable. Another two directions of NNE-SSW and NNW-SSE are also recognizable. The first two directions (lineaments) are more linear than the last two directions (lineaments), and this fact suggests that the first two lineaments are constructed in younger stage and the last two in older stage.

Major directions of intrusion of dolerite-basalt dykes in the Mahe island are NW-SE and E-W. This directions of intrusion are in close relationship with the first two lineaments. It can be said that the intrusion directions are controlled by the first two lineaments.

The first two lineaments are quite different from the general trend of the gneissose granodiorite (N20°E, 75°SE dip) and the first two lineaments are no relation with the distribution of various kinds of the Precambrian granitic rocks. These facts may suggest that the first two lineaments were constructed after the emplacement of the Precambrian granitic rocks.

The most recognizable lineament is NW-SE and this direction is parallel to the elongation of the present Mahe island and to the trend of the northern Mascarene Plateau.

Average chemical composition and C.I.P.W. norm of the dolerite-basalt dykes in the Mahe island are shown in Table 2. Petrography, mineralogy and petrochemistry of the dolerite-basalt dykes will be discussed in near future.

Syenitic and dioritic rocks in the Silhouette and North islands

Modal compositions of the syenitic and dioritic rocks in the Silhouette and North islands are shown in Table 3. Average chemical compositions and C.I.P.W. norms of the above rocks are shown in Table 4. These rocks are considered to be emplaced in the early Tertiary (60 Ma). Petrography, mineralogy and petrochemistry of the syenitic and dioritic rocks will be discussed in near future.

Table 1. Chemical compositions and C.I.P.W. norms of Seychelles granitic rocks (Analyst : R. Sugisaki)

		1 Gneissose granodiorite aver. (4)	2 Gneissose tonalite and amphibolite aver. (3)	3 Agmatitic amphibolite in gneissose granodiorite aver. (2)	4 Leuco-granite aver. (2)	5 Grey granite
	SiO_2	72.25	48.62	62.84	74.93	75.43
	TiO_2	0.34	1.27	0.79	0.24	0.22
	Al_2O_3	15.12	18.80	16.30	13.20	12.13
	Fe_2O_3	1.24	4.05	2.18	1.17	0.60
	FeO	1.10	5.77	2.76	0.69	1.67
	MnO	0.073	0.18	0.18	0.063	0.087
	MgO	0.52	4.65	1.73	0.23	0.17
	CaO	2.08	9.29	4.70	0.77	0.48
	Na_2O	5.23	3.63	5.22	4.99	4.60
	K_2O	2.41	1.46	2.22	3.98	4.06
	P_2O_5	0.075	0.24	0.30	0.033	0.024
	H_2O+	0.38	0.96	0.33	0.24	0.27
	H_2O-	0.13	0.67	0.13	0.14	0.23
	Total	100.948	99.59	99.68	100.676	99.971
				Norm		
	Q	27.33	0.00	12.61	29.14	31.22
	C	0.31	0.00	0.00	0.00	0.00
	Or	14.24	8.63	13.12	23.52	23.99
	Ab	44.26	29.51	44.17	42.23	38.93
	An	9.83	30.69	14.99	1.86	0.46
	Ne	0.00	0.65	0.00	0.00	0.00
	Ac	0.00	0.00	0.00	0.00	0.00
Di	En	0.00	3.67	1.76	0.57	0.12
Di	Fs	0.00	1.74	0.94	0.02	0.68
Di	Wo	0.00	5.77	2.87	0.68	0.74
	Wo	0.00	0.00	0.00	0.04	0.00
Hy	En	1.28	0.00	2.55	0.00	0.30
Hy	Fs	0.57	0.00	1.36	0.00	1.69
Ol	Fo	0.00	5.55	0.00	0.00	0.00
Ol	Fa	0.00	2.90	0.00	0.00	0.00
	Mt	1.80	5.87	3.16	1.70	0.87
	Il	0.65	2.41	1.50	0.46	0.42
	Ap	0.17	0.56	0.70	0.08	0.06
	H_2O	0.51	1.63	0.46	0.38	0.50
	Total	100.95	99.58	99.69	100.68	99.98
Specimen No.		KS-81101408 KS-81101410A-1 KS-81101502-1 KS-81101508-1	KS-81093004A-1 KS-81093004A-2 KS-81101708	KS-81101303 KS-81101409	KS-81101406 KS-81101508-2	KS-81100102

Table 1. (continued)

		6 Gneissose grey granite aver. (2)	7 Porphyritic granite aver. (2)	8 Pink granite	9 Average composition of granitic rocks (1, 4, 5, 6, 7, 8)
	SiO_2	75.50	74.00	73.54	74.28
	TiO_2	0.24	0.30	0.36	0.28
	Al_2O_3	11.96	12.94	13.16	13.09
	Fe_2O_3	0.83	0.81	1.30	0.99
	FeO	1.16	1.57	1.21	1.23
	MnO	0.029	0.078	0.097	0.071
	MgO	0.30	0.43	0.41	0.34
	CaO	0.27	1.11	0.88	0.93
	Na_2O	4.33	4.72	4.72	4.77
	K_2O	4.83	3.89	4.93	4.02
	P_2O_5	0.029	0.053	0.092	0.051
	H_2O+	0.21	0.36	0.18	0.27
	H_2O-	0.29	0.11	0.11	0.17
	Total	99.978	100.371	100.989	100.492
			Norm		
	Q	30.86	28.48	25.42	28.68
	C	0.00	0.00	0.00	0.00
	Or	28.54	22.99	29.14	23.76
	Ab	34.63	39.94	39.94	40.36
	An	0.00	2.63	0.16	2.43
	Ne	0.00	0.00	0.00	0.00
	Ac	1.77	0.00	0.00	0.00
Di	En	0.16	0.39	0.84	0.33
Di	Fs	0.34	0.68	0.60	0.44
Di	Wo	0.48	1.06	1.50	0.77
	Wo	0.00	0.00	0.00	0.00
Hy	En	0.59	0.68	0.18	0.51
Hy	Fs	1.27	1.18	0.13	0.67
Ol	Fo	0.00	0.00	0.00	0.00
Ol	Fa	0.00	0.00	0.00	0.00
	Mt	0.32	1.17	1.88	1.44
	Il	0.46	0.57	0.68	0.53
	Ap	0.07	0.12	0.21	0.12
	H_2O	0.50	0.47	0.29	0.44
	Total	99.99	100.36	100.97	100.48
Specimen No.		KS-81101706 KS-81101710	KS-81100103 KS-81100202	KS-81100604	

(2) 94.02 (2) 91.41 (2) 94.5 (2) 94.02 93.33

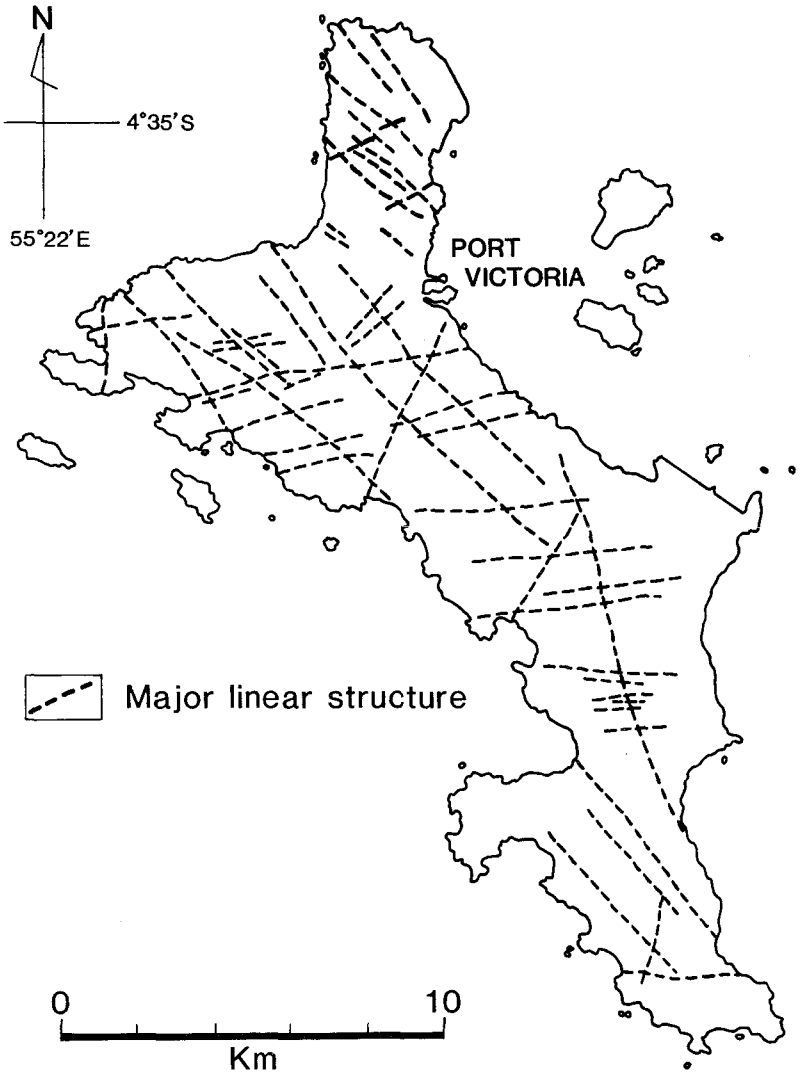

Fig. 3: Major linear structure, along which dolerite-basalt dykes are intruded, in the Mahe islands, Seychelles.

Table 2. Chemical compositions and C.I.P.W. norms of the Seychelles dolerite-basalt dyke, aver. (8) (Analyst: R. Sugisaki)

SiO_2	47.51		Or	6.62
TiO_2	2.37		Ab	26.99
Al_2O_3	15.51		An	24.69
Fe_2O_3	4.20	Di	En	3.22
FeO	8.69		Fs	1.78
MnO	0.19		Wo	5.30
MgO	6.48	Hy	En	7.11
CaO	8.47		Fs	3.93
Na_2O	3.19	Ol	Fo	4.07
K_2O	1.12		Fa	2.48
P_2O_5	0.71		Mt	6.09
H_2O+	1.33		Il	4.50
H_2O-	0.30		Ap	1.65
Total	100.07		H_2O	1.63

Specimen No.
KS-81093005A
KS-81093005B
KS-81093007B
KS-81100305A
KS-81100305B-1
KS-81100305B-2
KS-81101307-1
KS-81101307-2

Table 3. Modal compositions of the Cenozoic syenite and diorite occurring in the Silhouette and North islands, Seychelles

	Syenite MA-81100705 Silhouette	Syenite MA-81100706 Silhouette	Syenite MA-81100708 North island	Diorite MA-81100707A North island	Diorite MA-81100707B North island
Quartz	3.3	—	—	—	—
K-feldspar	85.2	77.8	91.8	—	—
Plagioclase	—	—	—	50.1	64.0
Biotite	—	3.8	—	17.2	15.7
Clinopyroxene	5.7	5.6	3.9	27.3	17.0
Hornblende	2.0	2.8	2.0	0.4	0.1
Actinolite	—	5.8	—	—	—
Orthoamphibole	2.2	—	—	—	—
Olivine	—	—	0.3	0.6	0.2
Opaque	0.9	3.2	1.2	3.8	2.5
Apatite	0.2	1.0	0.1	0.5	0.5
Zircon	tr	tr	—	tr	—
Chlorite	0.7	—	tr	tr	tr
Total	100.2	100.0	100.0	99.9	100.0

Table 4. Chemical compositions and C.I.P.W. norms of the Cenozoic syenite and diorite occurring in the Silhouette and North islands, Seychelles (Analyst: R. Sugisaki)

		Syenite aver. (3)	Diorite aver. (2)
	SiO_2	60.16	49.57
	TiO_2	1.08	1.73
	Al_2O_3	16.98	18.07
	Fe_2O_3	1.62	3.38
	FeO	4.54	6.43
	MnO	0.21	0.14
	MgO	0.96	4.56
	CaO	2.45	9.62
	Na_2O	5.87	3.77
	K_2O	4.64	1.74
	P_2O_5	0.36	0.34
	H_2O+	0.51	0.39
	H_2O-	0.41	0.21
	Total	99.79	99.95
		Norm	
	Q	0.80	0.00
	Or	27.42	10.28
	Ab	49.67	28.44
	An	6.28	27.25
	Ne	0.00	1.88
Di	En	0.46	4.61
Di	Fs	1.07	2.60
Di	Wo	1.47	7.62
Hy	En	1.93	0.00
Hy	Fs	4.53	0.00
Ol	Fo	0.00	4.73
Ol	Fa	0.00	2.95
	Mt	2.35	4.90
	Il	2.05	3.29
	Ap	0.83	0.79
	H_2O	0.92	0.60
	Total	99.78	99.95
	Specimen No.	MA-81100705 MA-81100706 MA-81100708	MA-81100707A MA-81100707B

From where the separation of Seychelles occurred ?

Fig.4 shows the locality map of the analysed granitic rocks belonging to the Mozambique belt, eastern Africa. Average chemical compositions and C.I.P.W. norms of the Precambrian granitic rocks from the several localities in Fig.4 are shown in Table 5. As can be seen in Table 5, it is very interesting that normative albite is more than normative orthoclase in the Precambrian granitic rocks occurring in the northern hemisphere and *vice versa* in the southern hemisphere.

Petrochemistry of the Precambrian granitic rocks in the Seychelles is very similar to that of the Precambrian granitic rocks occurring in the areas along the Red Sea and Gulf of Aden (northeastern Sudan and northern Somalia). Petrographical studies also show the same correlation, e.g., riebeckite granites are found in the northeastern Sudan and northern Somalia.

The separation of Seychelles is considered to be inaugurated probably from the areas of NE Sudan and northern Somalia in the African continent. This conclusion is concordant with the idea on separation of Madagascar from SE Somalia proposed by Rabinowitz *et al.* (1982).

Table 5. C.I.P.W. norms calculated from average analyses of the granitic rocks (500 – 720 Ma) in the Mozambique belt, Africa

	1 Aswan	2 N.E. Sudan	3 Somalia	4 Machakos	5 Malawi	6 Chirwa	7 Seychelles
Q	23.69	37.09	30.10	32.68	19.75	29.42	28.68
C	0.68	0.60	——	1.60	——	0.29	——
Or	28.90	22.93	24.35	22.81	37.24	27.37	23.76
Ab	37.65	35.37	34.77	32.75	30.88	26.82	40.36
An	4.13	1.58	5.65	5.73	4.52	9.58	2.43
Di	——	——	0.66	——	1.41	——	1.54
Hy	1.24	0.08	1.12	1.81	1.18	3.36	1.18
Mt	3.26	1.04	2.06	1.30	3.22	1.84	1.44
Il	0.42	0.25	0.51	0.40	0.80	0.80	0.53
Hm	——	0.30	——	——	——	——	——
Ap	0.21	0.17	0.38	0.25	0.38	——	0.12
H_2O+	0.39	0.42	0.27	0.30	0.44	0.45	0.27
H_2O-	——	0.08	0.09	0.15	0.14	——	0.17
Total	100.57	99.91	99.96	99.78	99.96	99.93	100.48
Specimen number	7	11	24	13	12	14	12
Reference	Rooke (1970)	Rooke (1970)	Rooke (1970)	Suwa *et al.* (1979)	Rooke (1970)	Rooke (1970)	This study (1983)

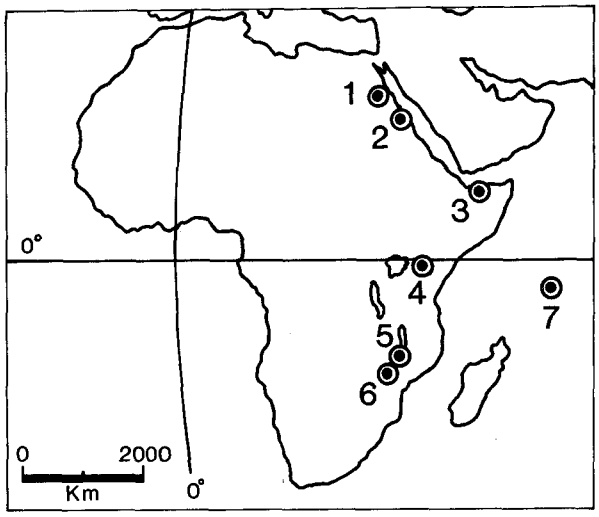

1: Aswan, 2: N.E. Sudan, 3: Somalia

4: Machakos, 5: Malawi, 6: Chirwa, 7: Seychelles

Fig. 4: Locality map of granitic rocks in the Mozambique belt, Africa.

Acknowledgements – We express our sincere thanks to Mr. P. Shilton, Secretary, National Research and Development Council, Ministry of Planning and Development, Republic of Seychelles and to Mr. G. Lionnet, Senior Education Officer, Ministry of Education and Information, Republic of Seychelles for their most esteemed and invaluable assistance.

The field work was made possible by the Grant-in-Aid for Overseas Scientific Survey from the Ministry of Education, Science and Culture, Japan, to which we express our thanks.

REFERENCES

AGATA, T. and SUWA, K. (1983): Opaque minerals from the Seychelles granitic rocks. *8th Prelim. Rept. Afr. Studies, Nagoya Univ.*, 63-74.

BAKER, B.H. (1963): Geology and mineral resources of the Seychelles Archipelago. *Memoir* No.**3**, *Geol. Survey Kenya*, 140p.

BAKER, B.H. and MILLER, J.A. (1963): Geology and geochronology of the Seychelles Islands and structure of the floor of the Arabian sea. *Nature,* **199**, 346-348.

DAVIES, D. and FRANCIS, T.J.G. (1964): The crustal structure of the Seychelles Bank. *Deep Sea Res.*, **11**, 921-927.

FRANCIS, T.J.G., DAVIES, D. and HILL, M.N. (1966): Crustal structure between Kenya and the Seychelles. *Phil. Trans. Roy. Soc.*, **A259**, 240-261.

FRANKEL, J.J. and KENT, L.E. (1964): On rocks from the Seychelles Islands, *22nd Intern. Geol. Cong.*, Sec.**10**, 161-190.

HEEZEN, B.C. and THARP, M. (1965): Physiographic diagram of the Indian ocean (with descriptive sheet). *Geol. Soc. Am.*, New York.

HOSHINO, M. and SUWA, K. (1983): Amphiboles in some granitic rocks from Mahe island and Cerf island, Seychelles. *8th Prelim. Rept. Afr. Studies, Nagoya Univ.,* 47-62.

LAUGHTON, A.S., MATTHEWS, D.H. and FISHER, R.L. (1970): The structure of the Indian ocean. *The Sea,* vol.**4**, Part **II**, 543-586.

MATTHEWS, D.H. and REILLY, T.A. (1964): Disappointing interium palaeomagnetic results from the Seychelles, *Nature,* **203**, 1160.

MATTHEWS, D.H. and DAVIES, D. (1966): Geophysical studies of the Seychelles Bank. *Phil. Trans. Roy. Soc.,* **A259**, 227-239.

MILLER, J.A. and MUDIE, J.D. (1961): Potassium-argon age determinations on granite from the Island of Mahé in the Seychelles archipelago. *Nature,* **192**, 1174-1175.

RABINOWITZ, P.D., COFFIN, M.F. and FALVEY, D. (1982): Salt diapirs bordering the continental margin of northern Kenya and southern Somalia. *Science,* **215**, 663-665.

ROOKE, J.M. (1970): Geochemical variations in African granitic rocks, and their structural implications. *In T.N.Clifford and I.G.Gass (eds.), African Magmatism and Tectonics, Oliver & Boyd, Edinburgh,* 355-417.

SUWA, K., NUREKI, T., INOUE, H., BIYAJIMA, K., and MIYAKAWA, K. (1979): Geology and petrology of the Machakos area, Kenya. *4th Prelim. Rept. Afr. Studies, Nagoya Univ.,* 3-20.

TOKIEDA, K., ITO, H. and SUWA, K. (1983): Remanent magnetization of granites and dolerites from Mahe Island, Seychelles. *8th Prelim. Rept. Afr. Studies, Nagoya Univ.,* 37-46.

WASSERBURG, G.J., CRAIG, H., MENARD, H.W., ENGEL, A.E.J. and ENGEL, C.G. (1963): Age and composition of a Bounty Islands granite and age of a Seychelles Islands granite. *Jour. Geol.,* **71**, 785-789.

YANAGI, T., WAKISAKA, Y. and SUWA, K. (1983): Rb-Sr whole rock age of granitic rocks from the Seychelles Islands. *8th Prelim. Rept. Afr. Studies, Nagoya Univ.,* 23-36.

PLATE I

1. West coast (4°35′ ~ 4°40′ S, 55°22′ ~ 55°26′ E) of the Mahe island seen from northwest. Left half is northern lower hills consisting of gneissose granodiorite and right half is southern higher hills consisting of grey granite and porphyritic granite (Photo. by K. S., 7 Oct., 1981).

2. Northeast coast of the Mahe island around Port Victoria (4°37′ S, 55°27′ E) seen from northeast (Photo. by K. S., 7 Oct., 1981).

1

2

PLATE II

1. Agmatite (angular blocks of amphibolite and gneissose granodiorite in leucogranite) at La Blache (4°35′ S, 55°26′ E) in the northwest coast of the Mahe island (Photo. by K. S., 14 Oct., 1981).

2. Grey granite around Anse Jasmin Estate (4°37.5′ S, 55°24′ E) in the northwest coast of the Mahe island (Photo. by K. S., 13 Oct., 1981).

1

2

PLATE III

1. Cerf island (4°38′ S, 55° 30′ E) seen from the northeastern coast of the Mahe island (Photo. by K. S., 4 July, 1981).

2. Dolerite dyke, being 125 cm in width and N45°W direction with easterly dipping at high angle (82°), intruding into porphyritic granite at Port Glaud (4°39.8′ S, 55°25.1′ E) in the west coast of the Mahe island (Photo. by K. S., 3 Oct., 1981).

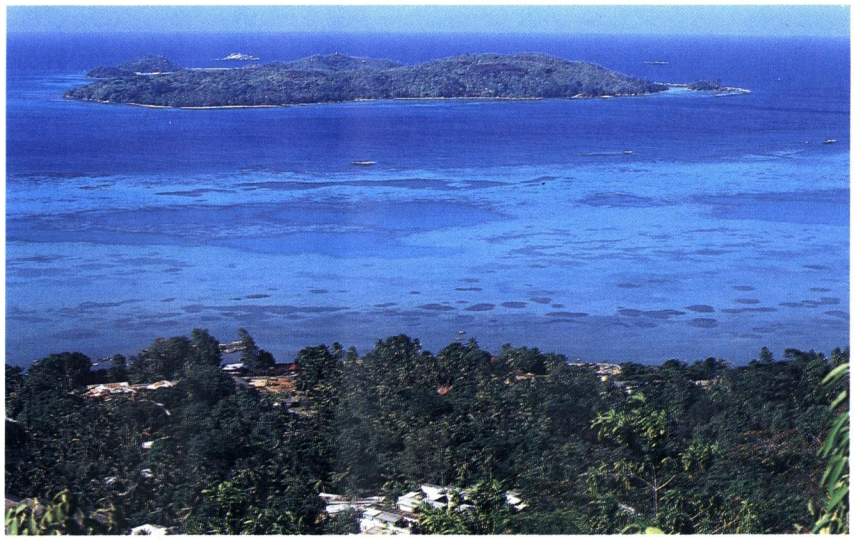

1

2

PLATE IV

1. Silhouette island (4°28′ S, 55°13′ E) seen from the northwest coast of the Mahe island (Photo. by K. S., 30 Sep., 1981).

2. Northeast coast (4°28.5′ S, 55°15′ E) of the Silhouette island (Photo. by K. S., 7 Oct. 1981).

1

2

PLATE V

1. Agmatite (angular blocks of gneissose granodiorite and amphibolite in leucogranite) at La Blache (4°35′ S, 55°26′ E) in the northwest coast of the Mahe island (Photo. by K. S., 14 Oct., 1981).

2. ditto (Photo. by K. S., 30 Sep., 1981)

PLATE V

1

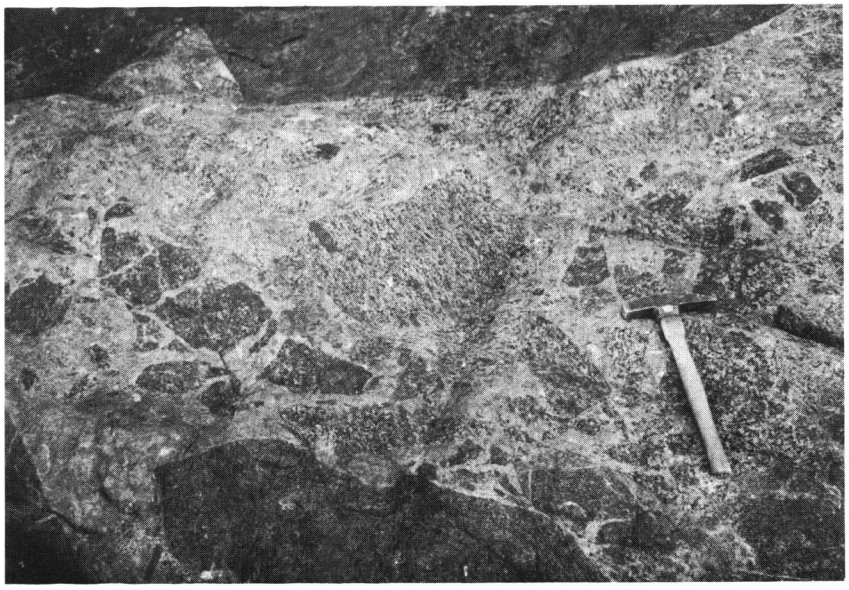

2

PLATE VI

1. Agmatite in leucogranite at La Blache (4°35′ S, 55°26′ E) in the northwest coast of the Mahe island (Photo. by K. S., 15 Oct., 1981)

2. Dolerite dyke intruding into agmatite at La Blache in the northwest coast of the Mahe island (Photo. by K. S., 14 Oct., 1981).

1

2

PLATE VII

1. Grey granite at Mt. Josephine (335 m above the sea level, 4°39′ S, 55°28.4′ E) in the northeast coast of the Mahe island (Photo. by K. S., 4 July, 1981).

2. Dolerite dyke, being 37 cm in width and N13°W direction with northeasterly dipping with high angle (84°), intruding into grey granite at the Wel Civil Quarry, Petit Paris (4°39.8′ S, 55°29.4′ E) in the northeast coast of the Mahe island (Photo. by K. S., 5 Oct., 1981).

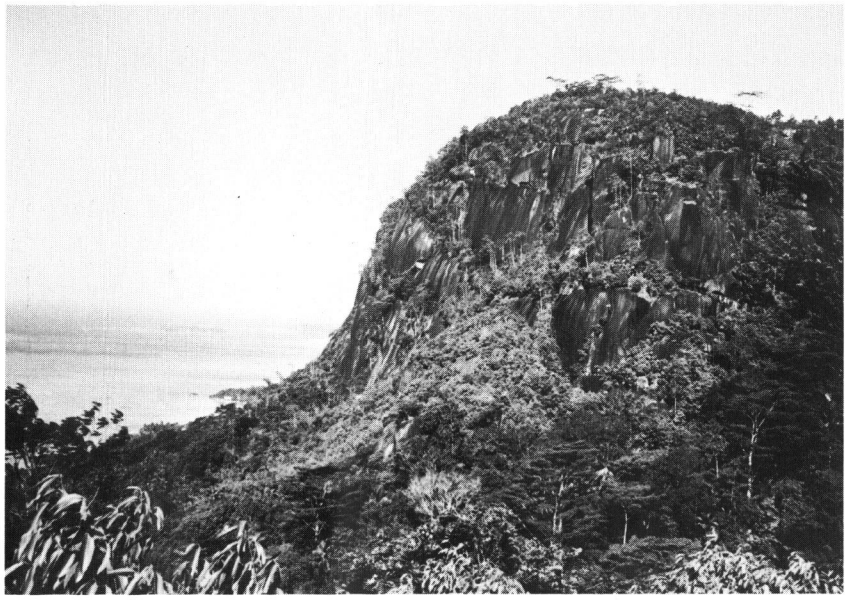

1

2

PLATE VIII

1. East coast (4°23.6′ S, 55°15.5′ E) of the North island (Photo. by K. S., 7 Oct., 1981).

2. ditto.

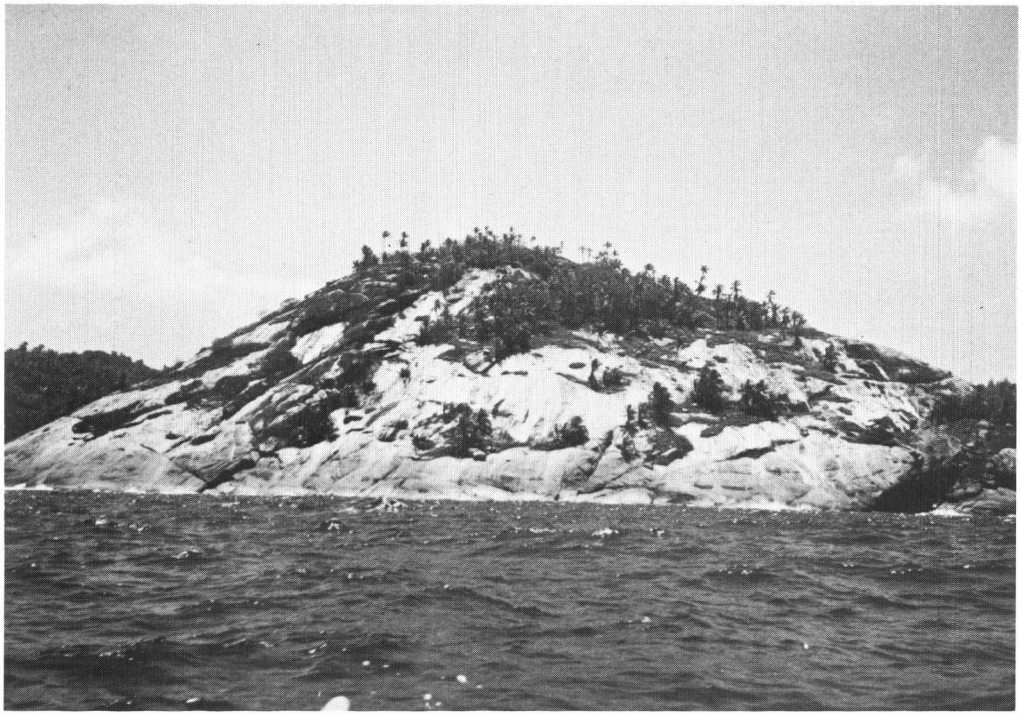

1

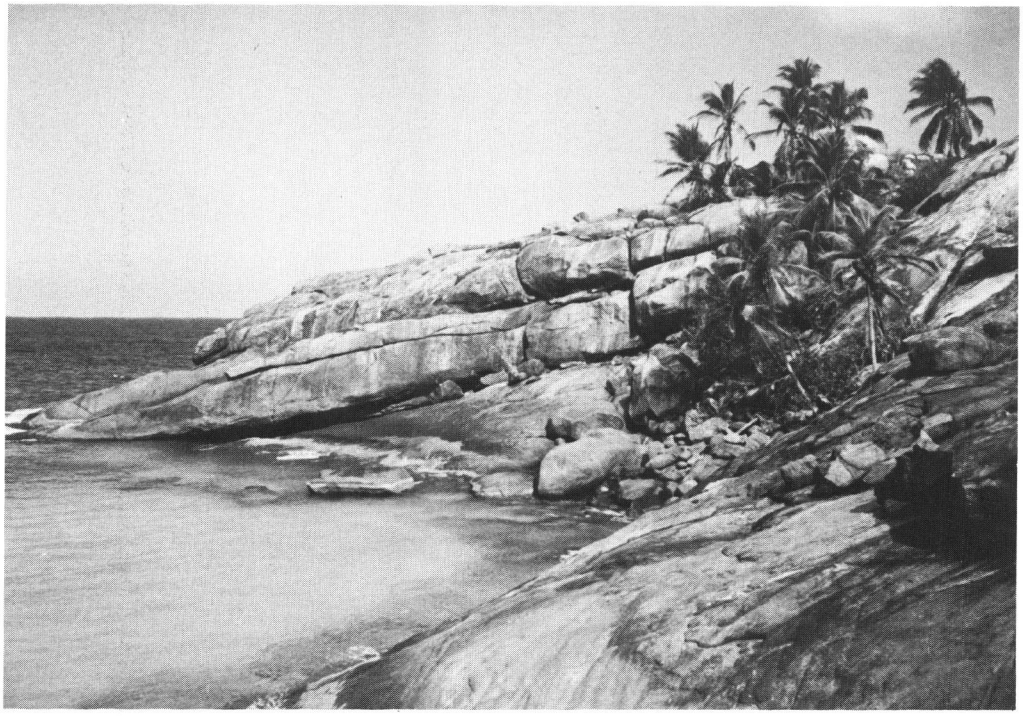

2

Rb-Sr Whole Rock Ages of Granitic Rocks from the Seychelles Islands

Takeru YANAGI*, Yasuhiko WAKIZAKA* and Kanenori SUWA**

* Department of Geology, Faculty of Science, Kyushu University
** Department of Earth Sciences, Faculty of Science, Nagoya University

Abstract

Rb-Sr radiometric dating was done on whole rock samples collected from the Mahe island, Seychelles. Analyses of these samples yielded isochron ages of 693 ± 16 Ma for the gneissose granite, 683 ± 16 Ma for the porphyritic granite. An apparent age of 570 ± 5 Ma which comes from the isochron plot for the grey granite is erroneous, due to the recrystallization of K-feldspar. A similar recrystallization texture is found in some gneissose granite samples. An age of 713 ± 19 Ma is recommended as a much reliable age of the gneissose granite. A Rb-Sr biotite age of the diorite in Ile Du Nord is very young at 60 ± 4 Ma and the associated initial ratio is 0.70361 ± 0.00010. It is an evidence of igneous activity occurred after the continental disruption.

These radiometric ages of the Precambrian granitic rocks are well correlated to the time of major magmatic activity in the Mozambique Belt in East Africa.

Introduction

Principal islands of Seychelles such as Mahe and Praslin are unique oceanic islands lying in the Western Indian Ocean, because they are composed of Precambrian granitic rocks (Miller and Mudie, 1961; Baker, 1963; Baker and Miller, 1963; Ben-Avraham et al., 1981). These islands are believed to be continental fragments left behind as a result of the disruption of Gondwanaland and the succeeding opening of the Indian Ocean. The object of this paper is to present a basic evidence for this idea by reporting Rb-Sr whole rock ages of Precambrian granitic rocks in the principal island, Mahe. In addition, this paper is to present another evidence of an igneous activity occurred after the continental disruption, which resulted in the emplacement of diorite in one of the Seychelles islands.

The comprehensive geological survey of almost all islands of the Seychelles archiperago was made first by B.H. Baker of Mines and Geological Department, Kenya, from 1960 to 1961. And the results were published in 1963, reporting that there are three main types of Precambrian granite, i.e., the grey Mahe granite, the grey faintly gneissose granite and the reddish Praslin-La Digue granite. The first two are main geological units found in Mahe and nearby islands, and the last composes the geology of Praslin with minor amounts of porphyritic granite and doleritic rocks. The porphyritic granite found rather extensively on the west coast of Mahe was

8th Prelim. Rept. Afr. Studies, Nagoya Univ., 23-36, 1983.

regarded by him as a facies of the grey Mahe granite. It was also reported that a swarm of doleritic dykes are found in all these three types of granite in Mahe and Praslin, but that no such dyke is found in Silhouette and Ile Du Nord, which consist of syenitic, microgranitic and dioritic rocks of early Tertiary in age.

Radiometric dating was done first on whole rock samples by Miller and Mudie (1961) with results that a K-Ar ages of grey and pink granites from Mahe is curiously young, ranging from 494 to 535 Ma, and that biotite of the pink granite, however, gives an older age of 653 Ma. The latter age is close to the results (624 and 667 Ma) of Wasserburg et al. (1963). Baker and Miller (1963) further tried on hornblende in granites and reported ages of 532 to 580 Ma. One hornblende sample of the pink granite in Praslin, however, was found to be 645 Ma. It is close to the biotite age and the results of Wasserburg et al. (1963). Baker and Miller reported an age of dolerite dyke in Mahe to be 643 Ma. It puts the youngest limit to the emplacement of Precambrian granites.

Syenitic rocks from Silhouette are very young with K-Ar ages of 34 to 62 Ma (Baker and Miller, 1963). Similar ages of 48 and 52 Ma were reported by them from olivine dolerites in Praslin. These are records of the latest event of igneous activity occurred in principal and associated islands of Seychells.

Geological Settings

The geological research team of Nagoya University made a field survey of Mahe and nearby islands during its stay from 26th September to 24th October 1981, and revised the geological map of the Mahe island (Suwa et al., 1983). Fig. 1 is the geological map in which sites of samples used for dating were plotted.

The geology of Mahe consists of four types of Precambrian granitic rocks, i.e., the gneissose granite, the grey granite, the pink granite and the porphyritic granite. All these plutonic rocks are cut by dykes of doleritic compositions, mostly with a WNW-ESE trend.

The gneissose granite, grey in colour, occurs in the northern part of Mahe and in such small islets lying east of Port Victoria as the St. Anne and Cerf islands. This intrusive body is petrographically heterogeneous with many ellipsoidal basic xenoliths. It has parallel banding and foliation, though these are faint. It is coarse-grained in some places, and fine-grained in other places. Rock facies with different grain sizes are distributed complicatedly in this intrusive body. The ellipsoidal basic xenoliths, 5 to 20 cm across, are arranged in parallel to the foliation. The foliation has a NNE trend and a steep dip to SE. On the west coast of north Mahe the gneissose granite is agmatitic in appearance, which are crushed into angular blocks and penetrated by veins of leucocratic granite in a network-like form.

The grey granite occupies the most part of the island. It is coarse-grained equigranular plutonic rocks with greenish grey to dark grey colours. It is massive with no foliation. Xenoliths are rather small and few. These petrographic characters are uniformly constant throughout the body. The rocks at quarries in Grand Anse

Village, however, are quite different and exceptional from other part of the body. It is porphyritic with K-feldspar and corroded quartz phenocrysts and has abundant basic xenoliths from 5 to 50 cm across. A body in a stock-like form found to the northwest of Port Victoria (Fig. 1) is the grey granite which seems to have been emplaced discordantly in the gneissose granite. On the west coast of Mahe, however, the boundary between the grey granite and the gneissose granite is not so sharp as it will be expected from a simple intrusion of magma. The gneissose granite seems to grade into the coarse-grained grey granite across the boundary zone.

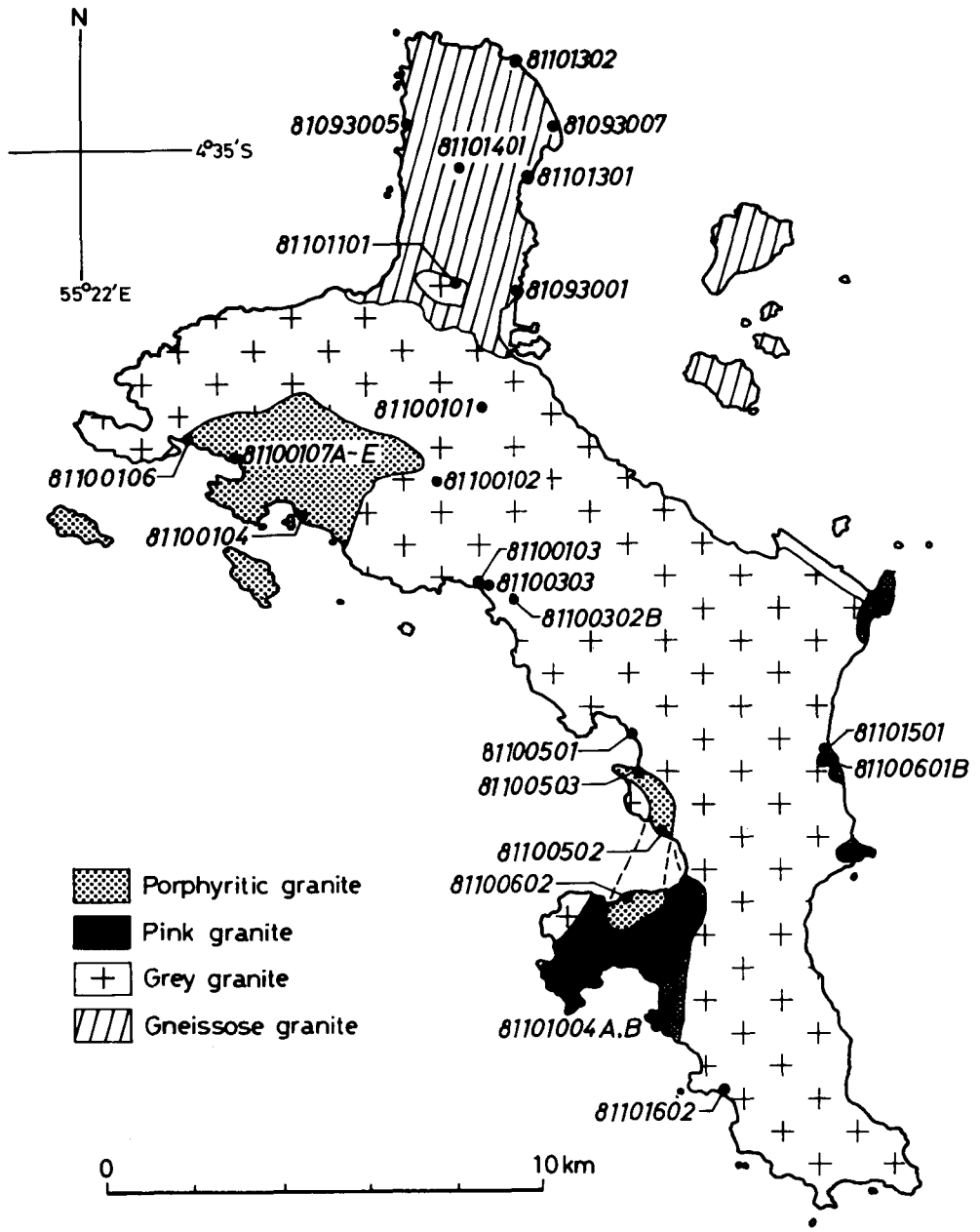

Fig. 1. Geological map of Mahe with sampling sites. Dolerite dykes are all excluded from this map.

The pink granite, reddish brown to orange in colour, is scattered as small masses in the grey granite. Besides those shown in Fig. 1, there are few other small masses in the grey granite. Among these masses of the pink granite, the one occurred in the Baie Lazare Village is exceptionally large with a surface extension of about 6 km^2. Besides their difference in colour, the pink granite and the grey granite are almost the same in petrographic aspects. The pink granite is discriminated from the grey granite by its stained K-feldspar with reddish brown to orange colours. Since the pink granite grades into the grey granite across the boundaries, these two seems to represent different facies of the same intrusive body.

The porphyritic granite is characterized by its porphyritic texture with phenocrysts of K-feldspar, which is unexceptionally mantled by sodic plagioclase. The porphyritic granite which consists of two intrusive bodies occurs on the west coast of Mahe (Fig. 1). The porphyritic granite in the north crops out around Port Launay Estate. This is grey in colour. The rock near the northwestern contact with the grey granite represents a chilled facies of the intrusion. This rock consists of very fine grained crystals of groundmass and a lesser amount of phenocrysts of K-feldspar mantled by plagioclase. Although the intrusive body is massive and homogeneous, in some places phenocrysts of feldspars accumulate to form pegmatitic masses or veins of a few centimeters across.

The porphyritic granite in the south intruded itself into both the grey granite and the pink granite in a dyke-like form of about 400 m in width. It is interesting that, although its half portion lying in the grey granite is grey in colour, the other half lying in the pink granite has K-feldspar phenocrysts stained in reddish brown to orange in colour.

The emplacement of parallel dykes of dolerites is the last event of magmatic activity recorded in Mahe.

Petrography

The gneissose granite consists mainly of sodic plagioclase, quartz, and K-feldspar with microperthitic texture. It contains green hornblende (<3%), sphene (<3%), opaque minerals (<3%) and biotite (<1%). It has an equigranular granoblastic texture with crystals of medium sizes. Quarts crystals unexceptionally display a recrystallization texture, which is very distinctive from those in other intrusions. The quartz crystals which had once been as large as associated plagioclase and K-feldspar became an aggregate of small grains of quartz with a granoblastic texture. All other intrusives, i.e., the grey, the pink and the porphyritic granite, lack this type of recrystallization texture, suggesting that the granoblastic aggregate of quartz was formed before or at the same time with the emplacement of these later intrusives, especially the grey granite.

The grey granite consists mainly of quartz and K-feldspar with a microperthitic texture. In most cases, the grey granite lacks plagioclase, or if any present, contains in a very small amount. This is one of discriminating characters. In addition to

these major minerals, it contains deep green hornblende (<4%), riebeckite (<4%), clinopyroxene (<2%), opaque minerals (<2%) and biotite (<1%). The grey granite has petrographic characters common to those of alkali granite. Riebeckite occurs ubiquitously in the grey granite as, in most cases, minute minerals overgrown around the ferrorichterite. In some places, however, amphibole is all riebeckite. Quartz in this granite shows no evidence of recrystalization. There is, however, recrystallization bands of albite along boudaries between K-feldspar grains. This recrystallization texture is found ubiquitously in the grey granite. In places the recrystallization proceeded to an extent that, in addition to broad recrystallization bands, new albite blobs were formed in the K-feldspar. Since Rb in the grey granite resides mostly in K-feldspar, it is reasonable to think that radiogenic $^{87}Sr^*$ in the granite is contained mostly in the same K-feldspar. The recrystallization texture indicates the alteration of the container of radiogenic $^{87}Sr^*$ in the rock. The same recrystallization texture, though much smaller in scale, is found in samples of the pink granite and also some samples of the gneissose granite. But it is not found in the porphyritic granite.

The pink granite is distinguished from the grey granite by the presence of sodic plagioclase with polysynthetic twin, although it is few. The recrystallization band found between K-feldspar grains is obscure in some samples and in other samples narrower in contrast to those found in the grey granite.

Phenocrysts of K-feldspar mantled by plagioclase give a unique appearance to the porphyritic granite. The mantling plagioclase is not poly crystals but a single crystal covering a core K-feldspar completely. The mantled texture is easily discernible even by naked eyes. The inner, rather transparent part of the phenocryst (K-feldspar) is concaved by weathering, and the peripheral, lactescent rim (plagioclase) is remained so that it gives a skeletal appearance on the weathered surface of rock. The porphyritic granite consists mainly of plagioclase, K-feldspar and quartz with minor amounts of augite, hornblende, biotite and opaque minerals. Augite is unexceptionally mantled by green hornblende rim. No recrystallization texture is found in this rock.

Samples and Analytical Methods

Six rock samples of the gneissose granite from six sites, six rock samples of the grey granite from six sites, six rock samples of the pink granite from five sites and ten rock samples of the porphyritic granite from five sites were analyzed to know whole rock isochron ages and geochemical relationships between them. Biotite was separated from one porphyritic granite (81100107B) to determine a mineral age of the rock. Another biotite sample was also separated from the diorite sample (81100703) from Ile Du Nord to limit an age of the latest igneous event in the Seychelles Islands.

Rock samples of 1-2 kg were crushed into chips of 0.5 −1 cm across. After washing them with distilled water, the chips were grounded into powder with a vibrating

Table 1. Analytical data

Rock/Sample No.	Rb (ppm)	Sr (ppm)	Rb^{87}/Sr^{86}	Sr^{87}/Sr^{86}
Gneissose Granite				
81093001	75.7*	126.0	1.742	0.72243 ± 0.00020
81093005	76.6*	202.7	1.095	0.71545 ± 0.00008
81093007	45.6*	136.0	0.970	0.71411 ± 0.00008
81101301	76.6*	68.1	3.25	0.73661 ± 0.00011
81101302	42.0	141.7	0.858	0.71278 ± 0.00006
81101401	77.1	46.6	4.82	0.75093 ± 0.00007
Grey Granite				
81100102	131.8*	28.6	13.49	0.83706 ± 0.00010
81100302B	117.0*	14.45	24.0	0.95575 ± 0.00009
81100303	119.3*	22.11	15.85	0.85672 ± 0.00009
81100501	118.7*	19.51	17.90	0.87315 ± 0.00009
81101501	110.0*	22.21	14.53	0.84557 ± 0.00013
81101602	136.8	21.51	18.72	0.87922 ± 0.00018
Pink Granite				
81100101	107.7	36.8	8.53	0.78831 ± 0.00008
81100103	131.7*	37.3	10.30	0.80492 ± 0.00018
81100601B	102.4	30.2	9.90	
81101004A	143.6*	41.1	10.22	
81101004B	146.8*	42.2	10.17	
81101101	159.1	48.2	9.65	0.79998 ± 0.00011
Porphyritic Granite (North)				
81100104	144.9*	106.2	3.94	0.74427 ± 0.00014
81100106	89.1	124.9	2.07	0.72680 ± 0.00015
81100107A-I	139.8*	139.4	2.91	0.73391 ± 0.00008
81100107B	137.4	141.4	2.82	0.73268 ± 0.00014
81100107C-I	171.6	160.9	3.10	
81100107C-II	137.2*	138.8	2.87	
81100107E	120.8*	155.2	2.26	0.72779 ± 0.00020
Porphyritic Granite (South)				
81100502	144.7	76.2	5.52	0.75874 ± 0.00015
81100503	169.5	67.4	7.34	0.78019 ± 0.00011
81100602	159.3*	69.4	6.69	0.77018 ± 0.00010
Diorite				
81100703	37.91	677	0.162	0.70375 ± 0.00009
Biotite (Porphyritic Granite, North)				
81100107B	743	11.49	222	2.6283 ± 0.0058
Biotite (Diorite)				
81100703	192	29.9	18.62	0.71974 ± 0.00024

sample mill (HEIKO TI-100) equipped with tungsten-carbide sample containers, and then analyzed on Rb and Sr contents and strontium isotopic composition. Rb and Sr contents were estimated at first with X-ray fluorescence method and then determined with the conventional isotopic dilution method. Relative errors of Rb/Sr rations were estimated to be less than 2%. Sr isotopic compositions were determined with two mass spectrometers, HITACHI RMU5G (r = 20 cm), and JEOL JM05RB (r = 30 cm), both equipped with digital output circuits, and normalized by adjusting $^{86}Sr/^{88}Sr$ ratio to 0.1194. All errors associated with isotopic ratios were listed in Table 1 at 1σ level.

The decay constant of Rb is 1.42×10^{-1} /year. K-Ar ages cited in this paper were recalculated with decay constants $\lambda_\beta = 4.962 \times 10^{-10}$/year and $\lambda_e = 0.581 \times 10^{-10}$/year (Steiger and Jäger, 1977).

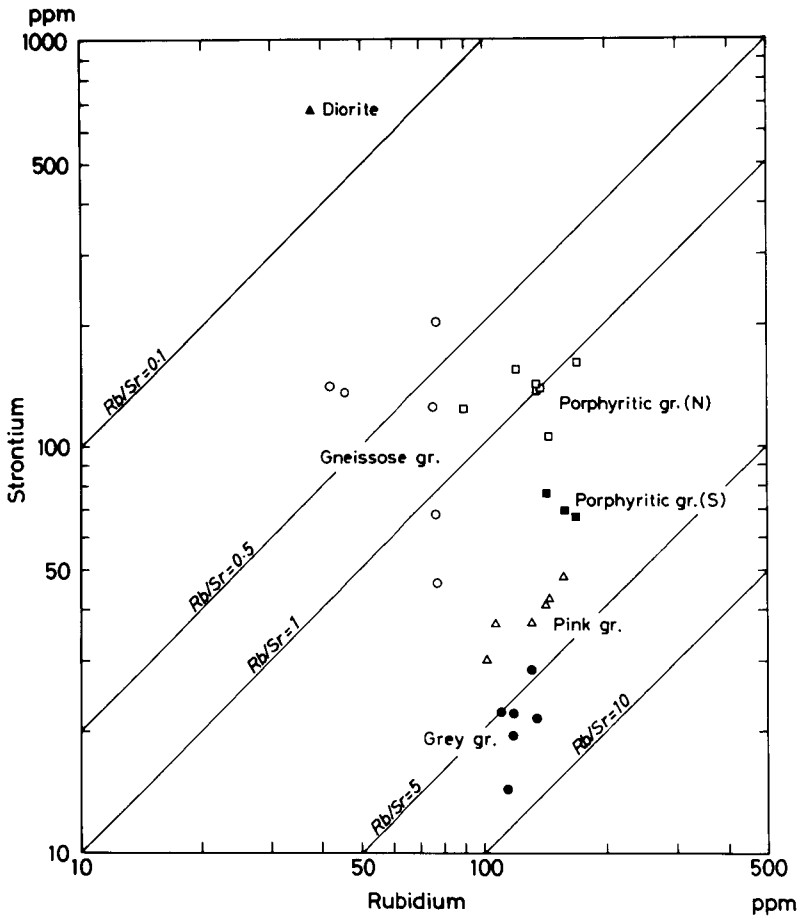

Fig. 2. Geochemical relations between different petrographic types of granite in Mahe.

Analytical Results

Analytical results were shown in Table 1. Data with an asterisk were determined with X-ray fluorescence method only. Rb and Sr contents were plotted in Fig 2 to show that four granitic plutons have their own specific fields in Rb vs. Sr diagram; Petrographically discriminated intrusive bodies have their own range of Rb and Sr contents.

Rb contents in the grey granite range from 100 to 150 ppm, and Sr contents from 14 to 30 ppm. The latter is very low. Rb/Sr ratios are in a range from 4.6 to 8.1. The grey granite marks the highest values of Rb/Sr ratio and has geochemical nature of the most evolved magma among the granitic plutons in Mahe.

The pink granite has intermediate compositions between the grey granite and other two types of intrusion (Fig. 2). Its Rb/Sr ratios are very limited in a range from 2.9 to 3.5, in spite of its scattered geological distribution.

Although they have the same petrographical characters, porphyritic granites in the north and in the south are so different in Sr content that they are plotted in separated areas in Fig. 2. The porphyritic granite in the south has less Sr contents and hence higher Rb/Sr ratios.

The gneissose granite marks the lowest values of Rb/Sr ratio. Rb content varies in a rather wide range from 40 to 80 ppm (Fig. 2). So far as available data are concerned, there is no rock sample with Rb more than 80 ppm. Although other three types of intrusion are limited in discrete and rather narrow areas in Fig. 2, the gneissose granite occupies a wider area, corresponding to its wide range of petrographic variation.

Fig. 3 is a Rb/Sr vs. Rb plot. In this diagram the granite samples are enclosed within an area bounded by broken lines. Samples of the gneissose granite lie on the side of low Rb contents and low Rb/Sr ratios, indicating their comparatively less evolved geochemical nature.

Fig. 4 is an isochron plot for the gneissose granite. In Fig. 4, an isochron for the porphyritic granite was also shown for comparison. The data for the gneissose granite define an isochron which yields an age of 693 ± 16 Ma and an initial ratio of 0.70450 ± 0.00029. This age is the oldest among those so far reported. The K-Ar age of biotite of the pink granite was reported by Miller and Mudie (1961) to be 653 Ma. A similar K-Ar age on hornblende in the pink granite was reported from Praslin, about 40 km northeast of Mahe. It is 643 Ma. Rb-Sr ages determined on a whole rock and a feldspar sample of the grey granite in Mahe are 667 and 624 Ma, respectively (Wasserburg et al., 1963). All other data are in the range from 494 to 580 Ma.

Fig. 5 shows an isochron of the porphyritic granite, the last granitic intrusive in the Mahe island. Eight analytical data, five from the northern and three from the southern intrusive bodies, define an isochron of 683 ± 16 Ma with an initial ratio of 0.70592 ± 0.00075. The reference isochron in Fig. 5 is of the gneissose granite, suggesting that the gneissose granite is older by about 10 Ma than the porphyritic granite. This age relation is consistent with the field observation.

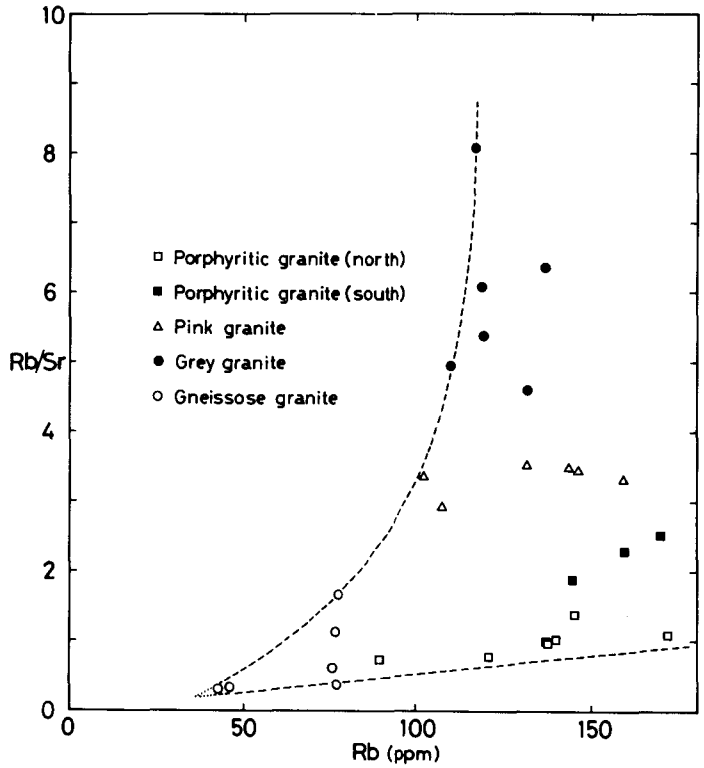

Fig. 3. Rb/Sr vs.Rb plot for granites in Mahe.

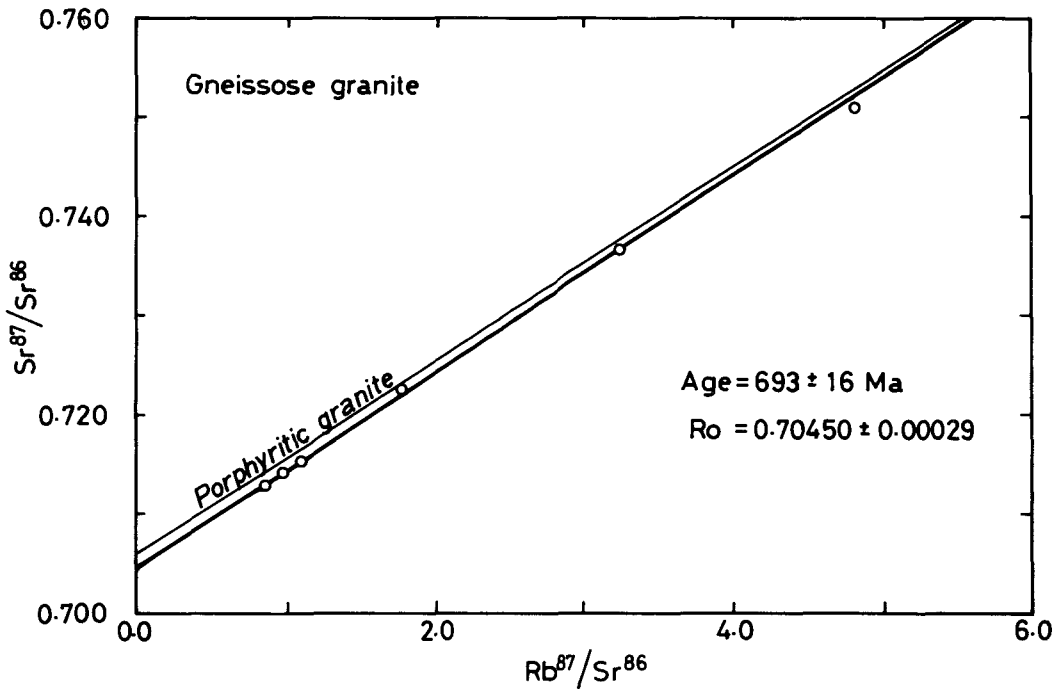

Fig. 4. Isochron plot for the gneissose granite. A thin line is an isochron of the porphyritic granite.

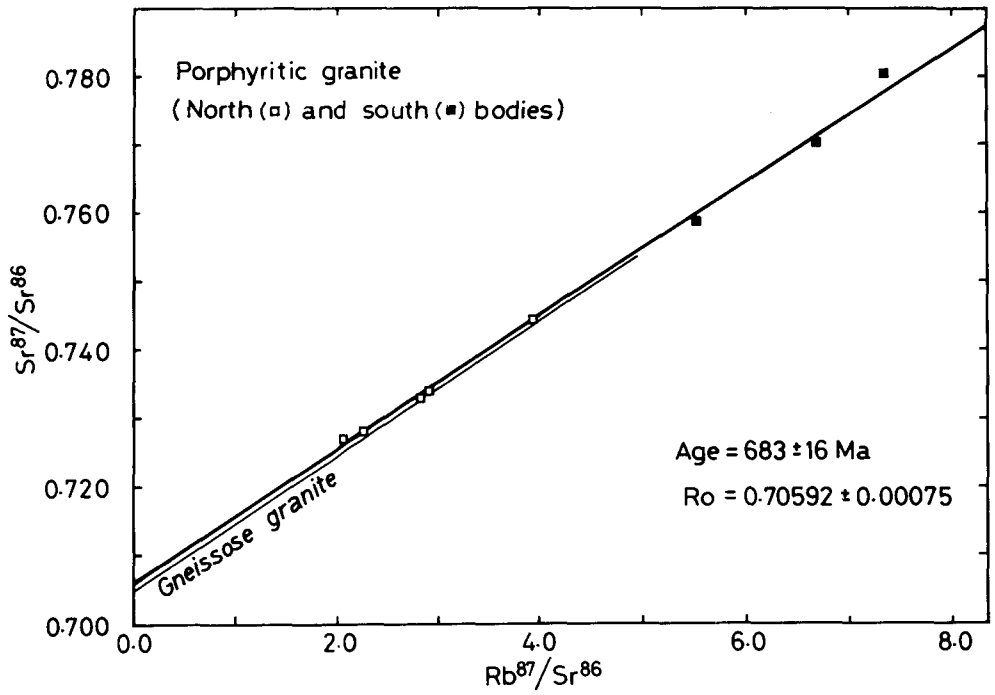

Fig. 5. Isochron plot for the porphyritic granite. A thin line is the isochron of the gneissose granite.

Fig. 6 is an isochron plot for the grey granite. Five data out of six well define an isochron of 570 ± 5 Ma with a high initial ratio of 0.7275 ± 0.00012. Remaining one is plotted far above the isochron. This datum was excluded from the regression to define the isochron. The apparent isochron age of the grey granite is younger than that of the porphyritic granite, which intruded itself into the former. The apparent age is rather close to K-Ar ages on hornblendes and whole rocks of the same granite. The discrepancy will be discussed later.

A pair of whole rock and biotite samples of the porphyritic granite gives a mineral age of 605 ± 15 Ma, and an initial ratio of 0.7083 ± 0.0012. Another pair come from the diorite in Ile Du Nord gives an age of 60 ± 4 Ma. An initial ratio of the diorite is very low at 0.70361 ± 0.00010.

Discussion

Recrystallization textures are observed in samples of the grey granite and the gneissose granite. Since much of Rb in these samples resides in K-feldspar which has low retentivity of radiogenic $*Sr^{87}$, the evidence of recrystallization should be evaluated properly.

There is no discernible recrystallization texture nor evidence of later alteration of

minerals in the porphyritic granite samples. Therefore its whole rock isochron age of 683 ± 16 Ma is the most reliable among those reported here. Grain size of biotite crystals in the porphyritic granite is very small, less than 300μm across. Therefore it is reasonable to think that a certain amount of radiogenic $*Sr^{87}$ has been lost during a cooling period of the granite. Therefore it could not be possible to assign this age to some geological event.

Many parallel dykes of dolerites cut all types of granitic plutons. The emplacement of these dykes represents the last magmatic event occurred in the Mahe island. One K-Ar age has been reported from the dyke by Baker and Miller (1963) to be 643 ± 55 Ma. This age and the whole rock isochron age of the porphyritic granite are consistent with the geological relationships found between them.

Quartz in the gneissose granite exclusively has a recrystallization texture, in which it occurs as a granoblastic aggregate of grains much smaller than associated K-feldspar and plagioclase. Some samples of the gneissose granite have recrystallization bands of albite along the boundaries between crystal grains of K-feldspar. Although the recrystallization texture is the same, the width of the band is narrower, and its number found under the microscope is smaller in the gneissose granite than in the granite. There seems to be such relation in the gneissose granite that the more the rock contains K-feldspar, the more present are the recrystallization bands in number. This type of recrystallization is so far proceeded in the sample numbered 81101401

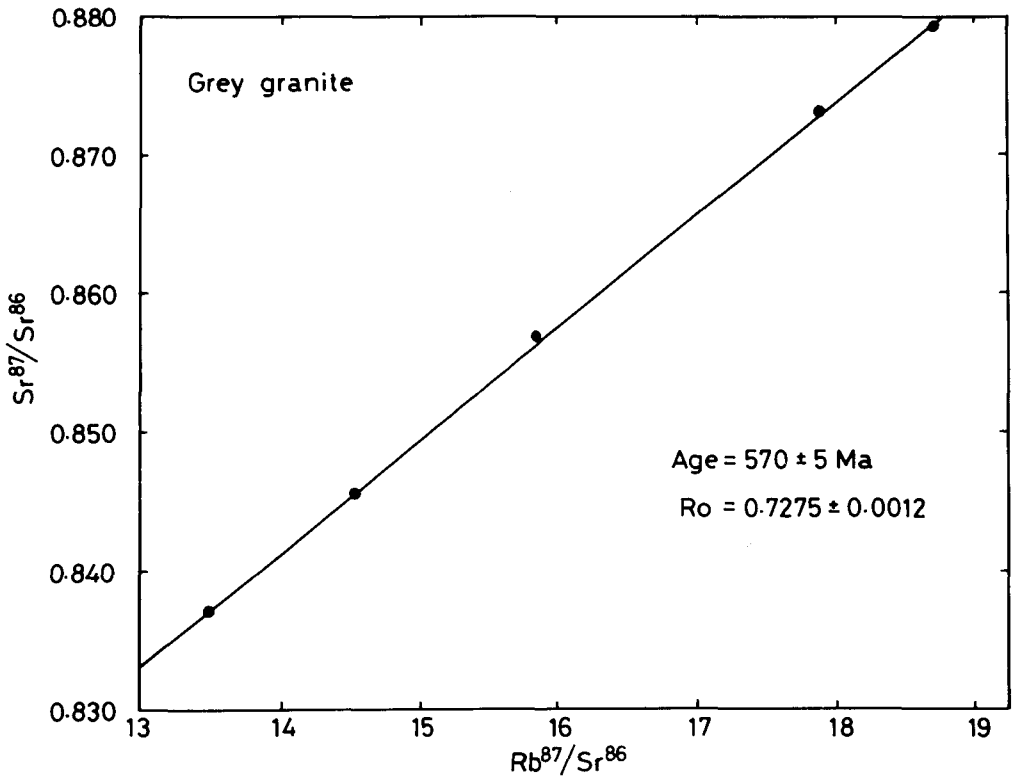

Fig. 6. Isochron plot for the grey granite.

that the small recrystallization blobs of albite are formed in K-feldspar. This sample should be discriminated and then excluded from others in which the recrystallization band is obscure or small in number and scale. Data for these less recrystallized five samples give an isochron of 713 ± 19 Ma with an initial ratio of 0.70419 ± 0.00032. This value is recommended as more reliable age or, more probably, a possible youngest limit of the gneissose granite.

The conflict found between the radiometric ages of the grey granite and the porphyritic granite may come from the recrystallization ubiquitously occurred in the grey granite. It is reasonable to think that a significant amount of radiogenic $*Sr^{87}$ has been lost during the recrystallization of K-feldspar, the most important container of radiogenic $*Sr^{87}$ in the rock. Five data for the grey granite, however, are not scattered but well define a straight line on the isochron plot. But an age come from the slope is mysterious, being far below even the biotite age of the porphyritic granite, and the age of the dolerite dyke. Therefore we must analyse how the linear arrangement is hold during the recrystallization, by which radiogenic $*Sr^{87}$ is partly removed from the rock system.

Let us assume the migration of radiogenic $*Sr^{87}$ out of the rock system to be a first order transportation phenomenon, and also assume that a rate of migration is constant throughout the system. Then the accumulation rate of radiogenic $*Sr^{87}$ at a certain site of the system is

$$\frac{d*Sr^{87}}{dt} = \lambda\, Rb^{87} - \alpha *Sr^{87}$$

Where λ and α are a decay constant of ^{87}Rb and a rate constant of the migration, respectively. In a case that the recrystallization begins after a period t_1 passed from the time of formation, the solution to this equation is

$$\left(\frac{Sr^{87}}{Sr^{86}}\right)_t = \left(\frac{Sr^{87}}{Sr^{86}}\right)_0 + \frac{Rb^{87}}{Sr^{86}} \left\{ (e^{\lambda t_1} - 1)\, e^{\lambda t - \lambda t_1 - \alpha t} + \frac{\lambda}{\alpha - \lambda} (e^{-\lambda t} - e^{-\alpha t})\, e^{\lambda (t - t_1)} \right\}$$

Where $(^{87}Sr/^{86}Sr)_0$ is the strontium isotopic ratio when the rock was formed. This equation indicates that the rock system defines a straight line on the isochron plot during and after the recrystallization. But its slope does not simply indicate the age of formation nor the period of recrystallization. It depends on unknown three parameters, t_1, t and α. If the rock system has been remained to be closed after the recrystallization, it may also define a straight line on the isochron plot. But this line is no more isochron because it depends on unknown parameters and hence it could not designate a specific time. The line may be significant only in a case that the rate constant is so great that the strontium isotopic ratio is reset completely during the recrystallization. In this case the slope of the line indicates a time passed after the recrystallization.

The recrystallization in the grey granite is partial, being limited along the bound-

aries between K-feldspar grains and, in addition to this, within some K-feldspar grains in places of the body. Therefore the straight line defined by data for the grey granite is regarded to be apparent, due to the partial loss of radiogenic $^{87}Sr^*$ during the incomplete recrystallization. The whole rock age of 570 ± 5 Ma could not be corresponded to a specific geological event.

Table 2. Results of radiometric dating

Rock type	Age (Ma)	Reference
(Early Tertiary magmatic event)		
Olivine dolerite in Praslin	50	1
Diorite in Ile Du Nord	60	2
Syenite in Silhouette	62	1
(Late Precambrian magmatic event)		
Dolerite in Mahe	643	1
Porphyritic granite in Mahe	683	2
Grey and pink granites in Mahe	?	
Gneissose granite in Mahe	713	2

1 Baker and Miller (1963); 2 This paper

Summary

The summary of radiometric dating is shown in Table 2. The emplacement of the diorite in Ile Du Nord 60 Ma ago represents the latest magmatic event in the Seychelles archipelago. The syenite and microgranite in Silhouette, and olivine dolerite dykes in Praslin may all be contemporaneous with the diorite.

The late Precambrian magmatic event in the Mahe and nearby islands commenced at some 720 Ma ago and then continued for about 70 Ma. The emplacement of the dolerite dyke swarm in Mahe about 650 Ma ago represents the last phase of this magmatic event. This event began with the emplacement of the gneissose granite which was followed by the successive intrusion of the grey and the porphyritic granite. The age of the porphyritic granite is 683 Ma. Therefore a period for the successive intrusion is about 40 Ma. This Precambrian magmatic event represented by the extensive granite emplacement may well be correlated to the major magmatic activity in the Mozambique Belt in East Africa (Shibata and Suwa, 1979; Kröner, 1980).

Acknowledgements — We thank Mr. P. Shilton, Secretary, National Research and Development Council, Ministry of Planning and Development, and also Mr. G. Lionnet, Senior Education Officer, Ministry of Education and Information, Republic of Seychelles, for their valuable suggestions and supports.

We are very grateful to Messrs. K. Tokieda, H. Umemura, M. Asami and M.

Hoshino for their laborious collaboration in the field survey in 1981. The field work was made possible by the Grant-in-Aid for Overseas Scientific Survey from the Ministry of Education, Science and Culture, Japan, to which we express our thanks. Miss R. Hamamoto assisted us in operating the mass spectrometers.

REFERENCES

BAKER, B.H. (1963): Geology and mineral resources of the Seychelles Archipelago. *Mem, Geol. Surv. Kenya,* **3**, 1-140.

BAKER, B.H. and MILLER, J.A. (1963): Geology and geochronology of the Seychelles Islands and structure of the floor of the Arabian Sea. *Nature,* **199**, 341-348.

BEN-AVRAHAM, Z., NUR, A., JONES, D.J. and COX, A. (1980): Continental accretion: From oceanic plateaus to allochtonous terrains. *Science*, **213**, 47-54.

KRÖNER, A. (1980): Pan African crustal evolution. *Episodes*, **1980**, (2), 3-8.

MILLER, J.A. and MUDIE, J.D. (1961): Potassium-argon age determinations on granite from the island of Mahe in Seychelles Archipelago. *Nature,* **192**, 1174-1175.

SHIBATA, K. and SUWA, K. (1979): A geochronological study on granitoid gneiss from the Mbooni Hills, Machakos area, Kenya. *4th Prelim. Rept. Afr. Studies, Nagoya Univ.*, 163-167.

STEIGER, H. and JÄGER E. (1977): Subcommission on geochronology: Convention on the use of decay constants in geo-and cosmochronology. *Earth Planet. Sci. Letters*, **36**, 359-362.

SUWA, K., YANAGI, T., TOKIEDA, K., UMEMURA, H., ASAMI, M. and HOSHINO, M. (1983): Geology and Petrology of the Seychelles Islands, *8th Prelim. Rept. Afr. Studies, Nagoya Univ.,* 3-21.

WASSERBURG, G.J., CRAIG, H., MENARD, H.W., ENGEL, A.E.J. and ENGEL C.G. (1963): Age and composition of a Bounty Islands granite and age of a Seychelles Islands granite. *Jour. Geol.*, **71**, 758-789.

PLATE I

1. Gneissose granite (Sample No. 81093005) with faint banding, from a road-cut 100m north of Sunset Hotel.

2. Grey granite (Sample No. 81101602) with abundant recrystallization bands of albite, from the northwest frank of Castle Hill.

PLATE I

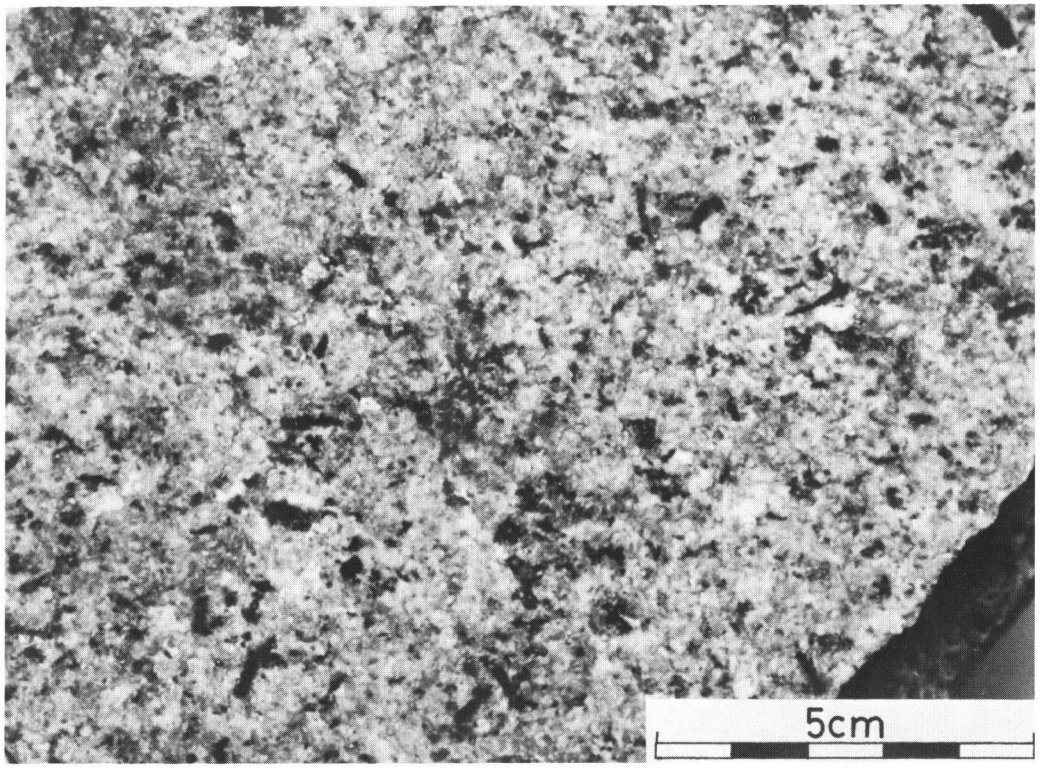

1

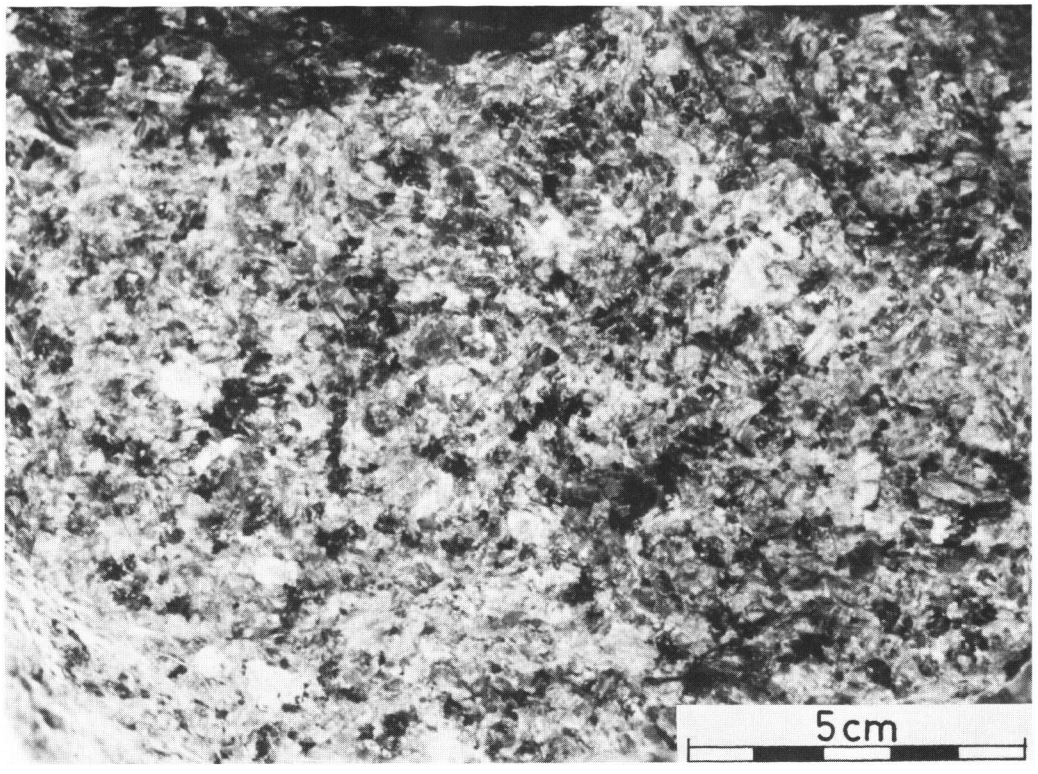

2

PLATE II

1. Pink granite (Sample No. 81101004A) from Pointe Maravi.

2. Porphyritic granite (Sample No. 81100503) with phenocrysts of K-feldspar mantled by sodic plagioclase. From a road-cut near the Agriculture Station, Anse Boileau.

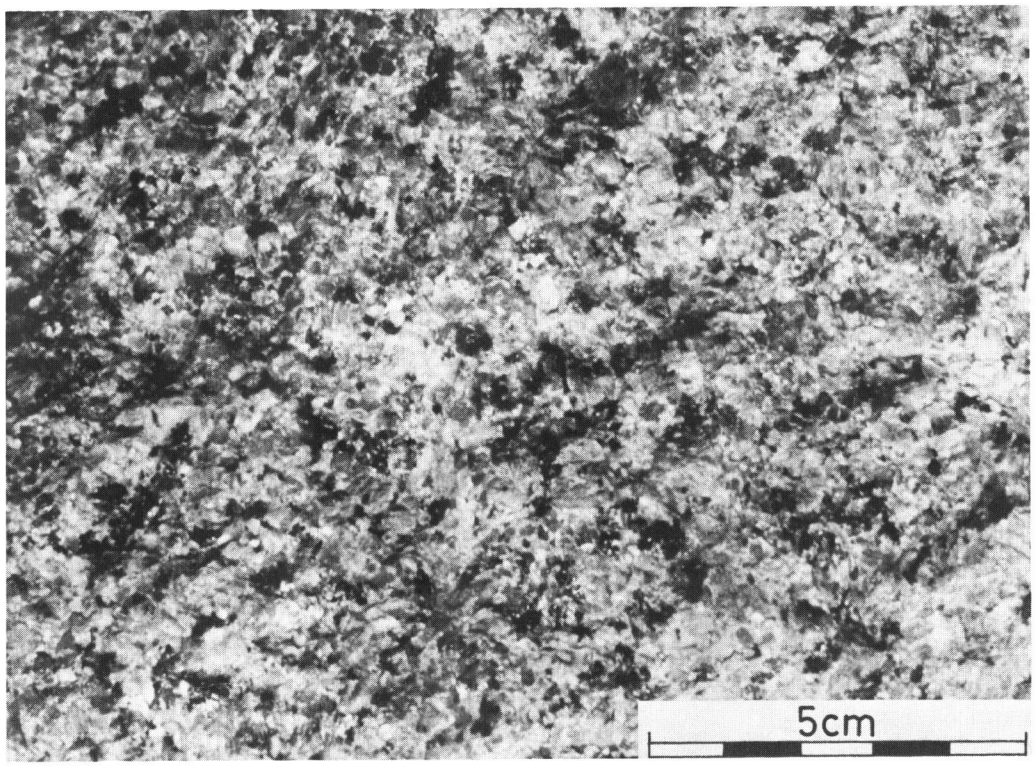

1

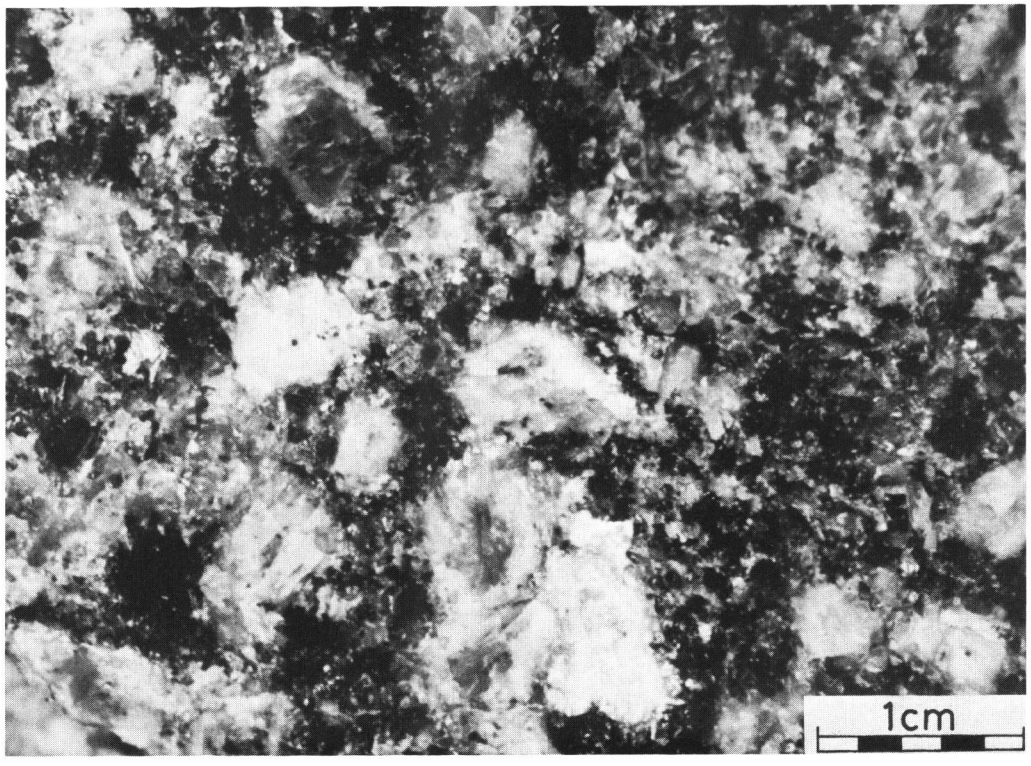

2

PLATE III

1. Photomicrograph of gneissose granite (Sample No. 81101302), from a road-cut, Carana Estate. No recrystallization band of albite between K-feldspar grains.

2. Photomicrograph of grey granite (Sample No. 81100501) with recrystallization bands of albite between K-feldspar grains. From near the shrine, Bon Espoir Estate.

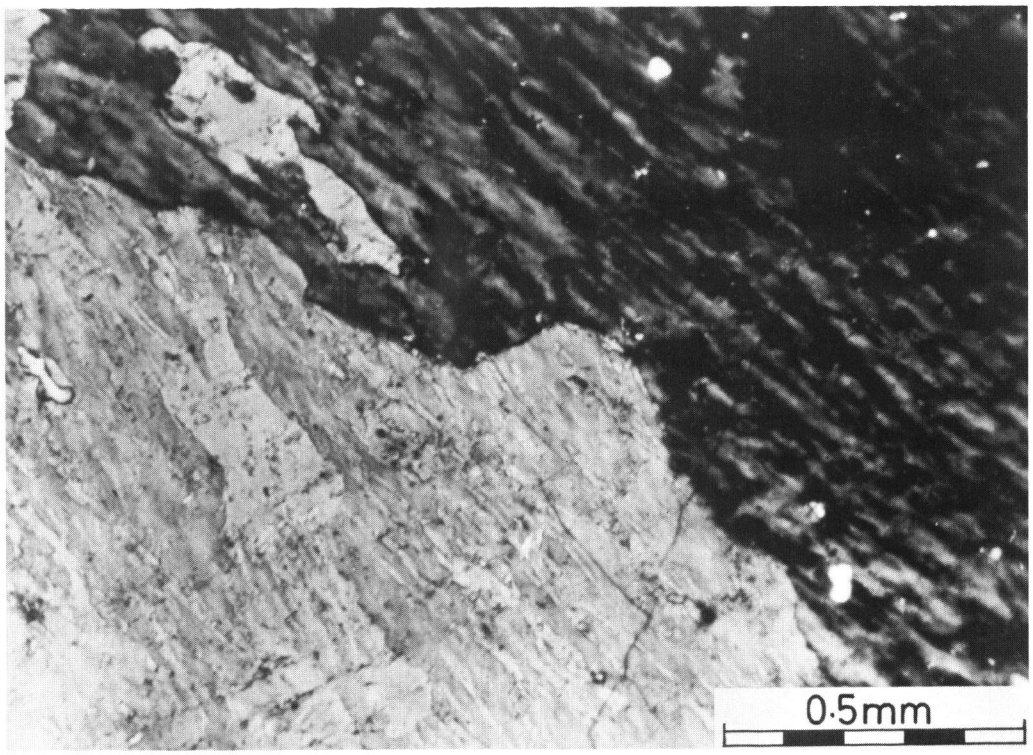

1

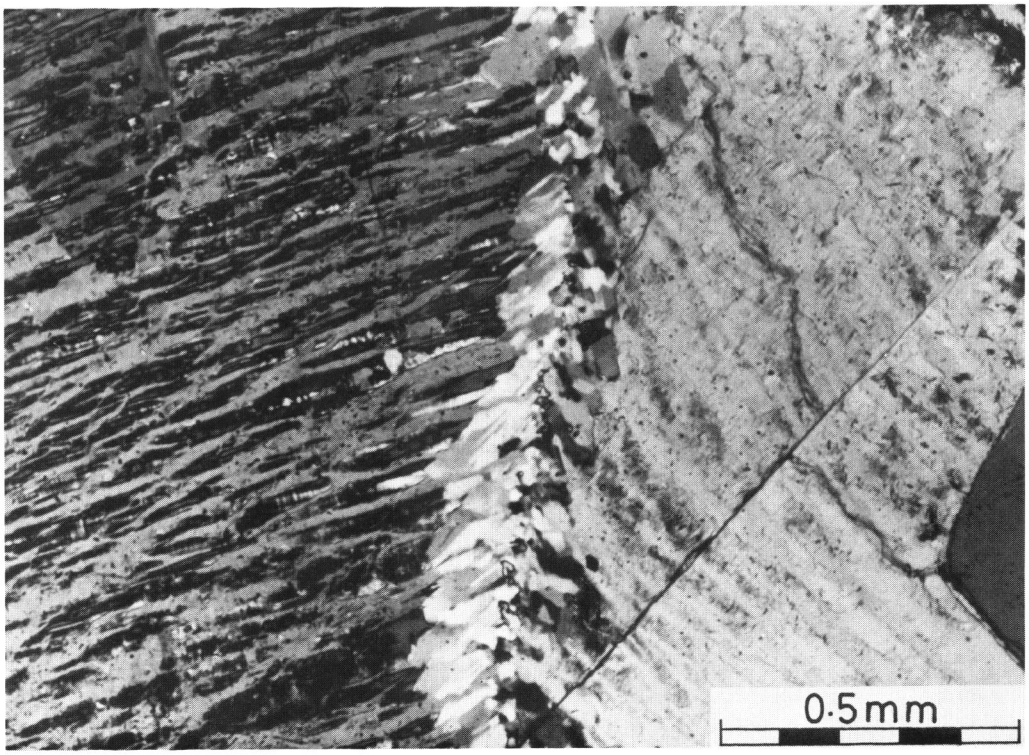

2

Remanent magnetization of granites and dolerites from Mahe Island, Seychelles

Katsuyasu Tokieda,* Haruaki Ito* and Kanenori Suwa**

* Department of Physics, Faculty of Science, Shimane University
** Department of Earth Sciences, Faculty of Science, Nagoya University

Abstract

Four hundred-eight late Precambrian granite specimens and eighty-six age-unknown dolerite specimens were collected from Mahe Island, Seychelles. Progressive alternating field demagnetization has been successfully performed to isolate stable remanence with well-grouped direction from natural remanent magnetization of the granites and the dolerites. The stable remanence of the granites falls to around a northerly mean direction, of which declination is 348.5° and inclination 48.7°. On the other hand, two groupings in direction of the cleaned remanence are found for the dolerite dykes. One falls to nearly the same northerly mean direction as the granite samples, other to a southerly mean direction, of which declination is 192.4° and inclination 67.7°. Some aspect to tectonic structure of Mahe Island and a paleoposition of Seychelles before the break-up of Gondwanaland are discussed.

Introduction

Seychelles has been suggested to represent a fragment left behind during the break-up of Gondwanaland which was first reconstructed by Du Toit (1937). Some geophysical studies made over the Seychelles Bank, have been confirmed this point of view: Baker and Miller (1963), using the K-Ar method, dated the granite of the Seychelles group at 650 m.y. and pointed out that this age was comparable to that of the Mozambique Belt in the eastern part of Africa and Madagascar; Seismic refraction data by Davies and Fransis (1964) showed that the bank had crustal structure of a continental type. Paleomagnetic study previously attempted by Matthews and Reilly(1964), however, failed to obtain meaningful results from remanent magnetization of the dolerite dykes in the Seychelles group, because of their treatment without demagnetizing technique. We made a intensive paleomagnetic study of Mahe Island, Silhouette Island, and North Island in the Seychelles group, expecting that effective demagnetizing technique could give significant information about tectonic structure of Mahe Island as well as a paleoposition of Seychelles before the break-up of Gondwanaland. This is a preliminary report mainly on the results of alternating field demagnetization applied to the granites and dolerite dykes from Mahe Island. Further experiments including thermal demagnetization are now going on.

8th Prelim. Rept. Afr. Studies, Nagoya Univ., 37-46, 1983.

Geological setting

The Seychelles archiperago comprises over hundred islands, of which fourty are granitic and the remainder coralline. The granitic group occurs as scattered islands in the north-center of the Seychelles Bank which is located at the northern part of the Mascarene Plateau in the West Indian Ocean. The largest island is Mahe. Geology of Mahe has been described in detail by Baker (1963) and revised by Suwa et al. (1983). Mahe is almost entirely formed of granite and numerous dolerite dykes cut across the granitic massif. Baker (1963) distinguished two types of granites: one was referred to Mahe granite which formed the basis of the greater part of the island; another was porphyritic granite which occupied the north-western and south-western coast of the island. Suwa et al. (1983) recognize that the Mahe granite described by Baker (1963) can be further classified into three types, gneissose granite, grey granite, and pink granite. According to Suwa et al. (1983), the gneissose granite, trending to NE 20° and dipping 75° SE in its gneissosity, occurs at the northern end of Mahe, including St. Anne Island and Cerf Island; the gneissose granite is cut by the massive grey granite which occupies the major portion of Mahe; the massive pink granite occurs as minor exposure along south-western and south-eastern coast of the island. A swarm of dolerite dykes is emplaced in all of the four types of the granites. These dykes are found mainly in north-westerly-trending joints developed in the granite bodies, and almost vertical in attitude. Distribution of the four types of the granites after Suwa et al. (1983) is shown in Fig. 1.

Radiometric age

Several radiometric age determinations reveal the Mahe Island granite to be of late Precambrian age. Miller and Mudie (1961) have obtained a K-Ar age of 654±17 m.y. on biotite and considerably low values for whole rock ages ranging from 495 to 536 m.y. Applying the Rb-Sr method, Wasserburg et al.(1963) have dated the granite of Mahe at 681±34 m.y. on whole rock and at 638±25 m.y. on felspar. K-Ar age determinations on hornblende by Baker and Miller (1963) gave a low average of 554 m.y. for the Mahe Island granite, but 647±55 m.y. for granite from Praslin which is also a granitic island belonging to the Seychelles group. Baker and Miller (1963) concluded that the true age of the Mahe Island granite was about 650 m.y. They attributed the low values of the K-Ar age from the Mahe Island granite to radiogenic argon loss due to slight alteration. Yanagi et al.(1983) newly determine some Rb-Sr ages on three types of the Mahe Island granite which have been classified by Suwa et al. (1983). According to Yanagi et al. (1983), whole rock ages of the gneissose granite and the porphyritic granite are determined at 713±19 and 683±16 m.y., respectively. These ages give older values than Baker's estimation. Baker and Miller (1963) determined a late Precambrian age of 645±55 m.y. for basalt dyke at Bel Ombre bay, north-west of Mahe, using the K-Ar method. Although no radiometric age determination was made, they supposed most of the dolerite dykes of Mahe to

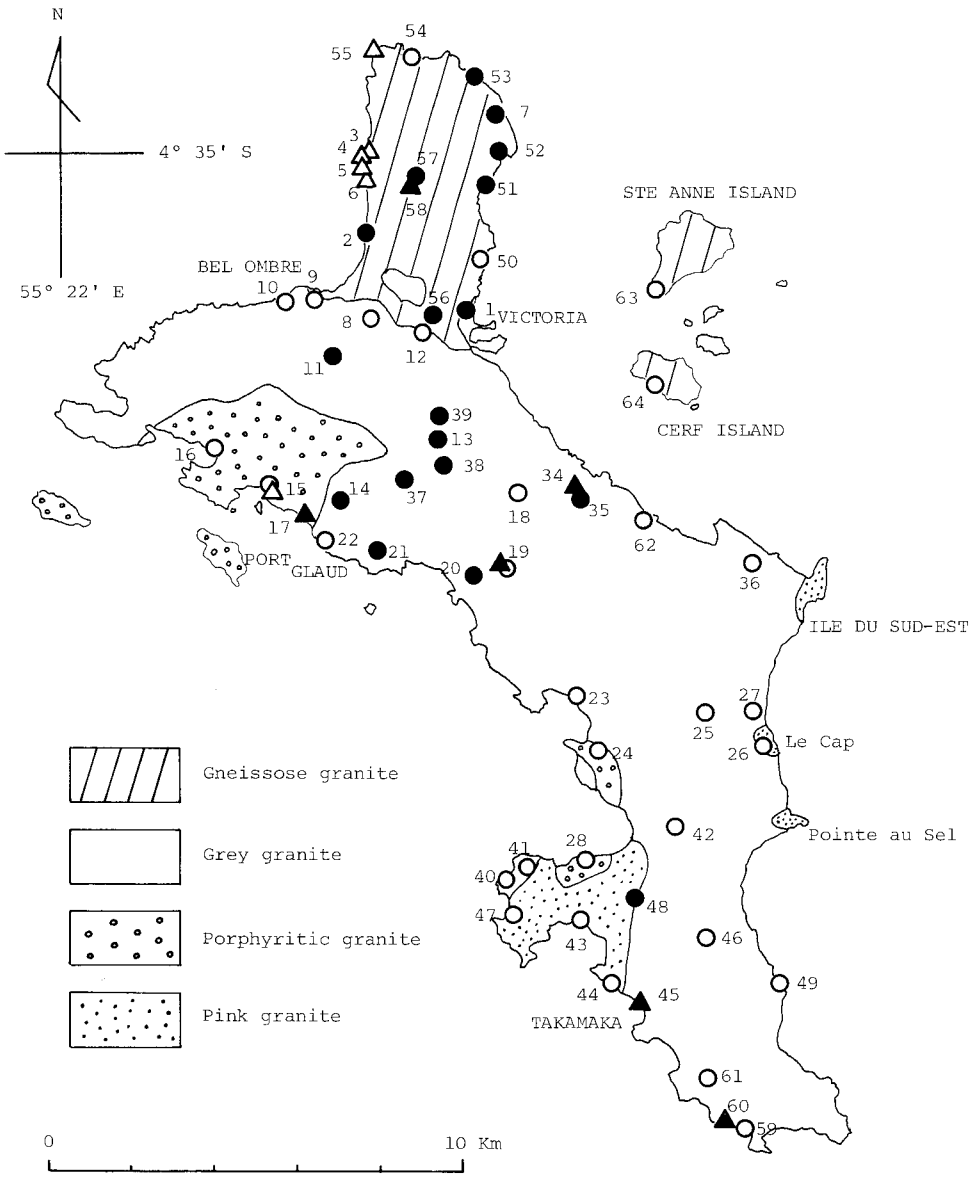

Fig. 1 Simplified geological map of Mahe Island after Suwa et al. (1983) with paleomagnetic sampling localities. Circles denote granites and triangles dolerite dykes. Solid symbols indicate sites of well-grouped samples. Open symbols indicate sites of non-grouped samples. Figures represent site numbers. Leucogranites were collected from sites 18, 36, 50 and 64.

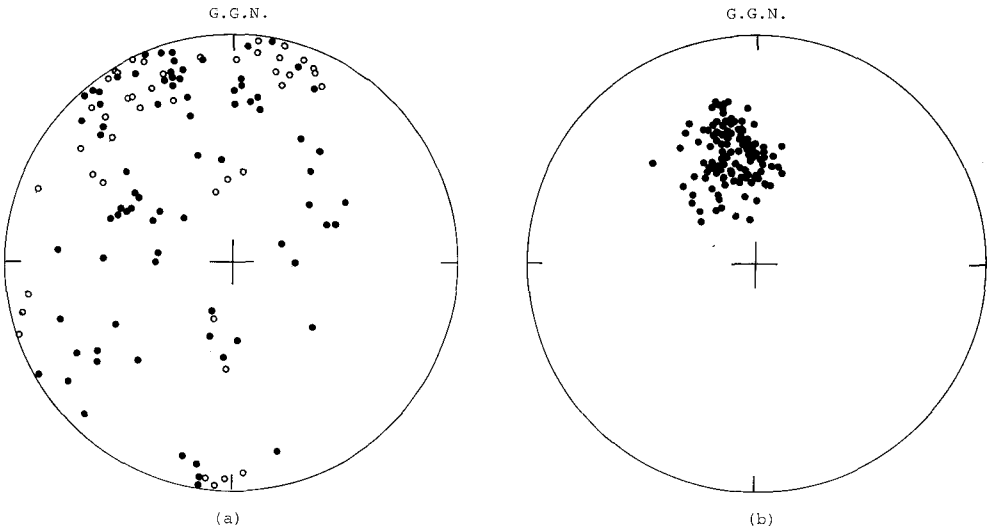

Fig. 2 Stereographic projection of NRM directions of granites from Mahe Island. (a) before cleaning. (b) after cleaning.

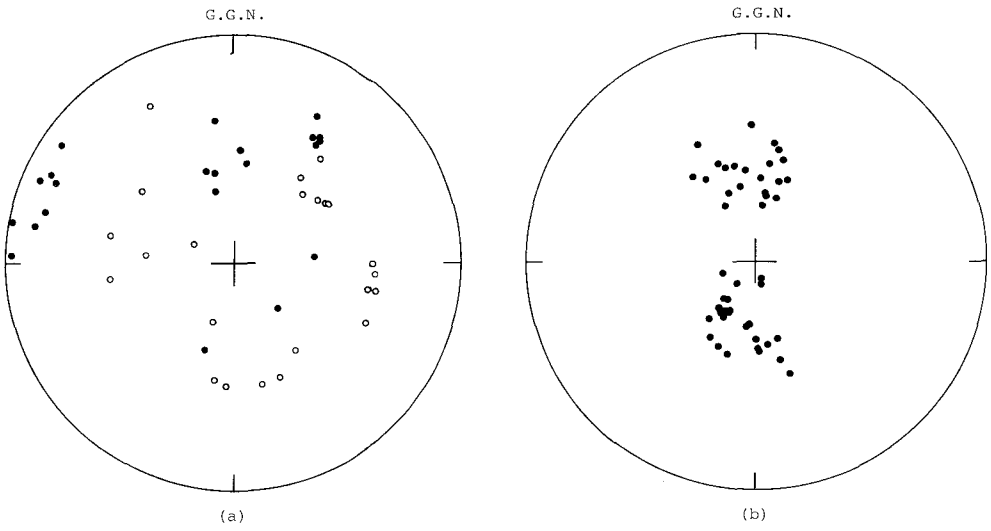

Fig. 3 Stereographic projection of NRM directions of dolerite dykes from Mahe Island. (a) before cleaning. (b) after cleaning.

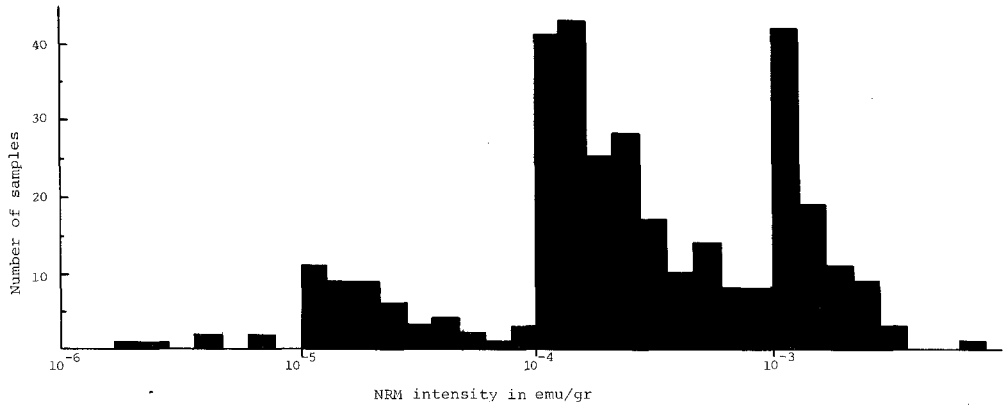

Fig. 4 Distribution of NRM intensity of granites from Mahe Island.

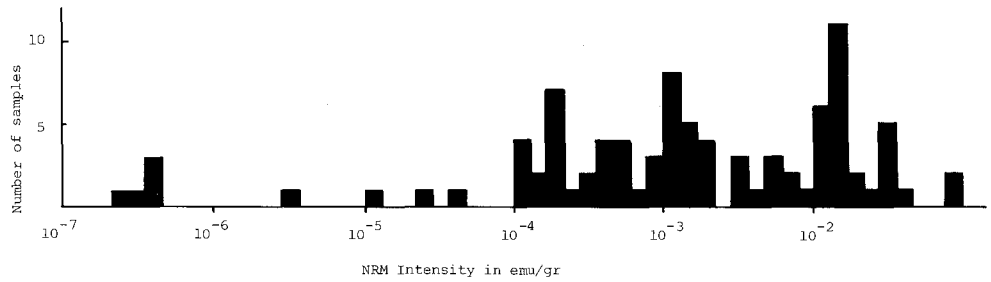

Fig. 5 Distribution of NRM intensity of dolerite dykes from Mahe Island.

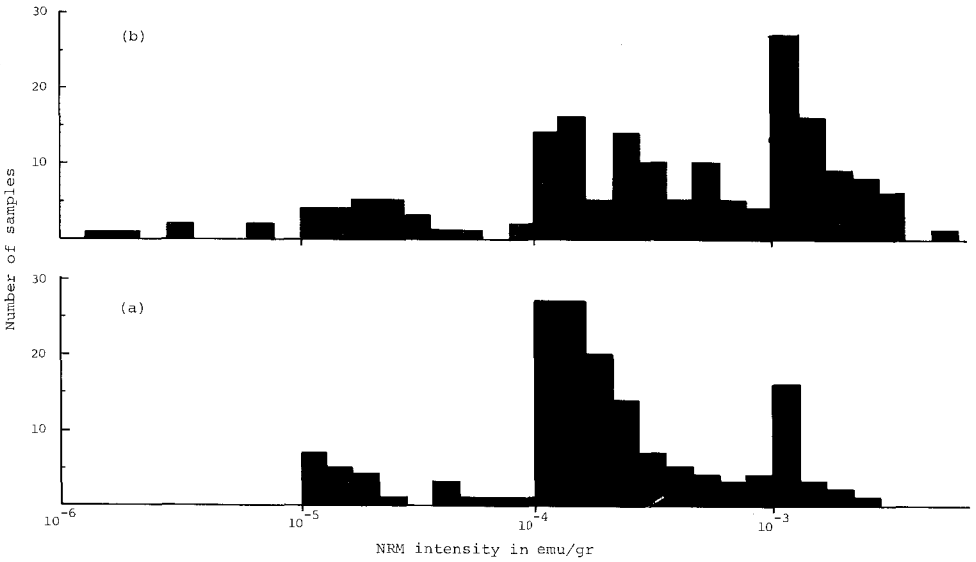

Fig. 6 Distribution of NRM intensity of granites from Mahe Island.
(a) for well-grouped samples after cleaning.
(b) for non-grouped samples after cleaning.

be of Tertiary age, based on the geological evidence that they were fresh or slightly altered.

Measurements of natural remanent magnetization (NRM)

Five hundred and ninety-four oriented hand specimens for paleomagnetic study were collected from sixty-one sites in Mahe Island. They consist of 408 granite specimens from 49 sites and 86 dolerite specimens from 12 sites. Sampling localities are shown in Fig. 1. Two or three core samples, 23 mm in diameter and 23 mm long, were drilled from each hand specimen in the laboratory. Direction and intensity of remanent magnetization of the core samples were measured in a spinner magnetometer having a noise level of 10^{-7} emu. The NRM directions of the granites and the dolerites are found to be widely scattered as shown in Figs. 2(a) and 3(a). Figs. 4 and 5 show distribution of the NRM intensity of the granites and the dolerites from Mahe Island, respectively. The NRM intensity of the dolerites is of the order between 10^{-4} and 10^{-2} emu/gr. And, most of the Mahe Island granite have strong NRM intensity, ranging from 10^{-4} to 10^{-3} emu/gr.

Alternating field (AF) demagnetization

Three to five pilot specimens from each site were subjected to the progressive AF demagnetization at 100 oersted field increments, up to the maximum peak field of 1000 oersted. The remainder were treated in the definite field which was fixed under the test demagnetization using a criterion of the minimum dispersion.

Granites

The results of the AF demagnetization reveal that the isolated stable remanence of the gneissose granite, the grey granite exposed only in the northern Mahe, and the pink granite from site 48, which is an only example from the southern part of the island, fall to around a northerly mean direction of D=348.5°, I=48.7° (N=121, k=40, α_{95}=2.0°). It is observed that the peak alternating field of 300~800 oersted is necessary for leaving the well-grouped direction, when the remanence intensity of the samples is reduced to 1/10~1/100 of the initial value. On the other hand, the remainder, the porphyritic granite, the pink granite except site 48, and the leucogranite, all show no significant improvement of grouping in remanence direction in spite of demagnetizing at 1000 oersted. The well-grouped directions after cleanig are plotted in Fig. 2(b). The distributions of the NRM intensity are again shown in Fig. 6, resolving them into two categories; one has the well-grouped remanence after AF demagnetization and another not. It is clearly seen that the well-grouped remanence is weaker than the non-grouped one.

Dolerite dykes

The cleaned remanence of the dolerite specimens from the northern part of the island (sites 17, 19, 34a, and 58), falls to around a northerly mean direction of D=355.9°, I=57.5° (N=22, k=41, α_{95}=4.9°). This is almost the same direction as the granite. On the other hand, the specimens from the southern end of Mahe (sites 45 and 65), together with those from site 34b, are found to have the stable well-grouped remanence with a southerly mean direction of D=192.4°, I=67.7° (N=24 k=39, α_{95}=4.8°). The well-clustering of the NRM direction has been reached after the AF treatment in the field of 200~1000 oersted with the associated reduction of the NRM intensity to 1/10~1/100 of the initial value. The well-grouped directions obtained from the dolerite specimens are plotted in Fig. 3(b). No sample from the north-western coast of the island (sites 3,4,5,6,15 and 55) is observed to group in remanence direction, even after the AF treatment in the field of 1000 oersted. It is of some importance to note that sites 34a, 34b and 35 represent the same place. Their relationship is that the grey granite (site 35) is cut by two closely occurring dolerite dykes; one (site 34a) trend NW 13° and dip 84° NE, another (site 34b) NW 50°, 28° SW.

Characteristic distribution of the remanence

The experiments demonstrate that the remanence of the Mahe Island granite has several marked characteristics. Some of them serve as a help to estimate what tectonic event took place in the past. The NRM directions of the granite from the northern part of the island were well-grouped after the AF demagnetization, but that from the southern part not. This fact suggests that the tectonic event, which affected the magnetic properties of the Mahe Island granite after acquisition of original thermoremanent magnetization, had the north-south directional feature. In the northern "well-grouped" region, a few examples of unstable remanence are found in the grey granite along a petrological boundary which devides the grey granite and the gneissose granite. This indicate that there is a tectonic line along the boundary extending perpendicularly to the north-south direction. The existence of the tectonic line is strongly supported by the petrological evidence that mylonites occur in the granite along the same boundary (Suwa, personal communication), because mylonites are generally caused by a dislocation metamorphism. Therefore, it seems that the tectonic event involved some mechanical force acting in the north-south direction at least in the northern part of Mahe Island. This mechanical force might be generated by a reaction of the northward movement of India during late Cretaceous and early Tertiary, which was examined in detail by Mackenzie and Scrater (1971) on the basis of the sea floor spreading model. The NRM intensity is observed to be considerably stronger than usual as a whole and distributed to be weaker in the northern "well-grouped" region than in the southern "non-grouped" region. Such a characteristic distribution of the NRM intensity can be hardly attri-

buted to iso-thermal remanent magnetization induced by a lightning, because the topography of Mahe shows higher altitude in the northern area, where the weaker NRM is observed, than in the southern area of the island, as described by Baker (1963). The characteristic distribution of the NRM intensity must have some significant meanings to solve the problem of how the tectonic event occurred in Seychelles. But, the present state of our experiments can not allow us to find it.

Interpretation of paleomagnetic mean direction

The stable remanence of the Mahe Island granite yields a paleomagnetic pole at 54.0°N, 38.2°E. Comparing paleomagnetic pole for Seychelles with that for Africa, it is possible to estimate a location of seychelles in late Precambrian Era. Fig. 7(a) shows the paleomagnetic pole obtained from the Mahe Island granite together with apparent polar wander (APW) path for Africa during the period from late Precambrian to Ordovician, which was compiled by Piper (1975). Break-up between East and West Gondwanaland was estimated to begin at 150 m.y. by geological evidence summarized by Powell et al. (1980). Then in late Precambrian, Seychelles was located somewhere along the opposing African continental margin, and the paleomagnetic pole for the Mahe Island granite agreed with that for Africa. In Fig. 7(a), this paleo-geophysical constraint leads us to the following conclusion: the geomagnetic field was in the reversed polarity when the remanence of the Mahe Island granite was acquired originally in late Precambrian Era; Seychelles came from near the north of east African coast to the present position. Piper et al. (1973) described the African south pole position at 653 and 743 m.y. to be 85°N, 228°E and 72°N, 68°E respectively. Calculation using these poles allows us to present a drift model that Seychelles first occupied near the present entrance of the Gulf of Aden, and had drifted to the present position with a counter-clockwise rotation of about 20° since continental break-up. Paleomagnetic study by Embleton and McElhinny (1975) showed that Madagascar was located off the east coast of Africa adjacent to Kenya and Tanzania before break-up of Gondwanaland. It is noted that there is a good consistensy in drifting direction between reconstruction model for Madagascar by them and that for Seychelles by us. It is interesting that Seychelles in the estimated pre-drift position provides a link between African, Arabian, and Indian plate in Gondwana reconstruction by Smith and Hallam (1970). The Mahe Island granite is peculiar in that the age is 650~700 m.y. and the NRM intensity is strong. Geological continuation of such characteristic granite is a crucial key to dermine a exact pre-drift position of Seychelles relative to Africa, Arabia, and India. As for the dolerite dykes, the northerly mean direction is consistent with that of the granite. This may imply that the dolerite with the northerly mean direction was emplaced in late Precambrian Era. though no specimen was collected from Bell Ombre where Baker and Miller (1963) obtained a K-Ar age of 645 m.y. on dolerite. Fig. 7(b) shows the paleomagnetic pole derived from the southerly mean direction of the dolerite, together with Phanerozoic APW path for Africa by McElhinny et al. (1968). This APW path

is that of the south pole. Then it is concluded that the geomagnetic field was in the reversed polarity when the remanence with the southerly mean direction was acquired. The paleomagnetic pole position of the dolerite deviates significantly from Tertiary pole position, and falls closely on upper Carboniferous pole position in APW path for Africa. But it must be remembered that Seychelles was at its pre-drift position until 150 m.y. By returning Seychelles to the estimated pre-drift position, the paleomagnetic pole position of the dolerite comes to near lower Carboniferous pole position. Accordingly, the dolerite with the southerly mean direction may be paleomagnetically of Carboniferous period.

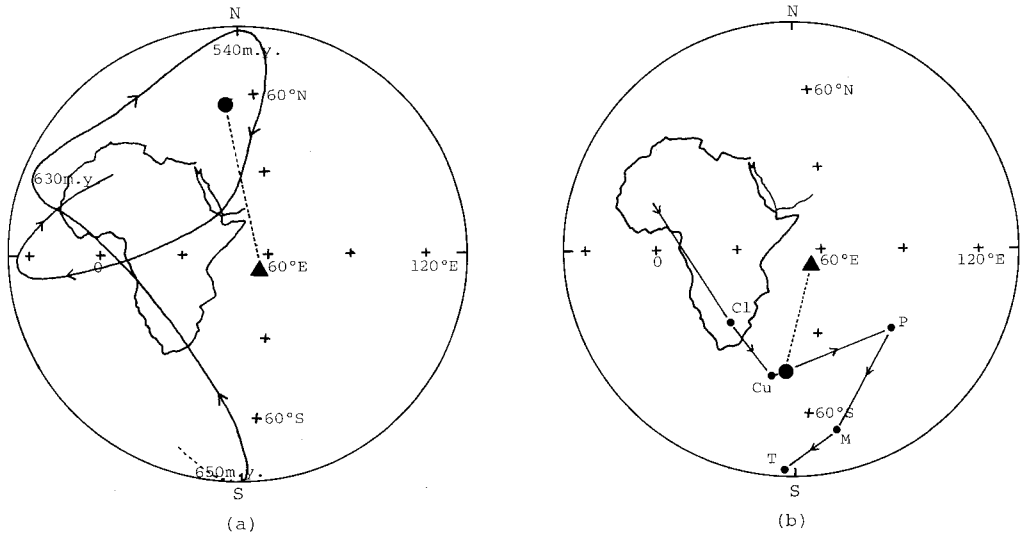

Fig. 7 Paleomagnetic pole for Mahe Island and apparent polar wander (APW) path for Africa.

(a) Paleomagnetic pole of the Mahe Island granite and APW path for Africa during the period from late Precambrian to Ordovician by Piper (1975).

(b) Paleomagnetic pole derived from southerly mean direction of the dolerite and Phanerozoic APW path for Africa by McElhinny et al. (1968).

Circle indicates paleomagnetic pole position for Mahe Island. Triangle indicates the present position of Seychelles. Cl, Cu, P, M, and T denote lower Carboniferous, upper Carboniferous, Permian, Mesozoic, and Tertiary poles.

Acknowledgements — We express our sincere thanks to Mr. P. Shilton, Secretary, National Research and Development Council, Ministry of Planning and Development, Republic of Seychelles and to Mr. G. Lionnet, Senior Education Officer, Ministry of Education and Information, Republic of Seychelles for their most esteemed and invaluable assistance.

We are very grateful to Drs. T. Yanagi and H. Umenura and Messrs. M. Asami and M. Hoshino for their laborious collaboration in the field survey in 1981.

The field work was made possible by the Grant-in-Aid for Overseas Scientific Survey from the Ministry of Education, Science and Culture, Japan, to which we express our thanks.

REFERENCES

BAKER, B.H. (1963): Geology and mineral resources of the Seychelles Archiperago. *Geol. Survey Kenya Mem.* **3**, 140pp.

BAKER, B.H. and MILLER, J.A. (1963): Geology and geochronology of the Seychelles Islands and the structure of the floor of the Arabian Sea. *Nature*, **199**, 346-348.

DAVIES, D. and FRANSIS, T.J.G. (1964): The crustal structure of the Seychelles Bank. *Deep-Sea Res.*, **11**, 921-927.

Du TOIT, A. (1937): *Our wandering continents*. Oliver and Boyd, Edinburgh, 366pp.

EMBLETON, B.J.J. and McELHINNY, M.W. (1975): The palaeoposition of Madagascar: Palaeomagnetic evidence from the Isaro group. *Earth Planet. Sci. Lett.*, **27**, 329-241.

MATTHEWS, D.H. and REILLY, T.A. (1964): Dissapointing interim palaeomagnetic results from the Seychelles. *Nature*, **203**, 1160.

McELHINNY, M.W., BRIDEN, J.C., JONES, D.L. and BROCK, A. (1968): Geological and geophysical implications of palaeomagnetic results from Africa. *Rev. Geophys.*, **6**, 201-238.

MckENZIE, D. and SCRATER, J.G. (1971): The evolution of the Indian Ocean since the Late Cretaceous. *Geophys. J. Roy. Soc.*, **25**, 437-528.

MILLER, J.A. and MUDIE, J.D. (1961): Potassium-argon age determinations on granite from the island of Mahe. *Nature*, **192**, 1174-1175.

PIPER, J.D.A., BRIDEN, J.C. and LOMAX. K. (1973): Precambrian Africa and South America as a single continent. *Nature*, **245**, 244-248.

PIPER, J.D.A. (1975): Palaeomagnetic correlations of Precambrian formations of east-central Africa and their tectonic implications. *Tectonophys.*, **26**, 135-161.

POWELL, C.M. LOHNSON, B.D. and VEEVERS, J.J. (1980): A revised fit of East and West Gondwanaland. *Tectonophys.*, **63**, 13-29.

SMITH, A.G. and HALLAM, A. (1970): The fit of the southern continents. Nature, **255**, 139-144.

SUWA, K., YANAGI, T., TOKIEDA, K., UMEMURA, H., ASAMI, M. and HOSHINO, M. (1983): Geology and Petrology of the Seychelles Islands. *8th Prelim. Rept. Afr. Studies, Nagoya Univ.*, 3-21.

WASSERBURG, G.J., CRAIG, H., MENARD, H.W., ENGEL, A.E.J. and ENGEL, C.G. (1963): Age and composition of a Bounty Island granite and age of a Seychelles Islands granite. *J. Geol.*, **71**, 785-789.

YANAGI, T., WAKIZAKA, K. and SUWA, K. (1983): Rb-Sr whole rock ages of granitic rocks from the Seychelles Islands. *8th Prelim. Rept. Afr. Studies, Nagoya Univ.*, 23-36.

Amphiboles in some granitic rocks from Mahe island and Cerf island, Seychelles

Mitsuo HOSHINO* and Kanenori SUWA**

* Laboratory of Geology, College of General Education, Nagoya University
** Department of Earth Sciences, Faculty of Science, Nagoya University

Abstract

The granitic rocks of Mahe island and Cerf island, Seychelles are composed of grey granite, pink granite, porphyritic granite, Mahe gneissose granite and Cerf island gneissose granite. Petrographical analyses indicate that the grey granite and the Cerf island gneissose granite belong to alkali-feldspar granite and others belong to granite to granodiorite.

Chemical analyses were made on the amphiboles from seven granitic rocks and one amphibolite xenolith in the Mahe gneissose granite. The amphiboles from the Mahe gneissose granite and the amphibolite xenolith are found to be Fe^{2+}-poor hornblende. The amphiboles from the porphyritic granite and the pink granite are found to be Fe^{2+}-rich hornblende and ferroedenite, respectively. The amphilboles from the grey granite and the Cerf island gneissose granite are found to be ferrorichterite rimmed with riebeckite. An aggregate of acicular riebeckites also occurs in the Cerf island gneissose granite.

Fe^{2+} and (Na + K)-enrichment was attained markedly in the ferrorichterites of the grey granite and the Cerf island gneissose granite. Riebeckite would have been stable instead of ferrorichterite at the later stage of the crystallization, due to the elevated oxygen fugacity of the rocks.

Introduction

It is well known that the late Precambrian granitic rocks widely occur in the Seychelles Islands in the southwestern Indian Ocean. According to Baker (1963), the late Precambrian rocks in the Seychelles Islands comprise Mahe granite with characteristic grey- to pink-coloured appearance, and porphyritic granite. Tertiary syenitic rocks and dolerite dykes are also found in subordinate amounts. Baker (1963) and Frankel and Kent (1964) clarified in their petrographical studies that some of the Seychelles granitic rocks exhibit alkalic nature with deep-coloured and strongly pleochroic amphiboles. However, not any detailed mineralogical and chemical study on the amphiboles in the Seychelles granitic rocks has been made so far.

In this paper some amphiboles from six kinds of Precambrian rocks of Mahe island and Cerf island are analysed optically and chemically. And the deep-coloured

8th Prelim. Rept. Afr. Studies, Nagoya Univ., 47-62, 1983.

amphiboles turned out to be ferrorichterite, ferroedenite and riebeckite. Some feldspars are also chemically analysed.

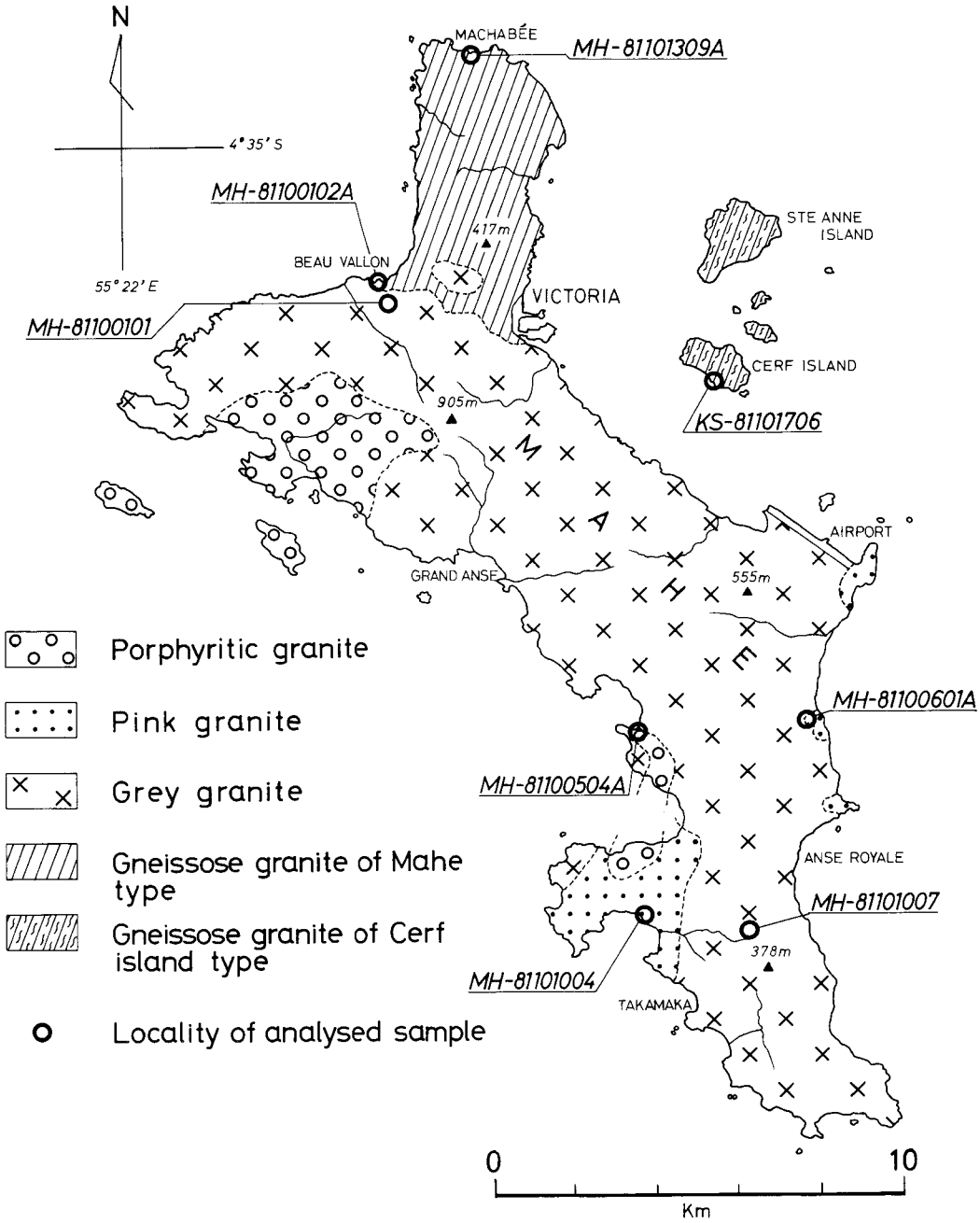

Fig. 1: Geological map of Mahe island and adjacent islets.

Geological setting of Mahe island and Cerf island

Baker's geological map of Mahe island was revised by Suwa et al. (1982) as shown in Fig. 1. In the Baker's geological map, grey granite, pink granite and gneissose granite in our geological map (Fig. 1) are treated together as Mahe granite. Among these three types of granite, petrographical differences are evident and they should be separated from each other as shown in Fig. 1.

Grey granite is massive and commonly coarse-grained. Grey- to greenish grey -colour is characteristic. Mafic xenoliths rarely occur in this rock. Major constituent minerals are microcline mesoperthite, quartz and ferrorichterite and subordinate amounts of biotite and riebeckite are also contained. Small amounts of ferro-actinolite, hedenbergite and albite occur in some grey granites.

Pink granite is massive and coarse-grained. This granite exhibits salmon-pink to brownish pink in colour. Major constituent minerals are microcline perthite to mesoperthite, quartz, albite, ferroedenite and biotite. A sizable body of the pink granite is found at the north of Takamaka and three small bodies of the pink granite are found at the eastern coast between Airport and Anse Royale.

Porphyritic granite varies in lithology and generally rich in mafic to dioritic xenolith. The common type of porphyritic granite has phenocrysts of alkali feldspar and quartz up to 1 cm in grain size and has a medium- to fine-grained groundmass composed of microcline perthite, quartz, albite, edenitic hornblende and biotite. Two bodies of the porphyritic granite are found, larger one occurs at the place between Beau Vallon and Grand Anse and smaller one occurs at the northern coast of Takamaka.

Gneissose granite exhibits diverse appearance in lithology. Predominant type found in the northern Mahe island is of medium- to coarse-grained rock with a faint gneissosity. General trend of the gneissosity is NNE. Major constituent minerals are plagioclase, quartz, microcline perthite to cryptoperthite, biotite and hornblende. Mafic to dioritic xenoliths are frequently found. Leucocratic granite sometimes invades into the gneissose granite.

On the other hand, gneissose granite found from a group of islets (Cerf island, Ste Anne island and so on) off shore of Port Victoria is markedly different in mineral association from the gneissose granite of Mahe island. The Cerf island gneissose granite is composed mainly of microline mesoperthite, quartz, ferrorichterite and riebeckite. This mineral association resembles to that of the grey granite.

The granitic basement mentioned above is intruded by a number of dolerite dykes with thickness of 0.2 m to 10 m. Dolerite dyke commonly contains plagioclese, titanaugite, hornblende, biotite and epidote.

Petrography of the analysed samples

Grey granite

a) MH-81100101: Biotite-riebeckite-ferroactinolite-ferrorichterite-quartz-microcline mesoperthite Alkali-feldspar Granite.

Allanite, apatite, zircon and iron ores are also contained as accessories. Equigranular texture with a grain size of 2 mm to 8 mm is observed. Considerable part of the rock is occupied by mesoperthite and quartz, and ferromagnesian minerals are contained only sparsely. Mesoperthite and quartz are subhedral to anhedral and the mesoperthite crystal is often surrounded with minute grains of microcline and quartz. Such minute grains are also found along the shear plane within the mesoperthite crystal. Plagioclase occurs only as exsolution lamella in the mesoperthite. Ferrorichterite is subhedral and short prismatic with a strong pleochroism. Abnormal interference colour is common. Riebeckite occurs as small flakes rimming and replacing the ferrorichterite (Plates I-A and I-B). Riebeckite exhibits a strong pleochroism and an abnormal interference colour. Ferroactinolite rarely occurs at the core of the ferrorichterite. Ferroactinolite is partly or mostly altered to carbonate minerals. Birefringence is higher and pleochroism is weaker than those of ferrorichterite. Small flakes of biotite occur around the ferrorichterite, along the grain boundary and along the shear plane.

Optical properties of the constituent minerals and chemical compositions of a mesoperthite are as follows;

Mesoperthite

Core of the host microcline = An 0.0 Ab 1.3 Or 98.7
Adjoining albite lamella = An 0.0 Ab 99.5 Or 0.5
Rim of the host microcline = An 0.0 Ab 1.2 Or 98.8
Adjoining albite lamella = An 0.0 Ab 99.7 Or 0.3

Ferrorichterite

Pleochroism- X = light greenish yellow, Y = deep bluish green
Z = deep yellowish green
$2V_X = 46°$, $c \wedge Z \fallingdotseq 13°$, $r < v$

Riebeckite

Pleochroism- X = deep blue, Y = dark blue, Z = light greenish yellow
$2V \fallingdotseq 90°$, $c \wedge X = 7°$

Ferroactinolite

Pleochroism- X = pale green, Y = greyish green, Z = bluish green
$2V_X \fallingdotseq 23°$, $c \wedge Z \fallingdotseq 0°$

Biotite

Pleochroism- X = pale brownish yellow, Y = Z = dark brown.

b) MH-81101007: Biotite-riebeckite-ferrorichterite-quartz-microcline mesoperthite Alkali-feldspar Granite.

Accessories are allanite, apatite, zircon and iron ores. This rock exhibits a similar microscopic feature to the rock (MH-81100101). Ferroactinolite is not found in this rock. Biotite aggregates are commonly found and some of them may be pseudomorphs after ferrorichterites.

Optical properties of the constituent minerals and chemical compositions of a mesoperthite are as follows;

Mesoperthite

Core of the host microcline = An 0.0 Ab 3.5 Or 96.5
Adjoining albite lamella = An 0.4 Ab 99.2 Or 0.4
Rim of the host microcline = An 0.0 Ab 2.3 Or 97.7
Adjoining albite lamella = An 0.0 Ab 99.6 Or 0.4

Ferrorichterite

Pleochroism- X = light yellowish green, Y = deep bluish green, Z = deep green
$2V_x = 44°$, $r < v$

Pleochroisms of the riebeckite and the biotite and optic axial angle of the riebeckite are identical with those in MH-81100101.

Pink granite

c) MH-81100601A: Biotite-ferroedenite-albite-quartz-microcline perthite Granite.

Accessories are allanite, apatite, sphene, zircon and iron ores. This rock exhibits an equigranular texture with a grain size less than 7 mm. Anhedral to subhedral crystals of perthite, quartz and albite occupy large volume of the rock. Albite shows lamellar twinning and weak zoning. Anorthite content in the plagioclase decreases slightly toward the rim. Ferroedenite is subhedral and short prismatic with a strong pleochroism. Poikilitic texture containing grains of feldspar and quartz is characteristic as shown in Plate II-A. Biotite flake commonly makes an intergrowth with the ferroedenite. Allanite reaches to 3 mm in grain size.

Optical properties of the constituent minerals and chemical compositions of the feldspars are as follows;

Perthite

Core of the host microcline = An 0.0 Ab 3.1 Or 96.9
Adjoining albite lamella = An 0.8 Ab 98.3 Or 0.9
Rim of the host microcline = An 0.0 Ab 3.4 Or 96.6
Adjoining albite lamella = An 1.8 Ab 97.6 Or 0.6

Albite

Core = An 8.1 Ab 90.4 Or 1.5
Rim = An 5.7 Ab 93.2 Or 1.1

Ferroedenite

Pleochroism- X = light greenish yellow, Y = yellowish green, Z = bluish green
$2V_x = 45°$ and $46°$

Biotite

Pleochroism- X = pale yellow, Y = Z = greenish brown.

d) MH-81101004: Biotite-albite-hornblende (ferroedenitic)-quartz-microcline mesoperthite Granite.

Accessories are allanite, apatite, sphene, zircon and iron ores. In the textural feature this rock is similar to MH-81100601A, but the amount of albite is small in this rock. Some mesoperthite crystals are rimmed with minute granis of microcline which can be observed also in the grey granite. Ferroedenitic hornblende exhibits strong pleochroism. Epidote is found as an alteration product.

Optical properties of the constituent minerals and chemical compositions of a mesoperthite are as follows;

Mesoperthite

Core of the host microcline = An 0.0 Ab 3.4 Or 96.6
Adjoining albite lamella = An 2.1 Ab 97.6 Or 0.3

Ferroedenitic hornblende

Pleochroism- X = light yellowish green, Y = brownish green
Z = deep bluish green

Biotite

Pleochroism- X = golden yellow, Y = Z = dark brown.

Porphyritic granite

e) MH-81100504A: Biotite-hornblende-microcline perthite-albite-quartz Porphyritic Granite.

Accessories are allanite, sphene, zircon and iron ores. Phenocrystic minerals are euhedral to subhedral microcline mesoperthite and quartz. Grain size of the phenocryst ranges from 0.5 cm to 1.0 cm. Mesoperthite phenocryst is commonly mantled with a cloudy albite. Groundmass is composed of microcline microperthite, albite, hornblende and biotite and they are less than 1.0 mm in grain size. Hornblende is subhedral and prismatic, and is strongly pleochroic. Biotite occurs as a stout crystal. Rim of the biotite is sometimes greenish. Aggregate of flaky biotite with epidote sometimes replaces the hornblende.

Optical properties of the constituent minerals and chemical compositions of the feldspars are as follows;

Mesoperthite phenocryst

Core of the host microcline = An 0.0 Ab 1.8 Or 98.2
Adjoining albite lamella = An 1.8 Ab 97.9 Or 0.3

Albite in the groundmass

Core = An 6.8 Ab 92.7 Or 0.5
Rim = An 1.4 Ab 98.3 Or 0.3

Hornblende

Pleochroism- X = light greenish yellow, Y = olive green, Z = bluish green

Biotite

Pleochroism- X = pale yellow, Y = Z = brown.

Gneissose granite

f) MH-81100102A: Hornblende-biotite-microcline microperthite-oligoclase-quartz Granodiorite

Accessories are apatite, sphene, zircon and iron ores. This rock shows an equigranular texture with a grain size of 0.5 mm to 1.5 mm. Constituent minerals are generally anhedral. Shear structure is found frequently. Oligoclase is twinned and zoned, and the core of the grain is saussuritized. Alkali feldspar occurs commonly as a microperthite and rarely as a cryptoperthite. Hornblende is long prismatic and commonly exhibits twinning. Along the shear plane minute grains of quartz, microcline and biotite recrystallize with a mosaic texture.

Optical properties of the constituent minerals and chemical compositions of the feldspars are as follows;

Oligoclase

Core = An 25.1 Ab 74.3 Or 0.6

Rim = An 18.9 Ab 80.6 Or 0.5

Cryptoperthite

Core = An 0.0 Ab 4.1 Or 95.9

Rim = An 0.0 Ab 3.4 Or 96.6

Hornblende

Pleochroism- X = light yellowish green, Y = yellowish green, Z = green

Biotite

Pleochroism- X = pale yellow, Y = Z = brownish green.

g) KS-81101706: Riebeckite-ferrorichterite-quartz-microcline mesoperthite Alkali-feldspar Granite.

Accessories are apatite, sphene, zircon, biotie and iron ores. This gneissose granite of Cerf island differs from the gneissose granite of Mahe island; i.e., the former has a feature of an alkali granite, on the other hand the latter has a feature of an ordinary granite. Following petrographical feature of this rock closely resembles to that of the grey granite. This rock shows an equigranular texture and the constituent minerals are almost anhedral with a grain size of 0.5 mm to 3.0 mm. Mesoperthite is commonly surrounded with minute grains of microcline. Ferrorichterite presents a strong pleochroism. Abnormal interference colour is also common. Riebeckite occurs as an aggregate of small flakes or as an aggregate of acicular crystals. Small flakes develop rimming the ferrorichterite (Plate II-B) and acicular crystals with a radial growth develop along the grain boundaries (Plates III-A and III-B). Riebeckite exhibits a strong pleochroism.

Table 1a: EPMA analyses of hornblende, ferroedenite, ferrorichterite and ferroactinolite in the granitic rocks and the amphibolite xenolith from Seychelles.

	1C	1R	2	3C	3R
SiO_2	45.32	48.48	49.48	46.25	46.08
TiO_2	1.11	0.16	0.11	1.37	1.39
Al_2O_3	3.87	1.51	0.54	2.81	2.66
Cr_2O_3	0.03	0.01	0.00	0.01	0.00
FeO*	32.19	33.15	34.04	34.82	34.11
MnO	1.06	0.84	1.23	1.49	1.62
MgO	1.39	1.35	0.99	0.36	0.32
CaO	8.35	7.38	8.82	7.03	7.05
Na_2O	2.75	5.15	1.79	3.10	3.33
K_2O	0.91	0.89	0.38	0.88	0.92
Total	96.99	98.92	97.36	98.12	97.49
	(O=23)	(O=23)	(O=23)	(O=23)	(O=23)
Si	7.378	7.754	7.988	7.514	7.532
Al^{IV}	0.622	0.246	0.012	0.486	0.468
Al^{VI}	0.121	0.039	0.090	0.052	0.046
Ti	0.136	0.019	0.013	0.167	0.171
Cr	0.004	0.002	0.000	0.002	0.000
Fe^{2+}	4.383	4.434	4.596	4.731	4.663
Mn	0.146	0.114	0.168	0.205	0.224
Mg	0.338	0.322	0.237	0.088	0.079
Ca	1.456	1.265	1.525	1.223	1.234
Na	0.869	1.596	0.561	0.977	1.055
K	0.190	0.183	0.078	0.183	0.193
$100Fe^{2+}/(Mg+Mn+Fe^{2+})$	90.1	91.0	91.9	94.2	93.9
Na + K	1.059	1.779	0.639	1.160	1.248

1C: Ferrorichterite in the grey granite (MH-81101007)-Core.
1R: ditto -Rim.
2 : Ferroactinolite in the grey granite (MH-81100101).
3C: Ferrorichterite in the grey granite (MH-81100101)-Core.
3R: ditto -Rim.
* : Total iron as FeO.

4C	4R	5C	5R	6C	6R
43.57	42.91	44.61	44.79	45.17	44.16
1.48	1.56	1.20	1.11	1.44	1.56
5.90	6.23	6.08	6.16	6.04	6.28
0.04	0.03	0.04	0.04	0.01	0.00
29.66	30.00	23.09	23.68	25.37	24.86
1.28	1.40	2.20	2.21	1.21	1.08
2.70	2.76	6.65	6.18	5.90	5.98
9.55	9.63	10.11	10.13	9.77	10.19
2.19	2.38	2.47	2.69	1.60	2.17
0.84	0.91	0.91	0.97	0.73	0.85
97.21	97.82	97.37	97.97	97.24	97.13
(O=23)	(O=23)	(O=23)	(O=23)	(O=23)	(O=23)
7.025	6.911	6.993	7.000	7.081	6.959
0.975	1.089	1.007	1.000	0.919	1.041
0.146	0.094	0.117	0.136	0.198	0.125
0.179	0.189	0.142	0.130	0.170	0.184
0.005	0.004	0.004	0.005	0.001	0.000
3.999	4.041	3.028	3.096	3.327	3.276
0.175	0.191	0.292	0.293	0.160	0.144
0.650	0.663	1.554	1.439	1.379	1.405
1.650	1.663	1.699	1.697	1.641	1.720
0.686	0.742	0.750	0.816	0.488	0.662
0.172	0.186	0.183	0.194	0.146	0.171
82.9	82.6	62.1	64.1	68.4	67.9
0.858	0.928	0.933	1.010	0.634	0.833

4C: Ferroedenitic hornblende in the pink granite (MH-81101004)-Core.
4R: ditto -Rim.
5C: Ferroedenite in the pink granite (MH-81100601A)-Core.
5R: ditto -Rim.
6C: Hornblende in the porphyritic granite (MH-81100504A)-Core.
6R: ditto -Rim.

Table 1b: Continued.

	7C	7R	8C	9C	9R
SiO_2	50.21	48.47	48.70	46.85	48.78
TiO_2	0.32	0.40	0.74	1.90	1.35
Al_2O_3	4.24	4.43	4.69	2.45	1.66
Cr_2O_3	0.01	0.00	0.00	0.00	0.00
FeO*	14.38	15.73	16.70	30.86	31.39
MnO	1.54	1.64	1.24	0.78	0.68
MgO	13.47	13.82	11.98	2.10	2.08
CaO	11.72	11.47	11.37	6.18	4.92
Na_2O	0.74	0.91	1.23	4.04	4.49
K_2O	0.38	0.52	0.67	1.22	1.09
Total	97.00	97.39	97.32	96.39	96.43
	(O=23)	(O=23)	(O=23)	(O=23)	(O=23)
Si	7.435	7.238	7.298	7.598	7.859
Al^{IV}	0.565	0.762	0.702	0.402	0.141
Al^{VI}	0.175	0.018	0.127	0.066	0.175
Ti	0.036	0.045	0.084	0.232	0.163
Cr	0.001	0.000	0.000	0.000	0.000
Fe^{2+}	1.781	1.964	2.093	4.186	4.229
Mn	0.193	0.208	0.157	0.108	0.093
Mg	2.972	3.075	2.675	0.507	0.500
Ca	1.860	1.835	1.825	1.075	0.849
Na	0.214	0.264	0.357	1.271	1.402
K	0.073	0.099	0.128	0.253	0.224
$100Fe^{2+}/(Mg+Mn+Fe^{2+})$	36.0	37.4	42.5	87.2	87.7
Na + K	0.287	0.363	0.485	1.524	1.626

7C: Hornblende in the Mahe gneissose granite (MH-81100102A)-Core.

7R: ditto -Rim.

8C: Hornblende in the amphibolite xenolith (MH-81101309A)-Core.

9C: Ferrorichterite in the Cerf island gneissose granite (KS-81101706)-Core.

9R: ditto -Rim.

* : Total iron as FeO.

Table 2: EPMA analyses of riebeckite in the granitic rocks from Seychelles.

	1	2
SiO_2	51.49	51.46
TiO_2	0.00	0.04
Al_2O_3	0.13	0.77
Cr_2O_3	0.00	0.03
Fe_2O_3*	14.67	9.64
FeO	22.94	26.40
MnO	0.89	0.18
MgO	0.54	0.77
CaO	0.85	0.02
Na_2O	6.03	6.81
K_2O	0.02	0.15
Total	97.69	96.26
	(O=23)	(O=23)
Si	8.034	8.143
Al^{VI}	0.024	0.143
Ti	0.000	0.005
Cr	0.001	0.004
Fe^{3+}	1.727	1.148
Fe^{2+}	3.003	3.494
Mn	0.118	0.024
Mg	0.127	0.181
Ca	0.142	0.005
Na	1.825	2.090
K	0.004	0.029
$100Fe^{2+}/(Fe^{2+}+Mg+Mn)$	92.5	94.5
$100Fe^{3+}/Fe^{3+}+Al^{VI}+Ti+Cr)$	98.6	88.3

1: Riebeckite in the grey granite (MH-81100101).

2: Riebeckite in the Cerf island gneissose granite (KS-81101706).

*: Fe_2O_3 content is roughly estimated so as to be $(Al^{VI}+Ti+Cr+Fe^{3+}+Fe^{2+}+Mn+Mg) = 5$ per formula unit on the basis of 23 oxygens.

Optical properties of the constituent minerals and chemical compositions of a mesoperthite are as follows;

Mesoperthite

(Rim of the host microcline = An 0.0 Ab 2.3 Or 97.7
\ Adjoining albite lamella = An 0.0 Ab 99.6 Or 0.4

Ferrorichterite

Pleochroism- X = light brownish yellow, Y = dark brownish yellow
Z = deep brownish green

$2V_X$ = 46° and 56°, $c \wedge Z \div 10°$, $r < v$

Riebeckite

Pleochroism- X = deep violet blue, Y = dark blue, Z = light greenish yellow

$2V_X \div 76°$

Biotite

Pleochroism- X = light brownish yellow, Y = Z = reddish brown.

Mafic xenolith in the Mahe gneissose granite

h) MH-81101309A: Biotite-hornblende-quartz-oligoclase Amphibolite.

Accessories are microcline, apatite, sphene, zircon and iron ores. This xenolith occurs in a rounded shape in the Mahe gneissose granite and the diameter is 30 cm. The boundary between this xenolith and the host rock is obscure due to gradual change in their mineral composition. This rock has an equigranular texture with a grain size less than 1.0 mm. Oligoclase is subhedral to anhedral and exhibits lamellar twinning. Subhedral long prismatic to anhedral granular hornblende commonly exhibits twinning. Microcline cryptoperthite is only trace in amount. Epidote also occurs as an alteration product.

Optical properties of the constituent minerals and chemical compositions of an oligoclase are as follows;

Oligoclase

Core = An 23.4 Ab 76.1 Or 0.5
Rim = An 8.7 Ab 90.9 Or 0.4

Hornblende

Pleochroism- X = greenish yellow, Y = yellowish green, Z = green

Biotite

Pleochroism- X = pale yellow, Y = Z = deep brownish green.

Chemistry of the amphiboles

Chemical analyses were made on various kinds of amphibole by means of Hitachi X-560 microanalyzer. Chemical compositions of calciferous and subcalciferous amphiboles are listed in Tables la and lb. For large amphibole crystals, chemical compositions are given on two analytical points, core and rim. Chemical composi-

tions of calciferous and subcalciferous amphiboles are plotted on (Na + K) vs. Al^{IV} diagram (Fig. 2).

Amphibole of each rock type has a unique compositional range. In the Mahe gneissose granite and the amphibolite xenolith, amphiboles are found to be hornblende. In the porphyritic granite, amphibole is of hornblende with edenitic rim. In the pink granite, amphibole is of ferroedenite to ferroedenitic hornblende. In the Mahe gneissose granite, porphyritic granite and pink granite, compositional zonings of their amphiboles are found, i.e., both (Na + K) atom and Al^{IV} atom increase toward the rim.

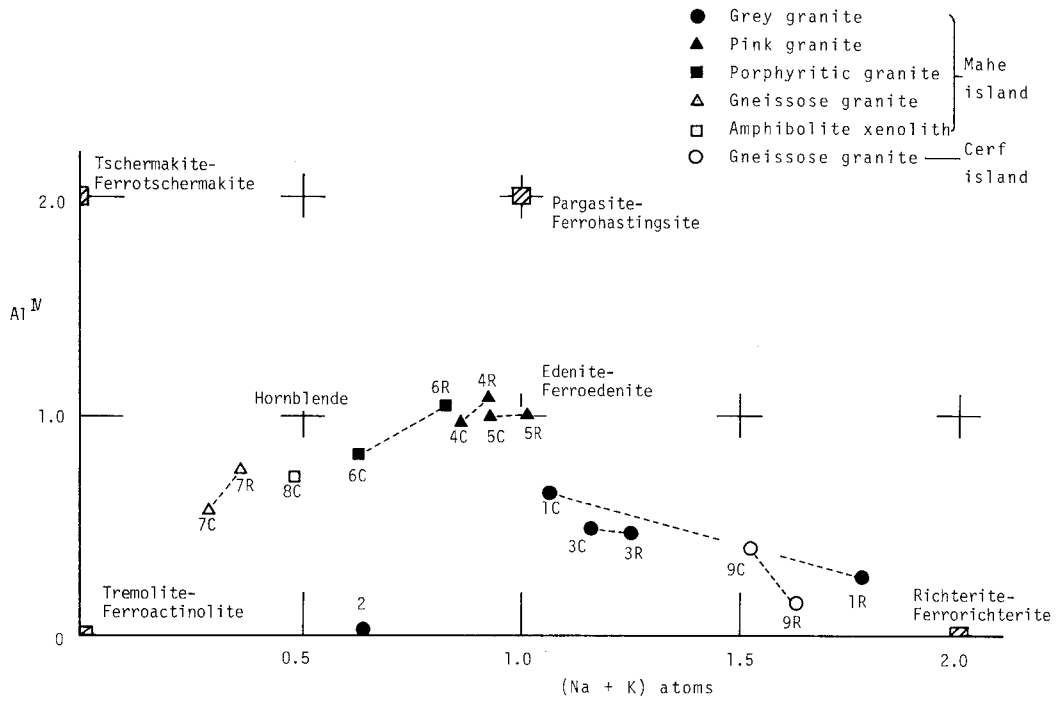

Fig. 2: (Na + K) atom and Al^{IV} atom per formula unit of calciferous and subcalciferous amphiboles.

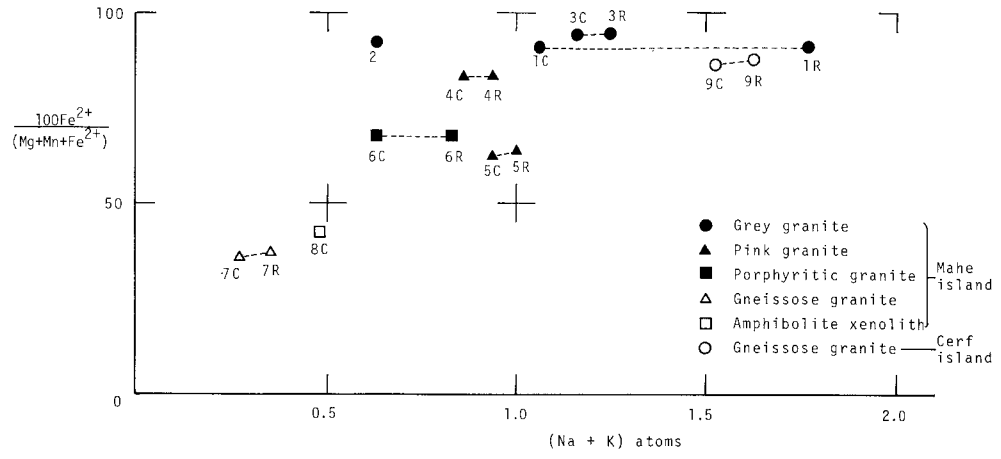

Fig. 3: (Na + K) atom per formula unit and $100Fe^{2+}/(Mg + Mn + Fe^{2+})$ atomic percentage of calciferous and subcalciferous amphiboles.

Amphiboles with compositions of Si > 7.25, (Ca + Na + K) > 2.50, Ca < 1.50 and Na > 1.00 are designated as richterite-ferrorichterite (Leake, 1968). According to this designation, amphiboles in the grey granite and in the Cerf island gneissose granite belong to ferrorichterite. Strictly speaking, the core compositions (Analyses 1C and 3C of Table la) cannot be defined as ferrorichterite, but are almost close to the above compositional limits. Ferrorichterite in both grey granite and Cerf island gneissose granite has such compositional zoning that (Na + K) atom increases and Al^{IV} atom decreases toward the rim. Marked compositional zoning can be detected in the amphibole of the grey granite, MH-81101007 (Points 1C and 1R of Fig. 2 and Analyses 1C and 1R of Table la). Light-coloured amphibole with a weak pleochroism, which rarely occurs at the core of ferrorichterite in the grey granite, MH-81100101, is found to be Al^{IV}-poor ferroactinolite (Point 2 of Fig. 2). In the alkali igneous rocks from Greenland, Na-poor ferromagnesian minerals are rimmed with Na-rich amphiboles, katophorite and arfvedsonite, at the later stage of the crystallization (Larsen, 1976).

Calciferous and subcalciferous amphiboles are plotted on (Na + K) vs. 100 Fe^{2+}/(Mg + Mn + Fe^{2+}) diagram (Fig. 3). Generally, Fe^{2+} content tends to increase with increasing the (Na + K) content in the amphibole, but Fe^{2+} content is nearly constant within each grain. It is possible in chemical composition to divide them into two groups, one is Fe^{2+}-poor and (Na + K)-poor amphibole in the Mahe gneissose granite and the amphibolite xenolith, and the other is Fe^{2+}-rich and (Na + K)-rich amphibole in the porphyritic granite, pink granite, grey granite and the Cerf island gneissose granite. Fe^{2+}-enrichment in the amphiboles of grey granite and the Cerf island gneissose granite is striking.

Two analyses of riebeckite are given in Table 2. Fe^{3+} content is roughly estimated by recalculating the sum of cations in the Y-position of the amphibole structure (Deer et al., 1963) equals to 5. Riebeckite in the grey granite (MH-81100101) is slightly higher in Mn and Ca contents and slightly lower in Al and Na contents than that in the Cerf island gneissose granite (KS-81101706). Both riebeckites are high in Fe^{2+}/(Fe^{2+} + Mg + Mn) atomic ratio.

Discussion

Petrographical and mineralogical features of the Seychelles granitic rocks can be summarized as follows.

1) The Mahe gneissose granite belongs to granodiorite with two feldspars, alkali-feldspar and oligoclase, and Fe^{2+}-poor hornblende. An amphibolite xenolith in the Mahe gneissose granite also contains Fe^{2+}-poor hornblende.

2) The porphyritic granite has two feldspars, alkali-feldspar and albite, and Fe^{2+}-rich hornblende. The rim of the hornblende is edenitic.

3) The pink granite contains two feldspars, alkali-feldspar and albite, and ferroedenite.

4) The grey granite and the Cerf island gneissose granite belong to alkali-feldspar

granite with one feldspar and ferrorichterite rimmed with riebeckite. Some grey granites contain ferroactinolite and hedenbergite which are considered to be the ferromagnesian minerals crystallized at the early stage.

Fe^{2+} content of the amphibole increases in the order of the above 1) → 2) → 3) → 4) and the most Fe^{2+}-rich amphibole is found to be a ferrorichterite ($100Fe^{2+}/(Mg + Mn + Fe^{2+}) = 94$ atomic %) in the grey granite. Alkali-enrichment at the later stage of the amphibole crystallization is attained in all types of rock. Especially a ferrorichterite in the grey granite contains 1.8 atoms of (Na + K) at the rim, which is nearly twice as high as that of the core (1.1 atoms of (Na + K)).

Stability of the richterite-ferrorichterite is studied in detail by Charles (1977). A few ferrorichterites are reported to occur from Al-poor alkali igneous rocks with a peculiar bulk composition of metasilicate normative. Oxygen fugacity (fo_2) is also an important factor controlling the stability of ferrorichterite. Ferrorichterite is stable only under very low fo_2 condition. If fo_2 is elevated by a certain episode, riebeckite will be stable instead of ferrorichterite.

Charles' above observation is enough to interpret the genesis of the Seychelles riebeckite-ferrorichterite rocks. Bulk chemical compositions of the grey granite and the Cerf island gneissose granite in Seychelles would be appropriate for crystallization of ferrorichterite. At the later stage of crystallization, oxygen fugacity of the rock would have been elevated to form the riebeckite, which is now observed as a mantle of the ferrorichterite and as an aggregate of acicular crystals. There is a possibility that the episode which has elevated the oxygen fugacity of the rock may be the shearing movement. But the tectonic setting of the Seychelles Islands including the shearing movement is not yet clear.

Acknowledgements – Mr. P. Shilton of the Ministry of Planning and Development, Seychelles and Mr. G. Lionnet of the Ministry of Education and Information, Seychelles kindly afford every facility for our field survey, to whom we would like to express our sincere thanks.

Our thanks are also due to Dr. T. Yanagi, Mr. K. Tokieda, Dr. H. Umemura and Mr. M. Asami for their laborious collaboration in the field survey.

The field work was made possible by the Grant-in-Aid for Overseas Scientific Survey from the Ministry of Education, Science and Culture, Japan, to which we express our thanks.

REFERENCES

Baker, B.H. (1963): Geology and mineral resources of the Seychelles archipelago. *Mem. Geol. Soc. Kenya,* **3**.

Charles, R.W. (1977): The phase equilibria of intermediate compositions on the pseudobinary $Na_2CaMg_5Si_8O_{22}(OH)_2$-$Na_2CaFe_5Si_8O_{22}(OH)_2$. *Am. J. Sci.,* **277**, 594-625.

Deer, W.A., Howie, R.A. and Zussman, J. (1962): *Rock-forming minerals*, **2**, 333-351, Longmans.

Frankel, J.J. and Kent, L.E. (1964): On rocks from the Seychelles islands. *22nd Inter. Geol. Congress,* Sec. **10**, 161-190.

Larsen, L.M. (1976): Clinopyroxenes and coexisting mafic minerals from the alkaline Ilimaussaq intrusion, south Greenland. *J. Petrology,* **17**, 258-290.

Leake, B.E. (1968) Catalogue of analysed calciferous and subcalciferous amphiboles together with their nomenclature and associated minerals. *Geol. Soc. Am. Spec. Paper,* **98**.

Suwa, K., Yanagi, T., Tokieda, K., Umemura, H., Asami, M. and Hoshino, M. (1982): Earth scientific studies of the Seychelles Islands, An introduction. *89th Annual Meet. Geol. Soc. Japan, Abst. Program*, 415 (in Japanese).

PLATE I

Microphotographs of the amphiboles from Seychelles.

A: Ferrorichterite rimmed with reibeckite (dark-coloured) in the grey granite (MH-81100101). One nicol.

B: Riebeckite (centre, dark-colured and light-coloured) replacing ferrorichterites (grey) along the grain boundary between ferrorichterites in the grey granite (MH-81100101). One nicol.

PLATE I

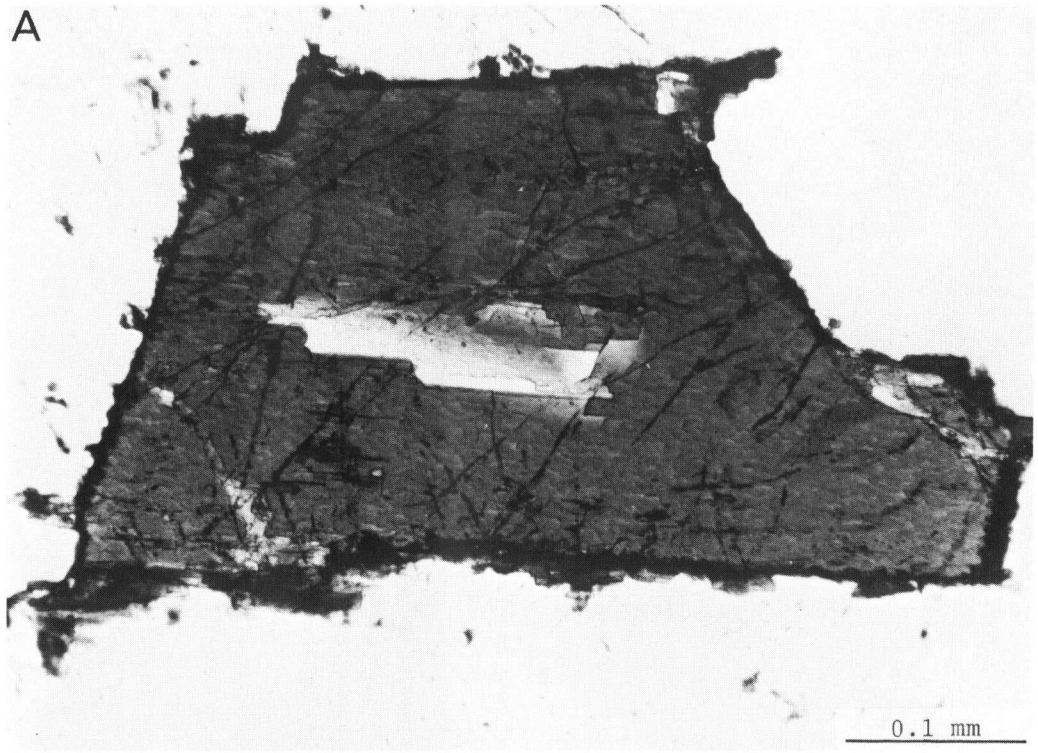

PLATE II

Microphotographs of the amphiboles from Seychelles.

A: Ferroedenite in the pink granite (MH-81100601A). One nicol.

B: Ferrorichterite partly rimmed with riebeckite (upper, dark-coloured) in the Cerf island gneissose granite (KS-81101706). One nicol.

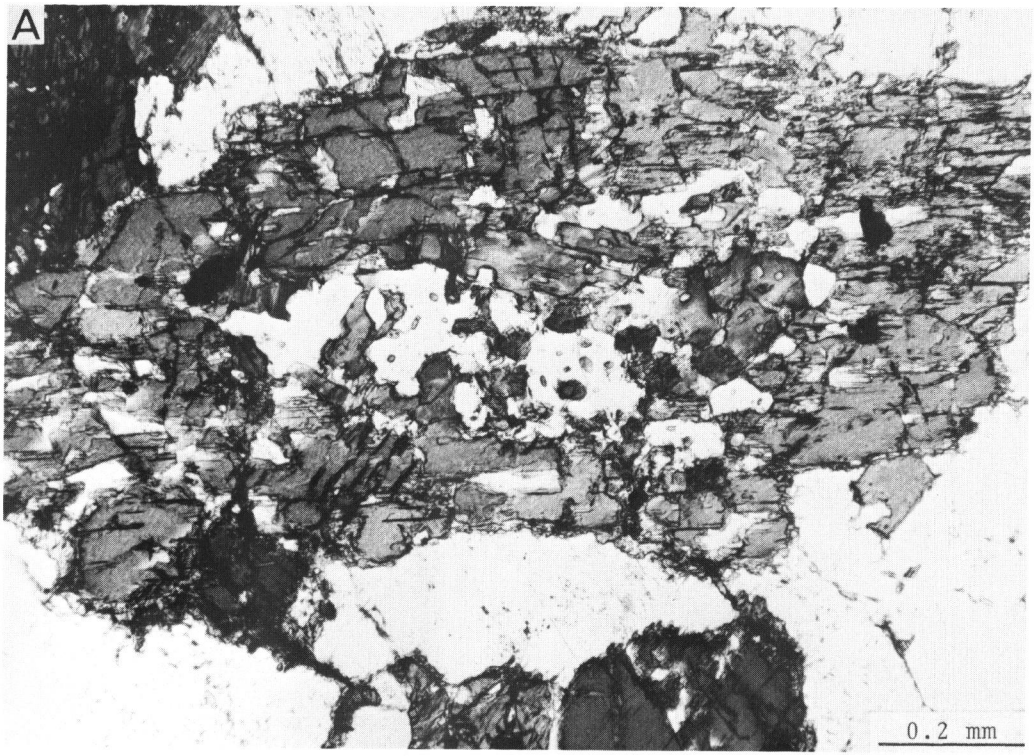
A
0.2 mm

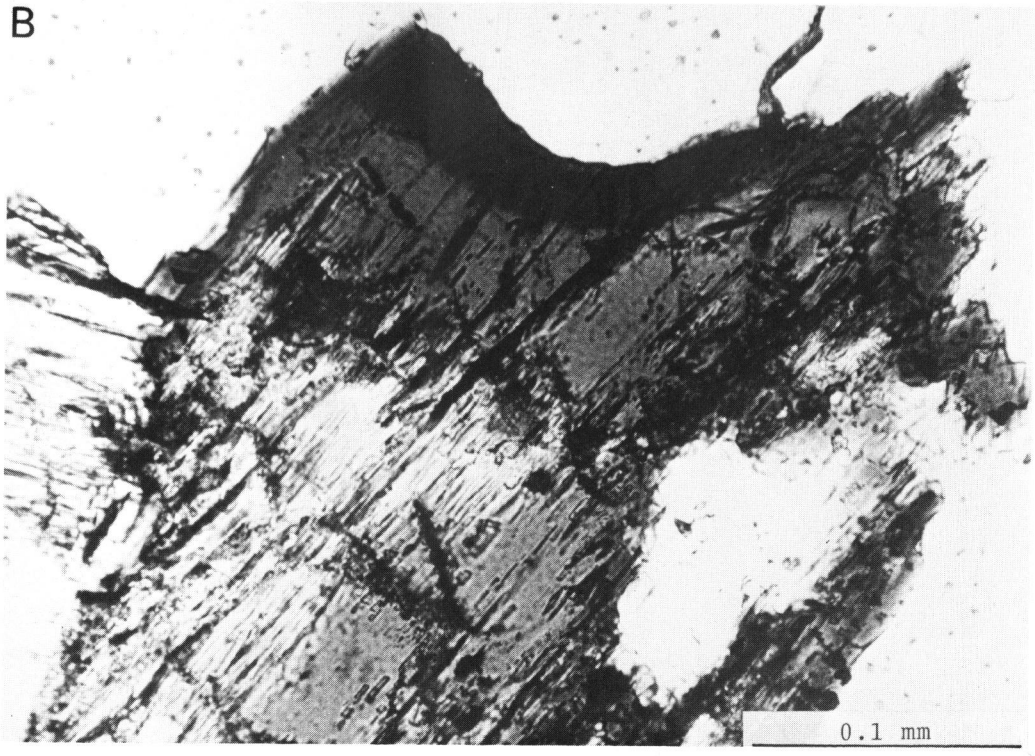
B
0.1 mm

PLATE III

Microphotographs of the amphiboles from Seychelles.

A: A radial aggregate of acicular riebeckites in the Cerf island gneissose granite (KS-81101706). One nicol.

B: An aggregate of acicular riebeckites along the grain boundary between mesoperthite and quartz in the Cerf island gneissose granite (KS-81101706). One nicol.

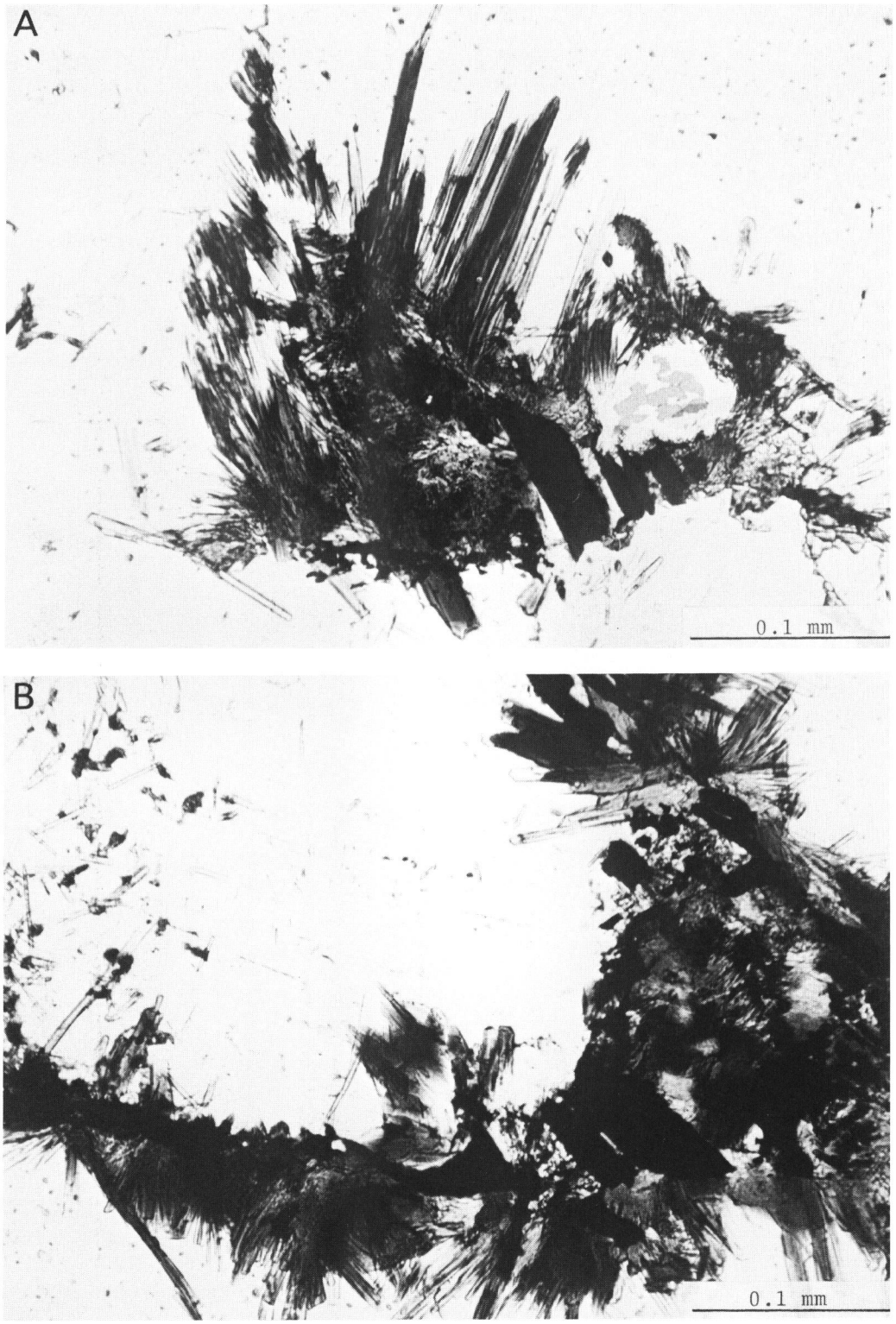
A
0.1 mm
B
0.1 mm

PLATE IV

A: Microphotograph of ferrorichterite (left) and riebeckite (centre, dark-coloured rim and acicular crystals) in the Cerf island gneissose granite (KS-81101706). One nicol.

B: Electron figure of the squared portion of the above.

C: Na-Kα X-ray image.

D: Ca-Kα X-ray image.

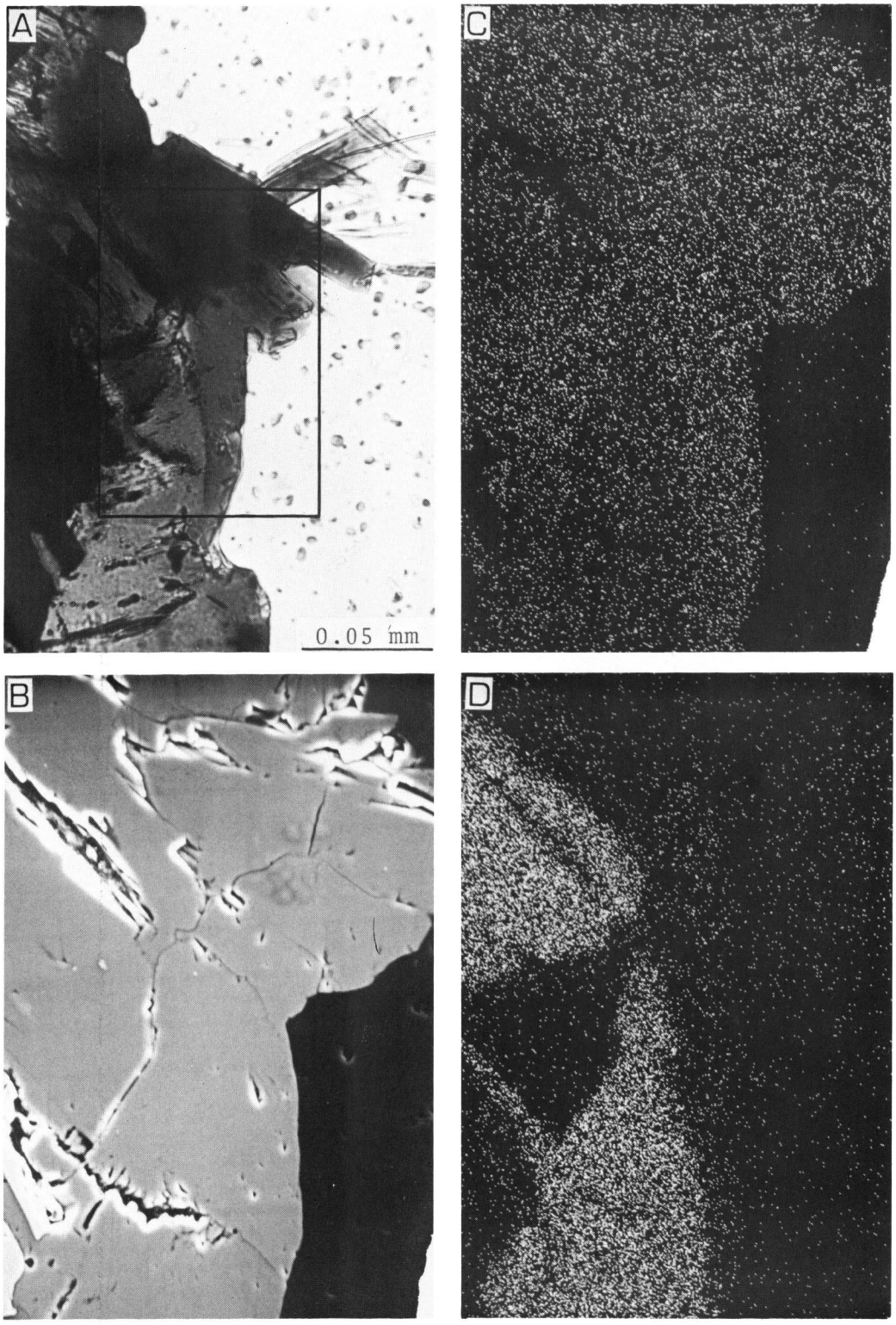
A
0.05 mm
C
B
D

Opaque minerals from the Seychelles granitic rocks

Takashi AGATA* and Kanenori SUWA**

* Faculty of Economics, Nagoya Economics University
** Department of Earth Sciences, Faculty of Science, Nagoya University

Abstract

An appreciable amount of opaque minerals occurs in Precambrian granitic rocks in Seychelles. The opaque minerals include magnetite, ilmenite intergrown with magnetite, and ilmenite occurring in discrete grains, and they were analyzed with an EPMA. Ilmenite is often manganoan and contains up to 32 wt. % MnO. The MnO content in ilmenite generally increases with the differentiation index of host granitic rocks rising, and the relations between the MnO content in ilmenite and the differentiation index indicates that there are at least three granitic rock series in Seychelles: (1) tonalite-gneissose granodiorite-leucogranite series, (2) gneissose granite-gray granite series, and (3) pink granite series. Ilmenite in the tonalite-gneissose granodiorite-leucogranite series is highly concentrated in MnO relatively to the differentiation index, while the gneissose granite-gray granite series is characterized by the low content of MnO in ilmenite; and the pink granite series contains ilmenite of an intermediate composition. The Fe^{2+} -Mn distribution coefficient ilmenite/magma ($=(Mn/Fe^{2+})_{ilmenite}/(Mn/Fe^{2+})_{magma}$) also appears to change correspondingly with these three rock series: 1.8-3.0 for the gneissose granite-gray granite series, 4.0-4.1 for the pink granite series, and 6.0-12.6 for the tonalite-gneissose granite-leucogranite series.

Introduction

Precambrian granitic rocks are developed in Seychelles, oceanic islands in the Indian Ocean and they contain an appreciable amount of opaque minerals. The opaque minerals are predominantly Fe-Ti oxides and subordinately sulfides. Recently, many petrologists have investigated Fe-Ti oxide minerals in igneous rocks and manganoan ilmenite or pyrophanite has been reported in some granitic rocks and pegmatites (e.g., Neumann and Bergstrøl, 1964; Tsusue, 1973; Elsdon, 1975). We found some ilmenite from Seychelles to be highly concentrated in MnO and the MnO content in ilmenite to vary strongly with the types of host granitic rocks. This study presents the description and chemistry of opaque minerals and discusses some of the genetical relations between the Seychelles granitic rocks.

The geological map of the Mahe and its adjacent islands, Seychelles, is shown in the previous paper of this report (Suwa et al., 1983, Fig. 1). On the basis of field appearance, granitic rocks in the Mahe island are classified into following five types

8th Prelim. Rept. Afr. Studies, Nagoya Univ., 63-74, 1983.

(Baker, 1963; Suwa et al., 1983): (1) gneissose granodiorite, (2) leucogranite, (3) gray granite, (4) pink granite, and (5) porphyritic granite. Tonalite additionally occurs as angular xenoliths in gneissose granodiorite. Leucogranite clearly cuts gneissose granodiorite in the field but is found only in association with gneissose granodiorite. Yanagi et al. (1983) have reported Rb-Sr isochron ages of 713 ± 18 Ma for gneissose granodiorite and 683 ± 16 Ma for porphyritic granite. Gneissose granite, probably Precambrian, also occurs in the Cerf island and it has the field appearance similar to that of gneissose granodiorite in the Mahe island. The representative chemical analyses of granitic rocks from Seychelles are given in Table 1. The differentiation index (normative Q + Or + Ab + Ne + Lc + Ks) of granitic rocks ranges from 71.2 to 96.7.

Description of opaque minerals

Opaque minerals from granitic rocks are essentially magnetite and ilmenite. Hematite, pyrite, chalcopyrite and pyrrhotite also occur but in most cases they are secondary hydrothermal or supergene products. The content of opaque minerals in granitic rocks from the Mahe island generally ranges from 0.4 to 1.6% by volume but some gray granite does not attain 0.2% in content of opaque minerals. Opaque minerals in the Cerf gneissose granite comprise 0.1 to 0.2 vol. % of the rocks.

Magnetite is observed in nearly all the granitic rock specimens but some of the Cerf gneissose granite does not contain magnetite. Magnetite is usually anhedral and measures about 1.0 mm in size. Magnetite grains are generally disseminated in the host rocks and are often associated with ferro-magnesian silicate minerals such as biotite and amphiboles. Magnetite is ubiquitously intergrown with ilmenite and the intergrowth mostly is granular: magnetite and ilmenite form granular aggregates. The ratio of ilmenite to magnetite in the granular intergrowth is generally close to 1 : 1 by volume, and the intergrown ilmenite rarely contains minute inclusions of hematite. Intergrown ilmenite sometimes forms thick lamellae parallel to (1 1 1) planes of host magnetite and trellis intergrowths are rarely observed.

Ilmenite is a ubiquitous mineral in the Seychelles granitic rocks. It is not only intergrown with magnetite but also occurs in discrete grains. Discrete ilmenite generally exhibits a subhedral to peri-euhedral crystal and measures about 1.0 mm in size. Relatively anhedral ilmenit is sometimes observed in the Cerf gneissose granite but it shows relatively angular outlines against ferro-magnesian silicate minerals. Euhedral ilmenite also occurs as minute inclusions in some silicate minerals but usually is very sparse. Some discrete ilmenite in leucogranite contains minute exsolved inclusions of hematite but exsolved hematite inclusions are generally rare in Seychelles. Most ilmenite specimens are, more or less, replaced by secondary sphene or rutile.

A small amount of secondary hematite occurs in most specimens and it usually replaces magnetite. Sulfide minerals including pyrite, chalcopyrite and pyrrhotite form veinlets in granitic rocks and replace igneous minerals.

Table 1. Representative chemical analyses of the Seychelles granitic rocks (analyst: R. Sugisaki)

	1	2	3	4	5	6	7
	Tonalite	Porphyritic granite	Gneissose granodiorite	Gneissose granite	Gray granite	Pink granite	Leuco-granite
Sample No.	KS-81101409	KS-81100202	KS-81101408	KS-81101706	KS-81100102	KS-81100604	KS-81101406
SiO_2	63.86	72.36	73.17	76.30	75.43	73.54	77.20
Al_2O_3	16.32	13.58	13.95	11.49	12.13	13.16	12.20
Fe_2O_3	2.01	0.93	0.89	0.84	0.60	1.30	0.93
FeO	2.58	1.61	1.19	0.98	1.67	1.21	0.78
MgO	1.67	0.55	0.44	0.16	0.17	0.41	0.15
CaO	4.89	1.61	1.75	0.32	0.48	0.88	0.26
Na_2O	5.53	4.71	4.48	4.20	4.60	4.72	4.92
K_2O	1.93	3.48	3.66	4.79	4.06	4.93	3.53
H_2O^+	0.18	0.31	0.74	0.19	0.27	0.18	0.19
H_2O^-	0.11	0.14	0.14	0.31	0.23	0.11	0.16
TiO_2	0.73	0.36	0.29	0.22	0.22	0.36	0.20
P_2O_5	0.28	0.08	0.07	0.02	0.02	0.09	0.02
MnO	0.16	0.08	0.06	0.02	0.09	0.10	0.06
Total	100.25	99.80	100.83	99.84	99.97	100.99	100.60
				Norms			
Q	12.96	27.20	28.64	33.14	31.22	25.42	34.22
Or	11.41	20.57	21.63	28.31	23.99	29.14	20.86
Ab	46.80	39.86	37.91	32.43	38.93	39.94	41.63
An	14.01	5.64	7.15	0.00	0.46	0.16	0.78
Ns	0.00	0.00	0.00	0.08	0.00	0.00	0.00
Ac	0.00	0.00	0.00	2.43	0.00	0.00	0.00
Wo	3.52	0.77	0.44	0.61	0.74	1.50	0.17
En	4.16	1.37	1.10	0.40	0.42	1.02	0.38
Fs	2.16	1.73	1.08	1.47	2.37	0.73	0.45
Mt	2.91	1.35	1.29	0.00	0.87	1.88	1.35
Il	1.39	0.68	0.55	0.42	0.42	0.68	0.38
Ap	0.65	0.18	0.17	0.04	0.06	0.21	0.04
H_2O	0.29	0.45	0.88	0.50	0.50	0.29	0.35
Total	100.26	99.80	100.84	99.83	99.98	100.97	100.61
DI	71.17	87.63	88.18	93.88	94.14	94.50	96.71

Chemistry of opaque minerals

Magnetite and ilmenite from the Seychelles granitic rocks were analyzed with EPMA (electron probe X-ray micro-analyzer) and their representative chemical compositions are given in Tables 2 and 3. Localities of analyzed specimens are shown in Fig. 1. Ferric iron was calculated assuming R_2O_3 stoichiometry for ilmenite and R_3O_4 stoichiometry for magnetite.

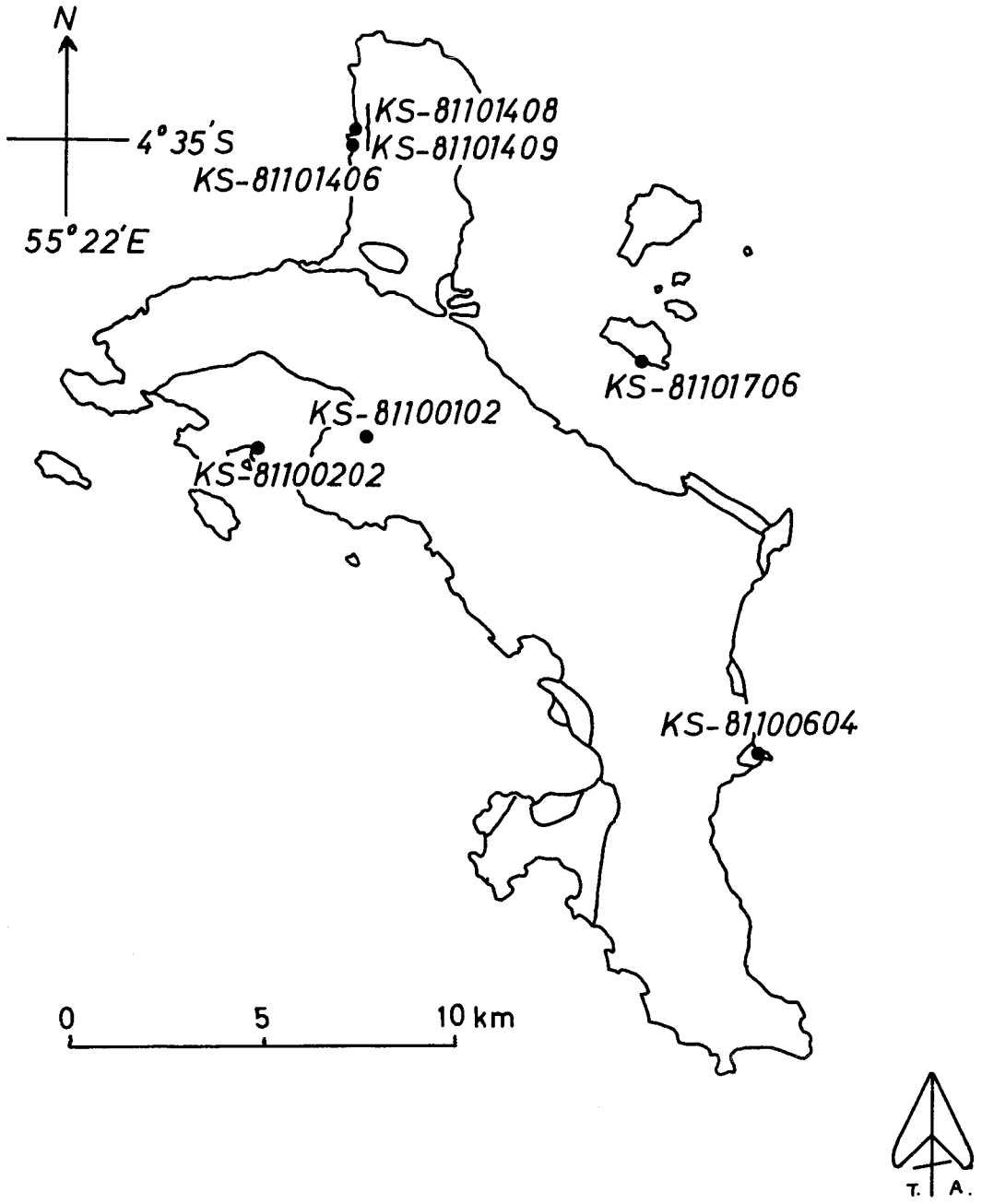

Fig. 1 Locality map of granitic rock specimens used for EPMA analysis.

Table 2. Representative EPMA analyses of magnetite from the Seychelles granitic rocks

	1	2	3	4	5	6
	Tonalite	Porphyritic granite	Genissose granodiorite	Gray granite	Pink granite	Leuco-granite
Sample No.	KS-81101409	KS-81100202	KS-81101408	KS-81100102	KS-81100604	KS-81101406
SiO_2	0.14	0.30	0.17	0.14	0.09	0.13
TiO_2	0.00	0.45	0.02	0.75	0.33	0.46
Al_2O_3	0.10	0.29	0.13	0.11	0.09	0.07
Cr_2O_3	0.05	0.01	0.04	0.00	0.03	0.01
Fe_2O_3*	68.11	66.89	68.98	67.44	68.67	67.43
FeO	30.89	31.71	31.42	31.35	31.64	31.08
MnO	0.17	0.09	0.17	0.75	0.14	0.44
MgO	0.00	0.01	0.00	0.00	0.00	0.00
CaO	0.01	0.01	0.00	0.00	0.00	0.00
Total	99.47	99.76	100.93	100.54	100.99	99.62
			O = 4			
Si	0.007	0.018	0.009	0.007	0.004	0.007
Al	0.005	0.013	0.003	0.005	0.004	0.003
Cr	0.002	0.000	0.001	0.000	0.001	0.000
Fe^{3+}	1.983	1.937	1.983	1.941	1.969	1.960
Ti	0.000	0.019	0.001	0.034	0.013	0.019
Fe^{2+}	0.999	1.021	1.008	1.003	1.008	1.004
Mn	0.006	0.003	0.005	0.024	0.005	0.014
Mg	0.000	0.001	0.000	0.000	0.000	0.000
Ca	0.000	0.000	0.000	0.000	0.000	0.000

* Calculated assuming the ideal chemical formula.

Magnetite from granitic rocks is usually close to pure Fe_3O_4 and generally contains traces of SiO_2, TiO_2, Al_2O_3, Cr_2O_3, and MnO. The amount of TiO_2 in some magnetite from gray granite is large relatively to those in other granitic rocks but is less than 1%.

Ilmenite is manganoan in many granitic rock specimens and the MnO content in ilmenite attains up to 32 wt.% (in leucogranite); but in some cases ilmenite does not contain any more than 2% MnO (in the Cerf gneissose granite). Ilmenite intergrown with magnetite is generally richer in MnO than co-existing discrete ilmenite but in gray granite the MnO contents in both ilmenites are nearly the same. The MnO concentration in each discrete and intergrown ilmenite often differs from grain to grain within the single hand specimens but each grain is generally homogeneous. The Fe_2O_3 content is generally less than 10% in both discrete and intergrown ilmenite, and other elements are only of trace.

Table 3. Representative EPMA analyses of ilmenite from the Seychelles granitie rocks

	Discrete ilmenite					
	1	2	3	4	5	6
	Tonalite	Gneissose granodiorite	Gneissose granite	Gray granite	Pink granite	Leuco-granite
Sample No.	KS-81101409	KS-81101408	KS-81101706	KS-81100102	KS-81100604	KS-81101406
SiO_2	0.21	0.13	0.11	0.12	0.39	0.11
TiO_2	47.33	51.23	51.02	50.67	48.03	53.01
Al_2O_3	0.06	0.08	0.04	0.04	0.08	0.04
Cr_2O_3	0.03	0.05	0.01	0.00	0.02	0.05
Fe_2O_3*	10.58	2.94	2.74	3.16	8.61	0.07
FeO	36.85	34.37	44.40	39.94	32.39	21.67
MnO	5.80	11.35	1.59	5.70	11.01	25.80
MgO	0.07	0.16	0.00	0.00	0.01	0.00
CaO	0.05	0.06	0.00	0.00	0.08	0.00
Total	100.98	100.37	99.91	99.63	100.62	100.75
			O = 6			
Si	0.012	0.007	0.006	0.006	0.020	0.005
Al	0.004	0.005	0.002	0.002	0.005	0.002
Cr	0.001	0.002	0.000	0.000	0.001	0.002
Fe^{3+}	0.397	0.111	0.104	0.121	0.325	0.003
Ti	1.768	1.935	1.941	1.932	1.815	1.991
Fe^{2+}	1.538	1.443	1.878	1.694	1.361	0.905
Mn	0.240	0.483	0.068	0.245	0.469	1.091
Mg	0.005	0.012	0.000	0.000	0.001	0.000
Ca	0.003	0.003	0.000	0.000	0.004	0.000

* Calculated assuming the ideal chemical formula.

Table 3 (continued).

	Intergrown ilmenite				
	7	8	9	10	11
	Tonalite	Porphyritic granite	Gneissose granodiorite	Gray granite	Leuco-granite
Sample No.	KS-81101409	KS-81100202	KS-81101408	KS-81100102	KS-81101406
SiO_2	0.21	0.30	0.12	0.07	0.11
TiO_2	48.66	50.04	49.66	50.55	51.14
Al_2O_3	0.00	0.28	0.15	0.04	0.04
Cr_2O_3	0.00	0.02	0.00	0.00	0.00
Fe_2O_3*	7.96	3.34	5.47	3.77	2.20
FeO	33.74	39.13	25.71	42.73	13.35
MnO	9.56	5.95	18.63	3.74	32.35
MgO	0.12	0.06	0.06	0.00	0.00
CaO	0.29	0.07	0.09	0.02	0.00
Total	100.54	99.19	99.89	99.92	99.19
			O = 6		
Si	0.011	0.015	0.006	0.003	0.006
Al	0.000	0.017	0.009	0.003	0.002
Cr	0.000	0.001	0.000	0.000	0.000
Fe^{3+}	0.301	0.128	0.208	0.144	0.084
Ti	1.839	1.912	1.886	1.923	1.951
Fe^{2+}	1.418	1.663	1.086	1.766	0.567
Mn	0.407	0.256	0.797	0.161	1.390
Mg	0.009	0.005	0.005	0.000	0.000
Ca	0.016	0.004	0.005	0.001	0.000

* Calculated assuming the ideal chemical formula.

Fe^{2+}-Mn distribution between ilmenite and magma

High concentration of MnO in ilmenite is characteristic of some of the Seychelles granitic rocks. Some authors (e.g., Tsusue, 1973; Neumann, 1974) have reported ilmenite enriched in MnO occurring in later crystallization products of granitic magma. Mn in ilmenite is usually divalent and substitutes Fe^{2+}. To explain the crystallization of manganoan ilmenite, it is necessary to make out the distribution of Fe^{2+} and Mn between ilmenite and magma (Tsusue, 1973).

Discrete ilmenite crystals in Seychells tend to display euhedral and/or angular outlines against ferro-magnesian minerals such as biotite and amphiboles, and

ilmenite is one of the earliest mafic minerals crystallizing from granitic magma. Mn/Fe^{2+} in granitic magma crystallizing ilmenite can be, therefore, represented by that in host granitic rock. Figure 2 shows distribution of Fe^{2+} and Mn between discrete ilmenite and host granitic rock. The chemical composition of tonalite forming xenoliths, probably a hybrid (Suwa et al., 1983), is not representative of the composition of magma and the Fe^{2+}-Mn distribution in tonalite is left out of consideration. Assuming Mn/Fe^{2+} in host rock to be that in magma, the distribution coefficient ($K_D = (Mn/Fe^{2+})_{ilmenite}/(Mn/Fe^{2+})_{magma}$) is estimated at 1.8-3.0 for gray granite and gneissose granite; gneissose granodiorite and leucogranite have conspicuously high K_D values (6.0-8.2 and 9.6-12.6, respectively), and pink granite shows an intermediate distribution coefficient (4.0-4.1). The distribution coefficient for gray granite and gneissose granite, Seychelles, is nearly identical with that estimated in the monzonite-granite suite near Oslo (Neumann, 1974), and pink granite and gneissose granodiorite have K_D values close to that in the Ōsumi diorite-granite suite (Tsusue, 1973). The distribution coefficient in Seychelles tends to increase with the MnO content in ilmenite rising (Fig. 2) and is

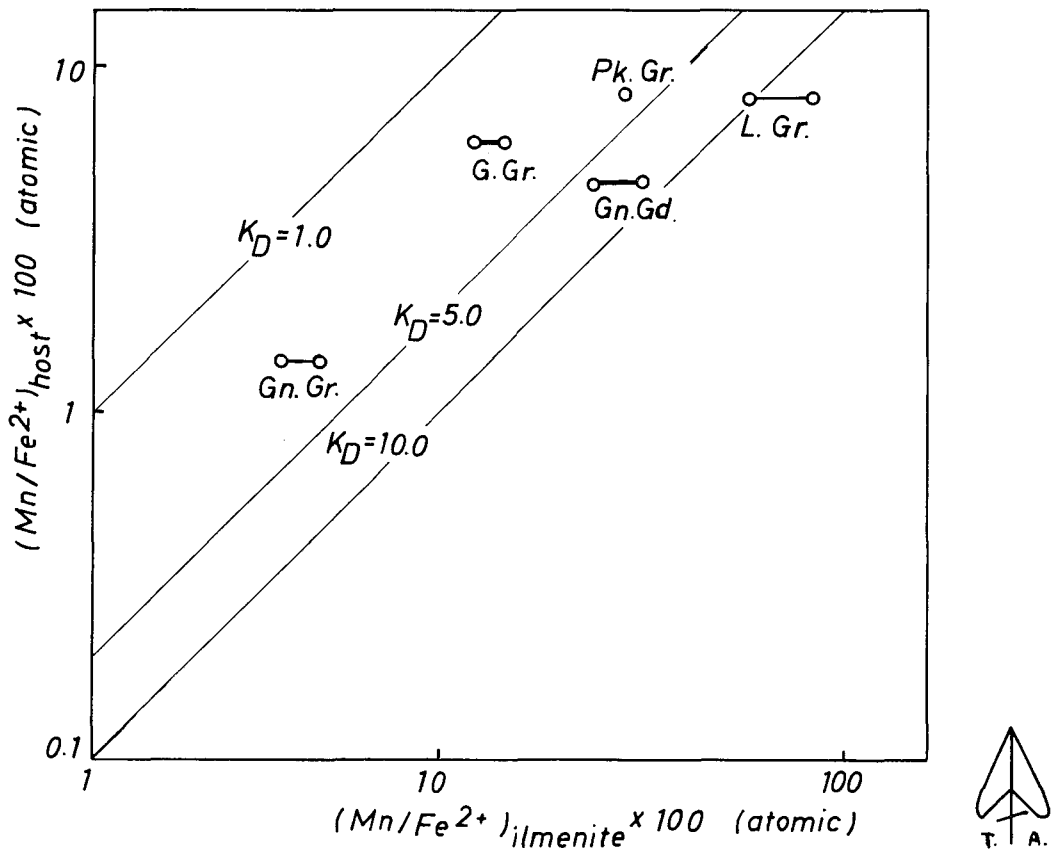

Fig. 2 Distribution of Fe^{2+} and Mn between ilmenite and host rock. Gn. Gr. = gneissose granite, G. Gr. = gray granite, Pk. Gr. = pink granite, Gn. Gd. = Gneissose granodiorite, L. Gr. = leucogranite.

different from the relatively constant coefficients reported in other granitic rock suites where manganoan ilmenite occurs.

Discussion

Ilmenite generally increases its MnO content with differentiation of magma proceeding, as shown by many authors (e.g., Elsdon, 1972; Duchesne, 1972; Tsusue, 1973). Figure 3 shows $Mn/(Mn+Fe^{2+})$ in discrete ilmenite plotted against the differentiation index of host rock. The MnO content in ilmenite varies with the differentiation index and there are recognized at least three granitic rock series present in Seychelles: (1) tonalite-gneissose granodiorite-leucogranite series, (2) gneissose granite-gray granite series, and (3) pink granite series. Ilmenite in the tonalite-gneissose granodiorite-leucogranite series has high $Mn/(Mn+Fe^{2+})$ relatively to the differentiation indices of host rocks, and the $Mn/(Mn+Fe^{2+})$ exceedingly increases, as the differentiation index rises. On the other hand, gneissose granite and gray granite, respectively distributed in the Cerf and Mahe islands, show low $Mn/(Mn+Fe^{2+})$ in ilmenite and are markedly different from tonalite, gneissose granodiorite and leucogranite. The pink granite series contains ilmenite of an intermediate composition. Figure 4 shows a similar diagram for the composition of intergrown ilmenite. Intergrown ilmenite is apparently an exsolution product formed as the result of titanomagnetite oxidizing, as discussed by Buddington and Lindsley (1964). Since magnetite intergrown with ilmenite is nearly of pure Fe_3O_4, $Mn/(Mn+Fe^{2+})$ in intergrown ilmenite is related to the contents of MnO and TiO_2 in pre-exsolved magnetite crystallized from magma. In this diagram, there is also distinct difference between the tonalite-gneissose granodiorite-leucogranite and the gneissose granite-gray granite series: intergrown ilmenite in the tonalite-gneissose granodiorite-leucogranite is dramatically Mn-rich. Intergrown ilmenite in porphyritic granite is plotted between those of the two series and porphyritic granite may belong to the pink granite series. The Fe^{2+}-Mn distribution coefficient ilmenite/magma also appears to vary correspondingly with these three rock series (Fig. 2).

The presence of three granitic rock series in Seychelles, divided on the basis of MnO content in ilmenite, may be also supported by the mineralogy of amphiboles, essential constituents in granitic rocks (Hoshino and Suwa, 1983). Rocks from the tonalite-gneissose granodiorite-leucogranite series contain Fe^{2+}-poor common hornblende, while ferro-richterite rimmed with riebeckite is characteristic of the gneissose granite-gray granite series; and Fe^{2+}-rich hornblende or ferro-edenite occurs in pink and porphyritic granites. Tonalite, gneissose granodiorite and leucogranite are all associated closely in the field and may also imply a cognate origin of them.

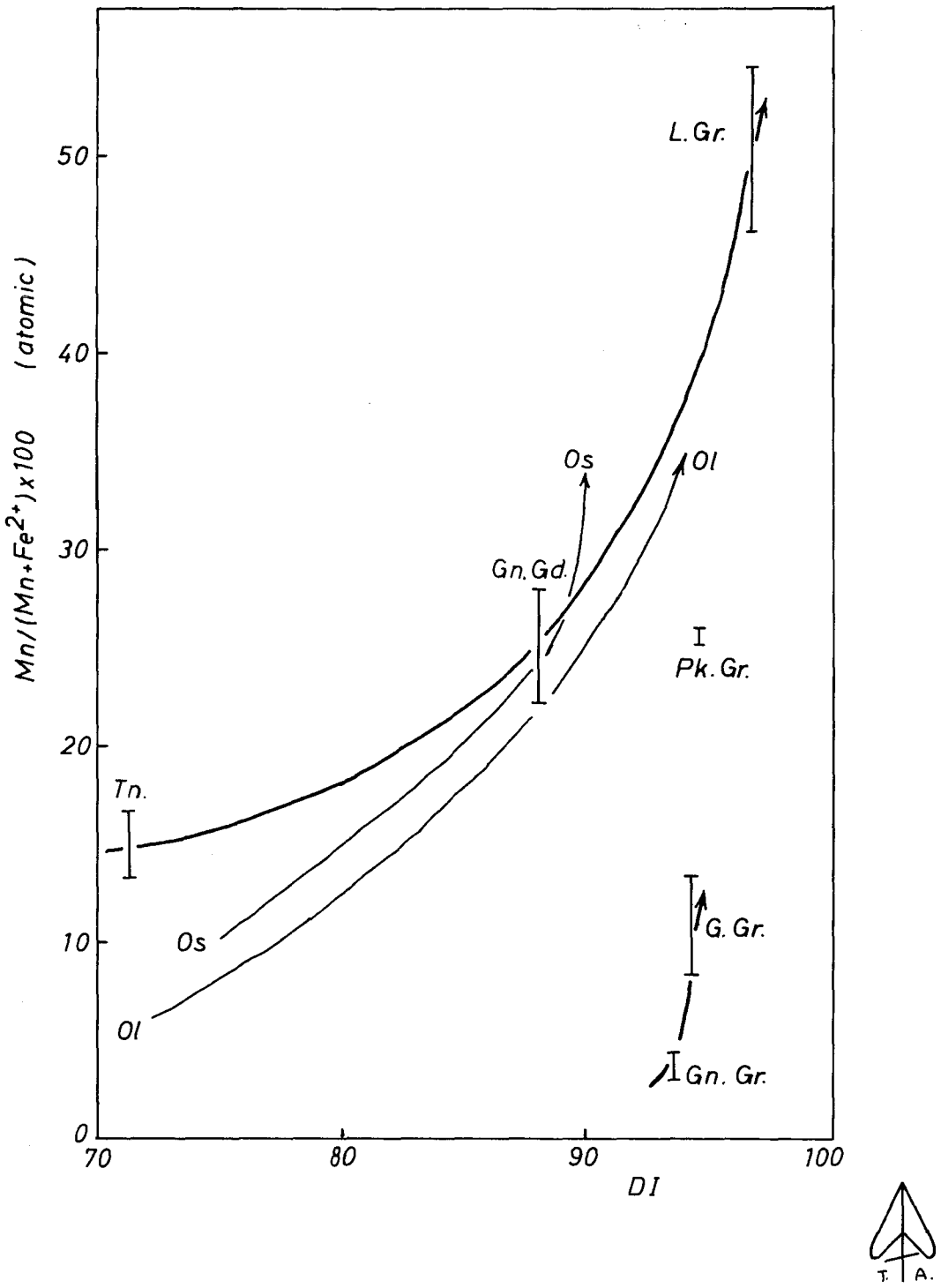

Fig. 3 Variation of Mn/(Mn + Fe^{2+}) in discrete ilmenite *vs* differentiation index (DI) of host rock. Tn. = tonalite; Ol = monzonite-granite suite near Oslo (Neumann, 1974); Os = diorite-granite suite, Ōsumi peninsula (Tsusue, 1973). Other symboles as Fig. 2.

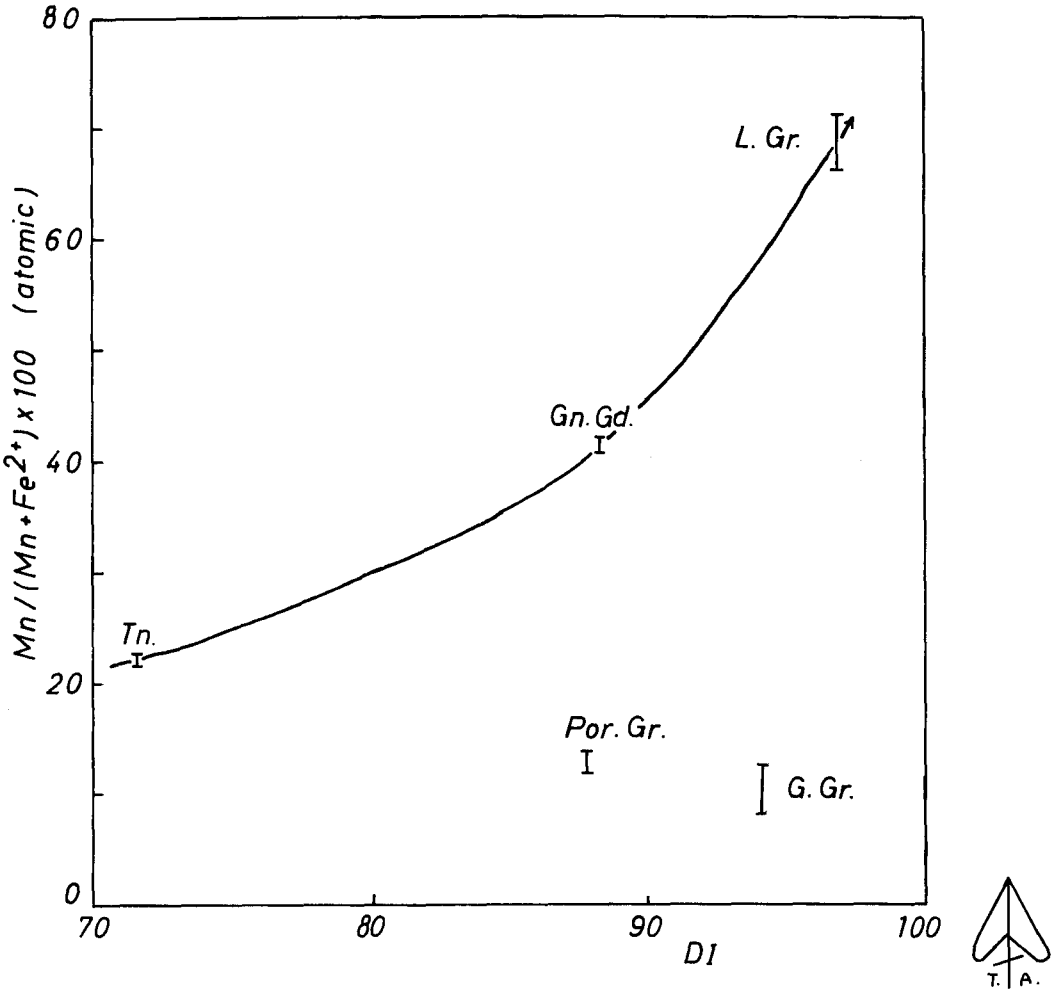

Fig. 4 Variation of Mn/(Mn + Fe^{2+}) in intergrown ilmenite *vs* differentiation index (DI) of host rock. Por. Gr. = porphyritic granite. Other symboles as Fig. 2.

Acknowledgments — We express our sincere thanks to Mr. P. Shilton, Secretary, National Research and Development Council, Ministry of Planning Development, Republic of Seychelles and to Mr. G. Lionnet, Senior Education Officer, Ministry of Education and Information, Republic of Seychelles for their most esteemed and invaluable assistance.

We are very grateful to Drs. T. Yanagi and H. Umemura and Messers. K. Tokieda, M. Asami and M. Hoshino for their laborious collaboration in the field survey in 1981.

The field work was made possible by the Grant-in-Aid Overseas Scientific Survey from the Ministry of Education, Science and Culture, Japan, to which we express our thanks.

REFERENCES

BAKER, B.H. (1963): Geology and mineral resources of the Seychelles archipelago. *Mem. Geol. Soc. Kenya,* **3.**

BUDDINGTON, A.E. and LINDSLEY, D.H: (1964): Iron-titanium oxide minerals and synthetic equivalents. *Jour. Petrol.,* **5,** 310-357.

DUCHESNE, J.G. (1972): Iron-titanium oxide minerals in the Bjerkrem-Sogndal Massif, South-Western Norway. *Jour. Petrol.,* **13,** 57-81.

ELSDON, R. (1972): Iron-titanium oxide minerals in the Upper Layered Series, Kap Edvard Holm, East Greenland. *Mineral. Mag.,* **38,** 946-956.

ELSDON, R. (1975): Manganoan ilmenite from the Leister granite, Iceland. *Mineral. Mag.,* **40,** 419-421.

HOSHINO, M. and SUWA, K. (1983): Amphiboles in some granitic rocks from the Mahe island and the Cerf island, Seychelles. *8th Prelim. Rept. Afr. Studies, Nagoya Univ.,* 47-62.

NEUMANN, E.R. (1974): The distribution of Mn^{2+} and Fe^{2+} between ilmenites and magnetites in igneous rocks. *Amer. Jour. Sci.,* **274,** 1074-1088.

NEUMANN, H. and BERGSTØL, S. (1964): Pyrophanite in the southern part of Oslo. Contributions to the Mineralogy of Norway, No. 25. *Norsk. Geol., Tidsskrift,* **44,** 39-42.

SUWA, K., YANAGI, T., TOKIEDA, K., UMEMURA, H., ASAMI, M. and HOSHINO, M. (1983): Geology and petrology of the Seychelles Islands. *8th Prelim. Rept. Afr. Studies, Nagoya Univ.,* 3-21.

TSUSUE, A. (1973): The distribution of manganese and iron between ilmenite and granite magma in the Ōsumi Peninsula, Japan. *Contri. Mineral. Petrol.,* **40,** 305-314.

YANAGI, T., WAKIZAKA, Y. and SUWA, K. (1983): Rb-Sr whole rock ages of granitic rocks from the Seychelles Islands. *8th Prelim. Rept. Afr. Studies, Nagoya Univ.,* 23-36.

PLATE I

1. Magnetite (light gray) intergrown with ilmenite (dark gray) in gray granite (KS-81100103). Width of field of the image is 0.43 mm. Reflected polarized light.

2. Ilmenite intergrown with magnetite in leucogranite (KS-81101406). Ilmenite contains minute inclusions of hematite (white). Magnetite is partly replaced by secondary hematite. Width of field is 0.13 mm. Reflected polarized light in oil.

PLATE I

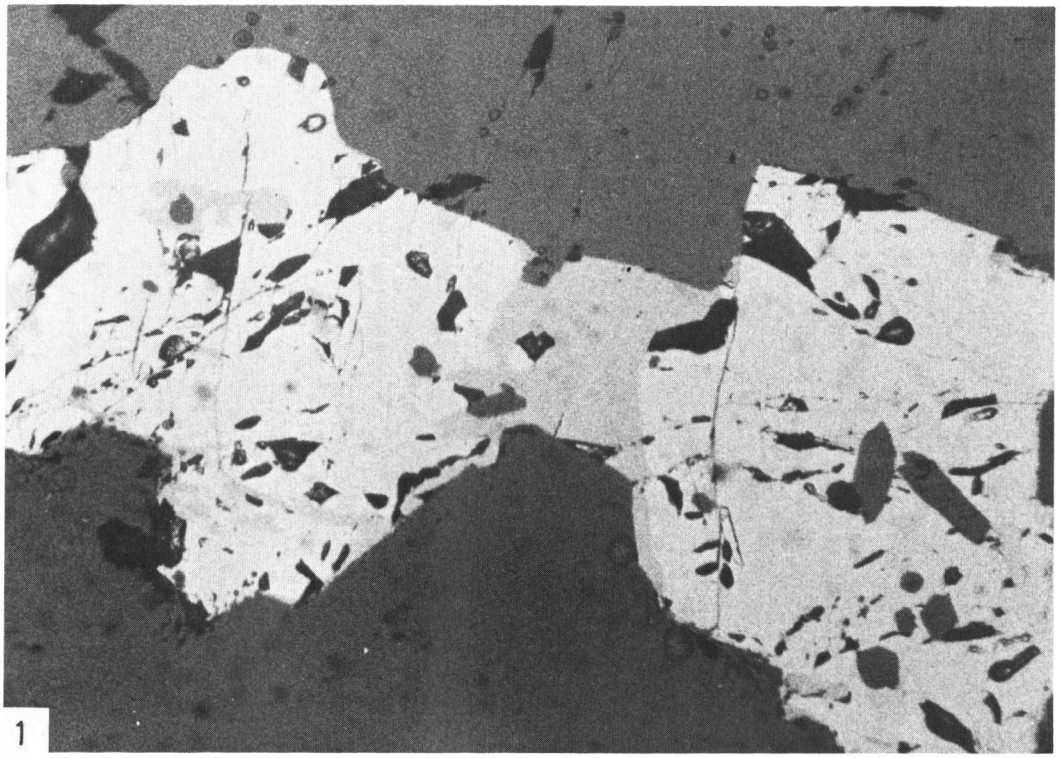

1

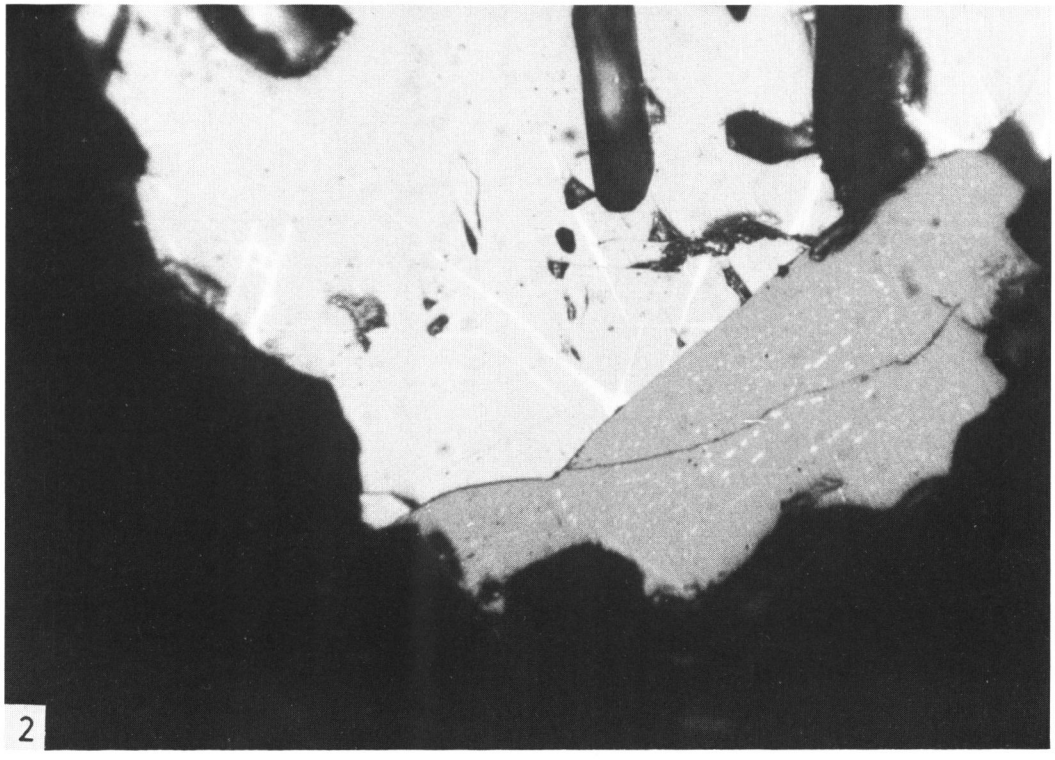

2

Petrological Study of Pelitic and Psammitic Gneisses in the Uvete Area, Kenya

Akira MIYAKE

Department of Earth Sciences, Faculty of Science, Nagoya University

Abstract

The late Precambrian Mozambique metamorphic rocks in the Uvete area, Kenya consist of pelitic, psammitic and basic gneisses. The pelitic and psammitic gneisses contain, in addition to quartz and plagioclase, kyanite-garnet-biotite-muscovite, kyanite-chlorite-biotite-muscovite, kyanite-garnet-chlorite-biotite-muscovite, staurolite-garnet-biotite-muscovite, microcline-garnet-biotite-muscovite and partial assemblages of the above types. These assemblages show that the rocks in the Uvete area was metamorphosed under conditions of the staurolite-kyanite zone in medium pressure type of facies series.

Since minerals of various mineral assemblages have the essentially unique composition according to mineral assemblages and the compositions of coexisting minerals, the assemblages are considered to be formed under narrow ranges of P-T conditions, in which kyanite-biotite join and kyanite-chlorite join are stable in the AFM diagram.

On the basis of the compositions of muscovite (with microcline and biotite) and pairs of garnet-biotite and garnet-plagioclase (with kyanite), temperature and pressure during metamorphism in the Uvete area are estimated at 530 ± 40°C and 6.5 ±0.5 Kb.

Mineral parageneses of pelitic gneisses are different between the Uvete area and its northward Machakos area. The estimated physical conditions and the chemical compositions of minerals in both areas show that the differences of the mineral parageneses in both areas are not due to the difference of the metamorphic grade but due to the bulk chemistry.

Introduction

The Precambrian Mozambique metamorphic rocks are widely exposed around the Uvete and Machakos areas. Geological studies of these areas were reported by Baker (1954), Biyajima et al. (1975), Biyajima (1976), Nureki et al. (1977), Suwa et al. (1979) and Miyake and Suwa (1981).

The foliations and lineations of paragneisses (pelitic, psammitic and basic gneisses) in the Uvete area are arranged nearly parallel around the central granitoid gneiss body of the Uvete dome and several synclines and anticlines are running in the paragneiss area around the granitoid gneiss body (Miyake and Suwa, 1981). Fig. 1 shows geological outline of the Uvete area with localities of samples studied in detail.

8th Prelim. Rept. Afr. Studies, Nagoya Univ., 75-95, 1983.

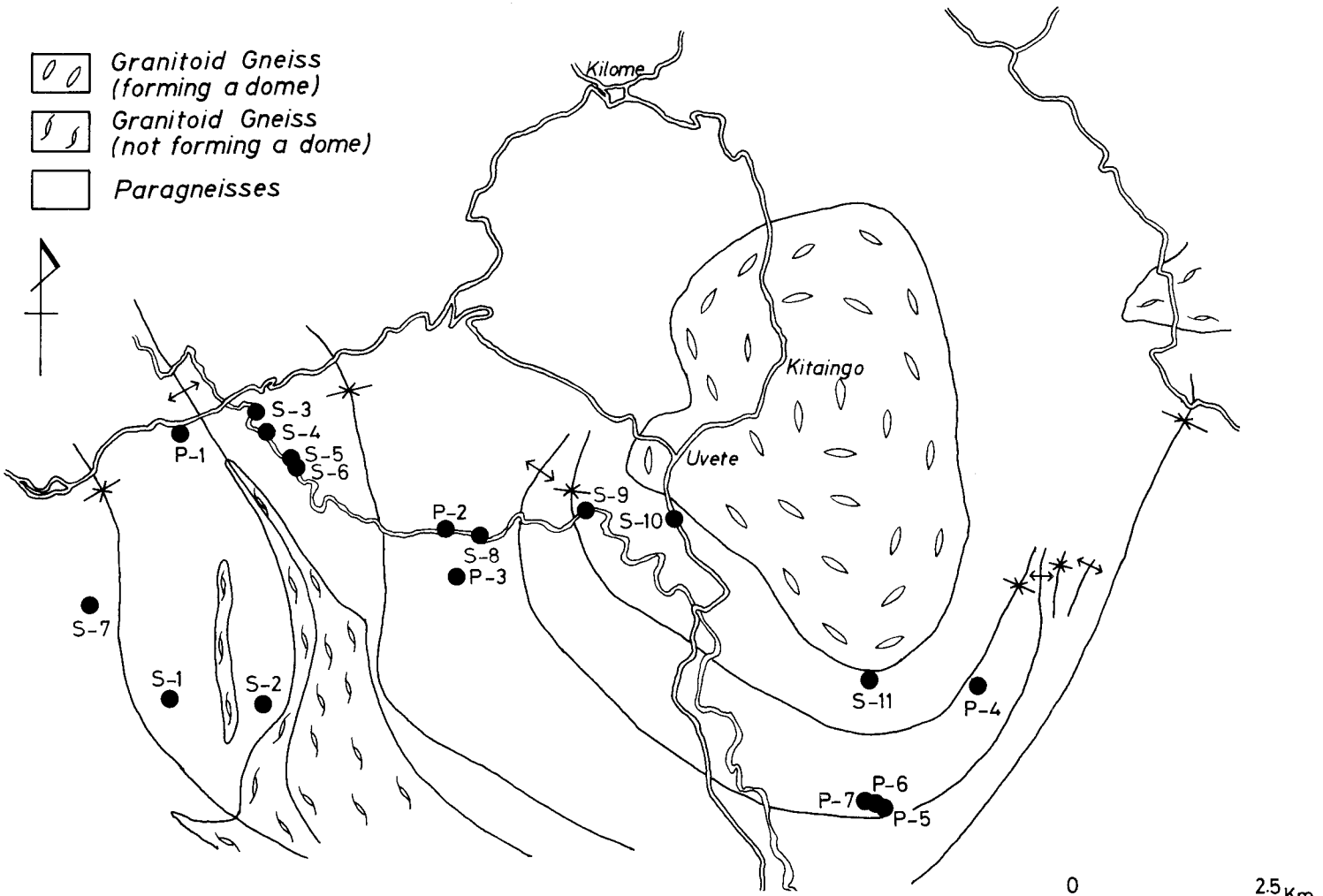

Fig. 1 Geological outline of the Uvete area with localities of samples.
P-1 to P-7 : localities of pelitic gneisses
S-1 to S-11 : localities of psammitic gneisses

The Mbooni dome in the Machakos area is situated about 20 Km north from the Uvete dome and has a similar geological structure to the Uvete dome. The maximum temperature and pressure around the Mbooni dome was estimated at 570-590°C and 6.8 Kb (Inoue and Suwa, 1979).

The present report gives analytical data of minerals in various mineral assemblages from the Uvete area. The main purpose of the report is firstly to correlate chemical variations in the rock-forming minerals to the mineral assemblages and compositions of coexisting minerals and secondly to estimate the physical conditions of metamorphism of the Uvete area.

Petrography

Psammitic gneisses in the Uvete area are light in colour owing to sparse coloured minerals and characterized by the presence of microcline. On the other hand pelitic gneisses are more micaceous and are characterized by the presence of kyanite or staurolite.

Mineral assemblages of pelitic and psammitic gneisses in the Uvete area are as follows:

(1) kyanite + garnet + biotite
(2) kyanite + garnet + biotite + muscovite
(3) kyanite + chlorite + biotite + muscovite
(4) kyanite + garnet + chlorite + biotite + muscovite
(5) kyanite + biotite + muscovite
(6) staurolite + garnet + biotite + muscovite
(7) garnet + biotite + muscovite
(8) biotite + muscovite
(9) microcline + garnet + biotite + muscovite
(10) microcline + biotite + muscovite

Quartz and plagioclase are present in all assemblages. Apatite and zircon are also present.

The assemblages (1) to (6) occur in pelitic gneisses and the assemblages (9) and (10) occur in psammitic gneisses. From the mineral assemblages, pelitic gneisses are considered to be more aluminous than psammitic gneisses. Since the assemblages (7) and (8) contain none of kyanite, staurolite and microcline, the rocks showing these assemblages have intermediate chemical compositions between typical pelitic and psammitic gneisses.

Kyanite, staurolite and chlorite occur in only pelitic gneisses. Kyanite occurs as a tabular poikiloblast which shows twins in some cases and sometimes reaches more than 2 cm in length. Elongated quartz crystals are included in kyanite crystals. Staurolite was rarely found in the Uvete area. Staurolite in sample P-3 occurs as a euhedral crystal about 0.2-0.7 mm in size. The mineral is pale yellow in colour and has weak pleochroism. Chlorite occurs being intimately associated with biotite and muscovite, and is very pale green in colour.

Garnet, biotite and muscovite occur in both pelitic and psammitic gneisses. Garnet in pelitic gneisses usually exhibits euhedral to subhedral crystal about 0.4-5.0 mm and garnet in psammitic gneisses usually has an irregular outline. Biotite in pelitic gneisses is brown to pale greenish brown in Z-axial colour, and biotite in psammitic gneisses is deep brownish green. Biotite in both gneisses forms the foliation of a rock together with muscovite. Muscovite in pelitic gneisses occurs as prismatic form being intimately associated with biotite. Muscovite in psammitic gneisses is symplectic or worm-eaten in appearance and is longer (~1 mm) in c-axial direction than that in pelitic gneisses.

Mineral chemistry

Garnet, chlorite, staurolite, biotite and muscovite of various mineral assemblages were analysed with EPMA, and ferric and ferrous contents of biotite and muscovite in some psammitic gneisses were determined with partial wet analysis. Chemical compositions of these minerals are given in Table 1-7. The analysed pelitic and psammitic gneisses are P-1 to P-7 and S-1 to S-11, respectively. The localities of these samples are shown in Fig.1 and the types of mineral assemblages of these samples are as follows;

Assemblage (1) : P-1
Assemblage (2) : P-2, P-4
Assemblage (3) : P-6, P-7
Assemblage (4) : P-5
Assemblage (6) : P-3
Assemblage (9) : S-1 to S-7, S-10, S-11
Assemblage (10) : S-8, S-9

Garnet

Compositions of garnet in the assemblages (1), (2), (4), (6) and (9) are presented in Table 1. Garnet usually exhibits chemical zoning characterized by Mg-richer core and Mn-richer rim. Core part of garnet in psammitic gneisses is richer in Fe than rim part. Garnet of pelitic gneisses, however, contains almost constant Fe content from core part to rim part. An example of zoning profile of garnet in sample P-3 is presented in Fig. 2. It is not sure whether these zoning patterns were formed during progressive or retrogressive metamorphism. On the other hand garnet in sample P-1 has Mn- and Ca-

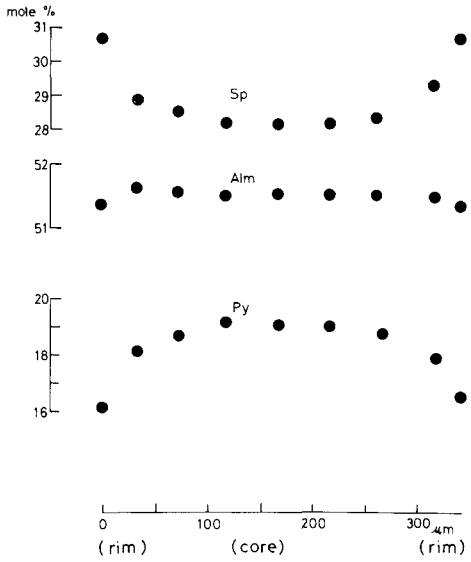

Fig. 2 Zoning profile of garnet in sample P-3.

Table 1. Chemical compositions of garnet.

	P-1		P-2		P-3		P-4	
	core	rim	core	rim	core	rim	core	rim
SiO_2	37.75	37.89	37.40	37.33	37.69	37.46	37.78	37.82
Al_2O_3	21.15	21.33	20.88	20.80	21.14	21.09	21.11	21.17
FeO*	29.34	33.97	31.19	31.80	23.31	23.38	28.73	28.05
MnO	2.42	0.46	5.39	5.84	12.65	13.57	8.97	9.63
MgO	1.52	3.80	4.21	3.58	4.88	4.08	3.96	3.72
CaO	8.65	2.93	0.57	0.54	0.45	0.38	0.58	0.57
Total	100.83	100.38	99.64	99.89	100.12	99.96	101.13	100.96
Si	3.001	3.009	3.008	3.009	3.001	3.002	3.002	3.009
Al	1.981	1.996	1.979	1.976	1.984	1.992	1.978	1.985
Fe	1.950	2.256	2.096	2.144	1.552	1.567	1.910	1.866
Mn	0.163	0.031	0.366	0.398	0.853	0.921	0.604	0.649
Mg	0.180	0.450	0.507	0.431	0.579	0.487	0.469	0.441
Ca	0.736	0.250	0.049	0.047	0.039	0.032	0.049	0.049

* Total iron calculated as FeO

(continued)

	P-5		S-1		S-2		S-3	
	core	rim	core	rim	core	rim	core	rim
SiO_2	38.17	38.13	36.31	36.49	36.79	36.85	36.26	36.22
Al_2O_3	21.27	21.58	19.66	20.21	19.91	19.77	18.89	19.56
FeO*	22.10	20.65	17.55	15.70	19.39	19.41	16.46	14.93
MnO	12.38	14.04	22.82	24.50	12.13	13.03	19.37	21.39
MgO	5.42	4.32	1.78	1.41	1.08	1.05	1.31	1.00
CaO	1.53	1.49	1.35	1.32	9.34	8.36	5.79	5.23
Total	100.87	100.21	99.47	99.63	98.64	98.47	98.08	98.33
Si	3.001	2.997	2.995	2.997	3.005	3.020	3.017	3.003
Al	1.971	1.997	1.911	1.956	1.917	1.910	1.852	1.911
Fe	1.453	1.444	1.211	1.079	1.334	1.330	1.146	1.036
Mn	0.825	0.940	1.594	1.704	0.840	0.904	1.365	1.502
Mg	0.635	0.507	0.219	0.172	0.131	0.128	0.163	0.124
Ca	0.129	0.139	0.198	0.116	0.817	0.717	0.516	0.465

*Total iron calculated as FeO

(continued)

	S-4		S-5		S-6	
	core	rim	core	rim	core	rim
SiO_2	36.80	36.84	36.57	36.61	36.69	36.55
Al_2O_3	19.58	19.63	19.47	19.34	20.09	19.87
FeO*	20.98	19.16	17.94	16.81	19.89	18.58
MnO	15.91	17.70	20.79	22.03	12.11	13.94
MgO	1.19	0.93	1.28	1.00	1.04	0.80
CaO	4.74	4.93	3.04	3.10	9.32	8.58
Total	99.20	99.19	99.09	98.90	99.14	98.32
Si	3.023	3.027	3.019	3.031	2.989	3.005
Al	1.896	1.901	1.895	1.887	1.929	1.925
Fe	1.441	1.317	1.239	1.164	1.355	1.284
Mn	1.107	1.232	1.455	1.546	0.835	0.971
Mg	0.147	0.114	0.157	0.123	0.127	0.098
Ca	0.417	0.434	0.274	0.275	0.813	0.756

* Total iron calculated as FeO

richer core and Mg- and Fe-richer rim. Such a zoning pattern is considered to be formed during progressive metamorphism. This sample does not contain muscovite and there may be a possibility that the difference between two zoning patterns is ascribed to presence or absence of muscovite.

Garnet contains various contents of the molecules of pyrope, almandine and spessartine. Garnet in pelitic gneisses has higher pyrope (14-17 mole %), higher almandine (48-75 mole %) and lower spessartine content (1-31 mole %) than garnet in psammitic gneisses (Py : 2-6 mole %, Alm : 35-52 mole %, Sp : 30-57 mole %).

Fig. 3 shows a relationship between the Mn/(Fe+Mg+Mn) and Mg/(Fe+Mg) value of garnet. Garnet in pelitic gneises is higher in Mg/(Fe+Mg) than that in psammitic gneisses. The Mn/(Fe+Mg+Mn) value increases with increasing of the Mg/(Fe+Mg) value in both pelitic and psammitic gneisses.

Staurolite

Staurolite in sample P-3 is very rich in ZnO (5-7 wt %).

Fig. 4 shows a relationship between ZnO and FeO contents of staurolite from pelitic gneisses in the Machakos area (Inoue and Suwa, 1979) and in sample P-3 (this study). Staurolite in this study is richer in ZnO and poorer in FeO than that from the Machakos area.

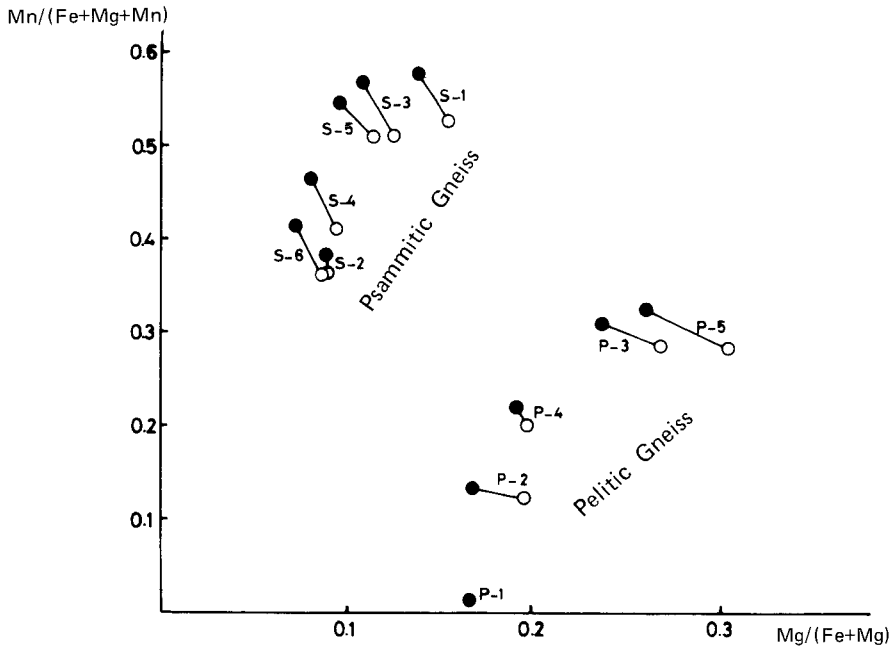

Fig. 3 Relation between Mn/(Fe+Mg+Mn) and Mg/(Fe+Mg) of garnet.
open circle : core part of garnet
closed circle : rim part of garnet

Table 2. Chemical compositions of staurolite in sample P-3.

	1	2	3
SiO_2	27.79	28.20	28.22
TiO_2	0.46	0.51	0.51
Al_2O_3	53.22	52.92	53.14
FeO*	8.05	8.65	8.79
MnO	0.98	1.08	0.97
MgO	2.23	2.48	2.42
ZnO	6.82	5.83	5.28
CaO	0.00	0.00	0.00
Na_2O	0.19	0.17	0.19
K_2O	0.00	0.00	0.00
Total	99.74	99.86	99.51
Si	7.845	7.934	7.941
Ti	0.098	0.108	0.107
Al	17.710	17.549	17.625
Fe	1.900	2.036	2.069
Mn	0.235	0.257	0.232
Mg	0.939	1.041	1.017
Zn	1.423	1.211	1.097
Ca	0.000	0.000	0.000
Na	0.103	0.094	0.101
K	0.000	0.000	0.000

* Total iron calculated as FeO

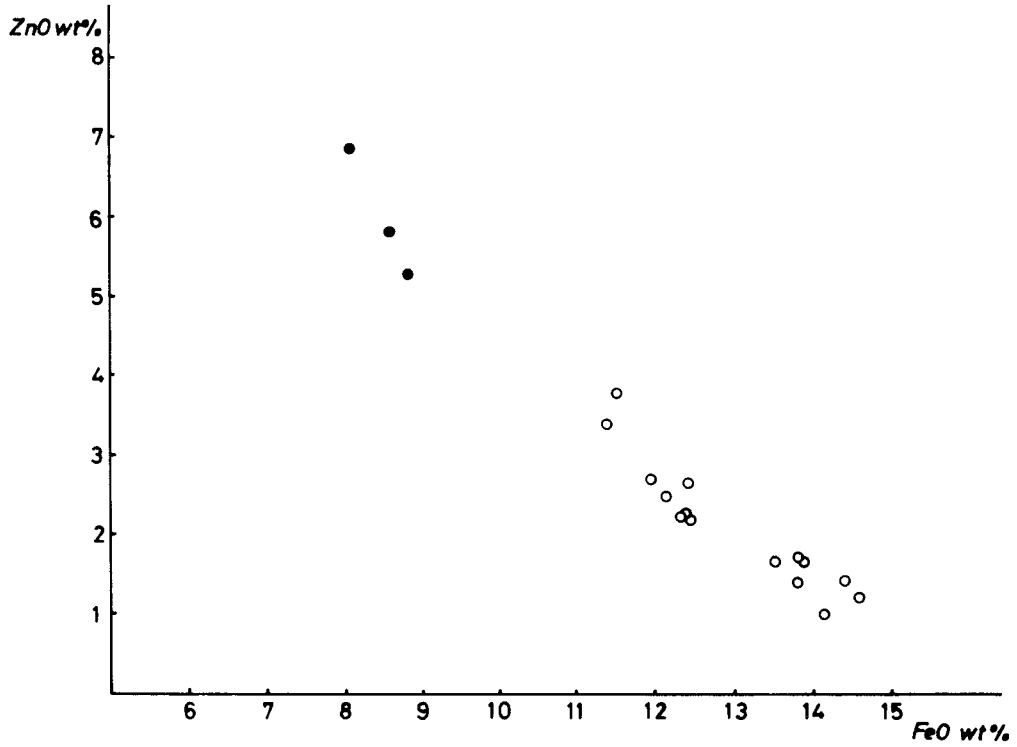

Fig. 4 Relation between ZnO and FeO of staurolite.
open circle : staurolite from the Machakos area (Inoue and Suwa, 1979)
closed circle : staurolite in sample P-3 (this study)

Chlorite

Compositions of chlorite in three samples (P-5, P-6 and P-7) are presented in Table 3. The three samples contain kyanite, biotite and muscovite, and the Mg/(Fe+Mg) values of chlorite in the three samples fall in narrow range (Mg/(Fe+Mg) = 0.75-0.77).

Biotite

Compositions of biotite in pelitic and psammitic gneisses are presented in Tables 4 and 5. In pelitic gneisses, the Mg/(Fe+Mg) value of biotite coexisting with chlorite is higher (Mg/(Fe+Mg) = 0.69-0.72) than that with garnet. Biotite coexisting with garnet has various Mg/(Fe+Mg) values ranging from 0.56 to 0.71 depending to samples. Biotite in pelitic gneisses contains uniform level of Al_2O_3 (19 ± 0.5 wt %) and TiO_2 (1.5 ± 0.5 wt %). Biotite in psammitic gneisses has lower Al_2O_3 content (16 ± 2 wt %) and higher TiO_2 content (3 ± 1 wt %).

Table 3. Chemical compositions of chlorite.

	P-5	P-6	P-7
SiO_2	26.67	26.63	26.55
TiO_2	0.07	0.09	0.06
Al_2O_3	22.87	23.19	22.91
FeO*	13.76	12.84	13.93
MnO	0.23	0.49	0.30
MgO	23.82	24.45	24.09
Total	87.42	87.69	87.84
Si	5.273	5.251	5.253
Ti	0.010	0.013	0.008
Al	5.362	5.389	5.343
Fe	2.287	2.092	2.316
Mn	0.040	0.082	0.051
Mg	7.063	7.153	7.105

* Total iron calculated as FeO

Table 4. Chemical compositions of biotite.

	P-1	P-2	P-3	P-4	P-5	P-6	P-7
SiO_2	36.95	36.99	37.82	37.36	38.04	38.12	38.08
TiO_2	2.01	1.08	1.70	1.74	1.13	1.63	1.70
Al_2O_3	19.09	19.02	19.01	18.30	19.36	18.80	18.82
FeO*	16.20	16.69	12.77	14.56	11.28	11.28	12.20
MnO	0.00	0.05	0.21	0.19	0.21	0.32	0.18
MgO	11.60	12.44	14.32	13.88	15.56	16.10	15.46
CaO	0.00	0.00	0.02	0.00	0.03	0.00	0.00
Na_2O	0.22	0.37	0.36	0.38	0.34	0.40	0.39
K_2O	8.61	8.41	8.00	8.86	8.64	8.62	8.63
Total	94.68	95.05	94.21	95.27	94.59	95.27	95.46
Si	5.522	5.518	5.566	5.526	5.544	5.535	5.537
Ti	0.226	0.121	0.188	0.194	0.124	0.179	0.187
Al	3.362	3.344	3.297	3.190	3.325	3.217	3.226
Fe	2.025	2.082	1.571	1.802	1.375	1.369	1.483
Mn	0.000	0.006	0.027	0.024	0.027	0.040	0.022
Mg	2.584	2.765	3.142	3.060	3.380	3.484	3.351
Ca	0.000	0.000	0.003	0.000	0.005	0.000	0.000
Na	0.065	0.106	0.102	0.108	0.095	0.114	0.111
K	1.642	1.601	1.501	1.671	1.609	1.597	1.601

* Total iron calculated as FeO

(continued)

	S-1	S-2	S-3	S-4	S-5	S-6
SiO_2	36.37	35.76	36.32	35.16	35.83	34.91
TiO_2	2.75	3.12	2.21	3.17	2.60	3.06
Al_2O_3	16.62	15.49	15.68	15.63	15.94	15.88
FeO*	16.68	23.29	20.99	22.35	20.60	24.17
MnO	0.65	0.56	0.35	0.41	0.50	0.57
MgO	11.34	7.71	9.96	8.00	9.38	6.59
CaO	0.00	0.00	0.02	0.00	0.00	0.00
Na_2O	0.06	0.02	0.03	0.04	0.06	0.06
K_2O	9.44	9.18	9.03	9.03	9.33	9.14
Total	93.91	95.13	94.59	93.89	94.23	94.38
Si	5.567	5.581	5.618	5.545	5.575	5.524
Ti	0.317	0.366	0.257	0.376	0.304	0.364
Al	2.998	2.850	2.860	2.905	2.923	2.962
Fe	2.135	3.041	2.716	2.948	2.756	3.199
Mn	0.083	0.074	0.046	0.054	0.066	0.076
MgO	2.586	1.795	2.297	1.882	2.177	1.554
Ca	0.000	0.000	0.004	0.000	0.000	0.000
Na	0.018	0.008	0.014	0.013	0.017	0.019
K	1.843	1.828	1.781	1.819	1.851	1.844

* Total iron calculated as FeO

Table 5. Chemical compositions of biotite.
Fe_2O_3 and FeO were determined with partial wet analysis.
and other oxides were analysed with EPMA.

	S-7	S-8	S-9	S-10	S-11
SiO_2	36.39	37.30	35.91	36.27	35.43
TiO_2	2.72	1.44	3.80	3.12	3.73
Al_2O_3	16.17	17.77	17.01	16.10	16.67
Fe_2O_3	6.89	3.30	1.67	3.78	2.11
FeO	17.40	11.30	22.40	19.20	22.00
MnO	0.71	0.54	0.21	0.36	0.39
MgO	7.84	13.80	6.14	7.55	6.62
CaO	0.00	0.01	0.01	0.00	0.00
Na_2O	0.05	0.05	0.06	0.06	0.07
K_2O	9.48	9.45	9.01	9.17	9.02
Total	97.65	94.96	96.22	95.61	96.04
Si	5.478	5.528	5.511	5.562	5.462
Ti	0.308	0.160	0.438	0.360	0.432
Al	2.868	3.103	3.076	2.909	3.028
Fe^{3+}	0.780	0.368	0.193	0.436	0.245
Fe^{2+}	2.190	1.400	2.874	2.462	2.835
Mn	0.091	0.068	0.027	0.047	0.051
Mg	1.758	3.047	1.404	1.725	1.520
Ca	0.000	0.002	0.002	0.000	0.000
Na	0.015	0.014	0.018	0.018	0.021
K	1.820	1.786	1.763	1.793	1.773

Muscovite

Compositions of muscovite in pelitic and psammitic gneisses are presented in Tables 6 and 7. Muscovite in pelitic gneisses has lower celadonite content and higher paragonite content than muscovite in psammitic gneisses.

Fig. 5 shows a relationship between the $Mg+Fe^{2+}$ and $Fe^{2+}/(Mg+Fe^{2+})$ values of muscovite coexisting with biotite and microcline. The $Mg+Fe^{2+}$ value increases with decreasing of the $Fe^{2+}/(Mg+Fe^{2+})$ value.

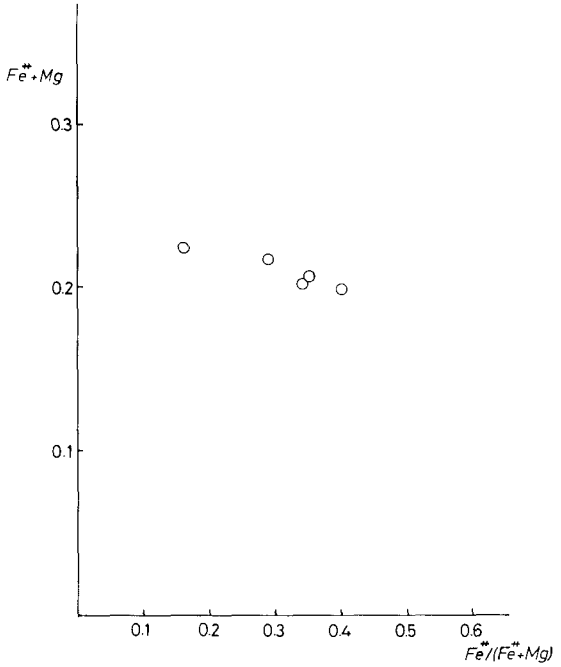

Fig. 5 Relation between $Mg+Fe^{2+}$ and $Fe^{2+}/(Mg+Fe^{2+})$ of muscovite coexisting with biotite and microcline.

Table 6. Chemical compositions of muscovite.

	P-2	P-3	P-4	P-5	S-1	S-2
SiO_2	46.22	47.11	46.06	46.64	46.11	46.24
TiO_2	0.15	0.74	0.50	0.42	1.18	0.94
Al_2O_3	35.26	34.70	34.45	35.75	30.90	29.02
FeO*	2.73	2.50	3.20	1.96	4.05	6.57
MnO	0.00	0.00	0.00	0.02	0.04	0.01
MgO	0.77	0.87	0.94	0.98	1.59	1.48
CaO	0.00	0.00	0.00	0.00	0.00	0.00
Na_2O	1.61	1.54	1.77	1.46	0.33	0.18
K_2O	8.24	8.36	8.18	8.76	10.30	10.39
Total	94.98	95.82	95.10	95.99	94.50	94.83
Si	6.153	6.210	6.149	6.135	6.289	6.369
Ti	0.015	0.073	0.050	0.041	0.122	0.098
Al	5.532	5.392	5.421	5.543	4.967	4.713
Fe	0.304	0.275	0.357	0.216	0.462	0.757
Mn	0.000	0.000	0.000	0.002	0.005	0.001
Mg	0.154	0.170	0.187	0.192	0.323	0.303
Ca	0.000	0.000	0.000	0.000	0.000	0.000
Na	0.416	0.393	0.457	0.373	0.088	0.047
K	1.399	1.406	1.393	1.471	1.792	1.825

* Total iron calculated as FeO

(continued)

	S-3	S-4	S-5	S-6
SiO_2	46.20	46.18	46.52	45.45
TiO_2	0.77	1.17	0.53	0.59
Al_2O_3	28.72	28.85	28.46	29.51
FeO*	6.84	6.07	6.04	6.09
MnO	0.01	0.03	0.03	0.03
MgO	1.74	1.39	1.71	1.31
CaO	0.00	0.00	0.00	0.00
Na_2O	0.21	0.25	0.24	0.22
K_2O	10.23	10.25	10.45	10.40
Total	94.72	94.19	93.98	93.60
Si	6.377	6.386	6.450	6.333
Ti	0.080	0.122	0.055	0.062
Al	4.672	4.702	4.650	4.846
Fe	0.790	0.702	0.700	0.711
Mn	0.001	0.003	0.002	0.003
Mg	0.358	0.288	0.354	0.272
Ca	0.000	0.000	0.000	0.000
Na	0.056	0.066	0.063	0.060
K	1.802	1.809	1.853	1.849

* Total iron calculated as FeO

Table 7. Chemical compositions of muscovite.
Fe_2O_3 and FeO were determined with partial wet analysis and other oxides were analysed with EPMA.

	S-7	S-8	S-9	S-10	S-11
SiO_2	46.57	46.68	47.68	46.41	46.94
TiO_2	0.81	0.47	0.81	0.71	1.09
Al_2O_3	28.55	31.91	32.19	30.23	31.67
Fe_2O_3	6.19	2.76	1.60	4.53	1.69
FeO	1.11	0.63	1.43	1.28	1.23
MnO	0.04	0.03	0.01	0.02	0.01
MgO	1.53	1.89	1.20	1.33	1.32
CaO	0.00	0.00	0.00	0.00	0.00
Na_2O	0.22	0.35	0.30	0.20	0.26
K_2O	10.44	10.28	10.07	10.17	10.34
Total	95.46	95.00	95.28	94.88	94.55
Si	6.328	6.268	6.358	6.296	6.326
Ti	0.083	0.047	0.081	0.072	0.110
Al	4.571	5.049	5.058	4.832	5.029
Fe^{3+}	0.633	0.279	0.160	0.462	0.171
Fe^{2+}	0.126	0.071	0.159	0.145	0.139
Mn	0.005	0.003	0.001	0.002	0.001
Mg	0.310	0.378	0.238	0.269	0.265
Ca	0.000	0.000	0.000	0.000	0.000
Na	0.058	0.091	0.078	0.053	0.068
K	1.809	1.760	1.712	1.759	1.777

Phase relation

AFM phase diagram

The mineral assemblages that occur in quartz + muscovite gneisses may be represented on the plane Al_2O_3-FeO-MgO (Thompson, 1957).

The assemblage (4) has four phases in this plane and although the assemblages (2) and (9) are three-phase assemblages, the compositions of garnet and biotite do not have constant Fe/(Fe+Mg) value for each assemblage. This is considered to result from the various Mn contents of garnet. Figs. 3 and 6 show that the Mn-richer

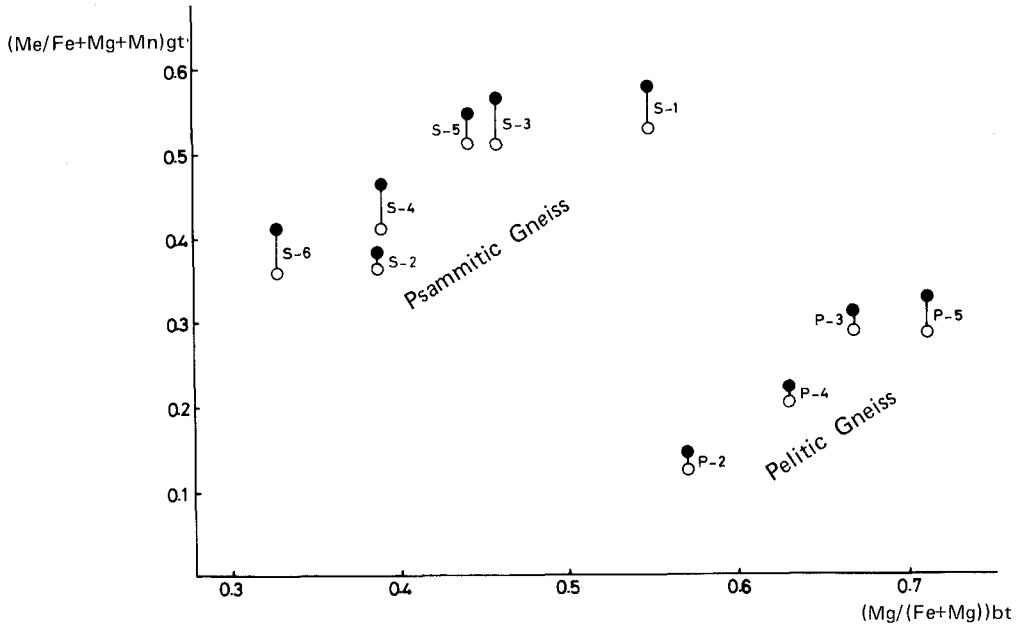

Fig. 6 Relation between Mn/(Fe+Mg+Mn) of garnet and Mg/(Fe+Mg) of biotite in muscovite-bearing rocks.
open circle : core part of garnet - biotite
closed circle : rim part of garnet - biotite

garnet in both core and rim parts has higher Mg/(Fe+Mg) value and that the Mn-richer garnet coexists with Mg-richer biotite for muscovite-bearing pelitic and psammitic gneisses, respectively. Compositions of pairs of garnet and biotite correspond regularly to their bulk chemical composition in the tetrahedron of Al_2O_3-FeO-MgO-MnO and only Mn-richest garnet in pelitic gneisses can coexist with chlorite (sample P-5). Clear trends in Fig. 3 and 6 indicate that the compositions of garnet and biotite in the three-phase assemblages are restricted when Mn-free rocks are concerned. On the other hand compositions of chlorite and coexisting biotite in pelitic gneisses have nearly constant Fe/(Fe+Mg) value. Furthermore

biotite coexisting with staurolite or kyanite is richer in Al than that with microcline. From the above, the schematic AFM diagram (Fig. 7) for Mn-free system is proposed.

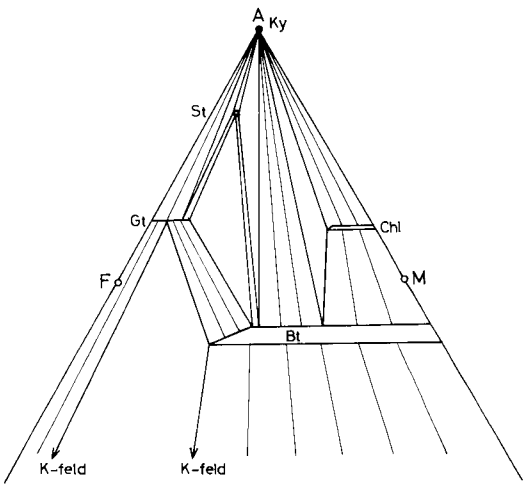

Fig. 7 Schematic AFM diagram.

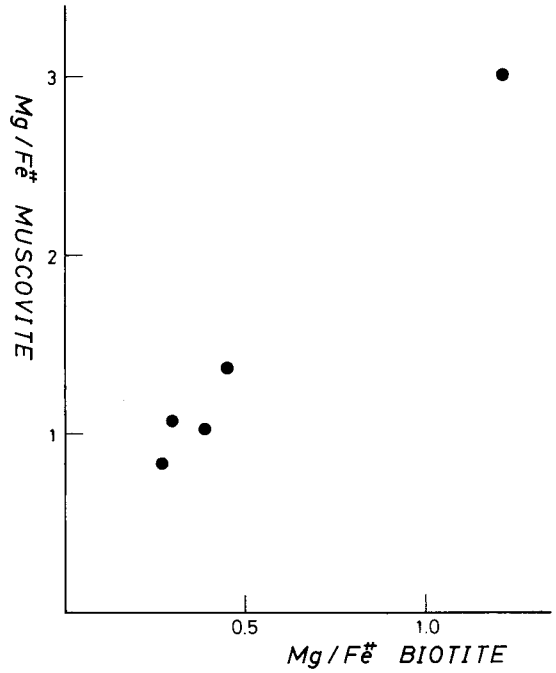

Fig. 8 Relation of Mg/Fe^{2+} between biotite and muscovite.

Muscovite and biotite in psammitic gneisses

The distribution of Mg/Fe^{2+} between biotite and muscovite is shown in Fig. 8. The distribution coefficient ($K_D = (Mg/Fe^{2+})^{mus}/(Mg/Fe^{2+})^{bt}$) shows only small variations, ranging from 2.4 to 3.5. Such values are very similar to the K_D value found by Butler (1967) in the Ardnamurchan area where K_D = 2.5-3.0, but are in contrast to 1.3 in that of Evans and Guidotti (1966) in western Main, to 1.56 in that of Guidotti(1970) in the Oquossoc area and 1.35 in that of Sharma and Narayan (1975) in the Rajasthan area. This difference is possibly not only due to the metamorphic grade but also due to the bulk chemical composition. The higher values in K_D (this study and Butler (1967)) are obtained from the mica pairs in microcline-bearing rocks, whereas the lower values (Evans and Guidotti (1966), Guidotti (1970) and Sharma and Narayan (1975)) are obtained from those in more aluminous rocks containing Al_2SiO_5 minerals or staurolite.

The Physical conditions

The parageneses of the AFM minerals show that the rocks in the Uvete area was metamorphosed under conditions of the staurolite-kyanite zone in medium pres-

sure type of facies series. Since the minerals of various mineral assemblages have the essentially unique compositions according to mineral assemblages and compositions of coexisting minerals, the assemblages are considered to be formed under essentially similar P-T conditions.

From the topology of the schematic AFM diagram (Fig. 7) only broadest region can be put on the P-T conditions at the metamorphism. Fig 9 shows the petrogenetic grid reconstructed by the method of Hess (1969). From the stable kyanite-biotite join and kyanite-chlorite join, the metamorphic conditions are considered to occupy a part of the shaded region of Fig. 9.

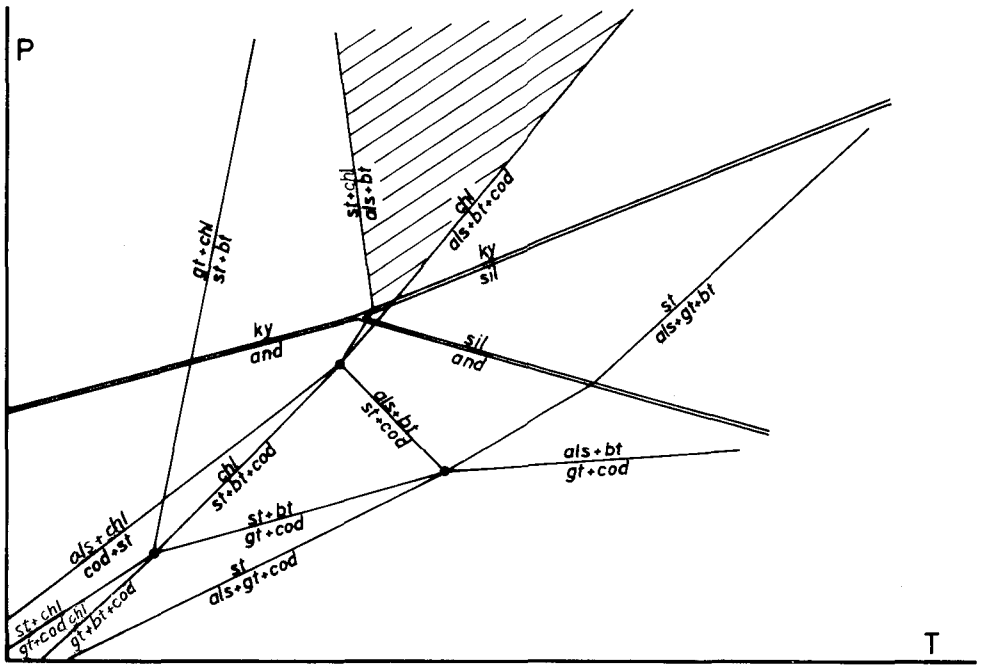

Fig. 9 Petrogenetic grid for the AFM phases.

Quantitative estimates of the physical conditions can be calculated from existing geothermometers. Temperature is estimated by the partitioning of Fe and Mg between garnet and biotite. Since it is not sure except for sample P-1 whether rim part or core part of garnet was formed under higher grade, rim garnet-biotite temperature and core garnet-biotite temperature were presented. Fig. 10 shows the compositions of coexisting garnet and biotite in terms of Mg/Fe. The distribution coefficient ($K_D = (Mg/Fe)^{bt}/(Mg/Fe)^{gt}$) provides temperature estimates for all garnet-biotite assemblages. The K_D values for rim garnet-biotite and core garnet-biotite are nearly constant, ranging from 6.39 to 7.62 and from 5.17 to 6.90, respectively. The variances of these values do not seem to depend on the Mn content of garnet (Fig. 11). The calibration of Thompson (1976) gives, for such K_D values, metamorphic temperature of 510 ± 20°C for rim garnet-biotite pairs and of 545 ± 35°C for core garnet-biotite pairs, respectively.

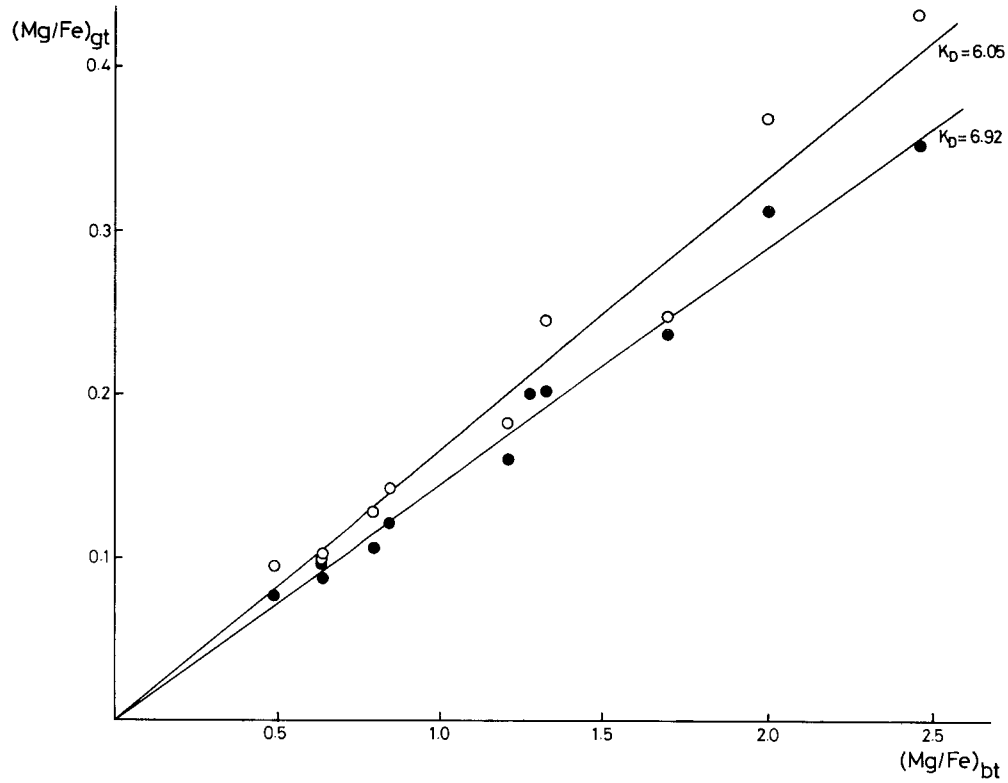

Fig. 10 Relation of Mg/Fe between biotite and garnet.

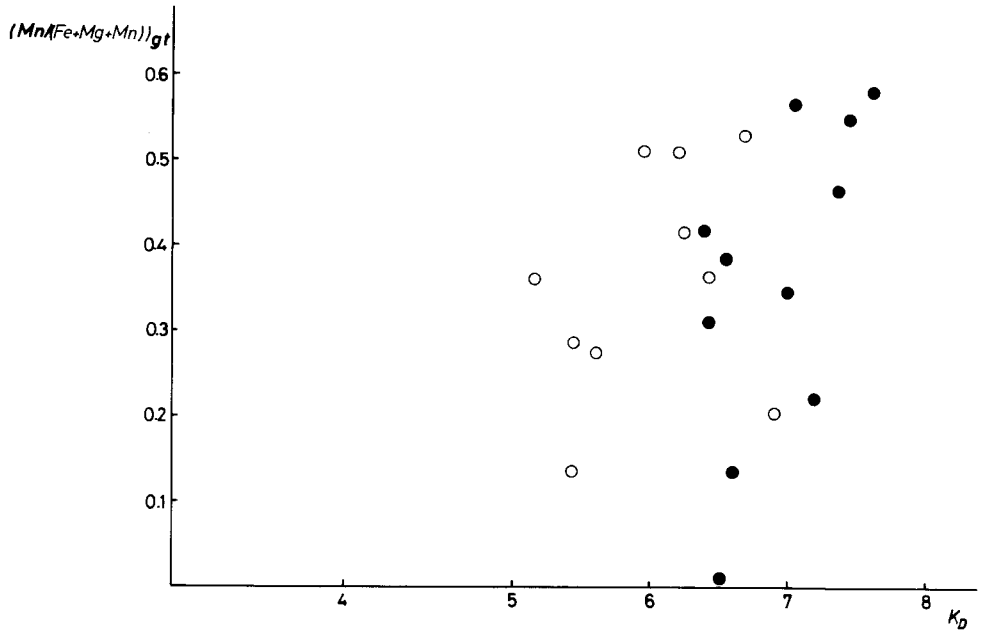

Fig. 11 Relation between K_D and Mn/(Fe+Mg+Mn) of garnet.
$K_D = (Mg/Fe)^{bt}/(Mg/Fe)^{gt}$
open circle : core part of garnet
closed circle : rim part of garnet

The pressure during metamorphism is usually estimated for given temperature. Since the difference between temperatures for garnet core and rim compositions is small (35°C), the intermediate temperature (530°C) was used for estimation of pressure.

Compositions of muscovite coexisting with microcline + biotite + quartz and of garnet-plagioclase pair coexisting with kyanite + quartz may allow the calibration of pressure.

Velde (1965) experimentally gave the relationship among temperature, pressure and celadonite content of muscovite coexisting with K-feldspar and biotite when $P = P_{H_2O}$. Figs. A and E of Velde (1965) present the following equations;

$$X = -(T - 973)(0.26 + \frac{0.21}{2.5}(P - 2000))/400 \quad \text{(when } Y = 1\text{)}$$

and

$$X = -(T - 973)(0.32 + \frac{0.06}{2.5}(P - 2000))/400 \quad \text{(when } Y = 0.5\text{)}$$

where X and Y represent the $Mg+Fe^{2+}$ and $Mg/(Mg+Fe^{2+})$ values, respectively. If we assume that the X value changes linearly according to the Y value, the relationship between composition of muscovite and pressure is obtained for T = 530°C (Fig. 12). The compositions of muscovite in five psammitic gneisses give metamorphic pressure ranging from 5.9 Kb to 6.5 Kb.

As a second geobarometer the following reaction is available (Ghent, 1976): 3 anorthite = grossular + kyanite + quartz.

The equibibrium constant is given by

$$0 = -\frac{3272}{T} - 8.3969 - \frac{0.3448\,(P-1)}{T} + \log a^{gt}_{gros} - 3 \log a^{pl}_{an}$$

(Ghent, 1976). The activity of anorthite in plagioclase is $\gamma^{pl}_{an} X^{pl}_{an}$, where $\gamma^{pl}_{an} = 1.28$ for sodic plagioclase (Orville, 1972). The activity of

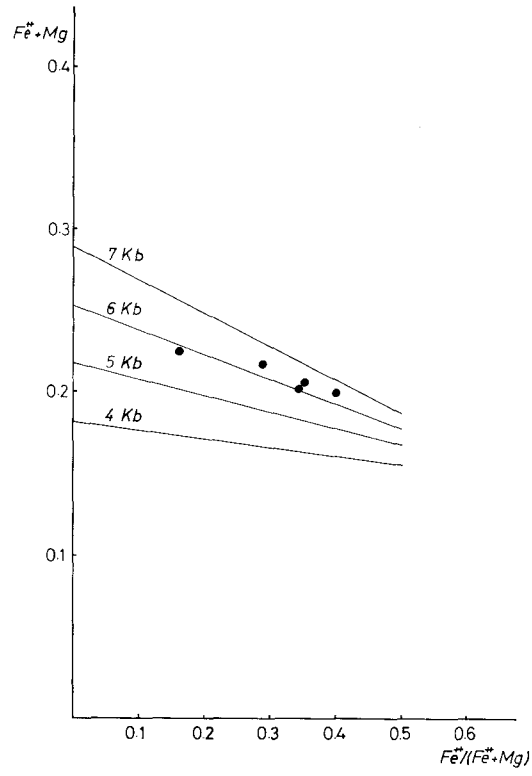

Fig 12 Relation between pressure and composition of muscovite coexisting with biotite and microcline for T = 530 °C.

grossular in garnet is given by $(\gamma^{gt}_{gros} X^{gt}_{gros})^3$, assuming random mixing in the three 8-fold sites. For a regular solution model for the binary solution grossular-almandine,

$$\ln \gamma^{gt}_{gros} = \frac{(1 - X^{gt}_{gros})^2}{RT} W$$

is given, where W is the regular solution parameter and estimated to be 1000 cal/mole by Ganguly and Kennedy (1974).

Pressure was calculated from three kyanite-bearing gneisses for T = 530°C. The result is shown in Table 8. The estimated pressure ranges from 6.5 Kb to 7.1 Kb and corresponds well to that obtained from the composition of muscovite.

Table 8. Estimation of pressure from garnet and plagioclase compositions.

sample	X^{pl}_{an}	X^{gt}_{gros}	γ^{gt}_{gros}	log K_D	P (Kb)
P-1 (rim garnet)	0.299	0.0837	0.526	−1.29	7.1
P-2 (core garnet)	0.064	0.0162	0.607	−1.32	7.0
P-2 (rim garnet)	0.064	0.0156	0.607	−1.37	6.9
P-4 (core garnet)	0.075	0.0162	0.607	−1.53	6.5
P-4 (rim garnet)	0.075	0.0163	0.606	−1.52	6.5

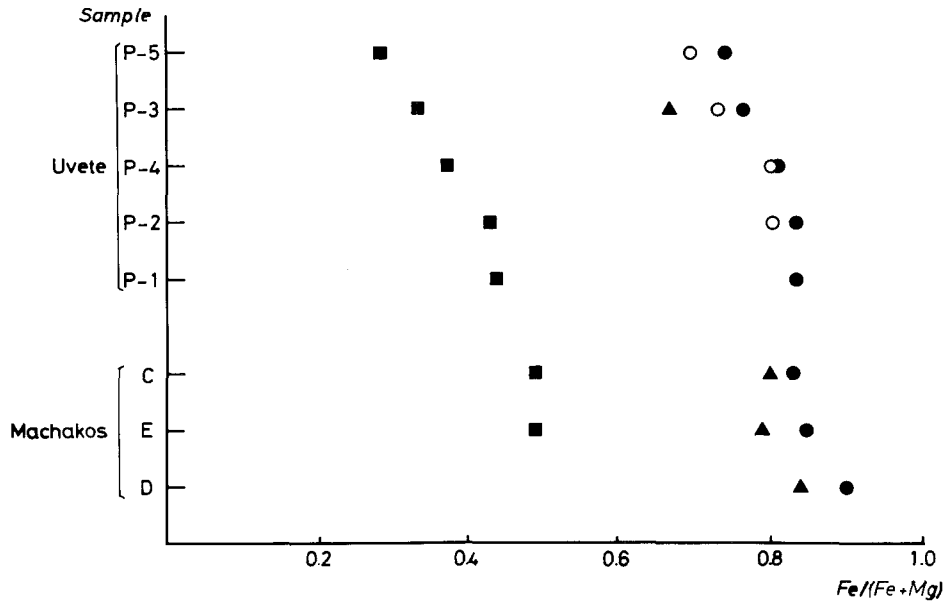

Fig. 13 The Mg/(Fe+Mg) values of staurolite, biotite and garnet in pelitic gneisses in the Uvete area (this study) and the Machakos area (Inoue and Suwa, 1979).
open circle : core part of garnet closed triangle : staurolite
closed circle : rim part of garnet closed square : biotite

The large uncertainty in temperature gives a tremendous uncertainty in pressure for above the two geobarometers. However both geobarometers gave almost similar pressure for a given temperature, which means that the temperature (530°C) is a good estimation.

Consequently the physical conditions during metamorphism in the Uvete area were estimated at 530 ± 40°C and 6.5 ± 0.5 Kb.

Comparison with the Machakos area

The petrological studies of pelitic gneisses in the Machakos area were reported by Inoue and Suwa (1979).

The dominant mineral assemblage of pelitic gneisses in the Machakos area is kyanite-staurolite-garnet-biotite-muscovite-plagioclase-quartz. On the other hand staurolite rarely occurs in pelitic gneisses in the Uvete area and the chemical composition of staurolite from the Uvete area is much higher in ZnO than that from the

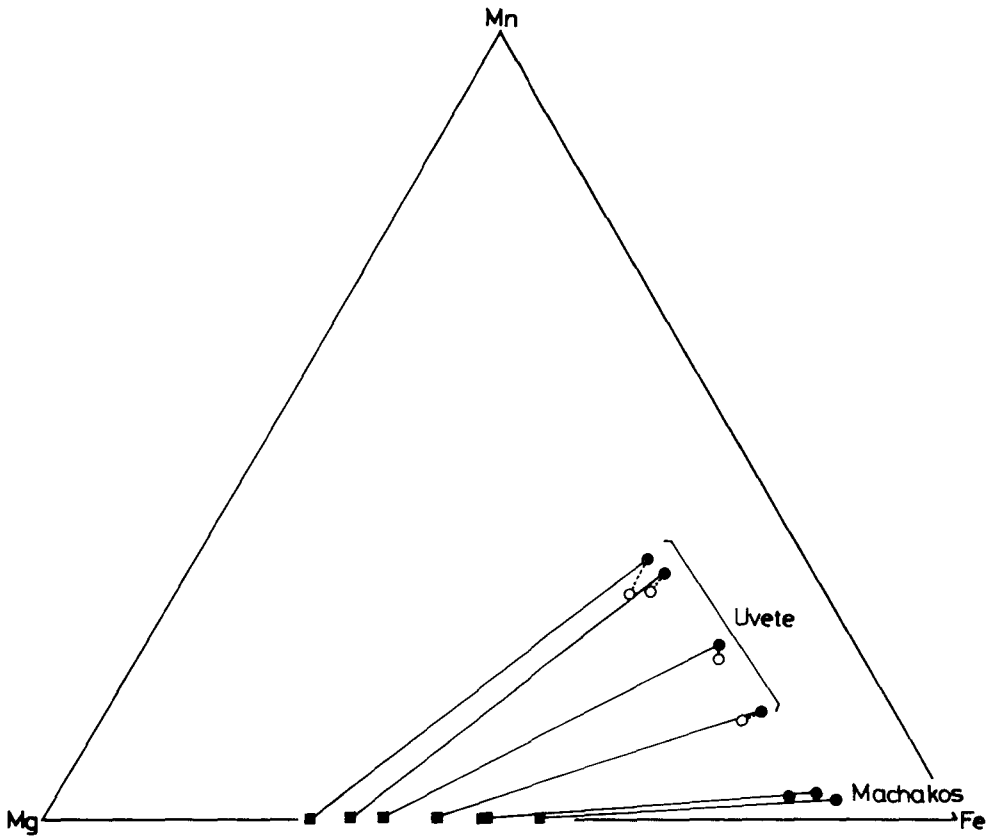

Fig. 14 Fe-Mg-Mn diagram of biotite and garnet in muscovite-bearing pelitic gneisses in the Uvete area (this study) and the Machakos area (Inoue and Suwa, 1979).
open circle : core part of garnet
closed circle : rim part of garnet
closed square : biotite

Machakos area (Fig. 4). Guidotti (1970) described that the ZnO content in staurolite increases with rising metamorphic grade and this means that sizable amounts of ZnO stabilize staurolite. Fig. 13 shows compositions of staurolite, biotite and garnet in pelitic gneisses in the Uvete and Machakos areas in terms of Fe/(Fe+Mg). The minerals from the Uvete area are more magnesian than those from the Machakos area.

There may be two ways of explaining for the above differences between the Uvete and Machakos areas.

The first explanation is that the metamorphic grade in the Uvete area is higher than that in the Machakos area. But the estimated temperature in the Uvete area (530 ± 40°C) is not higher than the temperature (525-590°C) in the Machakos area (Inoue and Suwa, 1979).

Another explanation is that the bulk composition of pelitic gneisses in the Uvete area is MgO-richer, MnO-richer and/or FeO-poorer than that in the Machakos area. Fig. 14 shows that garnet in the muscovite-bearing pelitic gneisses in the Uvete area is Mn-richer and coexists with Mg-richer biotite than that in the Machakos area and the tie lines between garnet and biotite in both areas never cut each other. Thus biotite in the Uvete area is considered to be too Mg-richer to coexist with staurolite with poorer ZnO. This could explain why staurolite rarely occurs in the Uvete area. However, because sizable amounts of ZnO stabilize staurolite, Mg-rich biotite can coexist with only Zn-rich staurolite.

Considering of the effect of MnO and ZnO, the phase parageneses of pelitic gneisses in the Uvete and Machakos areas are consistent with each other and the metamorphic grade in both areas is essentially similar.

Acknowledgements – I wish to express my sincere thanks to Dr. K. Suwa for his helpful guidance and encouragement throughout this study and for his critical reading of this manuscript. My thanks are extended also to Mr. I. Hiraiwa for providing many thin sections. Thanks are also due to Professor I. S. Loupekine and the late Dr. A. R. T. Hove of the University of Nairobi for their kind advice and encouragement during my stay in Kenya.

REFERENCES

BAKER, B. H. (1954): Geology of the southern Machakos district. *Report No.* **27**, *Geol. Surv. Kenya.*

BIYAJIMA, K. (1976): Petrological study of the Mozambique metamorphic rocks in the Machakos area, Kenya. *MS., Dept. Earth Sci., Nagoya Univ. (in Japanese)*

BIYAJIMA, K. SUWA, K. and MIYAKAWA, K. (1975): Mantled gneiss dome in the Mozambique belt around the Machakos area, Kenya. *1st Prelim. Rept. Afr. Studies, Nagoya Univ.*, 6-13.

BUTLER, B. C. M. (1967): Chemical study of minerals from the Moin scists of the Ardnamurchan area, Argyshire, Scotland. *J. Petrol.*, **8**, 233-267.

EVANS, B. W. and GUIDOTTI, C. V. (1966): The sillimanite-pottash feldspar isograd in western Main, U.S.A. *Contri. Mineral. Petrol.*, **12**, 25-62.

GANGULY, J. and KENNEDY, G. C. (1974): The energetics of natural garnet solid solution I. Mixing of the aluminosilicate endmembers. *Contri. Mineral. Petrol.*, **48**, 137-148.

GHENT, E. D. (1976): Plagioclase-garnet-Al_2O_3-quartz: a potential geobarometer-geothermometer. *Am. Mineral.*, **61**, 710-714.

GUIDOTTI, C. V. (1970): The mineralogy and petrology of the transition from the lower to upper sillimanite zone in the Oquossoc area, Main. *J. Ptrol.* **11**, 277-336.

HESS, P. C. (1967): The metamorphic paragenesis of cordierite in pelitic rocks. *Contri. Mineral. Petrol.*, **24**, 191-207.

INOUE, H. and SUWA, K. (1979): Petrographical note on staurolite-kyanite-almandine pelitic gneiss occurring at the western foot of the Mbooni Hills, Machakos area, Kenya - with special reference to the ZnO content in staurolite. *4th Prelim. Rept. Afr. Studies, Nagoya Univ.*, 97-111.

MIYAKE, A. and SUWA, K. (1981): Geological structure of the Uvete dome, Kenya. *6th Prelim. Rept. Afr. Studies, Nagoya Univ.*, 33-41.

NUREKI, T., SUWA, K., BIYAJIMA, K., SAKA, Y. and YUSA, Y. (1977): Tectonic evolution of the Mozambique belt in area southeast of Machakos, Kenya. *2nd Prelim. Rept. Afr.Studies, Nagoya Univ.*, 13-38.

ORVILLE, P. M. (1972): Plagioclase cation exchange equilibria with aqueous chloride solution: results at 700°C and 2000 bars in the presence of quartz. *Am. J. Sci.*, **272**, 234-272.

SHARMA, R. S. and NARAYAN, V. (1975): Distribution of elements between coexisting garnet-biotite and muscovite-biotite pairs from polymetamorphic schists of south-east beavar, Rajasthan, India. *Schweiz. Mineral. Petrogr. Mitt.*, **55**, 61-75.

SUWA, K., NUREKI, T., INOUE, H., BIYAJIMA, K. and MIYAKAWA, K. (1979): Geology and petrology of the Machakos area, Kenya. *4th Prelim. Rept. Afr. Studies, Nagoya Univ.*, 3-20.

THOMPSON, A.B. (1976): Mineral reactions in pelitic rocks: II. Calculation of some P-T-X(Fe Mg) phase relations. *Am. J. Sci.*, **276**, 425-454.

THOMPSON, J. B. (1957): The graphical analysis of mineral assemblages in pelitic schists. *Am. Mineral.*, **42**, 842-858.

VELDE, B. (1965): Phengite micas: synthesis, stability, and natural occurrence. *Am. J. Sci.*, **263**, 886-913.

Mozambique metamorphic rocks in the Kilungu area, central Kenya

Masao ASAMI*, Hayao UMEMURA**, Katsuyasu TOKIEDA***
and Kanenori SUWA****

* Department of Geological Sciences, College of Liberal Arts, Okayama University
** Department of Geology, Faculty of Science, Kochi University
*** Department of Physics, Faculty of Science, Shimane University
**** Department of Earth Sciences, Faculty of Science, Nagoya University

Abstract

Metamorphic rocks of the Mozambique belt in the Kilungu area have geologically and petrologically been investigated, and some results are preliminarily presented here.

Two types of metamorphic rocks are recognized; one is the paragneiss of pelitic, semi-pelitic, psammitic and basic compositions, and the other is granitoid gneiss. The paragneiss of this area conformably covers the paragneiss in the Uvete area to the south, and is covered with that in the Machakos area to the north. An antiform structure on a large scale, which represents the northern extention of the Uvete dome structure, is developed in the whole Kilungu area. The pelitic gneiss is characterized by the mineral assemblage kyanite-staurolite-garnet and the basic gneiss is by that garnet-hornblende-epidote-plagioclase. On the basis of the assemblage of the pelitic gneiss, the metamorphic grade of this area can be assigned to that of the kyanite zone in the Barrovian sequence.

Introduction

The Kilungu area is situated between the Machakos and the Uvete areas in central Kenya (Fig. 1).

B.H. Baker (1954) was the first to study the geology of the Machakos and adjacent areas. After Baker's work, geological and petrological studies of the Machakos and the Uvete areas have been made in more detail by the geologists mainly of Nagoya University since 1973 (Biyajima et al., 1975; Miyakawa and Suwa, 1975, 1977 and 1979; Nureki et al., 1977; Inoue and Suwa, 1979; Suwa et al., 1979; Miyake and Suwa, 1981; Miyata and Saka, 1981a and b; Saka and Miyata, 1981a and b). The Mozambique belt of these areas are characterized by development of granitoid gneiss domes and metamorphic rocks of the kyanite-zone grade. However, the granitoid gneiss domes in the Machakos and the Uvete areas are apart more than 20 km from each other as shown in Fig.1, so that it has been difficult to correlate geological relations between the two areas.

8th Prelim. Rept. Afr. Studies, Nagoya Univ., 97-104, 1983.

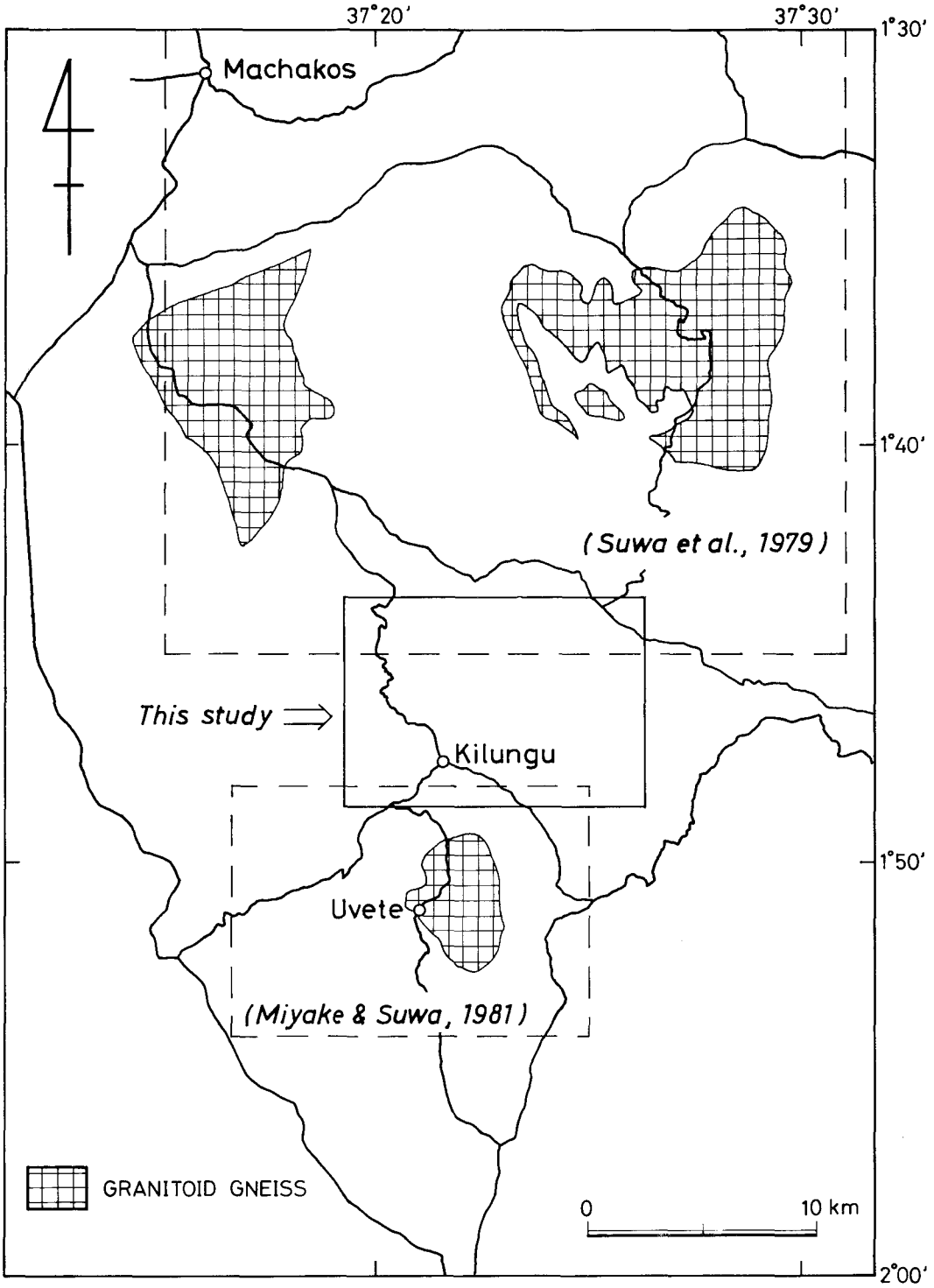

Fig. 1 Index map showing locations of the Kilungu area and the adjacent Machakos and Uvete areas.

We were engaged in geological survey of this area from 4th July to 14th August, 1981, during our stay in Kenya. This is a preliminary report on geology and petrology of the Mozambique metamorphic rocks in the Kilungu area.

Rock types and field occurrence

Fig. 2 shows the geological map of the kilungu area. This area occupies the northern slope of a ridge on which Kilungu, Kilome and Kikoko are located (Fig. 2 and Plate II-1).

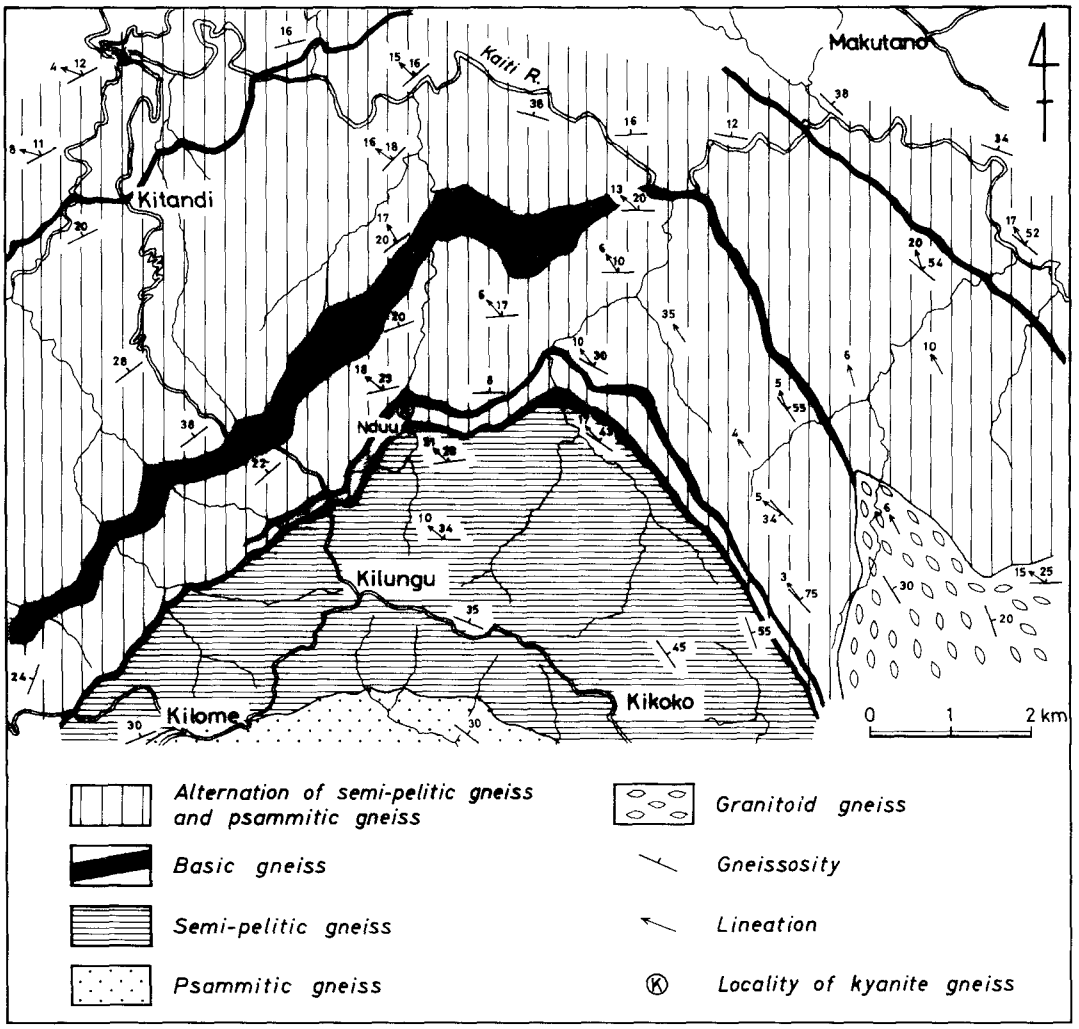

Fig. 2 Geological map of the Kilungu area.

Paragneiss is the dominant metamorphic rocks in the area. A small mass of granitoid gneiss is found, and dykes, veins and pools of pegmatite are also locally found. The paragneiss consists of pelitic gneiss, semi-pelitic gneiss, psammitic gneiss and basic gneiss. The semi-pelitic gneiss is the most predominant gneiss to occur among them and the pelitic gneiss is the most inferior.

Semi-pelitic gneiss is richer in mica than psammitic gneiss. The former occurs often in alternation with the latter (Plates I-1 and II-2) but occurs occasionally with seams of pelitic gneiss (Plate III-1). Garnet porphyroblasts are developed in some semi-pelitic gneiss (Plate III-2).

Psammitic gneiss is leucocratic and ill-foliated in appearance due to scarcity of mica minerals. At some exposures showing the alternation of psammitic gneiss with semi-pelitic gneiss, the former occurs as thicker layers, whose thickness reaches several ten metres, than the latter. Seams, veins and boudins of quartzose rock are often found in psammitic gneiss and semi-pelitic gneiss (Plate VIII-1 and 2).

Basic gneiss is essentially hornblende gneiss, and occurs as layers concordantly intercalated in semi-pelitic gneiss and psammitic gneiss. Basic gneiss shows conspicuous banded structure which is a result of alternation of hornblende-rich layers with plagioclase and/or epidote-rich layers (Plate IV-1). It is inferred from such field occurrence that the origin of basic gneiss may not be basic lava flows or sheets but sedimentary rocks such as basic tuff. In some localities, large hornblende porphyroblasts are found to be arranged on the gneissosity plane (Plate IV-2).

Pelitic gneiss occurs mostly as thin layers or rarely as thick layers, both of which are intercalated in semi-pelitic gneiss. An example of the thick layers is seen at an exposure along the river near Nduu (Plate V-1 and 2). The kyanite-bearing gneiss appears to be coarser-grained than adjacent semi-pelitic gneiss due to development of many porphyroblasts of kyanite, garnet, staurolite and plagioclase, especially the first of which reaches 25 cm in maximum length (Plates I-2, VI-1 and 2).

Granitoid gneiss is found as a discordant mass in the southeastern part of this area. This rock resembles psammitic gneiss at first glance, but it can be distinguished from the latter by uniform appearance in rock facies through the mass; i.e. it shows neither compositional banding nor marked variation in grain size.

Pegmatite is often found in semi-pelitic gneiss, psammitic gneiss and pelitic gneiss (Plate VII-1). Pegmatite sometimes contains garnet.

Stratigraphy

The paragneiss of the Kilungu area can be distinguished into four geologic units as shown in Fig.2; they are psammitic gneiss layer, semi-pelitic gneiss layer, basic gneiss layer and alternated unit of semi-pelitic gneiss and psammitic gneiss. Some layers of basic gneiss are useful as key beds to the stratigraphy because of their distinctive colour and lateral continuity. In this area, the gneissosity of the paragneiss is mostly parallel to the original bedding and is generally inclined to NE, N or NW (Fig. 2). Thus, the lowermost horizon of the paragneiss is represented by the psammitic

gneiss layer near Kilome, and the uppermost horizon by the alternated unit of semi-pelitic gneiss and psammitic gneiss which occurs north of Kitandi. The lowermost layer in this area corresponds to the layer of psammitic gneiss (6) in the Uvete area (Miyake and Suwa, 1981), and the uppermost layer corresponds to the alternated unit of semi-pelitic gneiss and psammitic gneiss occurring in the southernmost part of the Machakos area (Suwa et al., 1979).

Geological structure

The dominant planar structure of the metamorphic rocks is gneissosity of the paragneiss and granitoid gneiss. The gneissosity is defined by compositional banding developed parallel to the original bedding or by parallel alignment of mica minerals. Folds on a small scale are sometimes found (Plates VII-2 and VIII-1). The strike and dip of the gneissosity were measured and the results are plotted in Fig. 3. Some of the results are shown in Fig. 2. Figs.2 and 3A suggest the presence of an antiform on a large scale, the axis of which plunges gently northward. Clearly this structure represents the northern extention of a dome structure recognized in the Uvete area (Miyake and Suwa, 1981). The strike and dip of the gneissosity of granitoid gneiss vary from an exposure to the others, though it occurs as a small rock mass (Fig. 3B).

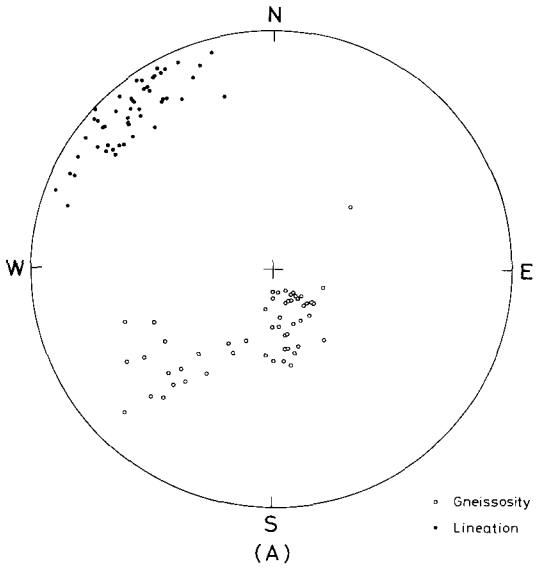

Fig. 3A Equal area projection of genissosity and lineation of paragneiss (lower hemisphere).

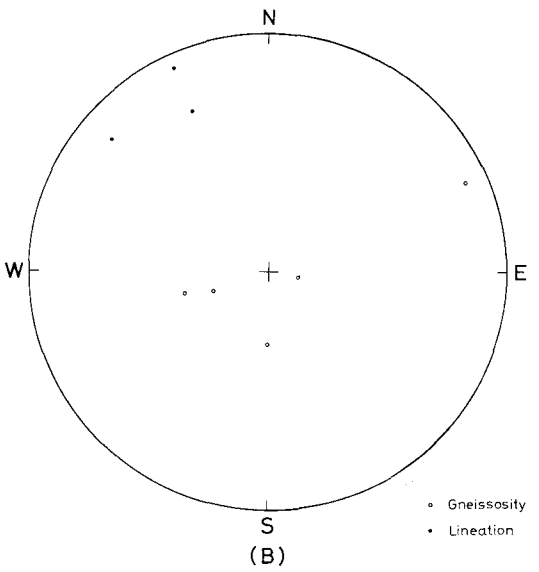

Fig. 3B Equal area projection of gneissosity and lineation of granitoid gneiss (lower hemisphere).

Crenulations are often found in the paragneiss. In many cases, lineation is defined by hinge lines of crenulations or minor folds. The other two types of lineation are also found in the paragneiss; one is intersections of the gneissosity and the axial plane cleavage which is accompanied with minor folds (Plate VII-2), and the other is necklines of boundins (Plate VIII-2). When all or some of types of lineation are developed together on one outcrop, they are parallel to each other. The results of measurement are shown in Figs. 2 and 3. The lineation of the paragneiss pitches gently towards NNW to WNW, and tends to be plotted around a great circle (Fig. 3A). Fig. 3A shows that the trends of lineation in the Kilungu area are similar to the general lineation trend observed in the Machakos area (Nureki et al., 1977; Suwa et al., 1979). The general trend of lineation in the granitoid gneiss seems to be concordant with that of the paragneiss (Fig. 3A and B).

Mineral assemblage

Mineral assemblages of the metamorphic rocks in the Kilungu area are presented in Table 1. Replacement textures of primary metamorphic minerals by secondary ones, such as kyanite altered to white mica, are observed in some rocks. The sec-

Table 1. Mineral assemblages of metamorphic rocks.

Semi-pelitic gneiss		
(1) Bi-Mu-Kf-Pl-Qu	(±Sph)	(+Ore)
(2) Ep-Bi-Mu-Kf-Pl-Qu	(+Sph)	
(3) Ga-Bi-Mu-Kf-Pl-Qu	(+Sph)	
(4) Ga-Ep-Bi-Mu-Kf-Pl-Qu	(+Sph)	
(5) Ga-Bi-Kf-Pl-Qu	(+Sph)	
Psammitic gneiss		
(1) Bi-Mu-Kf-Pl-Qu	(±Sph)	(+Ore)
(2) Ep-Bi-Mu-Kf-Pl-Qu	(+Sph)	
(3) Ga-Bi-Mu-Kf-Pl-Qu		
(4) Ga-Ep-Bi-Mu-Kf-Pl-Qu		
Basic gneiss		
(1) Hb-Ep-Bi-Pl-Qu	(+Sph)	(+Ore)
(2) Hb-Ep-Pl-Qu	(±Sph)	
(3) Ga-Hb-Ep-Bi-Pl-Qu	(+Sph)	
(4) Ga-Hb-Ep-Bi-Kf-Pl-Qu	(+Sph)	
Pelitic gneiss		
(1) Ky-St-Ga-Mu-Pl±Qu	(+Ru)	(+Ore)
(2) Ky-St-Mu-Pl	(+Ru)	
(3) Ky-Mu-Pl±Qu		
(4) St-Ga-Mu-Pl-Qu	(+Ru)	
(5) Ga-Mu	(+Ru)	
(6) Ga-Bi-Mu-Kf-Pl-Qu		
(7) Ga-Ep-Bi-Mu-Kf-Pl-Qu	(±Sph)	
(8) Ga-Ep-Bi-Mu-Pl-Qu	(±Sph)	
(9) Bi-Mu-Kf-Pl-Qu	(±Sph)	
(10) Ep-Bi-Mu-Kf-Pl-Qu	(+Sph)	
(11) Bi-Mu-Pl±Qu		
(12) Ep-Bi-Pl-Qu		
(13) Bi-Mu-Qu±Ga		
Granitoid gneiss		
(1) Hb-Ep-Bi-Kf-Pl-Qu	(+Sph)	(+Ore)
(2) Hb-Ep-Bi-Pl-Qu	(+Sph)	
(3) Bi-Kf-Pl-Qu	(+Sph)	

Abbreviations: Bi-biotite, Ep-epidote, Ga-garnet, Hb-hornblende, Kf-K-feldspar, Ky-kyanite, Mu-muscovite, Ore-ore mineral, Pl-plagioclase, Qu-quartz, Ru-rutile, Sph-sphene, St-staurolite.

ondary minerals of replacement origin are eliminated from the mineral assemblages given in Table 1, and only minerals which appear to coexist in texture are listed. K-feldspar is microcline in all the assemblages. Most of the metamorphic rocks contain apatite and zircon as accessories. The mineral assemblages of psammitic gneiss are essentially the same as those of semi-pelitic gneiss.

In basic gneiss, hornblende exhibits the Z-axial colour of bluish green to green and coexists with epidote and plagioclase, and often with garnet. The refractive index β of plagioclase in six specimens of basic gneiss is comparable with the refractive indices of quartz contacting with the plagioclase: $\omega_{Qu} < \beta_{Pl} < n_{e_{Qu}}$, i.e. $1.544 < \beta_{Pl} \leqq 1.553$. The plagioclase compositions may be estimated to be An_{20-40} after Smith (1958). On the other hand, the assemblage kyanite-staurolite-garnet in pelitic gneiss indicates the metamorphic grade to be of the kyanite zone in the Barrovian metamorphic sequence (Chinner, 1965). Thus, the hornblende-epidote-plagioclase assemblage in the present case is not that of the epidote amphibolite facies but of the amphibolite facies. Such characteristic mineral assemblages from this area may be correlated with those from the Machakos and the Uvete areas (Biyajima et al., 1975; Nureki et al., 1977; Inoue and Suwa, 1979; Miyake and Suwa, 1981).

Acknowledgement — The manuscript was critically read by Prof. T. Nureki of Okayama University, to whom we would like to express sincere thanks.

REFERENCES

BAKER, B.H. (1954): Geology of the southern Machakos district. *Report No.27, Geol. Surv. Kenya.*

BIYAJIMA, K., SUWA, K. and MIYAKAWA, K. (1975): Mantled gneiss dome in the Mozambique belt around the Machakos area, Kenya. *1st Prelim. Rept. Afr. Studies, Nagoya Univ.*, 6-13.

CHINNER, G.A. (1965): The kyanite isograd in Glen Clova, Angus, Scotland. *Mineral. Mag.*, **34**, 132-143.

INOUE, H. and SUWA, K. (1979): Petrographical note on staurolite-kyanite-almandine pelitic gneiss occurring at the western foot of the Mbooni Hill, Machakos area, Kenya — with special reference to the ZnO content in staurolite. *4th Prelim. Rept. Afr. Studies, Nagoya Univ.*, 97-111.

MIYAKAWA, K. and SUWA, K. (1975): An occurrence of staurolite from the Kioo pegmatite, Machakos District, Kenya. *1st Prelim. Rept. Afr. Studies, Nagoya Univ.*, 52-54.

MIYAKAWA, K. and SUWA, K. (1977): A note on the granitoid gneisses from the Machakos area, Kenya. *2nd Prelim. Rept. Afr. Studies, Nagoya Univ.*, 154-160.

MIYAKAWA, K. and SUWA, K. (1979): The Kalama psammitic gneisses from the Kalama Hills, Machakos area, Kenya. *4th Prelim. Rept. Afr. Studies, Nagoya Univ.*, 113-122.

MIYAKE, A. and SUWA, K. (1981): Geological structure of the Uvete dome, Kenya. *6th Prelim. Rept. Afr. Studies, Nagoya Univ.*, 33-41.

MIYATA, T. and SAKA, Y. (1981a): Strain distribution around the Uvete dome, Machakos, Kenya: Summary. *6th Prelim. Rept. Afr. Studies, Nagoya Univ.*, 67-71.

MIYATA, T. and SAKA, Y. (1981b): Boundinage structures in the Mozambiquian metamorphic rocks, south of Machakos, Kenya. *6th Prelim. Rept. Afr. Studies, Nagoya Univ.*, 73-81.

NUREKI, T., SUWA, K., BIYAJIMA, K., SAKA, Y. and YUSA, Y. (1977): Tectonic evolution of the Mozambique belt in area south-east of Machakos, Kenya. *2nd Prelim. Rept. Afr. Studies, Nagoya Univ.*, 13-38.

SAKA, Y. and MIYATA, T. (1981a): Primary sedimentary structures found in the gneisses of the Mozambique metamorphic belt near Machakos, Kenya. *6th Prelim. Rept. Afr. Studies, Nagoya Univ.*, 43-52.

SAKA, Y. and MIYATA, T. (1981b): Mega- and mesoscopic folds in the Mozambique metamorphic belt, south of Machakos, Kenya. *6th Prelim. Rept. Afr. Studies, Nagoya Univ.*, 53-66.

SMITH, J.R. (1958): The optical properties of heated plagioclases. *Am. Mineral.*, **43**, 1179-1194.

SUWA, K., NUREKI, T., INOUE, H., BIYAJIMA, K. and MIYAKAWA, K. (1979): Geology and petrology of Machakos area, Kenya. *4th Prelim. Rept. Afr. Studies, Nagoya Univ.*, 3-20.

PLATE I

1. Alternation of semi-pelitic gneiss and psammitic gneiss, 1km north of Kitandi.

2. Kyanite-bearing pelitic gneiss from Nduu, in which large porphyroblasts of kyanite, garnet, staurolite and plagioclase are developed.

1

2

PLATE II

1. A view of the northern slope of a ridge near Kilungu.

2. Alternation of semi-pelitic gneiss (lower half) and psammitic gneiss (upper half), dipping gently to the northwest, 1.5 km north of Kitandi.

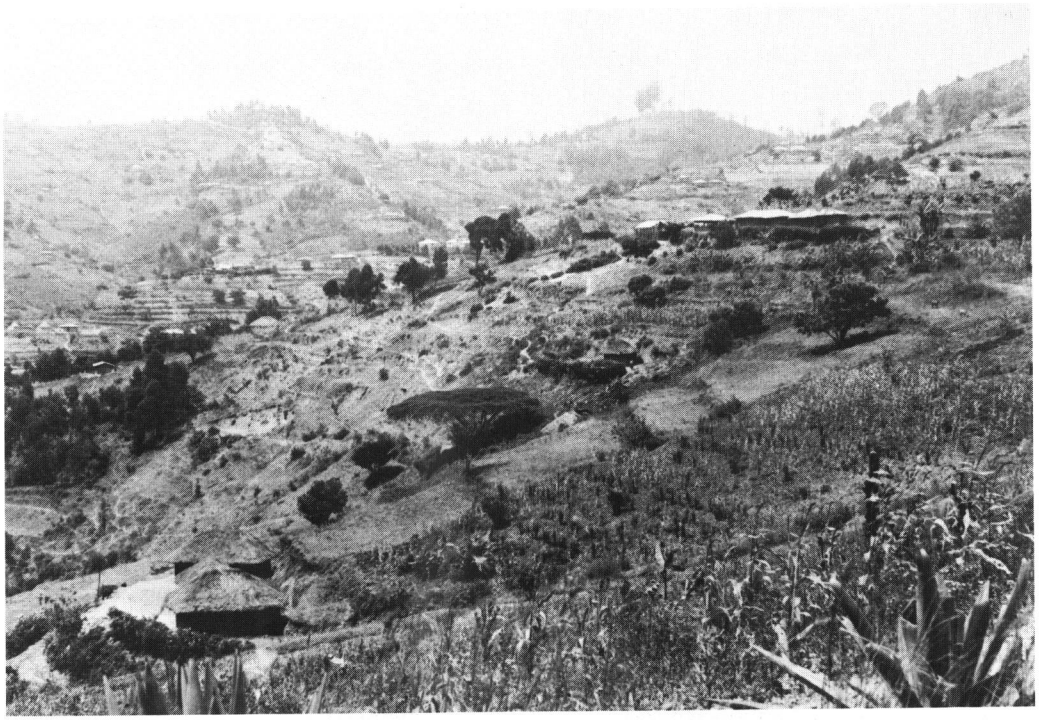

1

2

PLATE III

1. Pelitic gneiss seams intercalated in semi-pelitic gneiss, 1.5 km north of Kitandi.

2. Garnet-bearing semi-pelitic gneiss dipping steeply to the northeast, Kaiti River 3 km south-southeast of Makutano.

1

2

PLATE IV

1. Well-banded basic gneiss occurring comformably with semi-pelitic gneiss, Nduu.

2. Large hornblende porphyroblasts developed in basic gneiss, 1 km west of Kitandi.

PLATE IV

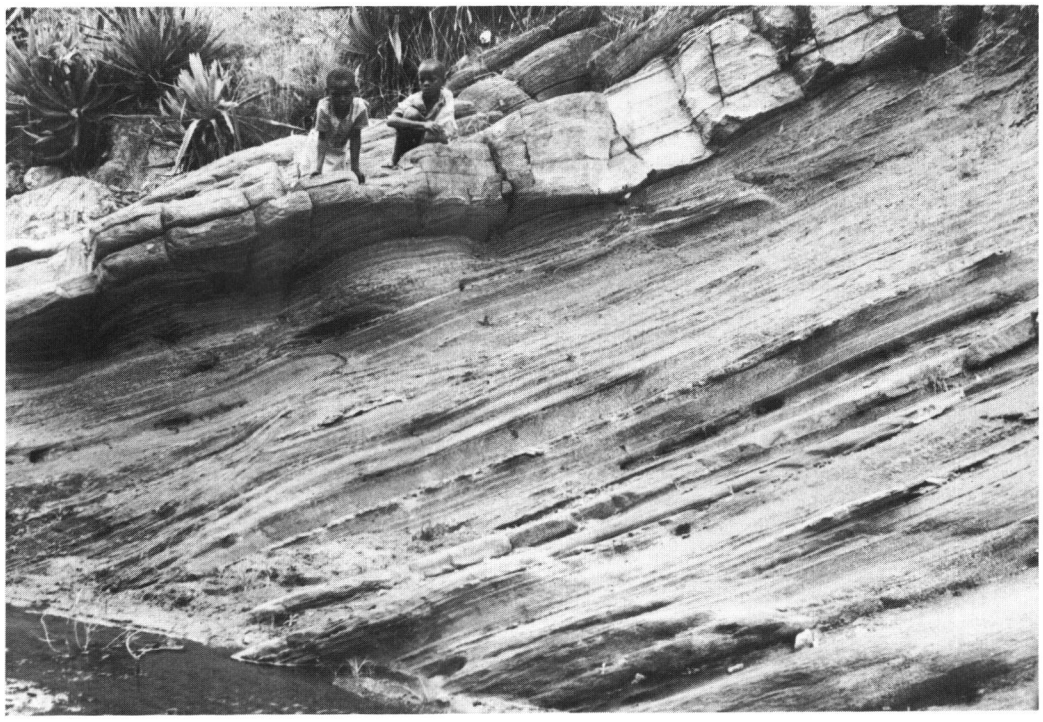

1

2

PLATE V

1. An outcrop of kyanite-bearing pelitic gneiss layers, Nduu.

2. Kyanite-bearing pelitic gneiss (lower left) with overlying semi-pelitic gneiss (centre) and basic gneiss (upper right) at the same outcrop.

PLATE V

1

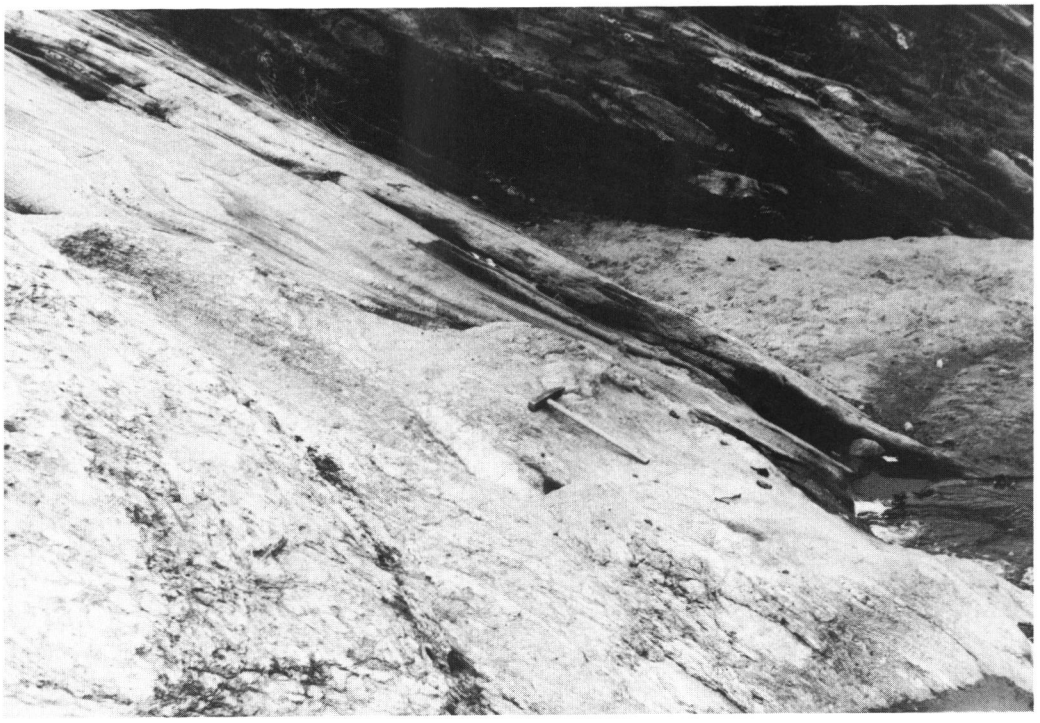

2

PLATE VI

1. Crose-up of kyanite-bearing pelitic gneiss, Nduu. Kyanite-rich part in which kyanite reaches 25 cm in maximum length.

2. Ditto. Garnet-bearing part.

PLATE VI

1

2

PLATE VII

1. A pegmatite dyke in semi-pelitic gneiss, 1 km northwest of Kitandi.

2. Minor folds with the axial plane cleavage found in semi-pelitic gneiss, 4 km northeast of Kilungu. Lineation is developed by intersections of the gneissosity plane and the axial plane cleavage.

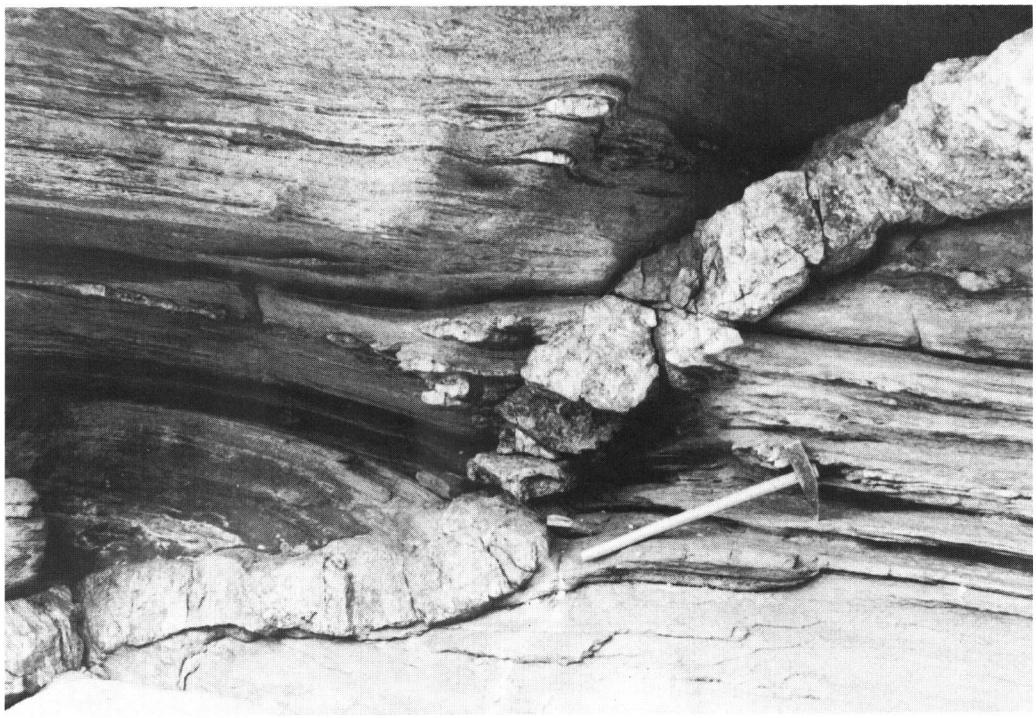

1

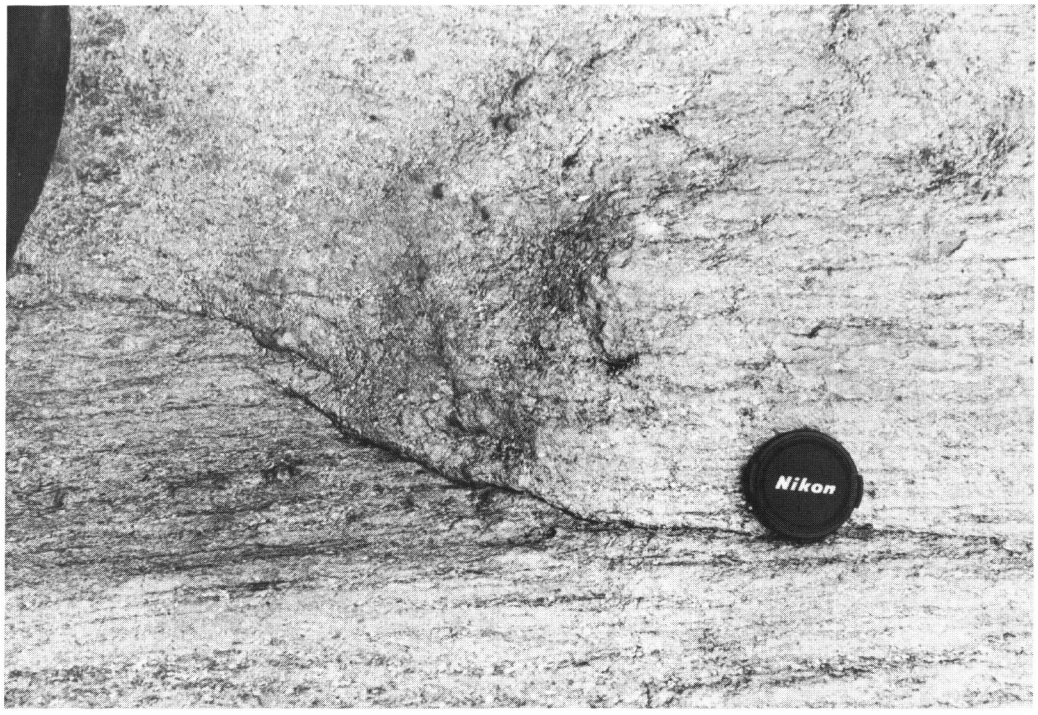

2

PLATE VIII

1. Minor folds in semi-pelitic gneiss, 1 km north of Nduu. A quartzose vein is also folded in the same manner as the surrounding gneiss.

2. Boudins of quartzose rock developed in psammitic geniss, 0.5 km north of Nduu. The direction of necklines is indicated by a pencil.

1

2

Chloritoid-bearing kyanite gneiss from the Kilungu area, central Kenya

Masao ASAMI

Department of Geological Sciences, College of Liberal Arts, Okayama University

Abstract

A chloritoid-bearing kyanite gneiss containing staurolite, garnet, muscovite, albite, quartz, ilmenite, rutile, paragonite and chlorite has been found in the Mozambique belt near Kilungu, central Kenya. Texture and mineralogy of the gneiss are presented and compatibility relations of chloritoid to the other constituents in this rock are discussed.

There is no textural and chemical evidence to suggest disequilibrium relations among kyanite, staurolite, garnet, muscovite, albite, quartz, ilmenite and rutile, setting aside a little difference in staurolite composition between porphyroblasts and small prisms in matrix. On the other hand, this rock characteristically shows some retrograde replacement textures of kyanite, staurolite and garnet by paragonite, of kyanite and garnet by chloritoid, and of garnet and staurolite by chlorite. The chemical compositions of paragonite and chlorite are evidently heterogeneous, $Mu_{10.7-45.9}$ and X_{Fe}=0.86-0.92 respectively, while chloritoid has uniform compositions (X_{Fe}=0.92-0.95). The chloritoid compositions fall within the kyanite-staurolite-garnet three-phase field on the AFM diagram. It is considered from the textural and compositional relations that chloritoid and paragonite in the gneiss were concomitantly formed by retrograde metamorphism. Hydration required for the retrograde reactions possibly resulted from a pegmatite dyke which was intruded into the chloritoid-bearing kyanite gneiss.

Introduction

Pelitic gneisses containing kyanite occur at many localities in the Mozambique belt of the Machakos and the Uvete areas, adjacent to the Kilungu area (Biyajima et al., 1975; Nureki et al., 1977; Suwa et al., 1979; Inoue and Suwa, 1979; Miyake and Suwa, 1981). Mineral assemblages of these kyanite-bearing gneisses have been considered to correspond to the kyanite-zone grade in the Barrovian metamorphic sequence (Chinner, 1965). The Mozambique belt around Kilungu is also composed of various kinds of gneiss of the kyanite-zone grade (Asami et al, 1983). During my petrological study on the pelitic gneisses of Kilungu, chloritoid was found to be in association with kyanite, staurolite and garnet. According to current view, the occurrence of chloritoid in rocks of the kyanite-zone grade appears to be unusual.

In this paper the chloritoid-bearing kyanite gneiss will be described to consider

8th Prelim. Rept. Afr. Studies, Nagoya Univ., 105-119, 1983.

the compatibility of chloritoid in the rock.

Field occurrence

The Mozambique belt around Kilungu consists of semipelitic gneiss, psammitic gneiss, basic gneiss and pelitic gneiss in descending order, whose mineral assemblages indicate metamorphic grade of this area to be of the kyanite-zone grade (Asami et al., 1983). Fig.1 shows the geological map of this area and the location of the chloritoid-bearing kyanite gneiss.

Two layers of kyanite-bearing pelitic gneiss crop out along the Kithembe River, 2.5 km north of Kilungu. They are alternated with semipelitic gneiss layers and the alternated gneiss members are interlayered between two layers of basic gneiss (Fig. 2). As noted by Inoue and Suwa (1979), it is also the case in this area that kyanite-bear-

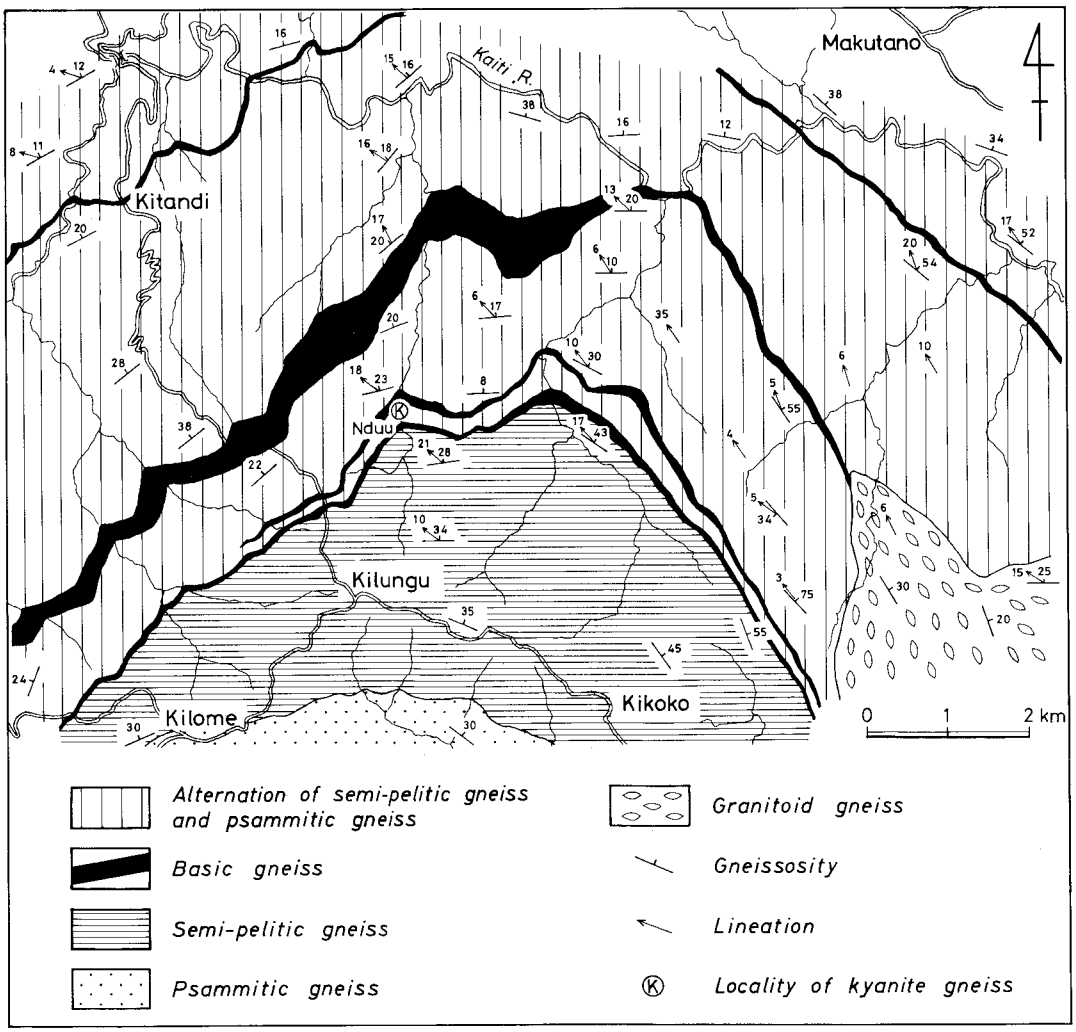

Fig. 1 Geological map of the Kilungu area (Asami et al., 1983). Locality from which the chloritoid-bearing kyanite gneiss was collected is shown.

ing pelitic gneiss occurs in close association with basic gneiss. The chloritoid-bearing kyanite gneiss is found in the upper pelitic gneiss layer (Pe II in Fig. 2). The metamorphic rocks are intruded by a pegmatite dyke (Fig. 2).

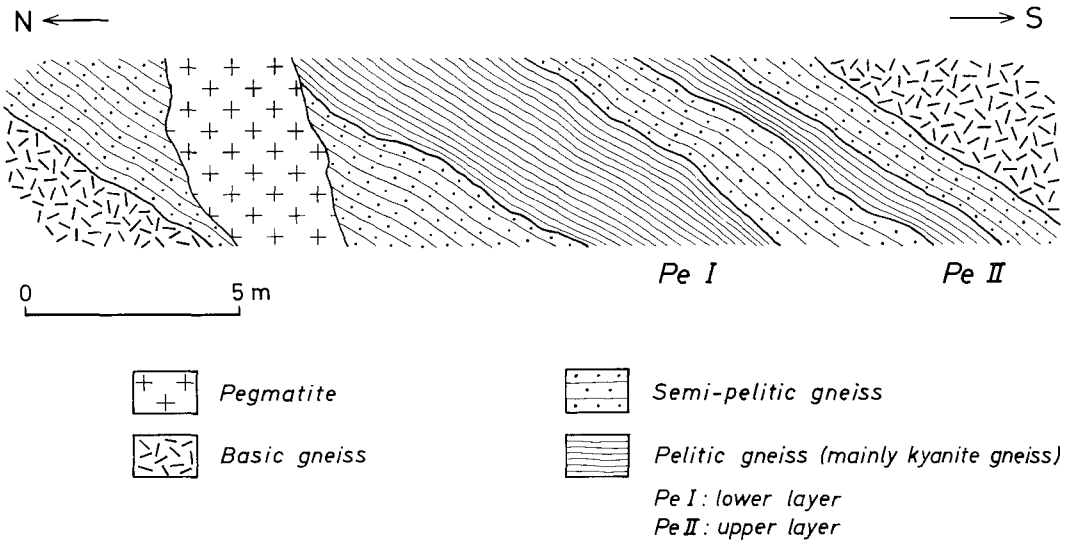

Fig. 2 Sketch showing an outcrop of kyanite-bearing pelitic gneiss and related rocks, along the Kithembe River near Nduu, 2.5 km north of Kilungu. Chloritoid-bearing gneiss is found in the upper layer of the pelitic gneiss (Pe II).

Petrography

Except for the chloritoid-bearing kyanite gneiss, pelitic gneiss now concerned has such mineral assemblages as (1) kyanite-staurolite-garnet-muscovite-plagioclase± quartz, (2) kyanite-staurolite-muscovite-plagioclase, (3) staurolite-garnet-muscovite-plagioclase-quartz, (4) kyanite-muscovite-plagioclase±quartz and (5) garnet-muscovite, with accessory ilmenite and rutile. Biotite is characteristically lacking in all the assemblages. The minerals in each assemblage described above appear to be texturally compatible with each other.

The chloritoid-bearing kyanite gneiss contains three minerals paragonite, chloritoid and chlorite, in addition to the constituents of the above assemblage (1). Plagioclase in this gneiss is albite. This rock is of coarse-grained in appearance, due to the development of many porphyroblastic crystals of kyanite, staurolite, garnet and albite.

Kyanite forms subhedral to anhedral prisms up to 2 cm in length. Its long axis is roughly oriented parallel to the gneissosity that is defined by parallel alignment of platy muscovite and prismatic ilmenite and rutile. Inclusions of albite, quartz, ilmenite and zircon are present in small amount.

Staurolite occurs in two modes: one is subhedral porphyroblasts 4 to 8 mm across and the other is stumpy prisms less than 2 mm long. Both types of staurolite show

the same pleochroism X≒Y: pale yellow and Z: golden yellow. Porphyroblastic staurolite includes poikilitically ilmenite, quartz, albite, rutile and zircon, among which prismatic ilmenite and fusiform quartz grains are arranged parallel to the gneissosity.

Garnet appears as subhedral porphyroblasts up to 8 mm across. It carries minute inclusions, though small in amount, of quartz, ilmenite, albite and zircon.

Muscovite commonly forms euhedral to subhedral flakes less than 1 mm across which are mostly arranged parallel to the gneissosity. Some muscovite flakes show ragged outline.

Albite occurs predominantly as large anhedral crystals up to 1.5 cm long which are elongated parallel to the gneissosity. It is also present as small grains. Most of albite crystals are polysynthetically twinned. Its large crystals include poikilitically fine grains of muscovite, ilmenite, rutile and quartz, the first three minerals of which are preferably oriented parallel to the gneissosity.

Quartz is present in small amount. It is found as small grains along grain boundaries between kyanite and albite, staurolite and albite, garnet and albite, chloritoid and albite and kyanite and staurolite. Quartz is also found as inclusions in these minerals themselves.

Ilmenite and rutile are scattered in the rock as prismatic fine crystals.

On the other hand, paragonite, chloritoid and chlorite are in many cases much smaller in size than the other minerals except quartz and show no preferred orientation parallel to the gneissosity. They are interpreted as replacement products, judging from textures under the microscope.

Paragonite occurs usually as shimmer aggregates of minute flakes and rarely as somewhat larger flakes. It is characteristically found as a replacement product filling the grain boundaries between kyanite and albite, some staurolite and albite and some garnet and albite (Plate IA and B). Although white micas here called paragonite are not always Na-rich ones in composition as will be described later, white micas of secondary origin are collectively called paragonite to distinguish them from primary muscovite.

Chloritoid has clear pleochroism of X: slaty green, Y: slaty blue-green and Z: pale yellow. It occurs sporadically but in three modes: (A) small tabular crystals associated with paragonite aggregates and sometimes being contact with corroded kyanite (Plate IC and D), (B) dendritic or veinlet-like crystals growing in albite crystals and at grain boundaries between albite crystals (Plate IIA and B), and (C) tabular crystals and aggregates of anhedral grains fringing or corroding garnet (Plate IIC) and corroding kyanite in association with paragonite (Plate IID). Chloritoid is also in contact with muscovite, quartz and chlorite (Plates ID, IIB and IIC). Some crystals of chloritoid include small amounts of quartz, albite, ilmenite, rutile and paragonite.

Chlorite is trace in amount. It occurs as anhedral to subhedral fine flakes which replace partially garnet and staurolite along their margins and cracks (Plates IB and IIC). Chlorite shows pleochroism of X: pale yellow and Y≒Z: green.

Mineral chemistry

Microprobe analyses were made using JXA-733 on two grains of kyanite, three grains of staurolite, two porphyroblasts of garnet, four flakes of muscovite, four grians of albite, six flakes of paragonite, eleven grains of chloritoid and four flakes of chlorite under conditions of 15 kV acceleration voltage, 0.01-0.02 μA beam current and 3μ beam diameter. Usually, two or more points on each mineral grain were analysed except for thin or fine crystals of muscovite, paragonite, chlorite and chloritoid. ZnO could be detected only for staurolite. Representative analyses are presented in Tables 1 to 3. Compositions of staurolite, garnet, chloritoid and chlorite are plotted on the Fe-Mg-Mn diagrams (Fig.3), and those of kyanite, muscovite, albite and paragonite are plotted on the Al_2O_3-$NaAlO_2$-$KAlO_2$ diagram (Fig. 4).

Fig.3 indicates that staurolite, garnet, chloritoid and chlorite are considerably poor in Mn except for garnet interiors, and that the first three minerals are always very rich in Fe, i.e. X_{Fe} (=Fe/(Fe+Mg)) >0.90. All of muscovite, albite and paragonite are very poor in Ca (Table 3).

The kyanite contains 0.35 to 0.61 wt% iron as FeO. These values are similar to iron contents of kyanite in a pelitic gneiss from the Machakos area (Inoue and Suwa, 1979).

Of the staurolite analysed, one (St-1) is a porphyroblast surrounded by garnet, kyanite, albite, muscovite and quartz, and the other two (St-2 and St-3) are small stumpy prisms in contact with albite, muscovite and paragonite. No compositional zoning has been detected in the staurolite crystals. X_{Fe} of the staurolite porphyroblast differs from that of the stumpy prisms, being 0.90-0.92 and 0.95-0.97 respectively (Fig.3). The ZnO contents differ a little between them, i.e. 0.96-1.02 wt% in the porphyroblast and 1.18-1.28 wt% in the others. The ZnO contents of the staurolite from Kilungu fall within the values (0.00-2.51 wt%) for poikiloblastic staurolite which was reported by Inoue and Suwa (1979) from the kyanite-garnet-biotite gneiss in the Machakos area.

The garnet porphyroblasts, one (Ga-1) being 6.5 mm and the other (Ga-2) 2.3 mm in diameter, were analysed at thirteen and eleven points running across each grain respectively. They are compositionally zoned with increasing Fe and Mg and decreasing Mn, Ca and X_{Fe} from core to rim. But the rim compositions of the two porphyroblasts are almost uniform (Fig.3 and Table 1). The zoning pattern of the garnet from Kilungu is generally similar to that in kyanite gneiss from the Machakos area (Biyajima et al., 1975; Inoue and Suwa, 1979), though some garnet grains from Machakos show a reverse relation about X_{Fe}.

Platy muscovite (Mu-1 to Mu-3) has uniform paragonite contents of Pa=26.8-29.6. A muscovite flake of ragged outline (Mu-4) which is in contact with paragonite, kyanite and chloritoid has a higher value of 33.9 (Fig.4). All the muscovite are relatively low in phengite contents (Si=6.040-6.102 and Fe+Mg=0.209-0.231 in atomic proportion), compared with those in the other kyanite-bearing rocks report-

Table 1 Representative analyses of garnet, staurolite and kyanite.

	Garnet				Staurolite				Kyanite	
	Ga-1		Ga-2		St-1		St-2		Ky-1	Ky-2
	Core	Rim	Core	Rim	Core	Rim	Core	Rim		
SiO_2	36.88	36.90	36.93	36.48	27.63	27.60	27.60	27.76	36.80	36.95
TiO_2	0.01	0.00	0.00	0.01	0.79	0.88	0.62	0.67	0.01	0.02
Al_2O_3	20.55	20.79	20.82	20.83	54.29	54.13	54.23	53.61	62.86	63.22
Cr_2O_3	0.01	0.02	0.00	0.04	0.01	0.05	0.11	0.00	0.04	0.00
FeO*	37.01	40.15	39.14	38.83	14.17	13.34	12.82	12.78	0.61	0.35
MnO	2.54	0.96	1.07	0.94	0.00	0.03	0.20	0.05	0.04	0.00
MgO	0.59	1.53	1.13	1.21	0.81	0.61	0.40	0.35	0.04	0.02
ZnO	0.00	0.00	0.00	0.00	1.00	1.00	1.20	1.13	0.00	0.00
CaO	2.49	0.55	0.88	0.64	0.00	0.01	0.00	0.02	0.05	0.00
Na_2O	0.00	0.03	0.00	0.00	0.01	0.05	0.02	0.08	0.00	0.00
K_2O	0.02	0.02	0.00	0.01	0.03	0.00	0.00	0.01	0.00	0.02
NiO	0.03	0.00	0.05	0.00	0.04	0.02	0.14	0.00	0.00	0.00
Total	100.13	100.95	100.02	98.99	98.78	97.72	97.34	96.46	100.45	100.58
	24 (0)				46 (0)				20 (0)	
Si	6.030	5.988	6.030	6.013	7.642	7.686	7.711	7.810	3.969	3.973
Al	3.960	3.977	4.006	4.046	17.700	17.767	17.858	17.778	7.991	8.010
Ti	0.001	–	–	0.001	0.164	0.184	0.130	0.142	0.001	0.001
Cr	0.001	0.002	–	0.006	0.002	0.011	0.024	–	0.003	–
Fe	5.061	5.450	5.345	5.353	3.278	3.107	2.995	3.007	0.055	0.032
Mn	0.352	0.132	0.147	0.131	–	0.007	0.047	0.012	0.003	–
Mg	0.143	0.370	0.276	0.297	0.334	0.253	0.167	0.147	0.006	0.003
Zn	–	–	–	–	0.204	0.206	0.248	0.235	–	–
Ca	0.437	0.096	0.155	0.113	–	0.003	–	0.006	0.005	–
Na	–	0.009	–	–	0.005	0.027	0.011	0.044	–	–
K	0.004	0.005	–	0.001	0.011	–	–	0.004	–	0.003
Ni	0.003	–	0.007	–	0.009	0.004	0.031	–	–	–
X_{Fe}	0.973	0.936	0.951	0.947	0.908	0.924	0.948	0.953		
Al	84.4	90.1	90.2	90.8						
Py	2.4	6.1	4.7	5.0						
Sp	5.9	2.2	2.5	2.2						
Gr	7.3	1.6	2.6	1.9						

* Total iron as FeO. X_{Fe}=Fe/(Fe + Mg).

Table 2 Representative analyses of chloritoid and chlorite.

	Chloritoid						Chlorite	
	Ct-2 (Mode A)		Ct-3 (Mode B)		Ct-11 (Mode C)		Ch-1	Ch-4
	Core	Rim	Core	Rim	Rim	Rim		
SiO_2	24.10	23.93	23.96	23.77	23.90	22.94	21.62	21.42
TiO_2	0.00	0.00	0.00	0.00	0.00	0.00	0.06	0.00
Al_2O_3	39.20	39.07	39.22	39.74	39.17	39.87	21.57	21.97
Cr_2O_3	0.00	0.00	0.02	0.07	0.09	0.04	0.04	0.07
FeO*	26.19	26.98	26.20	26.79	26.36	26.44	40.63	41.12
MnO	0.21	0.15	0.12	0.09	0.05	0.07	0.10	0.13
MgO	1.22	0.98	1.33	1.25	1.11	1.24	2.66	2.09
CaO	0.00	0.03	0.00	0.03	0.04	0.05	0.01	0.00
Na_2O	0.00	0.02	0.00	0.03	0.00	0.00	0.01	0.00
K_2O	0.00	0.00	0.06	0.00	0.00	0.01	0.01	0.00
NiO	0.00	0.00	0.00	0.04	0.07	0.00	0.07	0.07
Total	90.92	91.16	90.91	91.81	90.79	90.66	86.78	86.87
			12 (0)				28 (0)	
Si	2.045	2.034	2.035	2.005	2.034	1.951	5.060	5.022
Al	3.921	3.915	3.925	3.950	3.929	4.014	5.951	6.071
Ti	–	–	–	–	–	–	0.011	–
Cr	–	–	0.001	0.005	0.006	0.003	0.008	0.012
Fe	1.859	1.918	1.861	1.889	1.876	1.889	7.954	8.063
Mn	0.015	0.011	0.009	0.006	0.003	0.005	0.020	0.027
Mg	0.154	0.125	0.168	0.157	0.141	0.158	0.930	0.729
Ca	–	0.003	–	0.003	0.004	0.005	0.001	–
Na	–	0.003	–	0.004	–	–	0.003	–
K	–	–	0.006	–	–	0.001	0.001	–
Ni	–	–	–	0.002	0.005	–	0.012	0.012
X_{Fe}	0.923	0.939	0.917	0.924	0.930	0.923	0.895	0.917

* Total iron as FeO. $X_{Fe} = Fe/(Fe + Mg)$.

Table 3 Representative analyses of albite, muscovite and paragonite.

	Albite				Muscovite		Paragnonite	
	Ab-2		Ab-3		Mu-1	Mu-4	Pa-1	Pa-6
	Core	Rim	Core	Rim				
SiO_2	67.50	67.83	67.49	67.78	45.75	44.02	46.23	46.27
TiO_2	0.00	0.00	0.00	0.00	0.53	0.08	0.01	0.10
Al_2O_3	20.32	20.30	19.89	19.89	35.97	37.06	40.81	38.01
Cr_2O_3	0.01	0.05	0.07	0.04	0.02	0.00	0.08	0.02
FeO*	0.00	0.00	0.04	0.07	1.63	1.14	0.48	1.09
MnO	0.01	0.05	0.00	0.05	0.02	0.06	0.00	0.00
MgO	0.00	0.00	0.00	0.00	0.25	0.15	0.03	0.05
CaO	0.56	0.73	0.58	0.62	0.02	0.06	0.22	0.11
Na_2O	11.55	11.45	11.71	11.36	2.01	2.57	6.65	3.97
K_2O	0.04	0.01	0.05	0.01	8.35	7.62	1.21	5.11
NiO	0.00	0.00	0.06	0.04	0.02	0.00	0.00	0.00
Tatal	99.99	100.42	99.89	99.86	94.57	93.03	95.72	94.73
	32 (0)				22 (0)		22 (0)	
Si	11.817	11.826	11.847	11.880	6.102	5.959	5.892	6.055
Al	4.194	4.172	4.115	4.108	5.653	5.912	6.131	5.862
Ti	–	–	–	–	0.053	0.008	0.001	0.010
Cr	0.001	0.007	0.009	0.005	0.002	–	0.008	0.002
Fe	–	–	0.005	0.010	0.182	0.159	0.052	0.119
Mn	0.002	0.007	–	0.007	0.002	0.006	–	–
Mg	0.001	–	–	–	0.049	0.030	0.006	0.009
Ca	0.106	0.136	0.109	0.117	0.002	0.008	0.030	0.015
Na	3.922	3.870	3.984	3.860	0.521	0.674	1.643	1.008
K	0.008	0.003	0.012	0.002	1.421	1.315	0.197	0.854
Ni	–	–	0.008	0.005	0.002	–	–	–
Or	0.2	0.1	0.3	0.1				
Ab	97.2	96.5	97.1	97.0				
An	2.6	3.4	2.7	2.9				
Pa					26.8	33.9	89.3	54.1

* Total iron as FeO. Pa = 100Na/(K + Na).

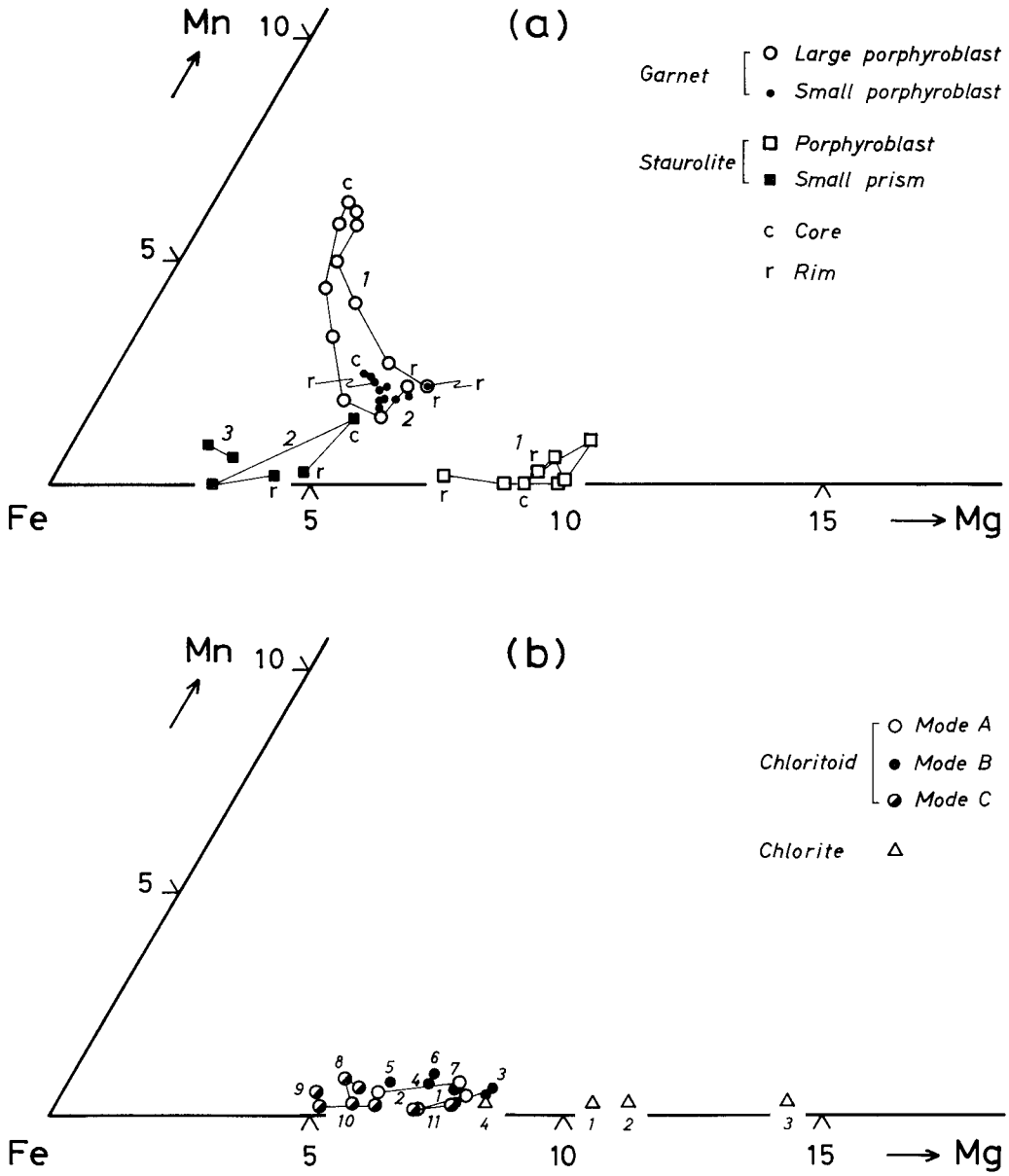

Fig. 3 Fe-Mg-Mn plot (atom. %) of analysed minerals: (a) garnet and staurolite and (b) chloritoid and chlorite. Analysed points on each mineral grain are connected by solid lines from rim through core to another side of the rim or from one point to the other, but the tie lines connecting rim with core of a small garnet porphyroblast (Ga-2) are omitted for avoiding confusion. Arabic numerals refer to numbers of mineral grain.

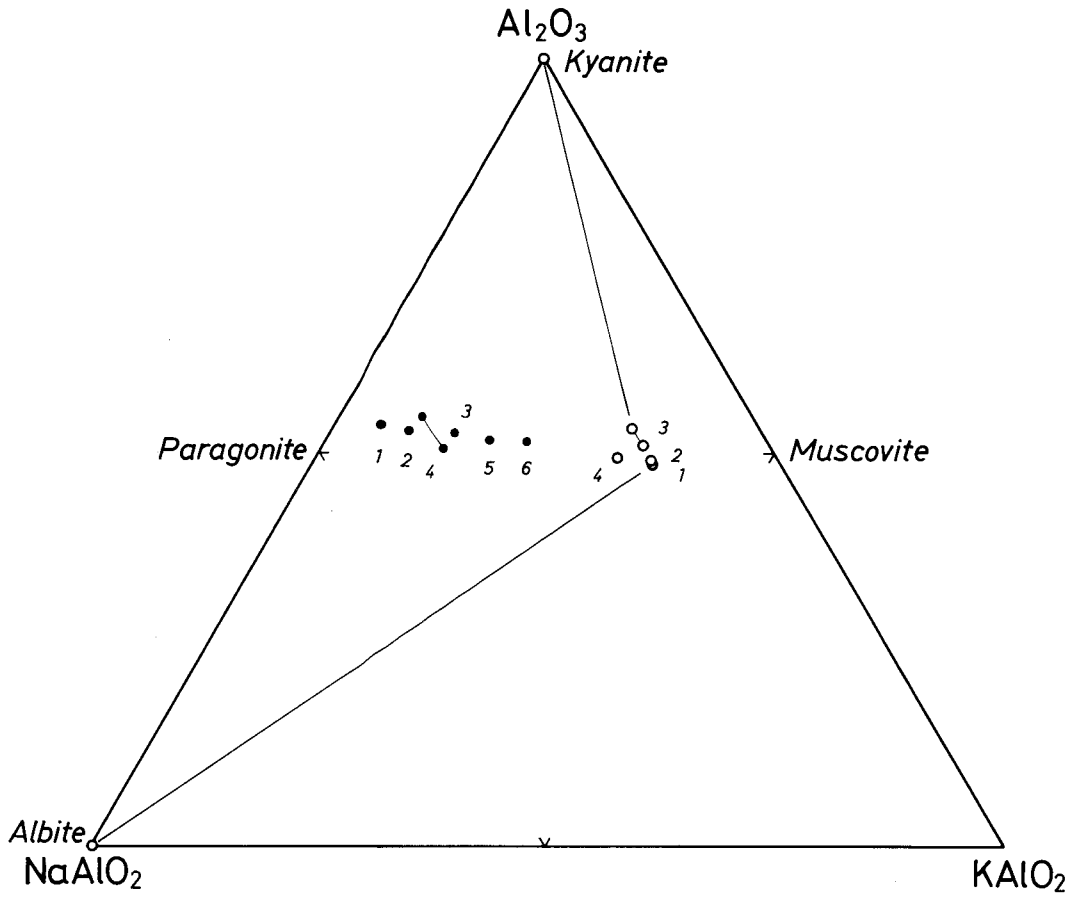

Fig. 4 Al_2O_3-$NaAlO_2$-$KAlO_2$ diagram showing compositions of kyanite, muscovite, albite and paragonite, and the primary mineral assemblage kyanite-muscovite-albite. Two analysed points are connected by a light solid line.

ed by Guidotti (1973) and Thompson et al. (1977). Muscovite in the kyanite gneiss from the Machakos area has lower Si and higher Fe+Mg values than that from Kilungu (Inoue and Suwa, 1979).

The albite reveals no compositional zoning and their An contents are arranged between 2.6 and 4.1 mol.%.

Setting aside staurolite, the uniform compositions of each mineral described above suggest that chemical equilibrium would be held among the minerals.

In contrast with the muscovite, the chemical compositions of paragonite vary considerably among flakes, ranging from 10.7 to 45.9 in muscovite molecule (Fig.4). In the system $NaAlO_2$-$KAlO_2$-Al_2O_3-SiO_2-H_2O, chemical compositions of muscovite and paragonite solid solutions are limited to narrow ranges due to the presence of the two-mica solvus and of the upper stability limit of paragonite according to the reaction $Pa_{ss}+Qu=Mu_{ss}+Ab_{ss}+Al_2SiO_5+H_2O$ (Thompson, 1974). For

example, after their estimated results, the solvus compositions of muscovite and paragonite which coexist with an Al_2SiO_5 mineral are about $Mu_{80}Pa_{20}$ and $Mu_{10}Pa_{90}$ under 2 kb P_{H_2O}. Thompson et al. (1977) described a coexisting pair of muscovite of $Mu_{75}Pa_{25}$ and paragonite of $Mu_{16}Pa_{84}$ in the kyanite-bearing Gassetts schist. The paragonite from Kilungu has intermediate compositions inside the muscovite-paragonite solvus (Fig.4), except one paragonite (Pa-1) that is in contact with muscovite (Mu-4). Two alternatives may be considered to explain such variable compositions of paragonite. One is that K-rich paragonite may be metastable, and the other is that muscovite-paragonite intergrowth on microscopic or submicroscopic scale may be present as reported by Höck (1974).

Eleven chloritoid grains (Ct-1 to Ct-11) occur in three modes as described above. Unlike the staurolite, the chloritoid shows no marked difference in composition and its X_{Fe} is restricted to a small range of 0.92 to 0.95 (Fig. 3).

The chlorite (Ch-1 to Ch-4), which partially replaces edges of garnet (Ga-2), is heterogeneous in X_{Fe} (0.86-0.96) (Fig.3).

Discussion

The mineral assemblages such as kyanite-staurolite-garnet, kyanite-staurolite-garnet-biotite, kyanite-garnet-biotite, kyanite-biotite and garnet-biotite have been found in pelitic gneisses from the Machakos-Kilungu-Uvete area (Biyajima et al., 1975; Nureki et al., 1977; Suwa et al., 1979; Inoue and Suwa, 1979; Miyake and Suwa, 1981; Asami et al., 1983). These mineral assemblages indicate that they correspond to a facies type of the kyanite-zone grade as schematically illustrated in Fig.5.

According to Albee (1972), chloritoid is generally no longer stable under the physical conditions of the kyanite-zone grade. Rumble (1970), however, regarded the chloritoid-staurolite-garnet assemblage in a biotite-free quartzite as an equilibrium one under physical conditions approaching to the kyanite-sillimanite isograd. The same three-phase assemblage was also found in a biotite-free semipelitic schist from the sillimanite-almandine-biotite zone (Lal and Ackermand, 1979). The stability of the assemblage has been attributed to the presence of such non-AFM components as Mn in chloritoid and garnet, and Ti or Zn in staurolite (Rumble, 1970; Lal and Ackermand, 1979). In the present case, however, it is considered from the textural evidence of the chloritoid-bearing kyanite gneiss that chloritoid would be secondarily formed along with paragonite and chlorite after the primary crystallisation of the other constituents.

AFM phases in this rock are kyanite, staurolite, garnet, chloritoid and chlorite. The chemical compositions of staurolite, garnet, chloritoid and chlorite are plotted on the AFM diagram (Fig.6). The compositions of staurolite (St-1) and garnet (Ga-1) which are connected by a tie line are those of rims in contact with each other. The staurolite and garnet have close X_{Fe} values, so that the three-phase field enclosed by kyanite, staurolite and garnet is extremely narrow as shown in Fig. 6.

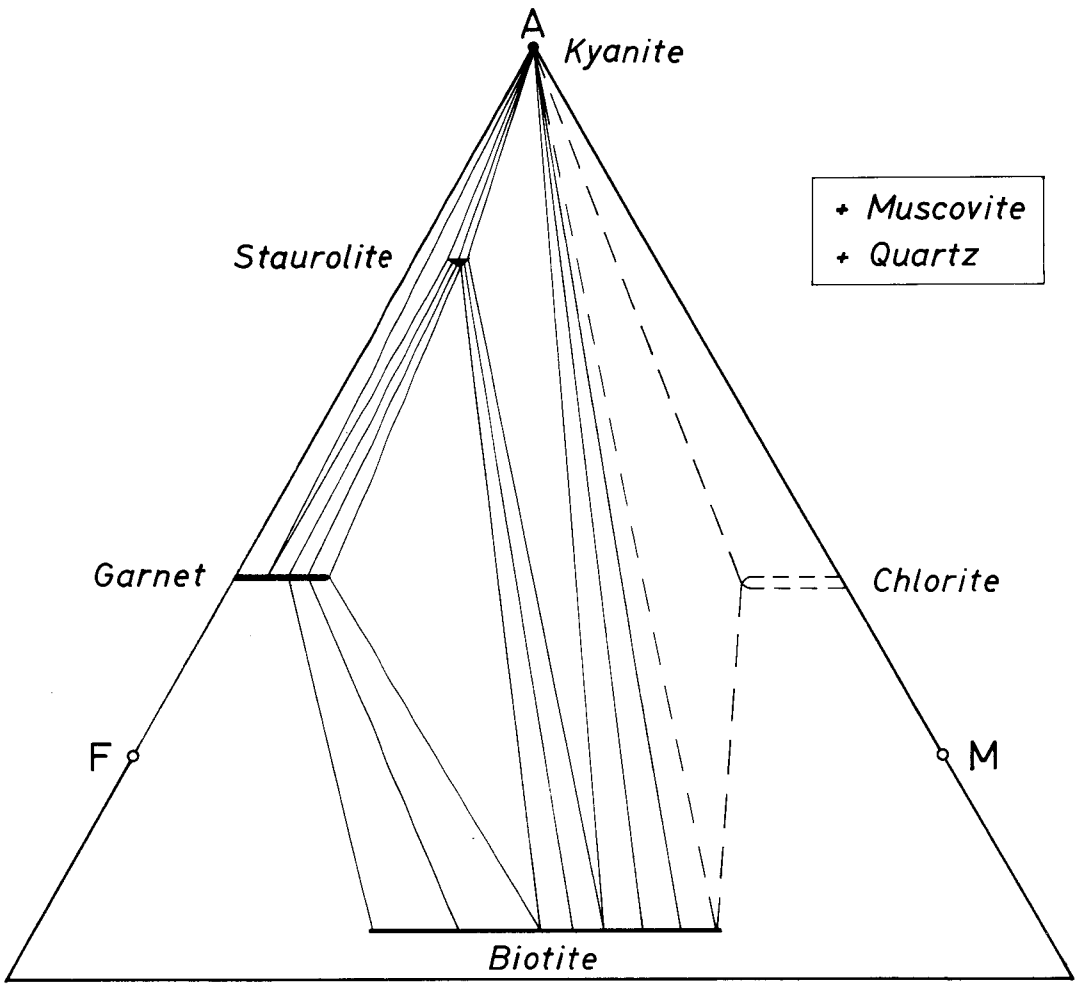

Fig. 5 Schematic AFM projection of the observed mineral assemblages in pelitic gneisses from the Machakos-Kilungu-Uvete area. Broken lines represent a possible assemblage which has not been found.

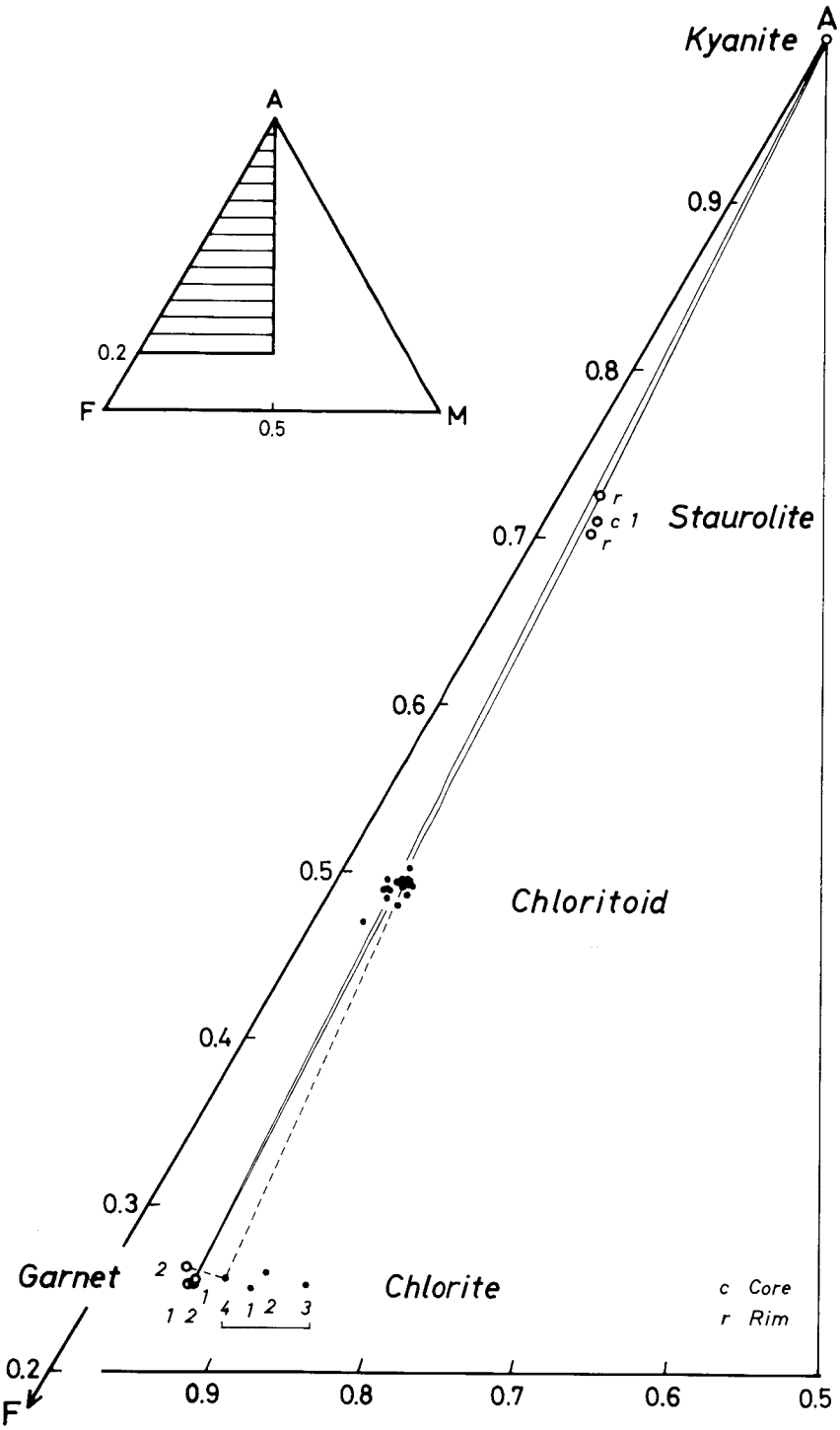

Fig. 6 AFM plot of staurolite, garnet, chloritoid and chlorite compositions. Plotted compositions of two garnet porphyroblasts (Ga-1 and Ga-2) are only those of the rim. Different minerals which are in direct contact with each other are connected by tie lines.

It is noted that most of the compositions of chloritoid are concentrated in a narrow area in the three-phase field. It has been known, when chloritoid coexists stably with staurolite, that X_{Fe}^{Ct} is commonly lower than X_{Fe}^{St} (Fox, 1971; Albee, 1972; Lal and Ackermand, 1979) or that the chloritoid composition lies on the Mg-rich side of the staurolite-garnet join in the AFM diagram (Rumble, 1970). The compositions of chloritoid plotted on Fig.6 are, however, not consistent with their conclusions, suggesting that chloritoid and staurolite are not in chemical equilibrium. This consideration is consistent with the textural evidence observed in this rock.

Chlorite (Ch-4) which partially replaces garnet rim (Ga-2) and is in contact with chloritoid (Ct-11) is connected with the last two by broken tie lines in Fig.6. The chloritoid-chlorite tie line does not cross both the kyanite-garnet and the staurolite-garnet tie lines. The chloritoid-chlorite association, therefore, could not be explained to have been produced by reactions of kyanite to garnet and/or of staurolite to garnet. Thus, chlorite does not appear to be in paragenetic relation to chloritoid but only to be a local replacement product after garnet, though explicit textural evidence to show the incompatible relation of chlorite to chloritoid has not been found. The compositional relations on Fig.6, together with resorbed texture on kyanite, staurolite and garnet, may indicate the following chloritoid-forming reaction:

$$Ky + St + Ga + H_2O \rightarrow Ct + Qu.$$

The common occurrence of paragonite along the grain boundaries between kyanite and albite suggests that paragonite would have resulted from a reaction:

$$Ky + Ab + H_2O \rightarrow Pa + Qu.$$

Paragonite in this gneiss, however, has a considerable amount of K_2O which is possibly differentiated as a muscovite component or muscovite lamellae intergrown. Moreover, muscovite, e.g. Mu-4, which is of ragged outline and is fringed with paragonite, is found in the gneiss. Thus, muscovite should be taken into account as a reactant. It is more likely to deduce that the following reaction took place:

$$Ky + Ab_{ss} + Mu_{ss} + H_2O \rightarrow Pa_{ss} + Qu.$$

As described previously, some chloritoid occur in close association with paragonite, and kyanite, staurolite and garnet are resorbed by paragonite. The formation of chloritoid is probably ascribed to retrograde metamorphism during which paragonite was also formed.

A pegmatite dyke is found near the chloritoid-bearing kyanite gneiss (Fig.2). It is considered that hydration for such retrograde reactions is probably closely related to the pegmatite emplacement.

Acknowledgements – I am grateful to Prof. T. Nureki of Okayama University for his critical reading of the manuscript, and Prof. K. Suwa of Nagoya University for his encouragement throughout this study. The field work was made with the co-operation of Mr. K. Tokieda of Shimane University and Dr. H. Umemura of

Kochi University, to whom I express my sincere thanks. Thanks are also extended to Dr. K. Suzuki, Mr. M. Enami and Mr. A. Miyake of Nagoya University for their useful discussion.

REFERENCES

ALBEE, A.L. (1972): Metamorphism of pelitic schists: reaction relations of chloritoid and staurolite. *Geol. Soc. Am. Bull.*, **83**, 3249-3268.

ASAMI, M., UMEMURA, H., TOKIEDA, K. and SUWA, K. (1983): Mozambique metamorphic rocks in the Kilungu area, central Kenya. *8th Prelim. Rept. Afr. Studies, Nagoya Univ.*, 97-104.

BIYAJIMA, K., SUWA, K. and MIYAKAWA, K. (1975): Mantled gneiss dome in the Mozambique belt around the Machakos area, Kenya. *Ist Prelim. Rept. Afr. Studies, Nagoya Univ.*, 6-13.

CHINNER, G.A. (1965): The kyanite isograd in Glen Clova, Angus, Scotland. *Mineral. Mag.*, **34**, 132-143.

FOX, K. (1971): Coexisting chloritoid and staurolite and the staurolite-chlorite isograd from the Agnew Lake area, Ontario, Canada. *Geol. Mag.*, **108**, 205-219.

GUIDOTTI, C.V. (1973): Compositional variation of muscovite as a function of metamorphic grade and assemblage in metapelites from N.W. Maine. *Contrib. Mineral. Petrol.*, **42**, 33-42.

HÖCK, V. (1974): Coexisting phengite, paragonite and margarite in metasediments of the Mittlere Hohe Tauern, Austria. *Contrib. Mineral. Petrol.*, **43**, 261-273.

INOUE, H. and SUWA, K. (1979): Petrographical note on staurolite-kyanite-almandine pelitic gneiss occurring at the western foot of the Mbooni Hills, Machakos area, Kenya – with special reference to the ZnO content in staurolite. *4th Prelim. Rept. Afr. Studies, Nagoya Univ.*, 97-111.

LAL, R.K. and ACKERMAND, D. (1979): Coexisting chloritoid-staurolite from the Sillimanite (fibrolite) zone, Sini, district Singhbhum, India. *Lithos*, **12**, 133-142.

MIYAKE, A. and SUWA, K. (1981): Geological structure of the Uvete dome, Kenya. *6th Prelim. Rept. Afr. Studies, Nagoya Univ.*, 33-41.

NUREKI, T., SUWA, K., BIYAJIMA, K., SAKA, Y. and YUSA, Y. (1977): Tectonic evolution of the Mozambique belt in area south-east of Machakos, Kenya. *2nd Prelim. Rept. Afr. Studies, Nagoya Univ.*, 13-38.

RUMBLE, D., III (1970): Chloritoid-staurolite quartzites from the Moosilauke quadrangle, New Hampshire. *Carnegie Inst. Washington Year Book*, **68**, 290-294.

SUWA, K., NUREKI, T., INOUE, H., BIYAJIMA, K. and MIYAKAWA, K. (1979): Geology and petrology of Machakos area, Kenya. *4th Prelim. Rept. Afr. Studies, Nagoya Univ.*, 3-20.

THOMPSON, A.B. (1974): Calculation of muscovite-paragonite-alkali feldspar phase relations. *Contrib. Mineral. Petrol.*, **44**, 173-194.

THOMPSON, A.B., LYTTLE, P.T. and THOMPSON, J.B. (1977): Mineral reactions and A-Na-K and A-F-M facies types in the Gassetts schist, Vermont. *Am. Jour. Sci.*, **277**, 1124-1151.

PLATE I.

Photomicrograph of chloritoid-bearing kyanite gneiss.

A: Paragonite aggregates (Pa) developed along the boundaries between kyanite (Ky) and albite (Ab) grains. One nicol.

B: Paragonite aggregates (Pa) and chlorite flakes (Ch) developed between staurolite (St) and albite (Ab). One nicol.

C: Chloritoid (Ct) in paragonite aggregates (Pa). One nicol.

D: Chloritoid (Ct) and corroded kyanite (Ky) in paragonite aggregates (Pa). One nicol.

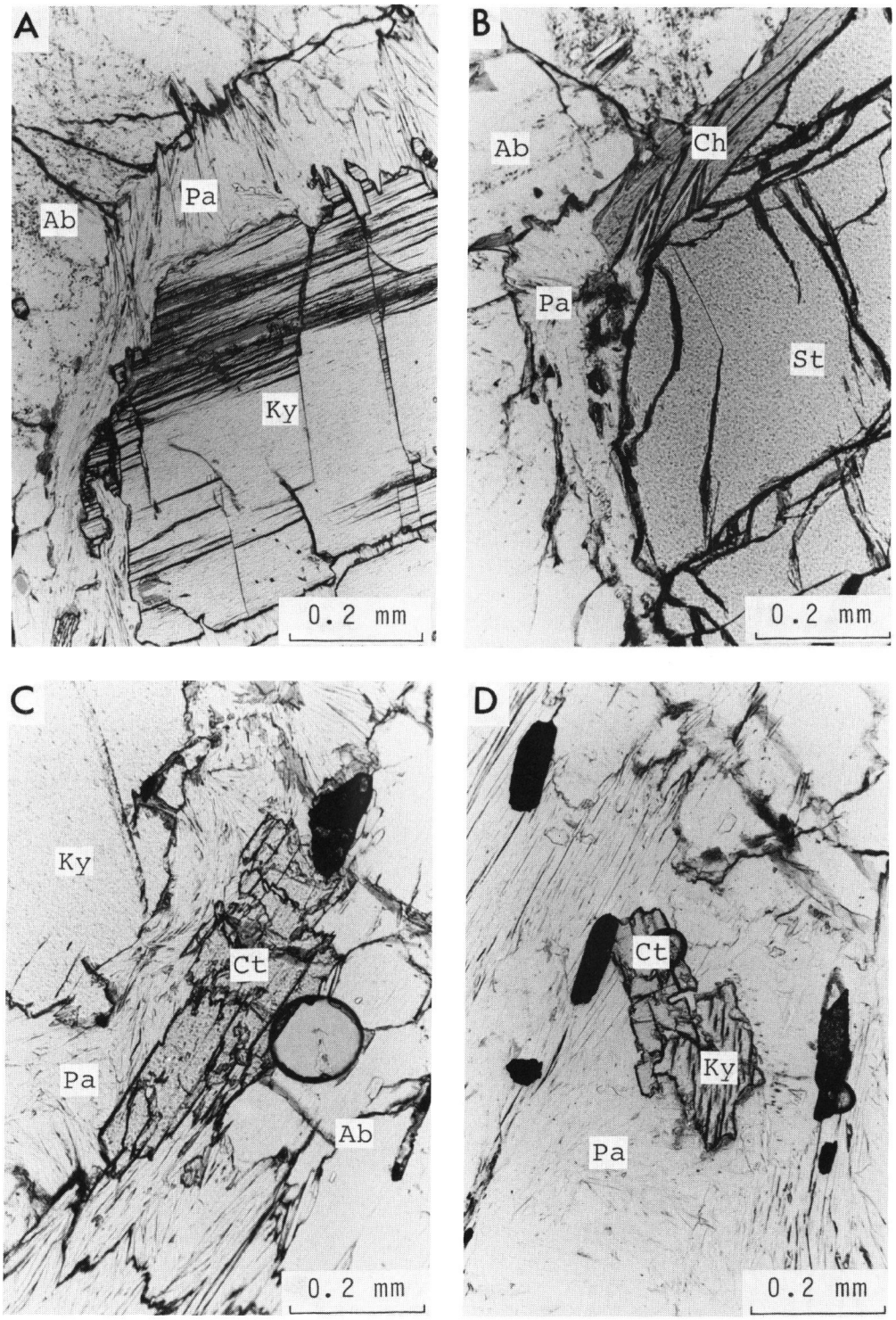
A
Ab
Pa
Ky
0.2 mm
B
Ab
Ch
Pa
St
0.2 mm
C
Ky
Ct
Pa
Ab
0.2 mm
D
Ct
Ky
Pa
0.2 mm

PLATE II.

Photomicrograph (ditto).

A: Dendritic chloritoid (Ct) in an albite porphyroblast (Ab.) One nicol.

B: Veinlet-like chloritoid (Ct) developed along the boundaries between albite crystals (Ab). One nicol.

C: Chloritoid (Ct) fringing and partially corroding a garnet porphyroblast (Ga). The garnet rim is also corroded by a small chlorite flake (Ch). Quartz grains (Qu) are found in the garnet and albite and between the chloritoid and albite. One nicol.

D: Chloritoid (Ct) and paragonite (Pa) invading the interior of a kyanite porphyroblast (Ky). One nicol.

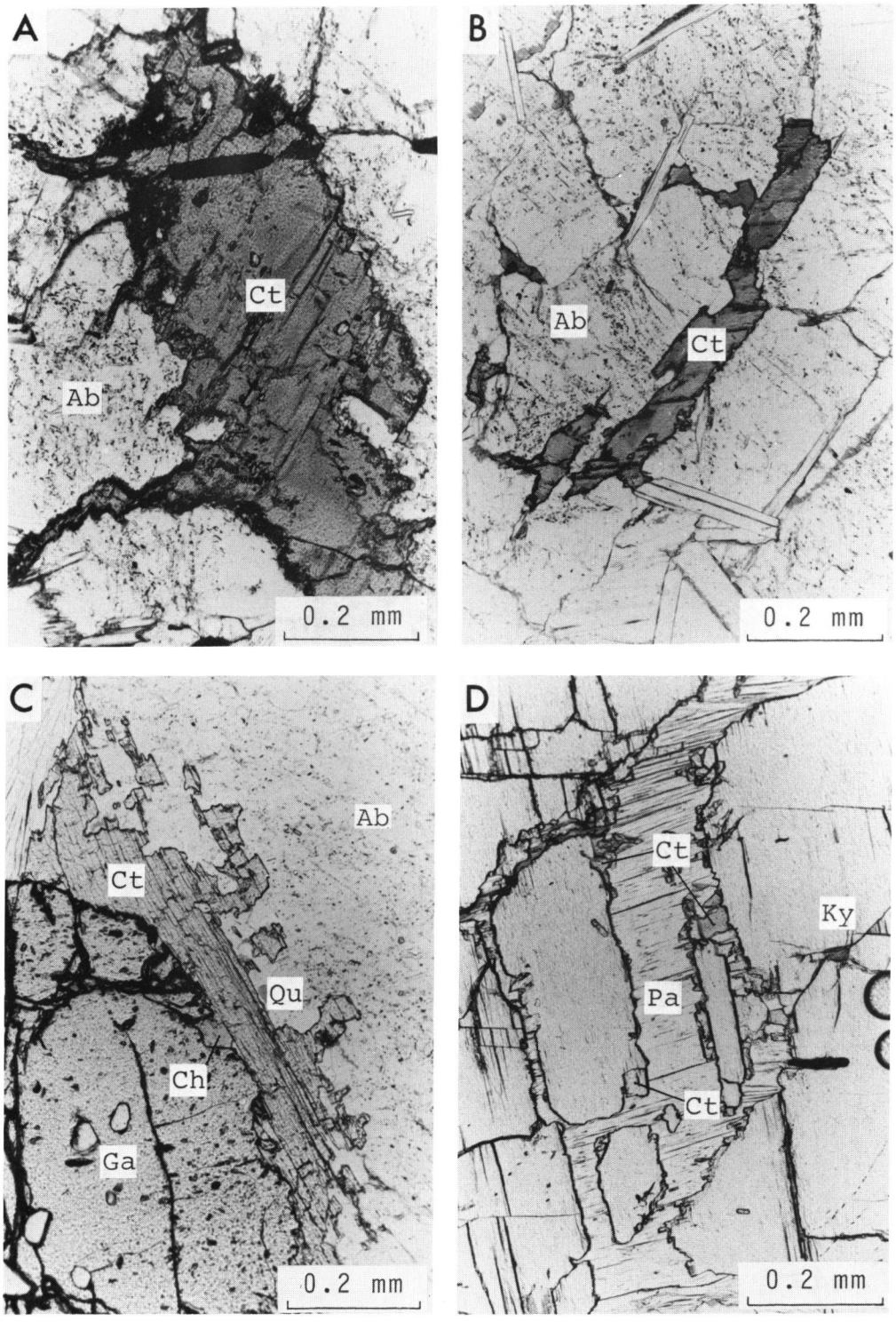
A
Ct
Ab
0.2 mm
B
Ab
Ct
0.2 mm
C
Ab
Ct
Qu
Ch
Ga
0.2 mm
D
Ct
Ky
Pa
Ct
0.2 mm

Magnetic susceptibility of the granitoid gneisses in the Mozambique metamorphic belt of Kenya

Heinosuke SHIOZAKI

Laboratory of Geology, College of General Education, Nagoya University

Abstract

In order to probe some metallogenic provinces in the Mozambique metamorphic belt, magnetic susceptibility of the granites, granitoid gneisses and paragneisses has been measured in-situ with an external flat coil of Bison model 3101A.

Granitoid gneiss forming a domed structure exhibits higher magnetic susceptibility and undomed granitoid gneiss and paragneiss exhibit lower magnetic susceptibility. Domed granitoid gneiss may be derived originally from the deep seated granitic pluton. Undomed and sheet-like granitoid gneisses may not be magmatic but be granitized paragneisses, even if these are magmatic, these are not coming from the deep seated layer of the earth's crust.

Any future prospecting for xenothermal mineral deposits should take aim in the nearby areas around the masses of domed granitoid gneiss.

Introduction

In 1971, I made geological reconnaissance on the Mozambique metamorphic rocks in Kenya, from Lasamba Hill(4°10'S) to Machakos area (1°30'S) through the Sagala Hills, the Taita Hills, Murka, Taveta, Voi, Kibini and Sultan Hamud with Prof. K. Suwa of Nagoya University. In the southeastern Machakos area, many kinds of metamorphic rocks including granitoid gneiss are widely and fully distributed with leading structural features. Remarkable out crops are numerous in the hills and along several large and many small rivers. This urged many geologists of Nagoya University to investigate further the geology and petrology of the area. Since 1973, the geological teams from Nagoya University have been frequently sent to investigate the Machakos-Kilungu-Uvete area and many reports based on their surveys have been published.

In order to probe some metallogenic provinces in the Mozambique metamorphic belt, I have carried out measurements of magnetic susceptibility of the granites, granitoid gneisses and paragneisses on the spots of their out-crops from the Machakos area of south-central Kenya and West Pokot and Nandi areas of west Kenya using a model of Bison 3101A. In this paper I described and discussed the measurement data in detail and proposed an object for the future prospecting of xenothermal mineral deposits.

8th Prelim. Rept. Afr. Studies, Nagoya Univ., 121-134, 1983.

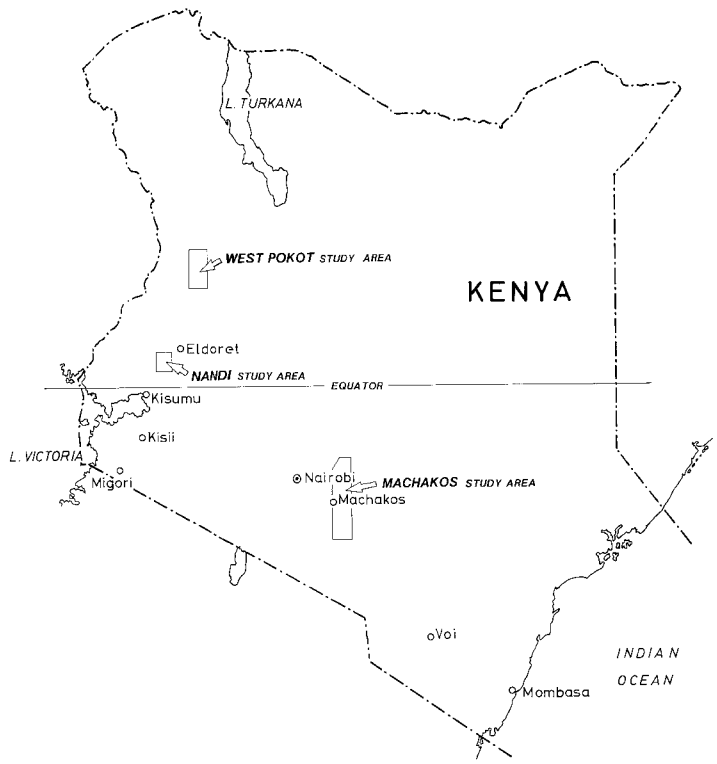

Fig. 1. Index map showing the studied areas in this work.

Measurements of magnetic susceptibility

1) Instrument and measuring procedure

Using a model of Bison 3101A I have carried out measurements of the magnetic susceptibility of the granitic rocks and metamorphic rocks on the spots of their out-crops in the Mozambique metamorphic belt in Kenya.

Two measuring procedures can be applied in the Bison model 3101A: the first is prepared for measurement of the weight magnetic susceptibility in $\times 10^{-6}$ emu. cgs./g, the second the in-situ measurement of the volume magnetic susceptibility in $\times 10^{-6}$ emu.cgs./cm^3. In the former procedure every samples must be pulverized and packed in a tube of sample holder. I performed my measurement by the latter procedure and the whole values obtained are expressed by the unit of $\times 10^{-6}$ emu. cgs./cm^3. We can obtain the values of weight magnetic susceptibility from the values of volume magnetic susceptibility by the division with the density of rocks concerned.

Magnetic susceptibility of the granitic rocks is considered mostly to depend on their magnetite contents. Ishihara (1979) proposed a simple formula on the relation between magnetic susceptibility and magnetite contents of the Japanese granitoids, that is $\chi = 0.001 \times V$ where χ is weight magnetic susceptibility in emu.cgs./g and V is modal volume of magnetite in percentage.

The Honshu Island, which is a major one of the Japanese Islands Arc, is divided into the Inner and Outer zones by the Median Tectonic Line. The Cretaceous granitic plutons widely distributed in the Inner zone of the southwestern Japan had brought about a development of many small deposits of xenothermal type. Three metallogenic provinces are set up in the Inner zone of the southwestern Japan (Ishihara, 1971), i.e., the first is molybdenum deposits province in the coastal area along the Japan Sea, the second is tungsten deposits province in the middle area, and the third is barren province in the nearby area along the Median Tectonic Line. The chemical characters of the granitoid rocks have been also noticed in relation with the ore bringers of the deposits by Ishihara (1977).

2) Calibration

The magnetic susceptibility of the granitoid rocks of Japan was measured by Kanaya and Ishihara(1973) using a same model of Bison 3101A. Before flight to Kenya, the instrument had been checked for these in-situ measurements at the various exposed surfaces of granitoid rocks belonging to both magnetite- and ilmenite-series in Japan. As the magnetite series, the Shirakawa granite was chosen and as the ilmenite series, the Toki granite. After come back from Kenya to Japan the instrument was checked again in the same ways.

3) Choice of measuring spots

The rock exposures for the in-situ measurement of magnetic susceptibility have been chosen to be fulfilled the following conditions;

(i) Being not weathered.

When any completely fresh and not weathered rock exposure is not found in the area concerned, any least or lesser altered rock exposured must be chosen and some considerations on weathering conditions are necessary.

(ii) Being not smaller than $1 \times 1 \times 1$ m^3 in size.

The size of fresh rock exposure must be greater than $1 \times 1 \times 1$ m^3. When the rock sample is found as a weathering boulder or weathered tor, the size of boulder must be greater than $1 \times 1 \times 1$ m^3, too.

(iii) Being a smooth and flat surface suitable for putting the external flat coil.

(iv) Being no electric power cable, water pipe line, and other big metal materials.

(v) Being dry conditions in the place, on which the instrument put for measurement.

4) Repetitions of measurement

Using the Bison model 3101A, the measured values less than 10×10^{-6} emu.cgs./cm^3 are not authorized, due to the accuracy of the instrument. Therefore, no discussion on measured value less than 10×10^{-6} emu.cgs./cm^3 has been done in this paper.

The distribution of magnetite grains in the granitoid rocks is not necessarily homogeneous, therefore, the modal composition of magnetite in granitoid rocks is

not necessarily good constancy and is statistically deviant. In the rock exposure, some repetitions of the measurement must be done for the above reasons. The five repetitions of a measurement at one exposure have done with intervals of about 0.5 meters and the five measured values are averaged.

5) Weatherring characters in the Machakos area and its neighbors

The magnetic susceptibility of granitoid rocks mostly depends on their magnetite contents. Iron minerals such as magnetite may be decomposed and turned to ferric oxides and/or hydroxides under a kind of weathering environments on the land surface. When the magnetic susceptibility is measured, therefore, the weathering environment of the area must be taken into account. The most important variables to control the characters of weathering are the climate and land form.

Baker(1954) described the climate in the Machakos area as follows: "The climate in the area is pleasant and similar to that of Nairobi except at levels about 1200 meters high where the heat in January and February become considerable".

	Machakos	Kilungu	Nairobi	Nagoya
Altitude (meter)	1500	1800	1650	20
Annual rainfall (mm)	910	990	930	1540
Annual mean temperature (°C)	21	18	18	15

In the above table, annual rainfall and annual mean temperature are shown on the Machakos area (Machakos, and Kilungu), Nairobi and central Japan (Nagoya). The climate of both Machakos and Nagoya may be designated as a humid subtropical climate. In the Machakos area, the annual rainfall is smaller than that of Nagoya and the annual mean temperature is slightly higher than that of Nagoya.

Regarding the following three characters of soil and weathered layers, the climate and weathering characters at the Kilungu area may be similar to that of the southwestern Japan.

(i) At the Kilungu area, a sort of soil, which color is yellow brown, are often found. The soil may be same with the yellow brown forest soil prevailing in the southwestern Japan. The yellow brown forest soil has been proposed as a soil type representing a humid subtropical climatic zone by Matsui (1964) and Gerasimov(1964).

(ii) At the Kilungu area no lateritic crust or related materials are recognized.

(iii) Under the yellow brown forest soil, a colorless or nearly colorless with pale

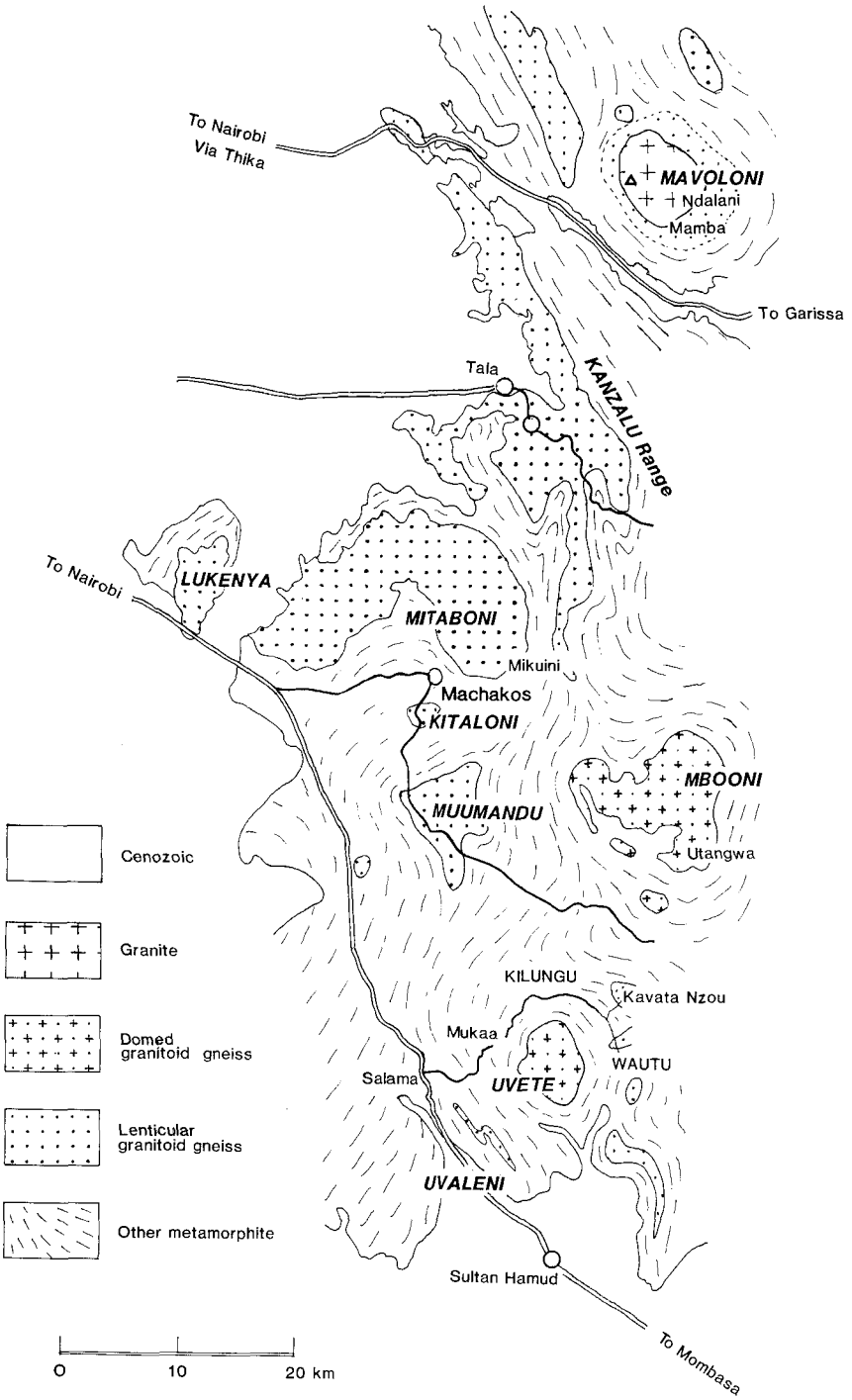

Fig. 2. Locality map showing the distribution of the granite and granitoid gneiss in the Mozambique metamorphic belt, Machakos, Kenya.
(After Baker, 1954, Fairburn, 1963, Biyajima et al., 1975, and Miyakawa and Suwa. 1979).

yellow brown tint saprolite is widely developed as a layer, which is underlain by the basement rocks.

The experiences in measurements at the Machakos area and the southwestern Japan show that the magnetic susceptibility is almost same between the fresh granitoid rocks and weathered granitoid saprolite. This may be due to the well reservation of magnetite without decomposition.

6) Detrital magnetite

In some places of Machakos and Kilungu areas, the detrital concentrates of magnetite sand derived by the rain wash are found in the bottom beds of small stream channels. At Utangwa situated in the Mbooni Hill, the granitoid gneiss shows high magnetic susceptibility. At Mukaa (Kilungu) and Kyanga (Wautu), the granitoid gneiss shows low magnetic susceptibility. Magnetite sand at Mukaa is derived from the upper most, dark brown fumic soil zone but not from the weathered in-situ granitoid gneiss zone.

All places of Utangwa, Mukaa and Kyanga are situated at higher altitudes than the sub-Miocene surface. The detrital magnetite sand are considered to be derived from the ancient detritus.

Magnetic susceptibility

1) "High magnetic" and "low magnetic"

All values obtained from the in-situ measurements by using an external flat coil of Bison model 3101A are shown as a volume magnetic susceptibility in units $\times 10^{-6}$ emu.cgs./cm^3. The volume magnetic susceptibility is easily recalculated to weight magnetic susceptibility ($\times 10^{-6}$ emu.cgs./g) by the division with the density of rock concerned. The densities of granitoid metamorphites in the Mozambique belt, Kenya, are measured as about 2.56 to 2.65 g/cm^3 by using an air comparison pycnometer, Beckman model 930.

Kanaya and Ishihara(1973) divided the Cretaceous granitoids of the southwestern Japan into two types of "high magnetic" magnetite-series and "low magnetic" ilmenite-series. The dividing point between two types has been set upon 50×10^{-6} emu. cgs./g, which corresponds with 130×10^{-6} emu.cgs./cm^3.

The granitoid gneisses in the Mozambique metamorphic belt of Kenya are also possible to divide into two types by the critical value of 130×10^{-6} emu.cgs./cm^3.

2) Granitoid metamorphites

(i) Previous works. Fairburn(1963) divided the Basement rocks into the following types:

A. Metasediments
B. Granitized sediments
   a. Migmatite, b. Granitoid gneiss, c. Augen-gneiss
C. Metamorphic intrusives

Table 1 Magnetic susceptibility of the granitoid gneisses from the Machakos areas ($\times 10^{-6}$ emu.cgs./cm^3)

Location	Rock	Minimum	Maximum	Average	Number of measured points
MAVOLONI					
Kathule	Mavoloni granite	260	1330	954	5
	"	700	800	750	2
	"	300	770	518	5
	"	160	580	383	6
	"	100	160	136	3
Nadalani	granitoid gn.	200	370	266	5
	"	50	590	280	5
	"	0	320	84	5
Mamba	granitoid gn.	40	70	60	4
	"	45	60	54	4
MITABONI					
Mikuini	granitoid gn.	50	110	80	5
	"	35	90	52	5
	"	20	60	28	5
	"	10	20	15	5
	"	20	110	62	6
	"	30	50	40	2
	basic gn.	20	52	36	2
	psammitic gn.	20	100	64	5
	"	50	70	60	3
KITALONI					
Kitaloni	granitoid gn.	65	125	96	4
	"	40	85	70	3
	"	11	15	13	4
MUUMANDU					
Muumandu	granitoid gn.	50	75	60	6
	"	35	85	60	8
	"	30	35	33	5
Mbondoni	granitoid gn.	20	45	33	8
MBOONI					
Utangwa	mica schist	700	800	730	6
	granitoid gn.	850	1100	970	6
	"	700	1000	970	6
Mukaatini	granitoid gn.	300	800	640	7
	"	600	700	650	4
	"	350	650	480	6
Yambae	granitoid gn.	700	800	720	4
Kitwii	granitoid gn.	350	500	440	6
	pegmatite	60	240	121	5
KILUNGU					
Kavata Nzou	granitoid gn.	1200	1500	1350	7
UVETE					
Kiwa Kiamba	granitoid gn.	170	210	191	5
Prim. Sch.	"	155	370	267	6
	"	155	405	273	5
	"	75	295	181	5
	"	100	410	228	6
	"	65	545	224	6
Uvete	granitoid gn.	50	170	115	8
Kyanga	granitoid gn.	35	50	45	3
	psammitic gn.	0	30	10	5
	"	40	70	52	5
KIONGWANI-UVALENI					
Kamuthini	granitoid gn.	20	20	20	5
	psammitic gn.	20	20	20	5
	pegmatite	5	15	9	7
	migmatite	15	20	16	5
	"	15	20	18	4
Uvaleni	granitoid gn.	20	25	21	7

Table 2. Magnetic susceptibility of the granitoid gneisses from the Nandi and West Pokot areas. ($\times 10^{-6}$ emu.cgs./cm^3)

Location	Rocks	Minimum	Muximum	Average	Number of measured points
NANDI					
Kaiboi	Gr.gn., (pink)	320	740	512	5
Kaiboi, north	Gr.gn.	400	700	590	5
Sarora Hill	Gr.gn.	330	540	442	5
Sarora, north	Gr.gn.	20	70	46	5
	Migmatite	155	1660	1049	8
	Migmatite	30	60	45	6
Kipkarum	Migmatite	60	150	125	8
	Migmatite	20	50	27	7
WEST POKOT					
Nguruch	Gr.gn.	40	140	87	3
	Gr.gn. (pink)	70	530	201	7
Akeriamet	Young granitic vein	0	0	0	9
Lomut	Gr.gn.	0	240	118	5

D. Intrusives
a. Granite, b. Pegmatite, c. quartz vein.

In this classification made by Fairburn, (i) all granitoid gneisses have been designated as a sort of paragneiss, (ii) the Mavoloni granite has been thought to be a younger intrusive. After my measurements of magnetic susceptibility, I have had an another idea differ from his opinion.

(ii) Granitoid gneisses Baker(1954) described that the granitoid gneisses often resemble the bedded quartz feldspathic gneisses and the Mbooni and Opete(Uvete) out crops are sub-circular with the concordantly surrounding gneisses. The larger bodies of granitoid gneiss suggest that they are considered to be granitoid domes resulting from the viscous upwelling of granitic material during metamorphism.

The granitoid gneiss of Kalama Hill is considered to be psammitic gneiss (Miyakawa and Suwa, 1979) and another granitoid gneiss of Muumandu Hill is designated as a concordant sheet-like body (Suwa et al, 1979).

Fairburn(1963) considered that some of the granitoid gneiss are a sort of granitized sediments. In the North Machakos-Thika area, he found a circular shaped granite body named "Mavaloni(Mavaloni) granite", which was considered to be a intrusive granite pluton. Both the Mavoloni granite and the surrounding granitoid gneiss show same mineral assemblies.

Petrogenesis of granitoid gneisses is in hot dispute among geologists. In Fig.4, changes of supposings to the origin of the granitoid gneisses in the Mozambique belt are shown. As clearly shown in Fig.3a and 3b, the magnetic susceptibility of granitoid gneiss forming domed structure is high and that of undomed granitoid gneiss and paragneisses is low.

Table 3. Magnetic susceptibility and the structural forms of rock body of the granitoid gneisses from the Mozambique metamorphic belt, Kenya.
(gr. = granite, gr.gn. = granitoid gneiss)

	High magnetic susceptibility		Low magnetic susceptibility
Locality	Discordant intrusive body	Domed body	undomed and concordant body
MACHAKOS			
NORTH MACHAKOS			
Mavoloni		Mavoloni gr.	
		Ndalani gr. gn.	Mamba gr. gn.
Mitaboni			Mikuini gr. gn.
SOUTH MACHAKOS			
Kitaloni			Kitaloni gr. gn.
Muumandu			Muumandu gr. gn.
Mbooni			Mbooni gr.gn.
KILUNGU			
Kilungu	Karongo gr. gn. (Kavata Nzou)		
Kitaingo		Uvete gr. gn.	
Uvaleni			Kamuthini gr. gn.
			Uvaleni gr. gn.
			Kasikeu gr. gn.
NANDI			
Kaiboi		Kaiboi gr. gn.	
Sarora Hill		Kaiboi gr. gn.	North Sarora gr. gn.
WEST POKOT			
Nguruch			Nguruch gr. gn.
Akeriamet	Pegmatite		
Lomut			Lomut gr. gn.

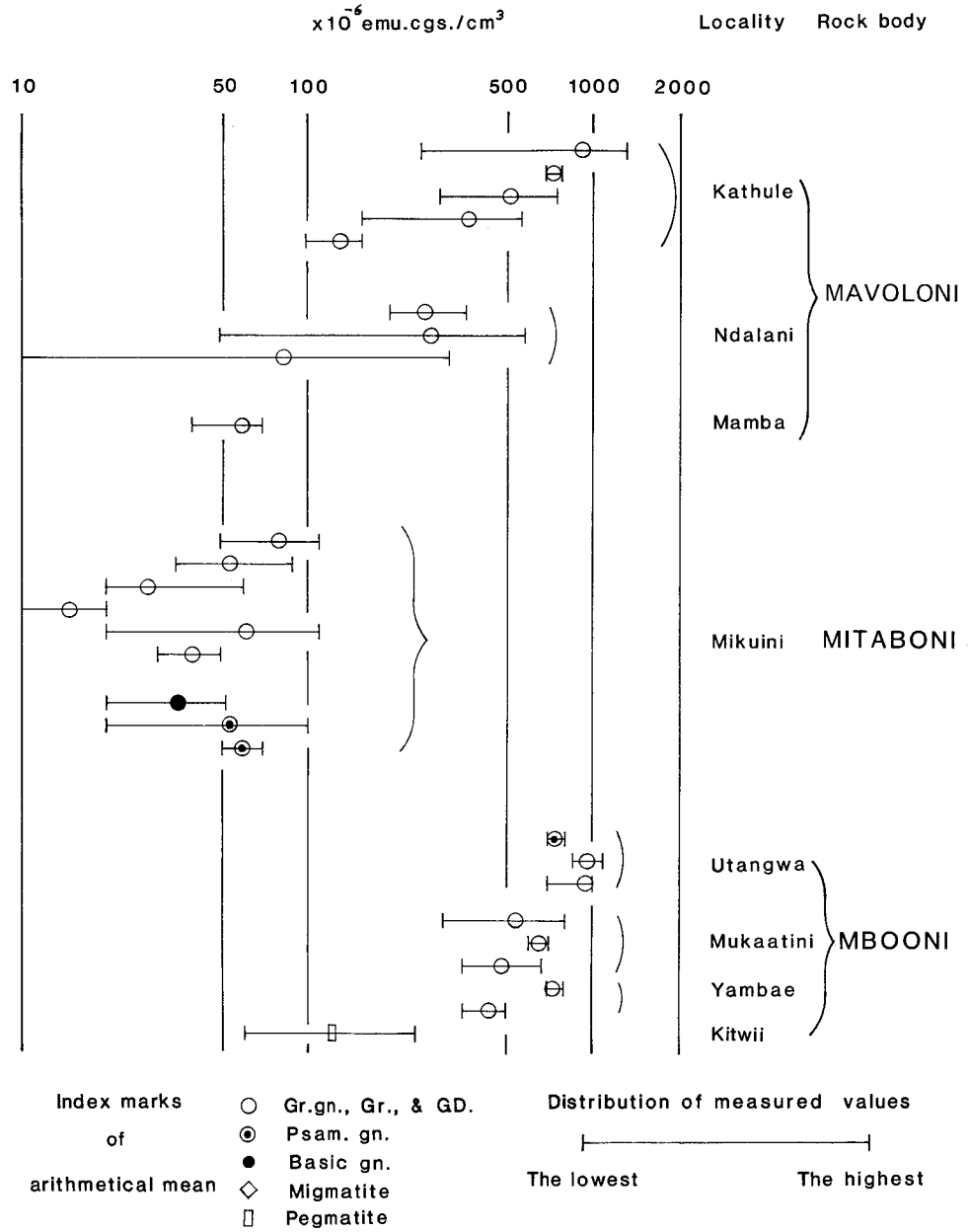

Fig. 3a. Magnetic susceptibility of the granitoid gneiss in the Mozambique metamorphic belt, Kenya.

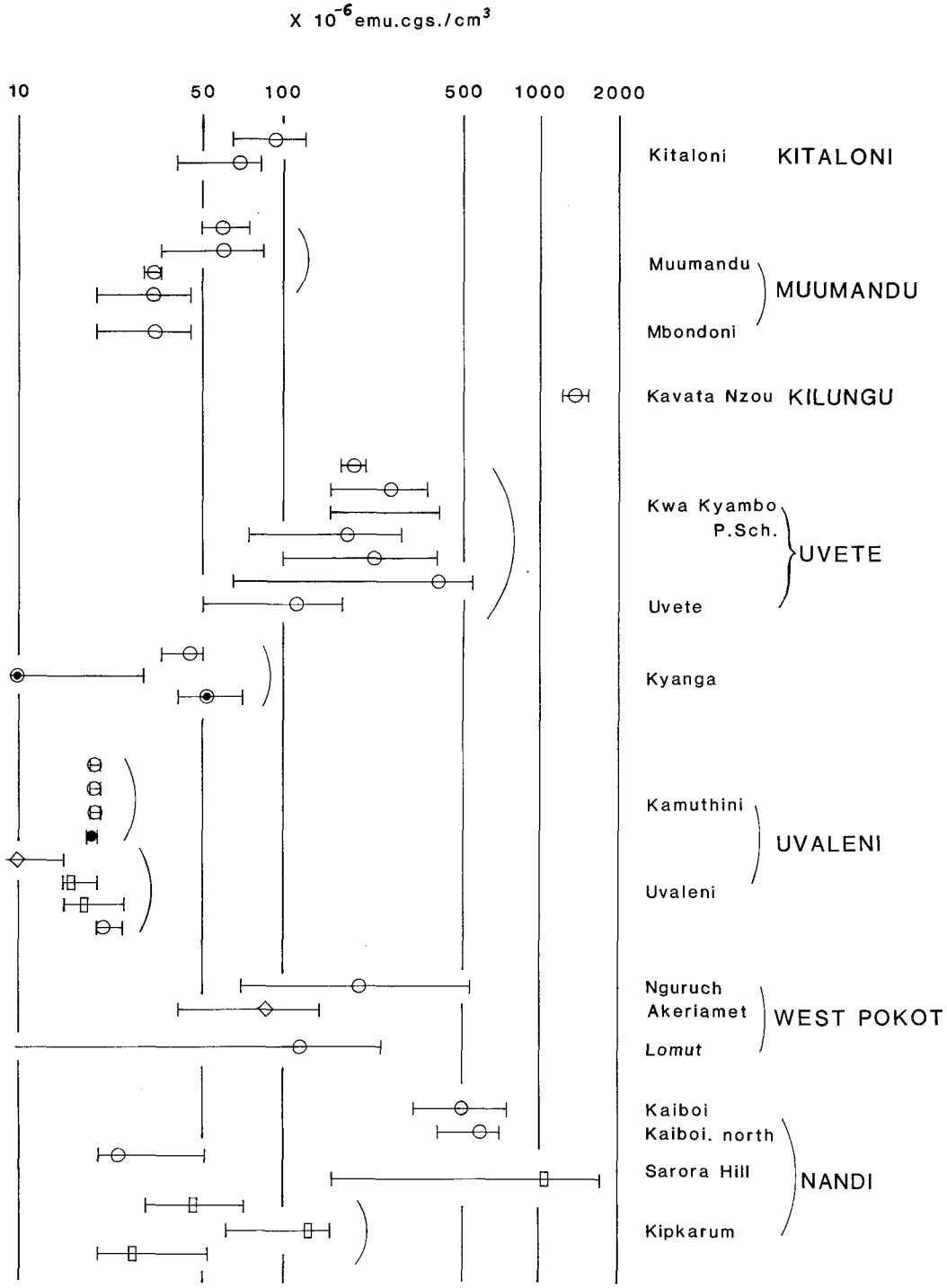

Fig. 3b. (continued from Fig. 3a.)

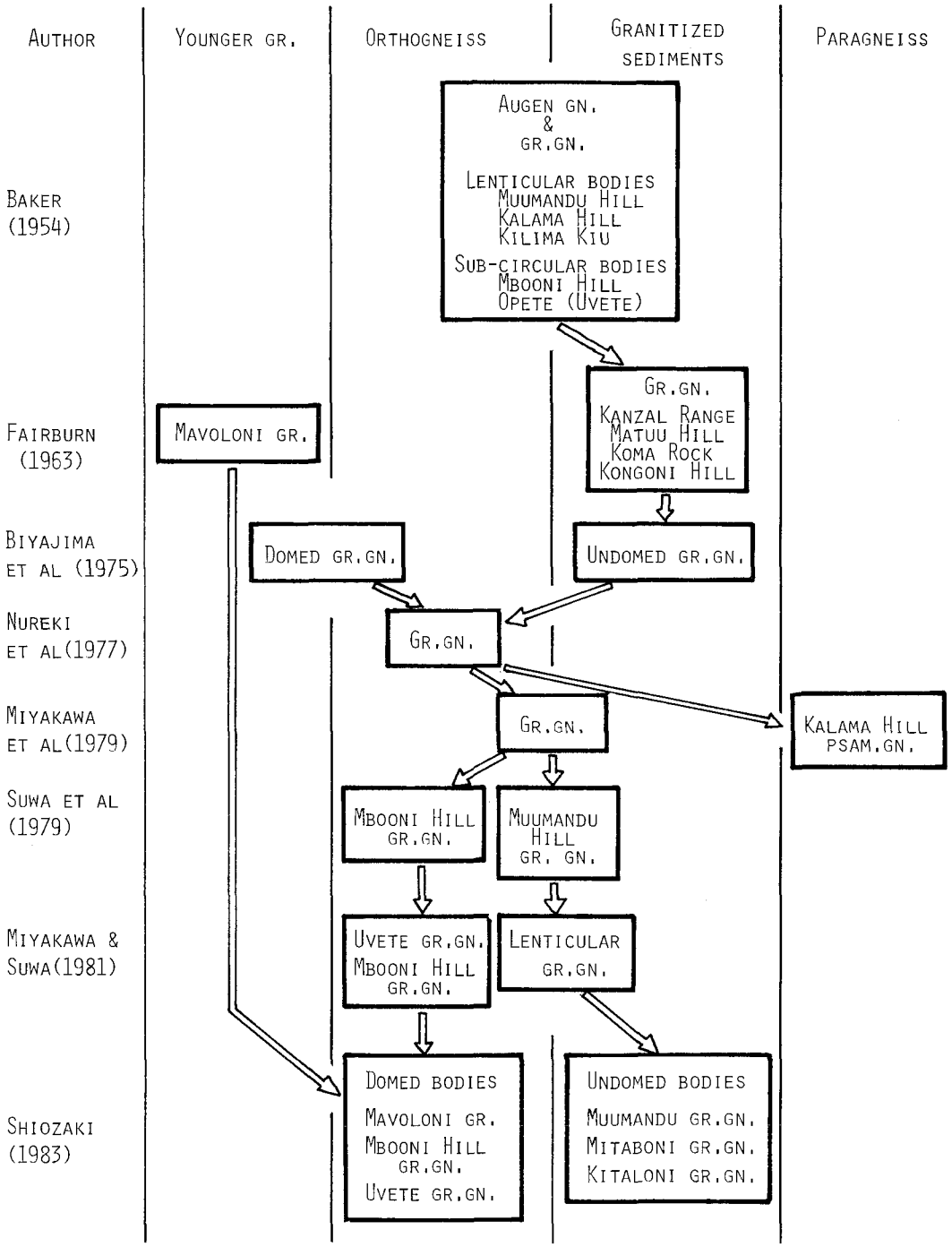

Fig. 4. Changes of supposings to the origin of the granitoid gneisses in the Mozambique metamorphic belt, Kenya.
(Gr. = granite, Gr. Gn. = granitoid gneiss, and Gn. = gneiss)

Considering the above results, "Mavoloni granite" around Kathule and Ndalani may be a domed granitoid gneiss.

The magnetic susceptibility of the granitoid rocks from the Kisumu area is higher than 130×10^{-6} emu.cgs./cm^3 (Shiozaki, 1983). These granitoid rocks constituting the Tanzania craton are considered to be derived from the deep seated layer. It may be said that the "low magnetic" concordant sheet-like granitoid gneiss is not magmatic or, even if it is magmatic, is not coming from deep seated layer of the earth's crust.

Hereafter, when anyone wishes to try to prospect any xenothermal mineral deposits, he should take aim at the surroundings of the domes of the granitoid gneisses.

Acknowledgement – I thank Mr. E.K. Ruchiami, Permanent Secretary of the Office of President of Kenya, for a research permission on my geological studies in Kenya. I thank also Prof. I.S.Loupekine of the University of Nairobi for his kind suggestions and helpful supports and I am very greatful to Mr.L.C.Butaki, Warden of Mines, Mines and Geological Department, Kenya, for his warm hospitality upon the export of my rock samples.

I would like to express my deep gratitude to Mr. T. Miyauchi, Mrs. and Mr. Kishida, Prof. J. Tanaka, Mr. J. Yamagiwa, Mr. M. Matsuda, Mr. I. Ota, Dr. S. Yagi, and Dr. T. Abe for their kind supports. I express my sincere thanks to Prof. K. Suwa of Nagoya University for his helpful assistances to this study.

This work in Kenya was made possible by the Grant-in-Aid from the Japan Society for Promotion of Science, to which I express my thanks. My sincere thanks are extended to Mr. N. Onozawa and others of the Japan Society for Promotion of Science for their kind assistance.

REFERENCES

BAKER, B.H. (1954): Geology of the Southern Machakos District, *Rept. Geol. Surv. Kenya*, **27**.

BIYAJIMA,K., SUWA,K., and MIYAKAWA,K. (1975): Mantled gneiss dome in the Mozambique belt around Machakos area, Kenya, *1st Prelim. Rept. Afr. Studies, Nagoya Univ.*, 6-13.

FAIRBURN,W.A. (1963): Geology of the North Machakos-Thika Area, *Rept. Geol. Surv. Kenya*, **59**.

GERASIMOV, I.P. (Ed., 1964): *Physico-geographical Atlas of the world*, AN.SSSR.

ISHIHARA, S. (1979): Lateral variation of magnetic susceptibility of the Japanese granitoids, *Jour. Geol. Soc. Japan*, **83**, 509-523.

KANAYA,H. and ISHIHARA, S. (1973): Regional variation of magnetic susceptibility of the granitic rocks in Japan, *Jour. Jap. Assoc. Min. Petr. Econ. Geol.*, **68**, 211-224.

MATSUI,T. (1964): An objection to the so-called "zonality" of the red soils in Japan, and a proposal of the yellow-brown earth as a newly established genetic soil type, *Pedologist*, **8**, 42-48 (in Japanese).

MIYAKAWA, K. and SUWA, K. (1979): The Kalama psammitic gneisses from the Kalama Hill, Machakos area, Kenya. *4th Prelim. Rept. Afr. Studies, Nagoya Univ.*, 113-122.

MIYAKE, A. and SUWA, K. (1981): Geological structure of the Uvete dome, Kenya. *6th Prelim.*

Rept. Afr. Studies, Nagoya Univ., 33-41.

NUREKI, T., SUWA, K., BIYAJIMA, K., SAKA, Y., and YUSA, Y. (1977): Tectonic evolution of the Mozambique belt in area south-east of Machakos, Kenya. *2nd Prelim. Rept. Afr. Studies, Nagoya Univ.*, 13-38.

SANDERS, L.D. (1965): Geology of contact between the Nyanza Shield and the Mozambique Belt in western Kenya. *Bull. Geol. Surv. Kenya,* **7**.

SUWA, K., NUREKI, T., INOUE, H., BIYAJIMA, K., and MIYAKAWA, K. (1979): Geology and petrology of the Machakos area, Kenya. *4th Prelim. Rept. Afr. Studies, Nagoya Univ.*, 3-20.

PLATE I

1. Inselberg consisting of granitoid gneiss, which shows a dome-like structure, near Kaiboi (south of Turbo), Nandi, west Kenya (Photo. by H.S., 12 Dec., 1981).

2. Magnetite sand washed out from fumic soil horizone, Utangwa, Mbooni · Hill, central Kenya (Photo. by H.S., 9 Oct., 1981).

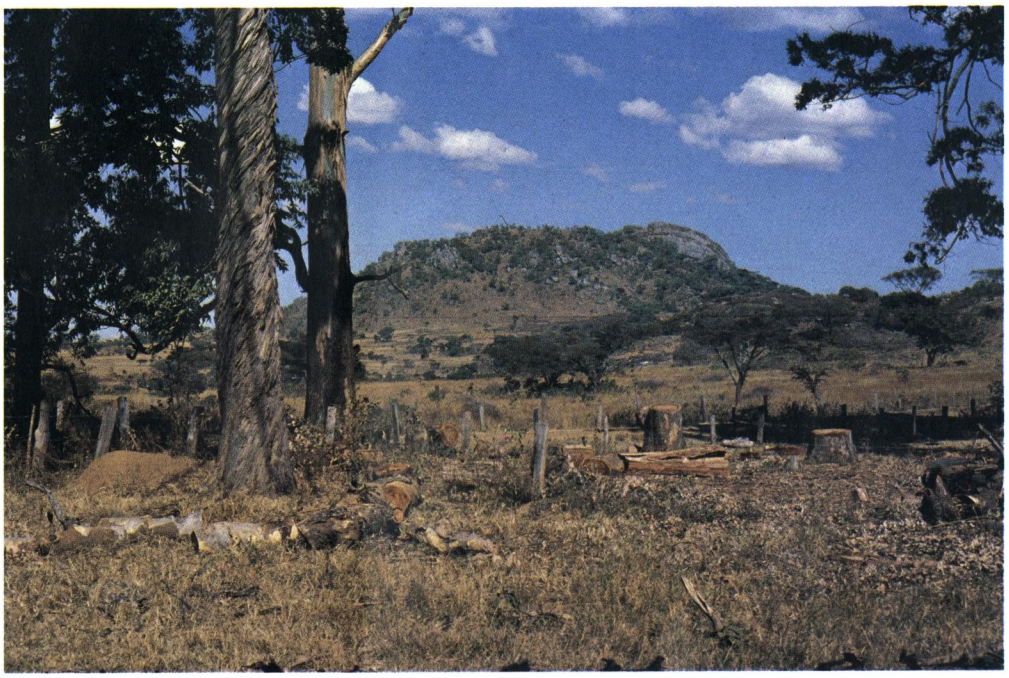

1

2

Chemical effect on AlK_β emission, with special reference to the melt-structure of olivine-nephelinite from the Kwa Nthuku cinder cone, central Kenya

Kazuhiro SUZUKI, Harufumi NORO, Akira MIYAKE,
Yoshiki YAMAMOTO and Ken-ichi YOKOI

Department of Earth Sciences, Faculty of Science, Nagoya University

Abstract

The AlK_β emission spectra of a metal, minerals and glasses have been measured with an electron probe microanalyser. The spectral peak of aluminium metal displaces about 18×10^{-3} Å towards the high-energy side relative to that of corundum. A strong correlation is observed between the average coordination number of aluminium in minerals and the peak displacement; the displacement amounts to 8×10^{-3} Å for feldspars and cordierite towards the low-energy side from the peak position of corundum. The peak displacement of anorthite glass agrees with those of feldspars, and show the preferable occurrence of aluminium as the network-former. The spectral peaks of the glasses of the anorthite-diopside system and of the olivine-nephelinite composition appear at positions between the peaks of corundum and feldspars with a shoulder on their high-energy envelope, indicating the presence of aluminium species other than network-forming one. Aluminium acts as network-former in silicate melts containing monovalent and/or divalent cations equivalent for aluminium, whereas in silicate melts containing excess charge-balancing cations, it does as both the network-former and network-modifier.

Introduction

Aluminium assumes the role of either a network-former (4-fold coordinated cation) or network-modifier (a cation with coordination number larger than 4) in silicate melts. The structure of simple silicate melts (glasses) was often studied by Raman spectroscopic and Radius Distribution Function techniques. On the basis of these studies, Taylor and Brown (1979a,b), Sharma et al. (1979), Mysen et al. (1981), Hess and Wood (1982), McMillan et al. (1982) and others proposed that aluminium occurs as network-former copolymerizing with silica tetrahedra whenever appropriate monovalent and/or divalent cations are available as charge-balancing species. On the other hand, Bruckner et al. (1978 and 1980) claimed the occurrence of octahedral aluminium in silicate melts containing larger amounts of charge-balancing monovalent and/or divalent cations than aluminium.

The structural state of aluminium in magma has received an attention among petrologists in relation to modeling of igneous processes. We examined the pre-

8th Prelim. Rept. Afr. Studies, Nagoya Univ., 135-144, 1983.

sence or absence of the network-modifying aluminium in the glass of an olivine-nephelinite composition by means of the AlK_β X-ray emission spectroscopy. In this paper, we describe first our precise measurement-technique for the displacement of the AlK_β spectral peak with an electron probe microanalyser, second the relationship between the degree of the displacement in AlK_β spectral peak and the average coordination number of aluminium in corundum and in silicate minerals, and third the state of aluminium in the glasses of an anorthite-diopside system and an olivine-nephelinite composition.

Experimental methods

(1) X-ray emission spectroscopy

The X-ray emission spectra were taken on JEOL JXA-5A electron probe microanalyser with Rowland circle diameter of 280 mm. The analysing crystal for the measurement was a TAP crystal (thallium acid phtharate; 2d = 25.757 Å and dimensions: length = 25 mm and width = 8 mm). The instrument operating conditions were 15 kv accelerating voltage, 0.1 μA specimen current, 20 second interval of counting time, and 5 μm beam diameter. A large beam diameter (about 50 μm) together with movement of the beam over a sample was used to prevent the loss of alkali elements in albite, adularia and the olivine-nephelinite glass.

Aluminium metal and corundum were used to calibrate the wavelength before and after each spectrum run. A manual drive mechanism enabled us to reproduce position of the spectrometer within about 0.002 Å in the region of the observed wavelength (0.025 unit of the instrument).

Spectral data were collected by manual step scanning over the peak in fixed time mode in intervals of 0.025 unit. The measurement of the X-ray intensity was repeated three times at each position on a spectrum, and the arithmetric mean of the readings was taken as true intensity. Special care was made on precise control and stabilization of beam current. The drift was monitored by continuous recording of the specimen current and the concomitant measurement of the $AlK\alpha$ intensity using another channel of the electron probe microanalyser, and was corrected linearly between those readings. When the drift was greater than 2 % during each spectral scan, or was suspected to be non-linear, those data were discarded.

(2) Syntheses of the glass samples

The glass of the olivine-nephelinite composition was prepared from the powder of olivine-nephelinite (sample No. KS-77072527) which was taken at the Kwa Nthuku cinder cone, Kenya. About 30 mg of the sample powder was put on a molybdenium film in a vacuum apparatus. In a bell jar below 10^{-5} Torr, the film was heated at 1270°C for 3 minutes to be melted completely and homogeneously. Then the temperature was quickly lowered to 1220°C and maintained for 5 minutes. After cutting off the heating current, the melt was frozen by injection of cooled air. Cooling rate was on the order 500°C/sec over the first 1000°C. The tempera-

ture was determined with an optical pyrometer; the uncertainty in the determination was usually less than ± 20°C.

Losses of Na_2O and K_2O by vaporization were inevitable during this melting. They were lossed almost completely by the 3 minutes melting at the super liquidus temperature (1500°C), but slightly by the melting at the liquidus temperature (1220°C). The compositions of olivine-nephelinite and the synthesized glass are shown in Table 1.

Table 1. Chemical compositions of olivine-nephelinite (A) and the synthesized glass (B)

	A	B
SiO_2	40.11	42.1
TiO_2	3.77	4.07
Al_2O_3	8.61	9.13
FeO*	13.71	13.4
MnO	0.14	0.17
MgO	15.42	15.2
CaO	11.78	12.4
Na_2O	2.12	1.94
K_2O	0.57	0.31
P_2O_5	0.67	–
H_2O	2.25	–
Total	99.15	98.72

*Total Fe as FeO

The starting materials for the glasses of the anorthite-diopside system were prepared from pure SiO_2, Al_2O_3, MgO and $CaCO_3$. The mixture was ground under alcohol in a motor for more than 30 minutes and dried at 110°C. About 30 mg of the each mixture was pressed into a pelet. The pelet was burnt at 700-1000°C for the complete decarbonation, and then was converted into a glass in the same way as the olivine-nephelinite glass. The melting was made at approximately 100°C above the liquidus temperature.

Results and discussions

(1) Emission spectra of aluminium metal and aluminium oxide

The K emission spectra of aluminium metal and aluminium oxide (corundum) are compared with each other in Fig. 1. Of aluminium metal, the principal $AlK\alpha_{1,2}$ doublet appears at 8.343 Å, and the peak of the $AlK\beta$ emission at 7.98 Å. The AlK_β peak is asymmetric and is broad compared with the $AlK\alpha_{1,2}$ doublet. The features suggest the presence of unresolved peak at low-energy envelope of the $K\beta$

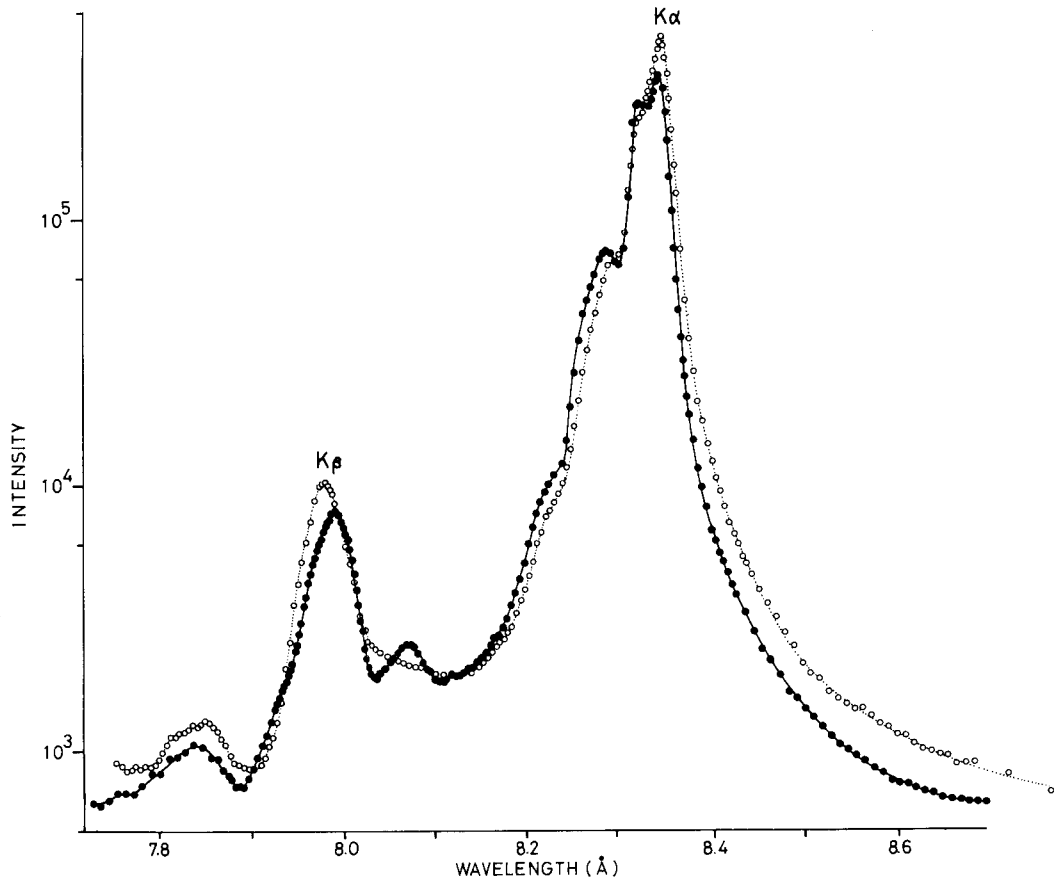

Fig. 1 X-ray emmision spectra of AlK$_\alpha$ to AlK$_\beta$ region for aluminium metal (open circle) and corundum (solid circle).

peak; the AlK$_\beta$ peak of aluminium metal should represent more than one kind of emission line. The broad peak at about 7.85 Å may be the high-energy satellite of the AlK$_\beta$ emission.

The X-ray emission spectrum of corundum differs from that of aluminium metal in peak position and in shape. The principal AlK$\alpha_{1,2}$ doublet of corundum displaces about 1×10^{-3} Å towards the high-energy side. Whereas, the AlK$_\beta$ peak displaces about 18×10^{-3} Å towards the low-energy side. The observed displacement of the AlK$_\beta$ peak agrees well with those reported in some literatures (e.g., Dodd and Glen, 1969; White and Gibbs, 1969).

Another significant difference between the emission spectra of aluminium metal and corundum is the appearance of the AlK$_\beta$ satellite at 8.07 Å in the spectrum of corundum. It is interpreted on the basis of molecular orbital model (Urch, 1970) that the 3p atomic orbital of aluminium participates in the σ bond orbitals of Urch's II and IV states upon oxidation. Hence, the Kβ transition will be splited into II→Al 1s and IV→Al 1s transitions; the main K$_\beta$ band and the low-energy satellite, respectively.

(2) Chemical effect on the AlK_β emission spectra

The ALK_β emission spectra of corundum and albite may represent the two extremes for rock-forming minerals; all aluminium atoms occupy 6-fold coordination site in corundum and 4-fold coordination site in albite. Figure 2 compares the spectra of corundum with albite. The spectral peak of albite displaces about 8×10^{-3} Å towards the low-energy side from the peak position of corundum. The displacement of the AlK_β spectral peak appears to reflect the chemical bonding.

The chemical effect on the AlK_β emission is exemplified in Fig. 3. The spectral peaks of corundum, jadeite and almandine all locate within the range of less than 2×10^{-3} Å. Similarly, the peaks of cordierite and adularia occur within the range of $7-8 \times 10^{-3}$ apart from the peak position of corundum. These two regions denote aluminium occupying 6-fold and 4-fold coordination sites, respectively.

The AlK_β spectral peaks of andalusite, sillimanite and muscovite occur at positions between the two regions. These intermediate displacements are not incon-

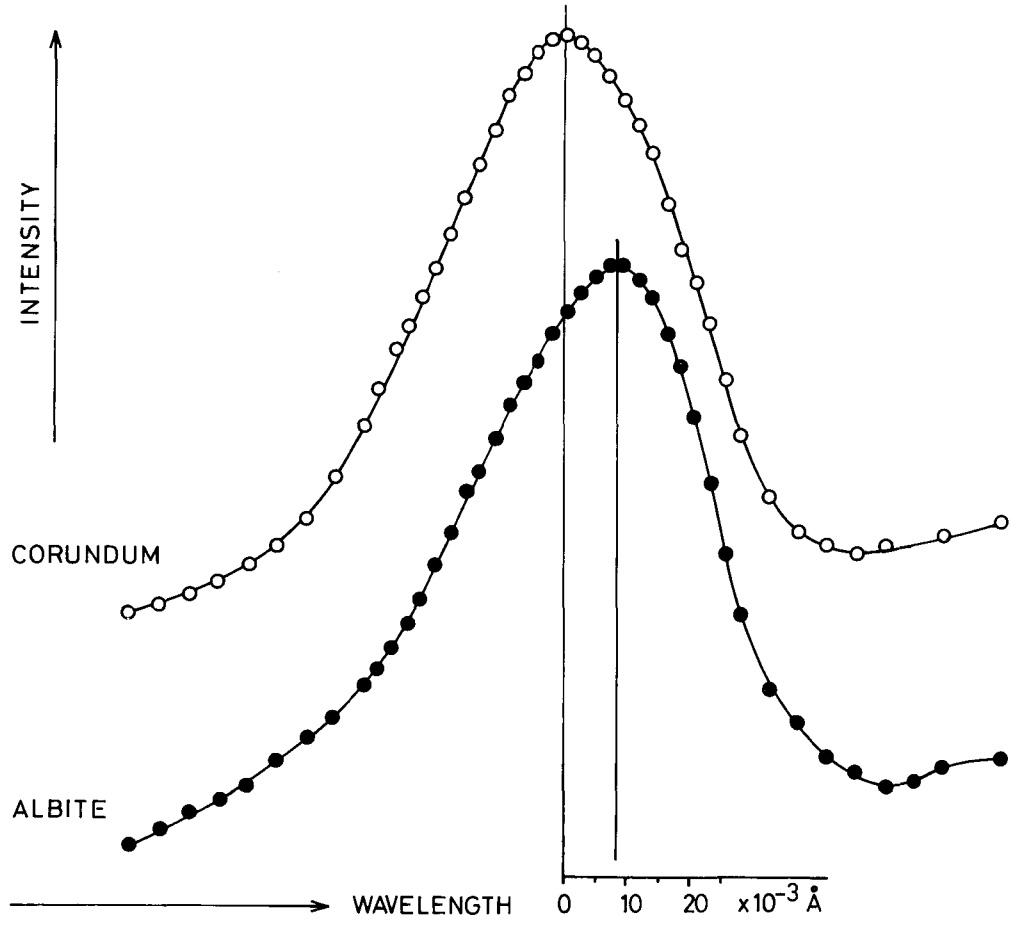

Fig. 2 X-ray emission spectra of $AlK\beta$ region for corundum and albite. Intensity is arbitrary scale. The scale of abscissa represents the displacement of peak position relative to the peak position for corundum.

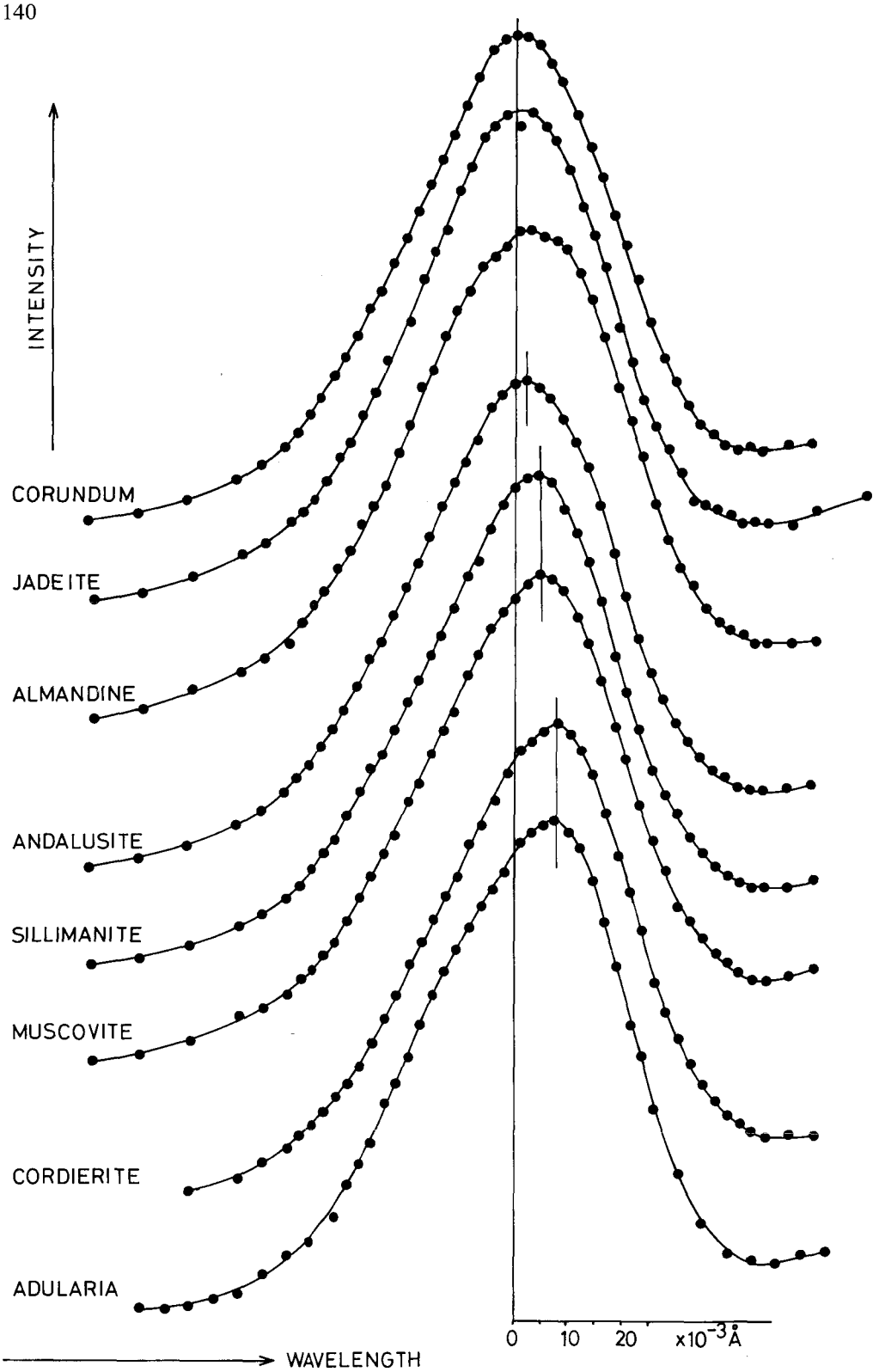

Fig. 3 X-ray emmision spectra of AlKβ region for aluminium containing silicate minerals with a reference spectrum of corundum. Explanations for the ordinate and the abscissa are the same for Fig. 2.

sistent with the view that aluminium in those minerals occupies more than one kind of coordination site. Andalusite is composed of chains of AlO_6 octahedra which are parallel to c-axis and are linked laterally with the alternations of silicon among four tertahedrally arranged oxygens and aluminium among five oxygens. The averaged coordination number of aluminium in andalusite becomes 5.5. Aluminium in sillimanite and muscovite is half in octahedrally coordinated site and half in tetrahedrally coordinated site, and hence the averaged coordination number of aluminium in these minerals amounts to 5. The displacement of AlK_β spectral peak is indicative of the change in the average coordination number of aluminium in crystalline minerals.

(3) The AlK_β emission spectra of glasses

The AlK_β emission spectra for the glasses of the anorthite-diopside system and the olivine-nephelinite composition are shown in Fig. 4. The peak position of the anorthite glass coincides with that of albite, displacing about 8×10^{-3} Å from the corundum peak. Since the anorthite crystal resembles the albite crystal in involving a three dimensional network of $(Si, Al)O_4$ tetrahedra, it will be envisaged that the structural state of aluminium in the mineral and in the glass of the same composition is similar to each other at least in such a simple system. Furthermore, this conclusion is supported by the observation of Velde and Kushiro (1978). They showed that the peak positions of AlK_α and AlK_β of 1 atm. quenched melt with the albite composition are similar to those of crystalline albite, respectively. We conclude that aluminium occurs as the network-former in the silicate melts containing monovalent and/or divalent charge-balancing cations equivalent for aluminium.

The glasses of the anorthite-diopside system show a progressive displacement of peak position toward the high-energy side from the peak position of the anorthite glass with increasing amount of the diopside component. The AlK_β peak for the $An_{35}Di_{65}$ glass occur at the position of 5×10^{-3} Å apart from the corundum peak. Dodd and Glen (1970) explained the AlK_β peak displacement for lithium aluminosilicate glasses as the result of weakening of Al-O bond in AlO_4 tetrahedra. On the other hand, Velde and Kushiro (1978) attributed the peak displacement for high pressure quenched albite glasses to the change in coordination number of aluminium. The observed displacements are too large to be attributed only to the weakening of the Al-O bond, because the Al-O bond length does not change significantly, so far as aluminium occupies 4-fold coordination site. In addition, the appearance of shoulder on the high-energy envelope of the spectral peaks indicates the presence of more than one kind of aluminium species. The displacement of the AlK_β spectral peak for aluminosilicate glasses seems to represent both the change of aluminium species and the weakening of the Al-O bond by depolymerization of the $(Si, Al)O_4$ network.

Above consideration suggests that it becomes increasingly difficult for the aluminosilicate melts to make AlO_4 tetrahedra and aluminium is forced to act as a network-modifier, when the $(M_2O+MO)/Al_2O_3$ ratio becomes larger than unity.

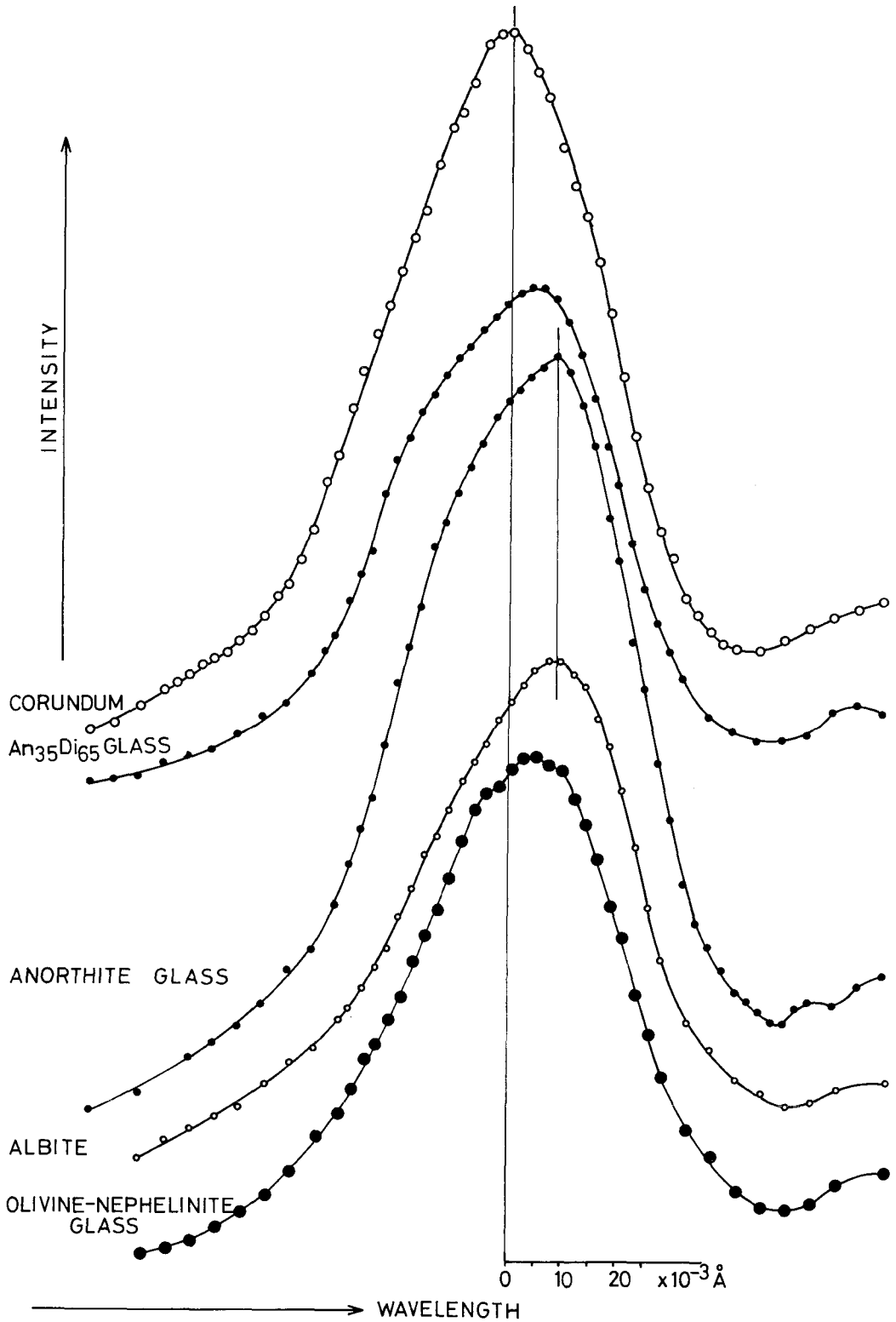

Fig. 4 X-ray emission spectra of K_β region for glasses of anorthite, $An_{35}Di_{65}$ and olivine-nephelinite compositions with reference spectra of corundum and albite. Explanations for the ordinate and abscissa are the same for Fig. 2.

The network-modifying aluminium may coordinate the non-bridging-oxygen of SiO_4 tetrahedra as like alkalies and alkaline earths in simple binary silicate melts (e.g., Mysen et al., 1980).

The AlK_β peak of the olivine-nephelinite glass occurs between the peak positions of corundum and the $An_{35}Di_{65}$ glass. The peak displacement clearly shows that aluminium in the olivine-nephelinite melt acts as both the network-modifier and the network-former at least at near liquidus temperature. Incidentally, the $(M_2O + MO)/Al_2O_3$ ratio of the olivine-nephelinite glass is 7.07, and is higher than that in the $An_{35}Di_{65}$ glass (4.71).

Our conclusion contradicts the previous view that as long as enough charge-balancing cations are present in silicate melts, aluminium acts exclusively as the network-former. But our conclusion is supported by the occurrence of octahedrally coordinated aluminium in phenocrystic olivine. Natural olivine in olivine-nephelinite contains about 210 ppm aluminium. Though the AlK_β emission from olivine is very weak, our careful measurement enables us the determination of the peak position. The peak position of the AlK_β emission from olivine coincides well with that for corundum, and shows that aluminium in olivine occupies preferentially 6-fold coordination site. Inasmuch as aluminium occurs in 6-fold coordination site in phenocrystic olivine, it is safely envisaged that part of aluminium in the olivine-nephelinite magma had acted as network-modifier.

Summary

The displacements of the AlK_β spectral peak have been correlated with change of the average coordination number of aluminium in crystalline minerals. As the degree of the long range order of atomic arrangements little affects the AlK_β emission spectrum, this X-ray spectroscopic technique is useful to study the state of aluminium not only in crystalline minerals but also in poorly crystallized materials and glasses which are not amenable to precise structural analysis.

In silicate melts, aluminium acts as network-former when melts contain monovalent and/or divalent charge-balancing cations equivalent for aluminium. With increasing amount of excess charge-balancing cations, it gradually becomes difficult for aluminium in silicate melts to act as network-former and some are forced to act as network-modifier.

Acknowledgements– We wish to express our sincere thanks to Drs. K. Suwa and R. Sugisaki for their helpful suggestions. Our thanks are extended also to Messrs. I. Hiraiwa and S. Yogo for providing many polished thin sections.

REFERENCES

BRUCKNER, R., CHUN, H-U. and GORETZKI, H. (1978): XPS measurements on alkali silicate and soda aluminosilicate glasses. *Jap. J. Applied Phys.*, **17**, 291-294.

BRUCKNER, R., CHUN, H-U., GORETZKI, H. and SAMMET, M. (1980): XPS measurements and structural aspects of silicate and phosphate glasses. *J. Noncrystalline Solids,* **42**, 49-60.

DODD, C.G. and GLEN, G.L. (1969): A survey of chemical bonding in silicate minerals by X-ray emission spectroscopy. *Am. Mineral.*, **54**, 1299-1311.

DODD, C.G. and GLEN, G.L. (1970): Studies of chemical bonding in glasses by X-ray emission spectroscopy. *J. Amer. Ceram. Soc.*, **53**, 322-325.

HESS, P.C. and WOOD, M.I. (1982): Aluminium coordination in metaaluminous and peralkaline silicate melts. *Contrib. Mineral. Petrol.*, **81**, 103-112.

McMILLAN, P., PIRIOU, B. and NAVROTSKY, A. (1982): A Raman spectroscopic study of glasses along the joins silica-calcium aluminate, silica-sodium aluminate and silica-potassium aluminate. *Geochim. Cosmochim. Acta,* **46**, 2021-2037.

MYSEN, B.O., VIRGO, D. and SCARFE, C.M. (1980): Relations between the anionic structure and viscosity of silicate melts — a Raman spectroscopic study. *Am. Mineral.*, **65**, 690-710.

MYSEN, B.O., VIRGO, D. and KUSHIRO, I. (1981): The structural role of aluminium in silicate melts — a Raman spectroscopic study at 1 atmosphere. *Am. Mineral.*, **66**, 678-701.

SHARMA, S.K., VIRGO, D. and MYSEN, B.O. (1979): Raman study of the coordination of aluminium in jadeite melts as a function of pressure. *Am. Mineral.*, **64**, 779-887.

TAYLOR, M. and BROWN, G.E. (1979a): Structure of mineral glasses — I. The feldspar glasses $NaAlSi_3O_8$, $KAlSi_3O_8$, $CaAl_2Si_2O_8$. *Geochim. Cosmochim. Acta,* **43**, 61-75.

TAYLOR, M. and BROWN, G.E. (1979b): Structure of mineral glasses-II. The SiO_2-$NaAlSiO_4$ join. *Geochim. Cosmochim. Acta,* **43**, 1467-1473.

URCH, D.S. (1970): The origin and intensities of low energy saterite lines in X-ray emission spectra: a molecular orbital interpretation. *J. Phys. C: Solid St. Phys.*, **3**, 1275-1291.

VELDE, B. and KUSHIRO, I. (1978): Structure of sodium alumino-silicate melts quenched at high pressure; infrared and aluminium K-radiation data. *Earth Planet. Sci. Lett.*, **40**, 137-140.

WHITE, E.W. and GIBBS, G.V. (1969): Structural and chemical effects on the AlK_β X-ray emission band among aluminium containing silicates and aluminium oxides. *Am. Mineral.*, **54**, 931-936.

Geological structure of the Archaean greenstone belt, northwest of Kisumu, Kenya

Mitsuo HOSHINO*, Takeru YANAGI**, Kanenori SUWA***
and Peter WINANI****

* Laboratory of Geology, College of General Education, Nagoya University
** Department of Geology, Faculty of Science, Kyushu University
*** Department of Earth Sciences, Faculty of Science, Nagoya University
**** Lake Basin Development Authority, Kenya

Abstract

Archaean greenstone belt occurs in the northwestern part of Kisumu. The Nyanzian System of the oldest rocks in the area, is composed mainly of basalt, andesite and rhyolite and their pyroclastics. Basaltic rocks are predominant in the lower stratigraphic unit, andesitic rocks in the middle unit and rhyolitic rocks in the upper unit. The ratio pyroclastics/lavas of the Nyanzian rocks increases from lower to upper. The Nyanzian System is characterized by the gentle fold with general trend of ENE-WSW and the Kavirondian rocks occur as outliers within the synclinal part.

The Kavirondian System also has three stratigraphic units. The lower unit is composed mainly of conglomerate, the middle unit of sandstone and the upper unit of mudstone. The Kavirondian System is characterized by the open fold with general trend of ENE-WSW to E-W.

The Nyanzian and the Kavirondian Systems were deformed together under the same fold system and the post-Kavirondian intrusives are also constrained to occur in concordant with the general trend of the fold system.

Thickness of the Nyanzian and the Kavirondian Systems are roughly estimated, more than 5,500 m and more than 9,000 m, respectively.

Introduction

Archaean greenstone belts extending around Lake Victoria form a part of the Tanzanian craton. Greenstone belts in Kenya widely occur in the northwestern part and the southern part of Kisumu.

Since 1973, geological investigations on the greenstone belts in Kenya have been made by the Nagoya University geological teams and some papers are published (Kagami, 1975; Suwa, 1981; Nakai and Suwa, 1981; Yanagi and Suwa, 1981 and Yanagi, 1982). In 1981, our field work in western Kenya was concentrated in the northwestern part of Kisumu and many lines of field evidence about the geology of the greenstone belt were obtained.

8th Prelim. Rept. Afr. Studies, Nagoya Univ., 145-156, 1983.

This is a preliminary report in which the geological structure of the greenstone belt occurring in the northwestern part of Kisumu is dealt with.

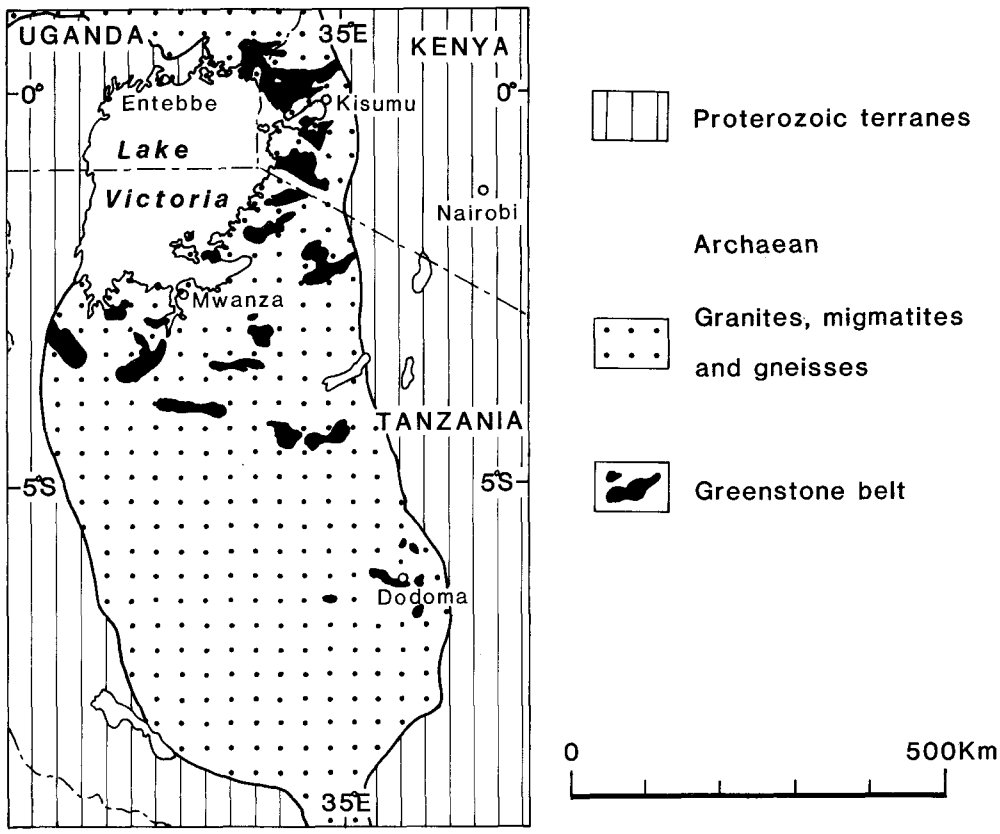

Fig. 1: Geological sketch map of the Tanzanian craton (Phanerozoic cover removed). (After Cahen and Snelling, 1966 and Cahen *et al.*, 1976)

Geological setting

Three rock associations are known in Archaean provinces of the World (Condie, 1981): the granite-greenstone association, the high-grade association, and the cratonic association in the descending order in occurrence. Fig.1 is a generalized geological map of the Tanzanian craton. The craton has an elongated outline in north-south direction and continues northwestward to the West Nile craton. On both sides the Tanzanian craton is cut by Proterozoic mobile belts, Mozambique belt at the east and Ubendian belt at the southwest. The northern half of the Tanzanian craton is typical of the granite-greenstone terrane. On the other hand, the southern half of the Tanzanian craton belongs to the high-grade terrane.

Geological map of the studied area is shown in Fig.2, where Huddlestone (1952) and Saggerson (1952) were partly referred. Archaean rocks in this area are principally of the Nyanzian System, the Kavirondian System and the post-Kavirondian

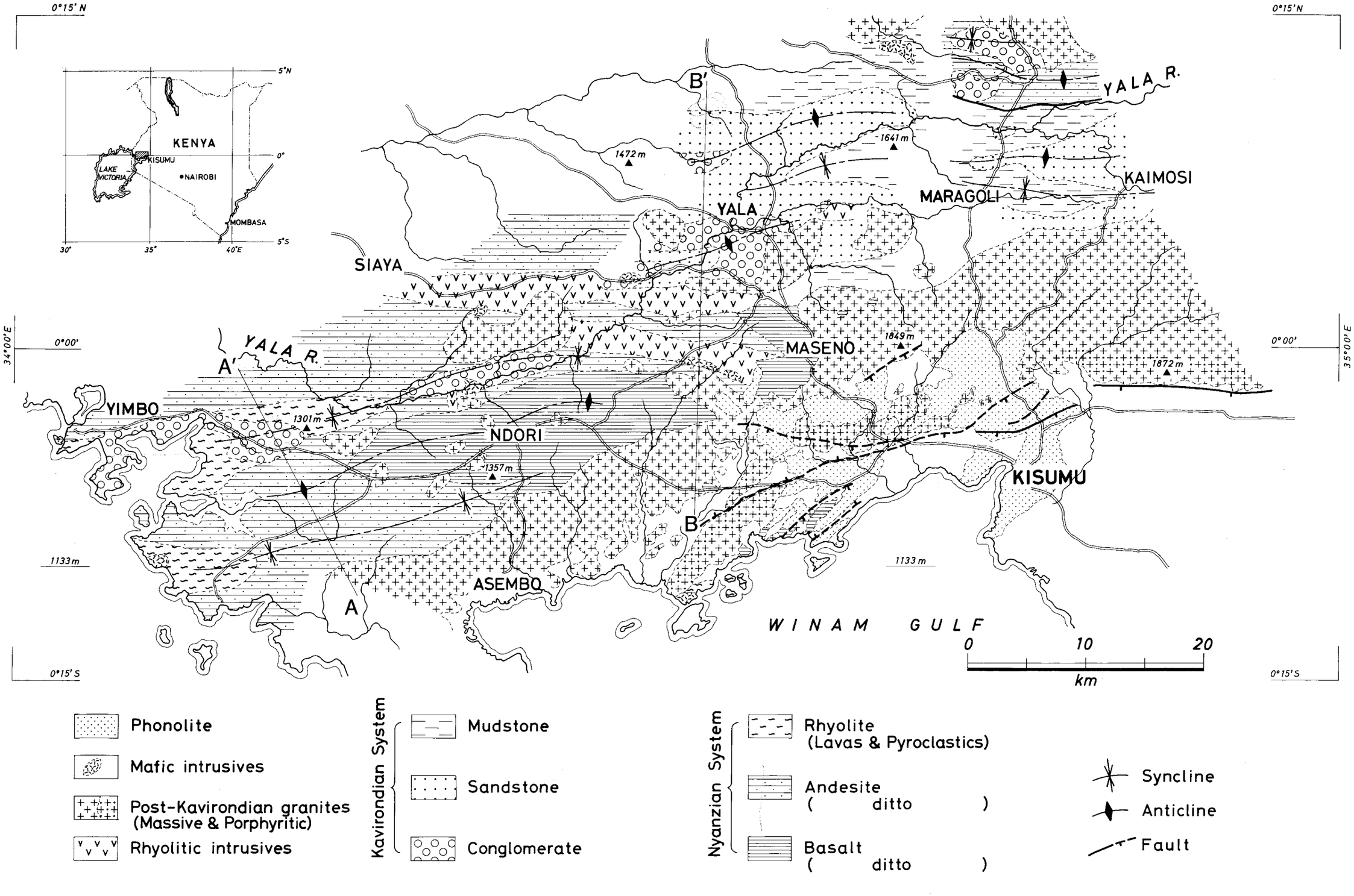

Fig. 2: Geological map of the greenstone belt, northwest of Kisumu, Kenya.

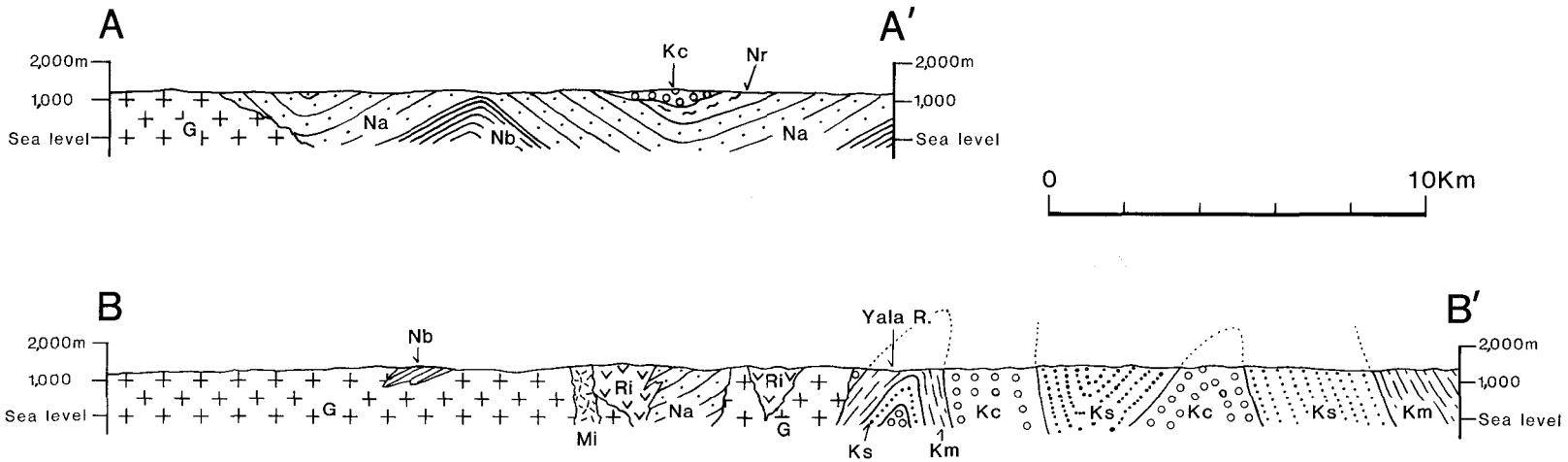

Fig. 3: Geological sections along A-A′ and B-B′ lines in Fig. 2. Abbreviations are as follows; Mi: Mafic intrusives, Ri: Rhyolitic intrusives, G: Post-Kavirondian granites, Km: Kavirondian mudstone, Ks: Kavirondian sandstone, Kc: Kavirondian conglomerate, Nr: Nyanzian rhyolite, Na: Nyanzian andesite, Nb: Nyanzian basalt.

granites. The Nyanzian System, the oldest one in this area, is composed mostly of lavas of basalt, andesite and rhyolite and their pyroclastics. This System is thought to be older than 2,800 Ma (Yanagi and Suwa, 1981 and Yanagi, 1982). The Kavirondian System is composed of conglomerate, sandstone and mudstone and deposited unconformably on the Nyanzian System. The age of the sedimentation of the Kavirondian System is thought to be between 2,800 Ma and 2,500 Ma (Yanagi and Suwa, 1981 and Yanagi, 1982). Post-Kavirondian granites occur as batholithic masses or stock-like bodies. Contact aureoles are clearly found in the Nyanzian and the Kavirondian rocks around the granite plutons. The ages of the post-Kavirondian granites are around 2,450 Ma (Dodson et al., 1975 and Yanagi and Suwa, 1981). Emplacement of the granites is followed by the activities of minor mafic intrusives. From the field occurrence, rhyolitic intrusives found in the central part are thought to be older than the post-Kavirondian granites and younger than the Kavirondian System. Yanagi and Suwa (1981) give the age of 2,700 Ma for the rhyolitic intrusives. These Archaean rocks are covered in part by the Tertiary phonolite lavas. Many faults are observed along the coast and are due to rift movement.

Nyanzian System

The Nyanzian rocks are well exposed in the western and the central parts. The Nyanzian basaltic rocks are weakly foliated and rarely exhibit pillow structures. Plate I-A shows pillow structures found at the point between Ndori and Asembo. Near the contact with the granite plutons, the foliation of basaltic rock is strengthened markedly (Plates IV-A, B and V-A).

The Nyanzian andesitic rocks are generally massive. Pillow structures are sometimes found in the andesite lavas. Sizable extention of the andesite pillow lava is known at Chausu point, 10 Km south-southeast of Yimbo (Suwa, 1981). Andesitic tuff breccia develops around Port Southby, 15 Km south-southeast of Yimbo (Plate I-B).

The Nyanzian rhyolitic rocks are also massive. A sizable body of rhyolitic rocks occurs only at the western part of the studied area. As shown in Plate II-A, the rhyolitic rocks tend to form small hills. The rhyolitic rocks sometimes occur as intercalations within the basaltic and the andesitic rocks (Plate V-B).

Some workers reported banded ironstone, chert and shale occurring in the Nyanzian System which is distributed in the southern part of Kisumu (e.g., Saggerson, 1952 and Le Bas, 1977). These rocks can be, however, found only in trace amounts in the studied area.

Petrochemical study (Suwa, 1981) reveals that the Nyanzian volcanic rocks having $<60\%$ and $>70\%$ in SiO_2 content belong to the tholeiitic rock series and those having 60-66% in SiO_2 content belong to the calc-alkaline rock series; and some rocks show affinities with low-K oceanic tholeiite.

Kavirondian System

The Kavirondian System comprises clastic sediments such as conglomerate, sandstone and mudstone. They frequently alternate with one another.

There are two types of the Kavirondian conglomerates; one is rich in cobbles and pebbles of granitic rocks and the other is rich in boulders, cobbles and pebbles of andesitic rocks. The former type of conglomerate is shown in Plate II-B, and the latter type of conglomerate in Plate VI-B. Plate VI-A shows an alternation of conglomerates and sandstones which seems to exhibit a graded bedding.

Gritty sandstones and mudstones (Plate VII-A) are well-exposed at the road cut between Maseno and Siaya (Fig. 5).

Post-Kavirondian intrusives and extrusives

Rhyolitic intrusives occur in the central part of the studied area and are often accompanied by pyroclastics (Plate VII-B). The intrusives are mainly of porphyritic rhyolite and quartz porphyry.

Porphyritic rhyolite occurring at Ohera church, 13 Km west-southwest of Yala (Fig. 5) was analysed petrochemically and geochronologically by Suwa (1981) and Yanagi and Suwa (1981), who originally thought this rock to be the Nyanzian rhyolite. The Ohera church rhyolite may also belong to the rhyolitic intrusives of the post-Kavirondian age. Comparative petrography on Nyanzian and post-Kavirondian rhyolitic rocks is now under study.

Post-Kavirondian granites widely occur throughout the area. A batholithic mass extends from the west of Asembo to farther east of Kaimosi (Plates III-A and III-B). This mass is named the Maragori granite (Huddlestone, 1952). Many stock-like bodies of granites intrude into the Nyanzian and the Kavirondian Systems and the rhyolitic intrusives.

The post-Kavirondian granites vary in mineral composition. Mineral composition is dominantly of granite and subordinately of granodiorite and diorite. They are generally homogeneous, but porphyritic granite and gneissose granite are sometimes found. Some granites include mafic xenoliths. Kagami (1975) classified the Maragori granite into eight types in lithological features. Plate VIII-A shows a pink K-feldspar porphyritic granite which characteristically occurs in the Maragori granite mass.

Mafic intrusives are dolerite, gabbro and diorite and occur mainly as dykes.

Phonolite lavas in Tertiary age cover the Archaean rocks. Plate VIII-B shows a quarry of the phonolite lavas.

Geological structure

The Nyanzian and the Kavirondian rocks have folded structures. The general trend of the axial traces is ENE-WSW in the western part and is E-W in the eastern

part. The fold axes generally plunge gently or moderately toward both directions.

Synclinal structure is found at the point of 7 Km northwest of Ndori (Fig. 4) and can be traced eastward. The contact relations between the Nyanzian and the Kavirondian System of Fig. 4 cannot be observed in the field. They may contact with each other through reverse fault or thrust. The Kavirondian conglomerates are megascopically distributed along the axial trace of the syncline. At the western extension of this axial trace, the south and the east of Yimbo, the Kavirondian conglomerates overlie the Nyanzian rhyolitic rocks. Anticlinal structure is found within the Nyanzian basaltic rocks, 4 Km northeast of Ndori and both rimbs of the anticline dip 30° to the north and the south, respectively. Fig. 5 exhibits a route map showing the Kavirondian rocks which would form the southern rimb of the anticline just south of Yala. Bedding planes of the Kavirondian rocks of Fig. 5 steeply dip southward.

Based on all this field evidence, we made the geological map and the geological sections (Fig. 3). Geological structure of the Nyanzian System would be represented by the A-A' section of Fig. 3. The Nyanzian System is characterized by the gentle fold and the Kavirondian basal conglomerate occurs as an outlier within the synclinal part of the older rocks. The lower stratigraphic unit in the Nyanzian System is composed mainly of basaltic rocks and the thickness of this unit is estimated more than 1,500 m. The middle stratigraphic unit is composed mainly of andesitic rocks and the thickness is about 3,000 m. The upper stratigraphic unit is composed mainly of rhyolitic rocks and the thickness is more than 1,000 m. Total thickness is estimated more than 5,500 m.

Each stratigraphic unit contains other types of volcanic rocks in considerable amounts. Yanagi (1982) analysed the lithological constitution of the Nyanzian System as given in Table 1. It is clear that basaltic rocks, andesitic rocks and rhyolitic rocks have been repeatedly extruded and the ratio pyroclastics/lavas increased as time proceeded.

The B-B' section of Fig. 3 shows a geological structure at the central part of the studied area. The Kavirondian System of the central part is characterized by the open fold with axial plane being inclined slightly toward the south. From the geological section, following stratigraphic succession can be inferred; lower unit mainly of conglomerate with thickness of more than 3,500 m, middle unit mainly of sandstone with thickness of about 3,500 m and upper unit mainly of mudstone with thickness of more than 2,000 m. Total thickness is estimated more than 9,000 m.

Post-Kavirondian granite plutons have outlines which are concordant with the general trend of the fold axes found in the older rocks. Rhyolitic intrusives also show outlines which are subconcordant with the general trend. The Nyanzian rocks and the Kavirondian rocks near the contact with the granite plutons suffer thermal metamorphism and the metamorphic grade attains up to amphibolite facies. The basaltic rocks in contact directly with the granites as shown in Plates IV-B and V-A, are completely recrystallized and converted into strongly foliated amphibolites.

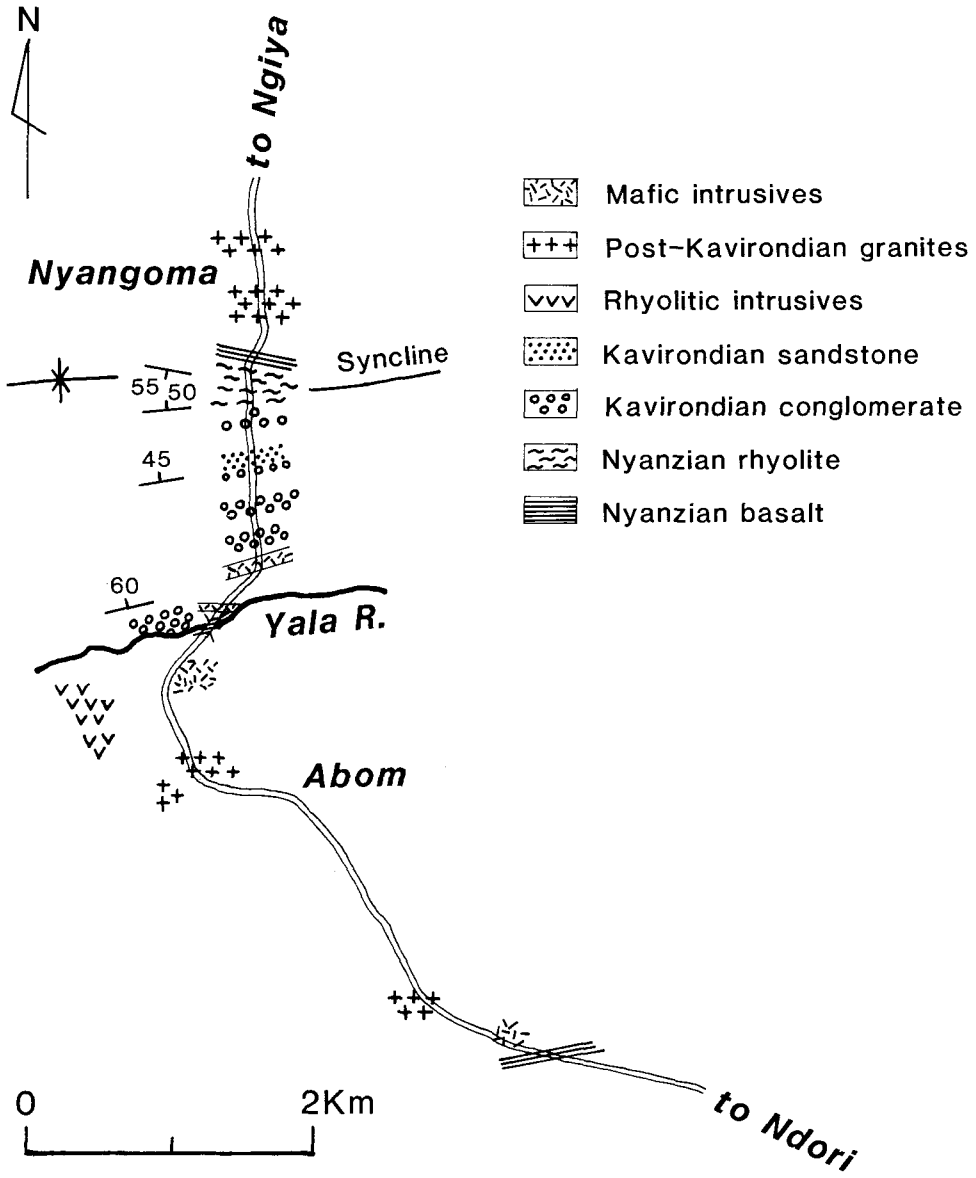

Fig. 4: Route map along the road near Yala bridge, 7 Km northwest of Ndori.

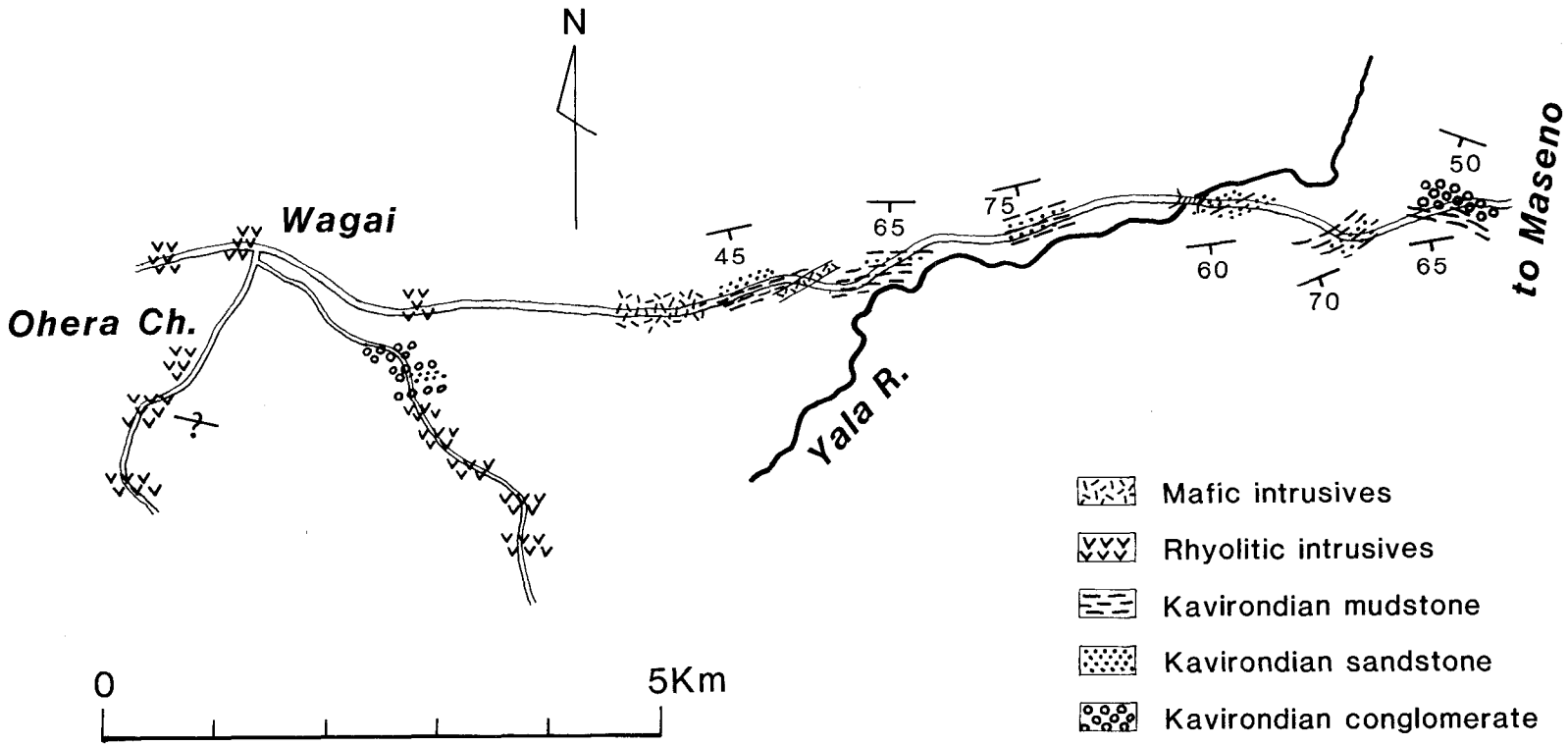

Fig. 5: Route map along the road near Ohera church, 13 Km west-southwest of Yala.

Table 1: Lithological constitution of the Nyanzian System. (after Yanagi, 1982).

Nyanzian System	Felsic Unit (Upper)	Rhyolites	(60%)	Lavas	(45%)
				Pyroclastics	(55%)
		Andesites	(40%)	Lavas	(65%)
				Pyroclastics	(35%)
	Intermediate Unit (Middle)	Rhyolites	(15%)	Lavas	(60%)
				Pyroclastics	(40%)
		Andesites	(80%)	Lavas	(80%)
				Pyroclastics	(20%)
		Basalts	(5%)		
	Basic Unit (Lower)	Rhyolites	(10%)		
		Andesites	(15%)	Lavas	(80%)
				Pyroclastics	(20%)
		Basalts	(75%)	Lavas	(90%)
				Pyroclastics	(10%)

From the fact that some Kavirondian conglomerates contain granite cobbles and pebbles, some of the granite plutons in this area are considered to be pre-Kavirondian in age. Petrology of thermally metamorphosed rocks is now under study.

In conclusion, the Nyanzian System and the Kavirondian System were deformed together under the same fold system and the post-Kavirondian intrusives are also constrained to occur in concordant with the general trend of the fold system.

Acknowledgements – We would like to express our gratitude to Mr. A.S. Segero, Geologist of Kenya Mines and Geological Department for his kind suggestion in the field.

Our thanks are extended to Prof. I.S. Loupekine of the University of Nairobi for his many supports and warm hospitality, and Mr. K. Tokieda and Drs. H. Umemura and M. Asami for their laborious collaboration in the field survey. Our thanks are also due to Mr. H. Shiozaki of Nagoya University for his kind suggestion.

The field work was made possible by the Grant-in-Aid for Overseas Scientific Survey from the Ministry of Education, Science and Culture, Japan, to which we express our thanks.

REFERENCES

CAHEN, L. and SNELLING, N.J. (1966): *The geochronology of Equatorial Africa.* North-Holland, Amsterdam, pp. 195.

CAHEN, L., DELHAL, J. and LAVREAU, J. (1976): The Archaean of Equatorial Africa: A review. *The early history of the Earth* (ed. by B.F. Windley), John Wiley & Sons, New York, 489-498.

CONDIE, K.C. (1981): *Archean greenstone belts.* Elsevier, Amsterdam, pp.434.

DODSON, M.H., GLEDHILL, A.R., SHACKLETON, R.M. and BELL, K. (1975): Age differences between Archaean cratons of eastern and southern Africa. *Nature,* **254**, 315-318.

HUDDLESTON, A. (1954): Geology of the Kakamega District. *Rep. Geol. Survey Kenya,* **28**.

KAGAMI, H. (1975): Maragori granite in Tanganyika craton. *1st. Prelim. Rept. Afr. Studies, Nagoya Univ.,* 14-16.

LE BAS, M.J. (1977): *Carbonatite-nephelinite volcanism.* John Wiley & Sons, London, pp.347.

NAKAI, Y. and SUWA, K. (1981): Zircons in the Precambrian granites from the Kisumu area, western Kenya. *6th Prelim. Rept. Afr. Studies, Nagoya Univ.,* 145-150.

SAGGERSON, E.D. (1952): Geology of the Kisumu District. *Rep. Geol. Survey Kenya,* **21**.

SUWA, K. (1981): Petrochemical and petrographical notes on some Nyanzian volcanic rocks, west Kenya. *6th Prelim. Rept. Afr. Studies, Nagoya Univ.,* 15-32.

YANAGI, T. (1982): Geological process of the African continent. Rept. Colloquium of Japan Overseas Sci. Survey, *"Geological process of the Gondwana land",* 3-16 (in Japanese).

YANAGI, T. and SUWA, K. (1981): Rb-Sr radiometric dating on Precambrian rocks in the western part of Kenya. *6th Prelim. Rept. Afr. Studies, Nagoya Univ.,* 163-172.

PLATE I

A: Nyanzian basalt lava with pillow structures at the point of 8 Km north of Asembo. (Photo by M.H.)

B: Nyanzian andesitic pyroclastics at Port Southby, 15 km south-southeast of Yimbo. (Photo by M.H.)

A

B

PLATE II

A: A distant view of Usengi Hill composed of Nyanzian rhyolite lava. This point is 5 Km west-southwest of Yimbo. (Photo by M.H.)

B: Kavirondian conglomerate rich in cobbles and pebbles of granitic rocks at Nyangoma, 5 Km north-northwest of Ndori. (Photo by M.H.)

A

B

PLATE III

A: A distant view of the post-Kavirondian granite at the point of 12 Km north of Kisumu. (Photo by K.S.)

B: A distant view of the post-Kavirondian granite at the point of 25 Km west of Kisumu. (Photo by K.S.)

A

B

PLATE IV

A: Nyanzian basalt lava along the road at the point of 27 Km west of Kisumu. Its bedding plane dips about 50° to the south. (Photo by K.S.)

B: Thermally metamorphosed Nyanzian basaltic pyroclastics near the contact with the post-Kavirondian granite (white). This point is 7 Km east of Ndori. (Photo by K.S.)

PLATE IV

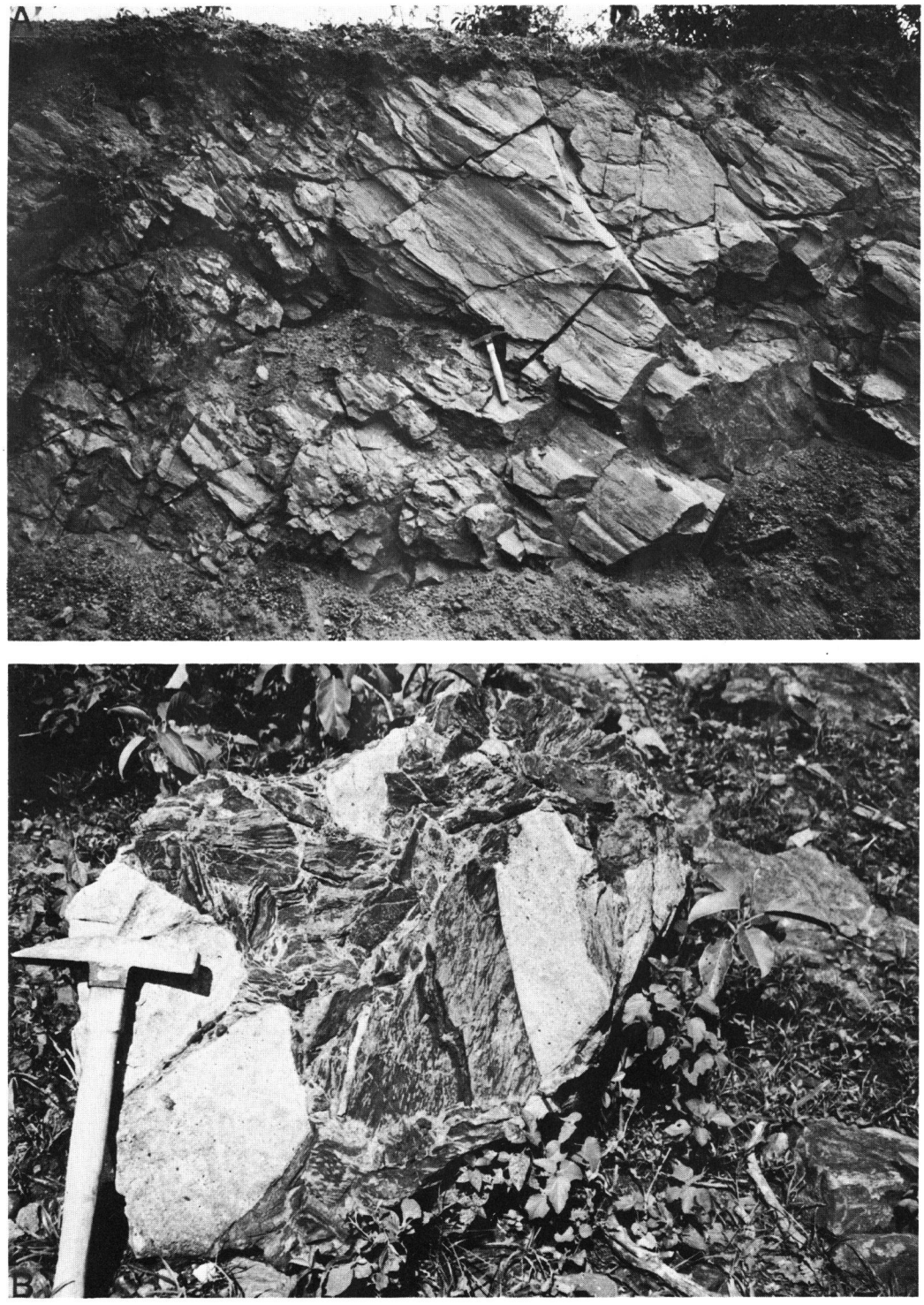

PLATE V

A: Thermally metamorphosed Nyanzian basalt lava at the contact with the post -Kavirondian granite (grey). This point is 2 Km south of Maseno. (Photo by M.H.)

B: Nyanzian basalt lava (right) and Nyanzian rhyolite lava (left) are in contact through minor fault (strike of N80°W and nearly vertical). This point is 5 Km north of Ndori. (Photo by M.H.)

PLATE V

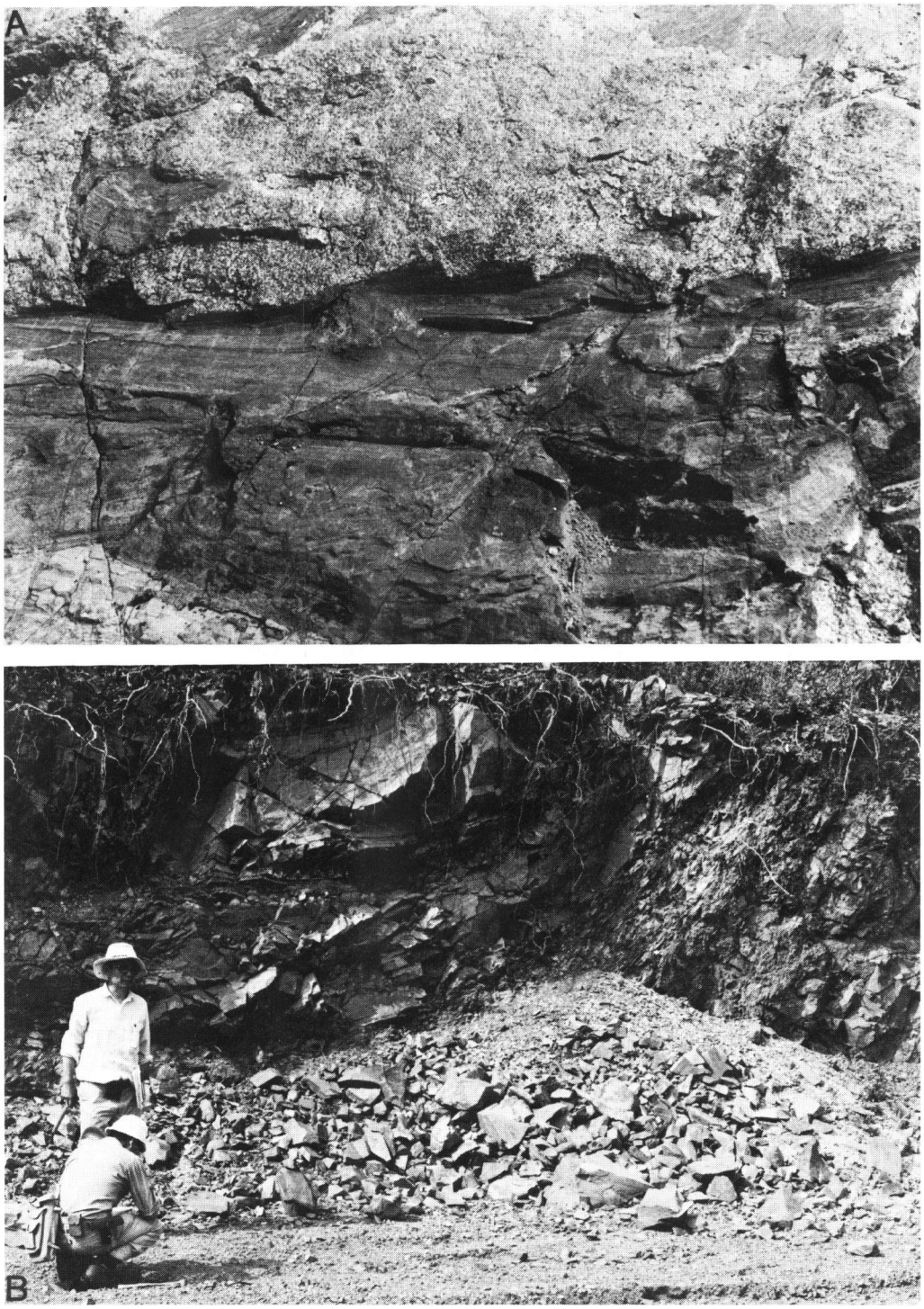

PLATE VI

A: Kavirondian conglomerate alternating with sandstone. This point is 4 Km south of Yala. (Photo by K.S.)

B: Kavirondian conglomerate rich in andesite cobbles at the point of 6 Km northwest of Ndori. (Photo by K.S.)

PLATE VI

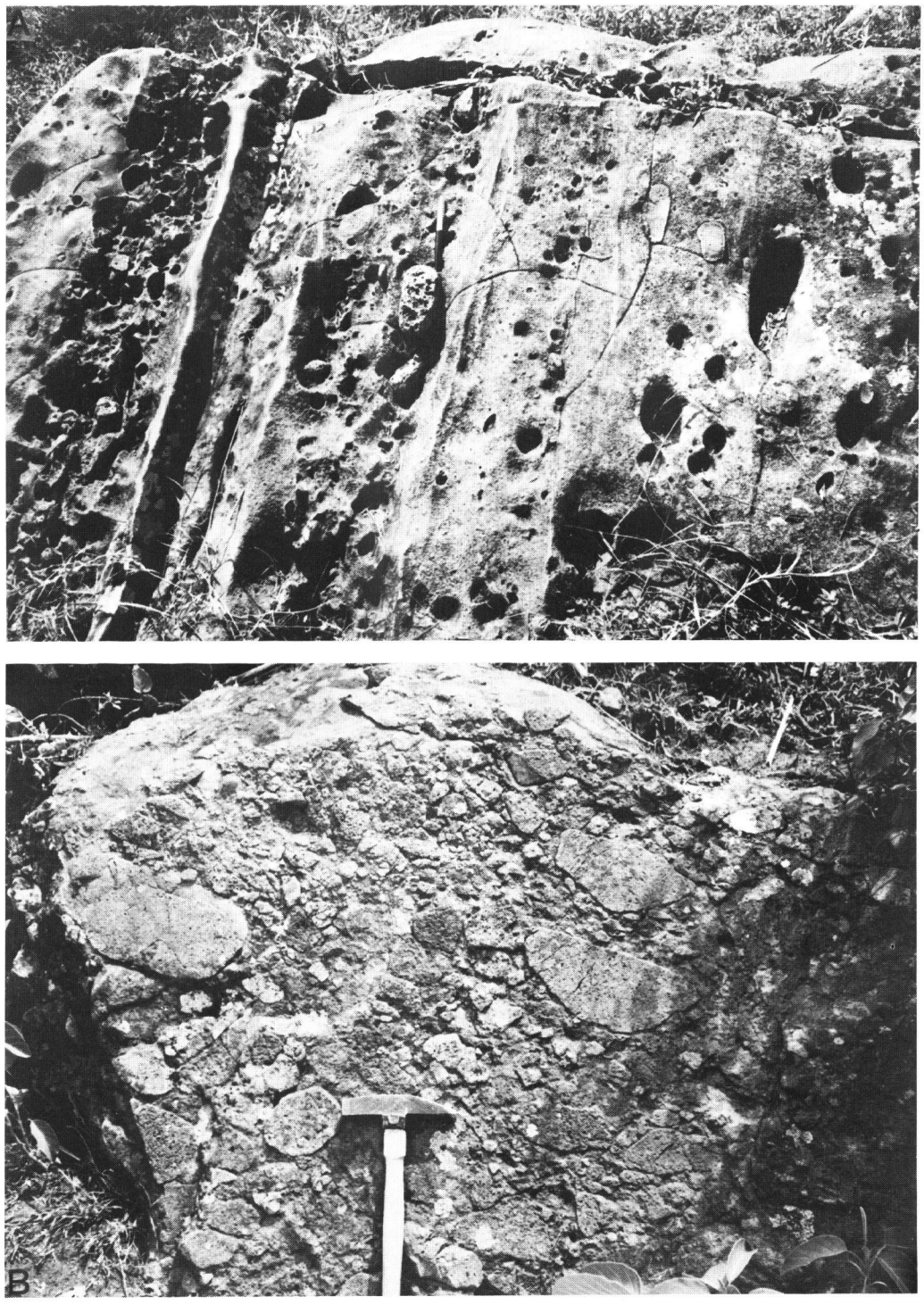

PLATE VII

A: Kavirondian mudstone with dip of about 70° to the south. This point is 8 Km southwest of Yala. (Photo by M.H.)

B: Rhyolitic intrusives (pyroclastics) at the point of 13 Km west-southwest of Yala. (Photo by M.H.)

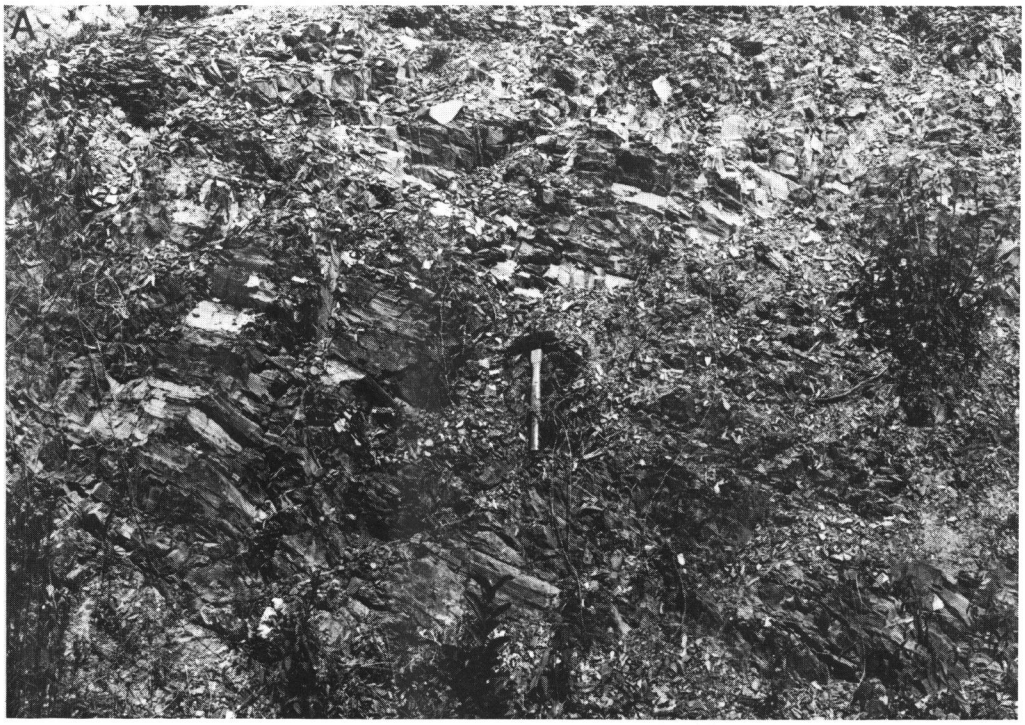
A

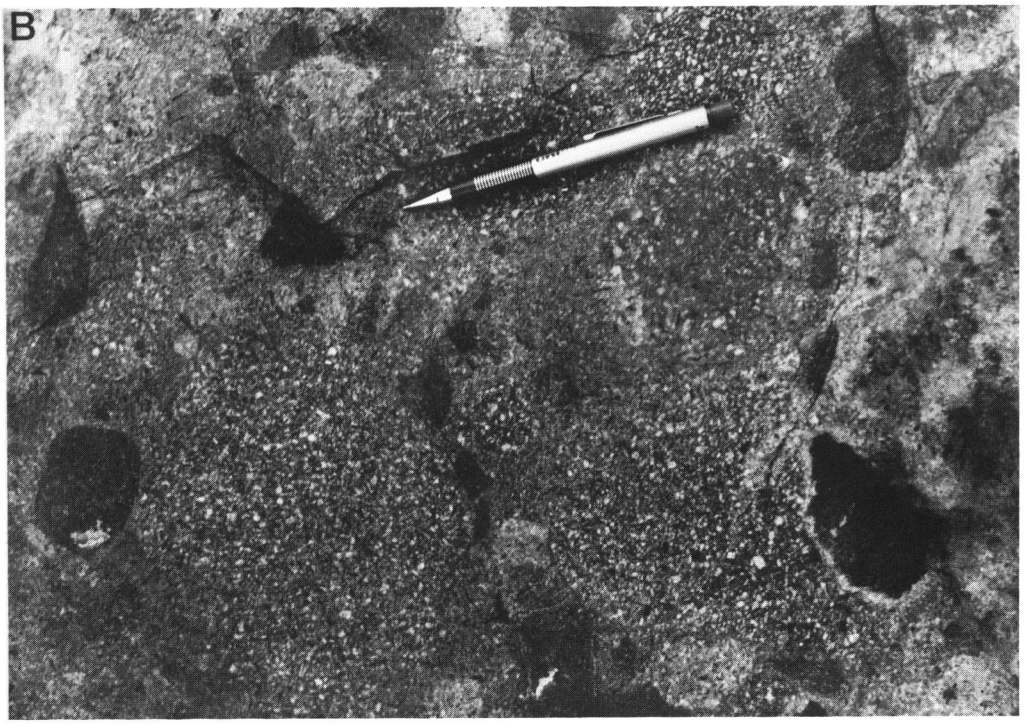
B

PLATE VIII

A: Post-Kavirondian K-feldspar porphyritic granite at the point of 11 Km west of Kisumu. (Photo by M.H.)

B: A quarry of the phonolite lava at the point of 13 Km west of Kisumu. (Photo by M.H.)

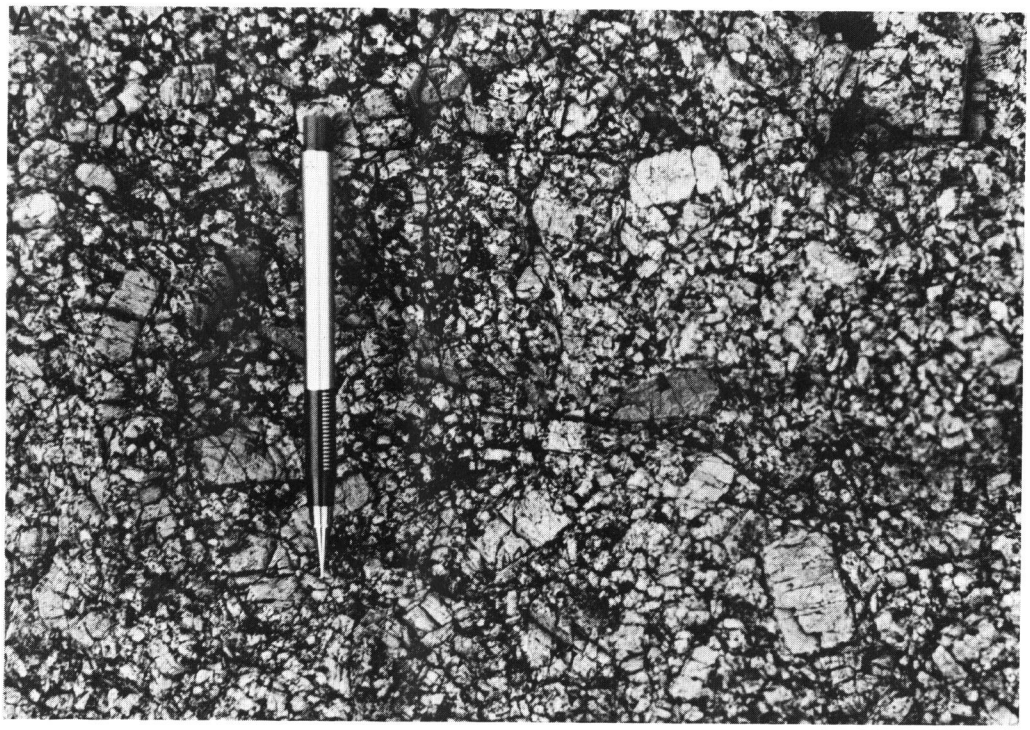

B

Geochronological study of the Maragori granite in the Tanganyika Craton

Hiroo KAGAMI*, Takahiko MARUYAMA**, Mamoru ADACHI***
and Kenji YAIRI****

* Institute for Thermal Spring Research, Okayama University
** Institute of Mining Geology, Mining College, Akita University
*** Department of Earth Sciences, Faculty of Science, Nagoya University
**** Institute of Earth Sciences, Faculty of General Education, Gifu University

Abstract

Whole-rock samples of the Maragori granite in northwestern Kenya give a Rb-Sr isochron age of 2595.4 ± 29.0 Ma with an initial $^{87}Sr/^{86}Sr$ ratio of 0.70139 ± 0.00002. This age coincides with older ages (2300-2800 Ma) of granites in the Tanganyika Craton.

Introduction

The Maragori granite is distributed in the northern part of Kisumu, western Kenya (Fig. 1). The eastern and southern ends of this granite are bounded by the Nandi fault and the Kavirondo rift, respectively. On the other hand, this granite is in contact with the Nyanzian and Kavirondian Systems in the northwestern part.

On the basis of megascopic features, the Maragori granite is classified into eight types (Kagami, 1975) (Table 1), although the mutual relationships among them had not been clarified.

The writers have measured Sr isotopic ratios, Rb and Sr concentrations, and obtained Rb-Sr whole rock ages of this granite. In this paper, the writers preliminarily report the result.

Modal Composition

The modal composition for the analysed rocks is given in Table 2. As the majority portion of epidote and sericite appears to have been derived from plagioclase, the values of epidote and sericite have been added to that of plagioclase. The recalculated composition is plotted in the modal Q-A-P diagram (Fig. 2) and the Mf-(Q+A)-P diagram (Fig. 3); the analysed rocks fall in the field between granite and quartz-diorite of IUGS (1973).

8th Prelim. Rept. Afr. Studies, Nagoya Univ., 157-164, 1983.

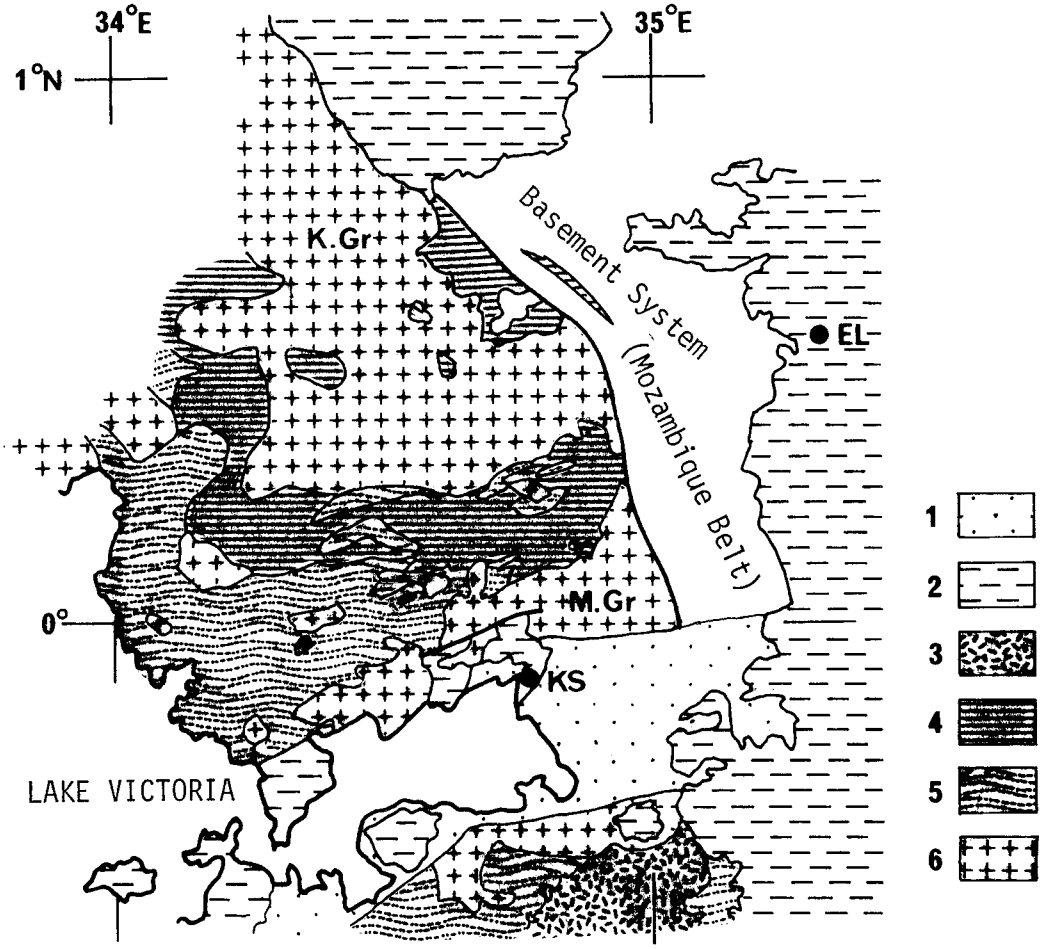

Figure 1 Generalized geological map of the northeastern area of Lake Victoria. 1; Quaternary, 2; Tertiary lavas, 3; Bukoban System, 4; Kavirondian System, 5; Nyanzian System, 6; Granite, K.Gr; Kitoshi granite, M.Gr; Maragori granite, El; Eldoret, KS; Kisumu.

Table 1 Megascopic features of eight rock types.

Type	Coarse (C) Medium (M) Fine (F)	Porphyritic (P) Non-porphyritic (N)	Schistose (S) Massive (M)	Other Features
A-type	Groundmass: F	P	S	
B-type	M	weakly P	M	Leucocratic granite
C-type	M	P	weakly S	This granite has conspicuous crystals of long prismatic euhedral hornblende.
D-type	M	N	S	Many mafic inclusions, aplite and pegmatite are discernible.
E-type	M	N	M	
F-type	C	N	weakly S	Leucocratic granite
G-type	C	N	M, weakly S	Quartz-diorite
H-type	F	N	M	

Table 2 Modal compositions for analysed rocks.
1-11; Maragori granite, 12, 13; Rocks collected from the Mozambique Belt.

Sample No.	Sample Name	Pl	Kf	Qt	Bt	Hd	Ap	Ca	Ch	Ep	Ore	Se	Ti	Rock type
1	7372903	32.9	35.8	23.2	2.4	0.5	0.3	0.0	1.7	1.0	0.3	1.4	0.5	A
2	7380513	33.8	1.8	15.3	10.0	13.3	0.7	0.0	0.0	14.9	0.0	9.8	0.4	G
3	7380515	39.0	3.2	19.8	13.0	13.8	0.0	0.6	0.0	6.0	0.6	3.2	0.8	G
4	7381102	39.6	1.3	22.0	7.8	7.0	0.0	0.0	0.0	15.2	0.1	6.0	1.0	G
5	7381507	29.1	37.8	10.2	5.6	7.7	0.2	0.0	0.0	7.8	0.0	1.2	0.4	C
6	7381801	28.2	15.0	9.1	0.0	26.5	1.8	0.0	1.6	6.7	0.0	8.7	2.4	C
7	7381822	27.3	34.2	23.3	3.3	1.5	0.0	0.0	1.3	4.6	0.5	2.7	1.3	E
8	7381835	37.0	25.7	31.3	0.0	0.0	0.0	0.0	0.7	0.3	0.0	4.8	0.2	E
9	7381836	37.1	22.6	23.8	4.8	0.0	0.4	0.0	0.6	7.6	0.4	2.0	0.7	H
10	7382211	37.1	20.2	15.9	13.9	0.0	0.4	0.2	0.2	6.0	0.2	4.1	1.8	Inclusion
11	7382212	39.5	31.5	18.4	3.0	0.0	0.0	1.0	0.4	3.2	0.0	1.2	1.8	F
12	7380407-A	33.8	3.5	10.5	0.0	50.5	0.5	0.0	0.0	0.5	0.0	0.0	0.7	
13	7381408	24.1	0.0	1.1	1.6	72.4	0.3	0.0	0.0	0.0	0.0	0.0	0.5	

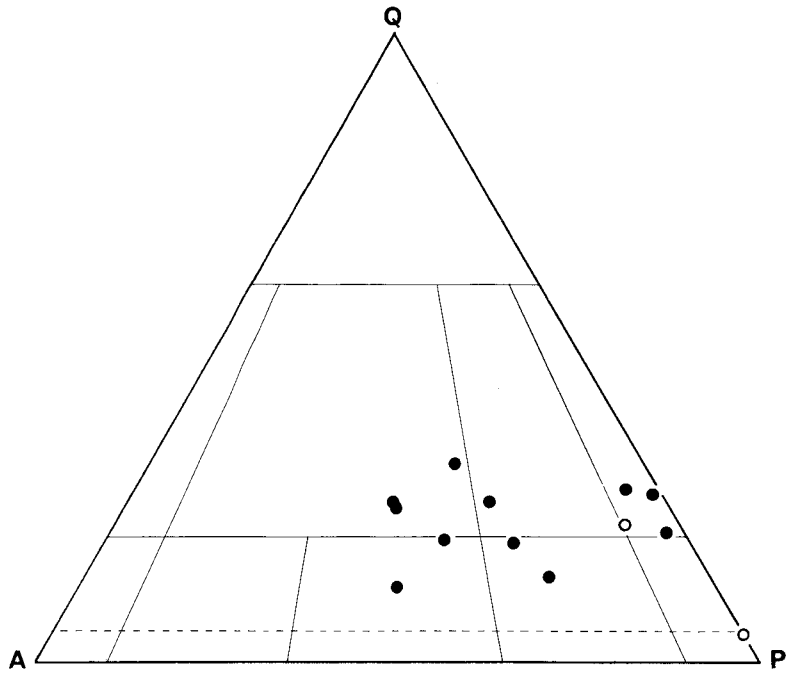

Figure 2 Modal Q-A-P diagram. Closed circles; Maragori granite, open circles; rocks collected from the Mozambique Belt.

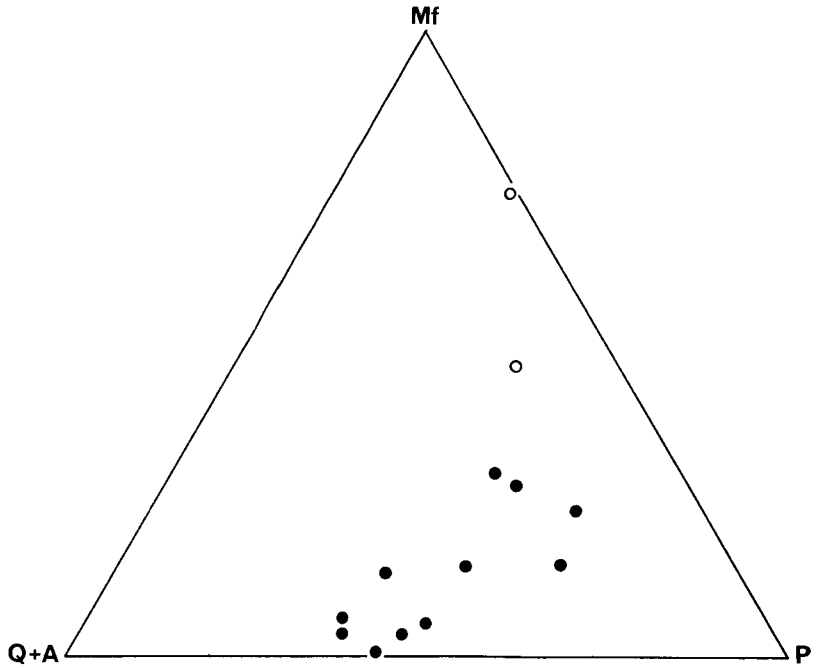

Figure 3 Modal Mf-(Q+A)-P diagram. Symbols are the same as in Figure 2.

Analytical Method

Sr isotopic ratios have been determined by the Varian MAT261 modified from MAT260. All $^{87}Sr/^{86}Sr$ ratios have been normalized to $^{88}Sr/^{86}Sr = 8.375209$, and the average value of $^{87}Sr/^{86}Sr$ ratio on 60 separate runs of NBS987 is 0.710239 ± 0.000007 (2σm); the within-run precision for this ratio is 0.0038% (2σm). Rb and Sr concentrations have been measured by isotope dilution method and X-ray fluorescence method (X-ray Spectrometer Assembly SeN, 3134P, Rigaku Denki Kogyo Co. Ltd.). The precision of Rb/Sr ratio for the former method is 0.68%. On the other hand, the latter has been estimated to be 1%.

Isochron ages have been calculated by the least-square method of York (1969) using a decay constant of $\lambda\ ^{87}Rb = 1.42 \times 10^{-11}\ y^{-1}$ (Steiger and Jäger, 1977). Analytical results are given in Table 3.

Table 3 Analytical result of Sr isotopic ratios, Rb and Sr concentrations.
* isotope dilution method.

Sample No.	Sample Name	$^{87}Sr/^{86}Sr$	$\pm 2\sigma$	$^{87}Rb/^{86}Sr$	Rb (ppm)	Sr (ppm)
1	7372903	0.76827	0.00002	1.7978	166.4	269.4
2	7380513	0.71657	0.00003	0.4064	73.8	525.8
4	7381102	0.70938	0.00007	0.2116	52.4*	716.3*
5	7381507	0.71768	0.00002	0.4382	102.8	679.3
6	7381801	0.72187	0.00003	0.5464	153.0	811.3
7	7381822	0.76612	0.00003	1.7121	194.7	330.9
		0.76615	0.00002			
8	7381835	1.21482	0.00006	16.6677	410.0	74.7
9	7381836	0.73098	0.00004	0.7789	154.2	574.1
10	7382211	0.72615	0.00003	0.6646	140.1	611.1
11	7382212	0.76112	0.00008	1.5813	238.2	438.1
12	7380407-A	0.70485	0.00004	0.0789	16.6*	610.1*
13	7381408	0.72257	0.00007	0.0891	35.5*	1154.4*

Result

Nine samples excluding one (No. 8) define an isochron of 2595.4 ± 29.0 (2σ) Ma with an initial $^{87}Sr/^{86}Sr$ ratio of 0.70139 ± 0.00020 (2σ) (Fig. 4A). The isochron connecting No. 8 and No. 9 which were collected from the same area gives 2112Ma (Fig. 4B).

Two samples (Nos. 12, 13), collected from the Mozambique Belt and rich in hornblende (Table 2), are not plotted on the two isochrons mentioned above (Fig. 5).

The age result of 2595Ma of the Maragori granite is compatible with ages of other granites occurring elsewhere in the Tanganyika Craton; similar ages have been reported by Old and Rex (1971), Wendt et al. (1972), Bell and Dodson (1980) and Yanagi and Suwa (1981). These age data arranged in the frequency distribution

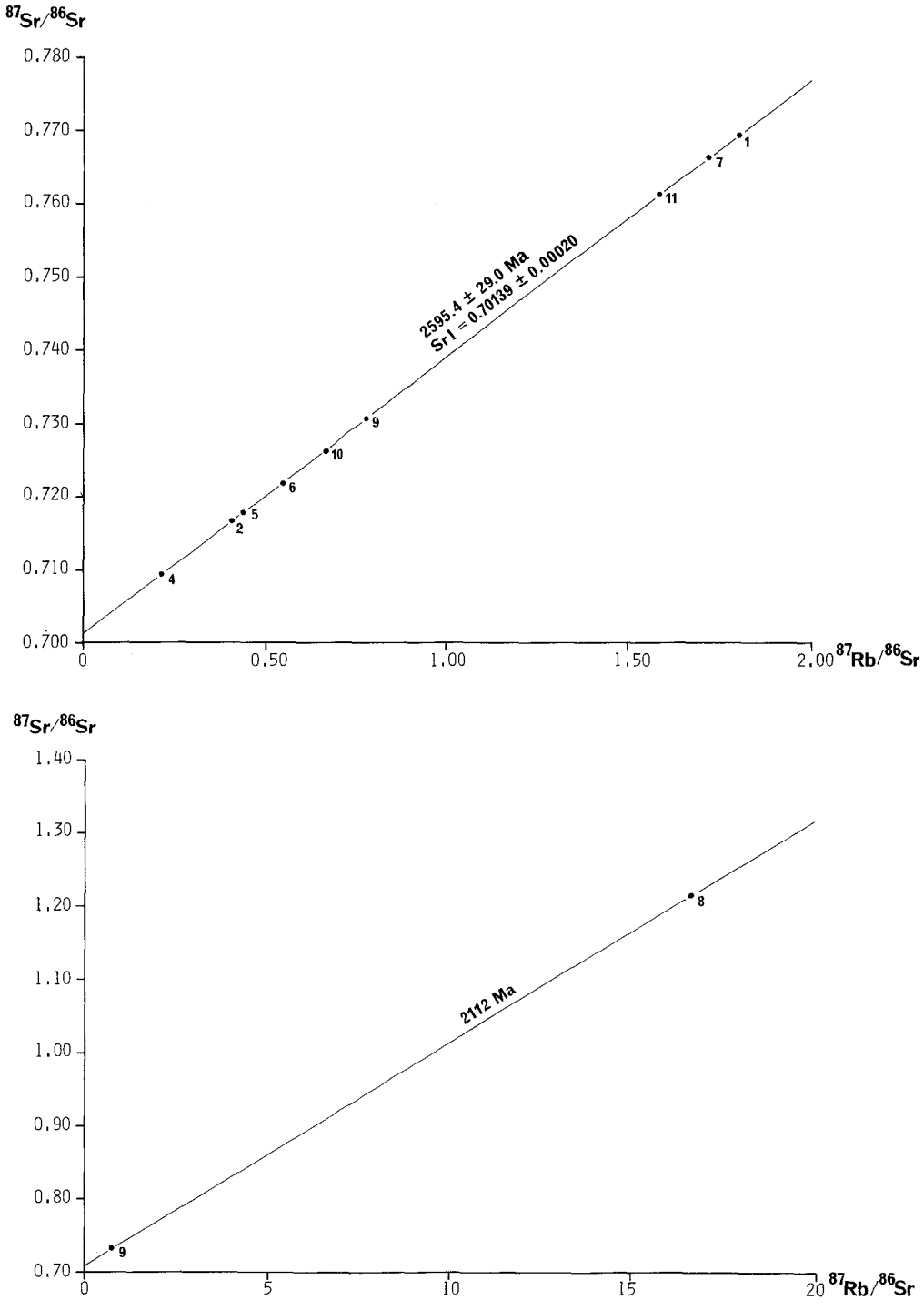

Figure 4A, B Rb/Sr isochron diagram of the Maragori granite.

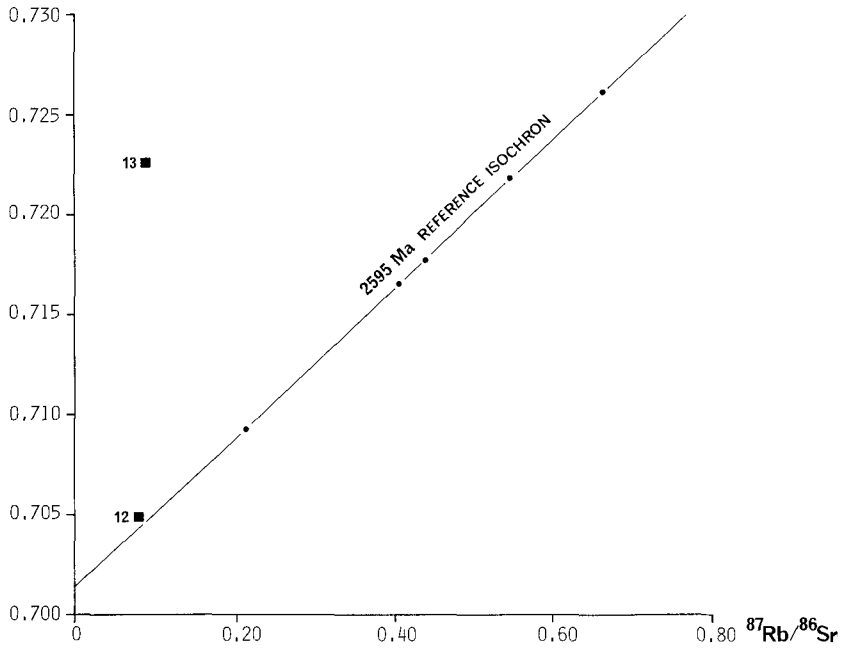

Figure 5 Relation between the reference isochron of the Maragori granite and the data obtained from the Mozambique Belt (closed squares).

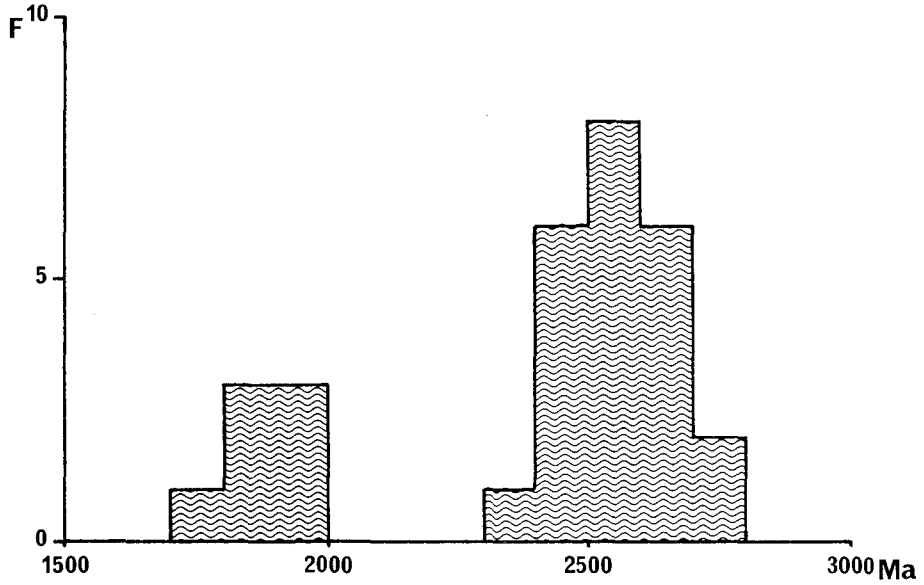

Figure 6 Frequency distribution diagram of isotopic ages for the granites in the Tanganyika Craton.

diagram (Fig. 6) show that the ages of granites in the Tanganyika Craton are distinctly divided into two stages, namely, 1700-2000Ma and 2300-2800Ma. The age of the Maragori granite belongs to the latter older stage. However, the 2112Ma is not consistent with age ranges of the two stages, and further study is needed to examine this age.

Acknowledgements — We would like to express our sincere gratitude to Professor K. Suwa of Nagoya University for his constructive comments on this report.

REFERENCES

BELL, K. and DODSON, M.H. (1980): The geochronology of the Tanzanian shield. *Jour. Geol.*, **89**, 109-128.

IUGS SUBCOMMISSION ON THE SYSTEMATICS OF IGNEOUS ROCKS (1973): Classification and nomenclature of plutonic rocks. *Geotimes*, **18**, 26-30.

KAGAMI, H. (1975): Maragori granite in Tanganyika Craton. *1st Prelim. Rep. Afr. Studies, Nagoya Univ.*, 14-16.

OLD, R.A. and REX, D.C. (1971): Rubidium and strontium age determination of some Precambrian granitic rocks, S.E. Uganda. *Geol. Mag.*, **108**, 353-360.

STEIGER, R.H. and JÄGER., E. (1977): Subcommission on geochronology: Convention on the use of decay constants in geo- and cosmochronology. *Earth Planet. Sci. Letters*, **36**, 359-362.

WENDT, I., BESANG, C., HARRE, W., KREUZER, H., LENZ, H. and MÜLLER, P. (1972): Age determinations of granitic intrusions and metamorphic events in the Early Precambrian of Tanzania. *Proc. 24th Int. Geol. Congr., Montreal*, Section **1**, 295-314.

YANAGI, T. and SUWA, K. (1981): Rb-Sr radiometric dating on Precambrian rocks in the western part of Kenya. *6th prelim. Rep. Aft. Studies, Nagoya Univ.*, 163-172.

YORK, D. (1969): Least squares fitting of a straight line with correlated errors. *Earth Planet. Sci. Letters*, **5**, 320-324.

Magnetic susceptibility of the granitic bodies in the Tanzania craton of western Kenya

Heinosuke SHIOZAKI

Laboratory of Geology, College of General Education, Nagoya University.

Abstract

In order to probe some metallogenic provinces in the Tanzania craton of western Kenya, magnetic susceptibility of the granites has been measured in-situ with an external flat coil of Bison model 3101A.

The magnetic susceptibilities of the granites in this area are considerably higher than those of the granites and granitoid gneisses in the Mozambique metamorphic belt of south-central and west Kenya.

Magnetic susceptibility of G2 granites in South Nyanza is exclusively higher than 500×10^{-6} emu.cgs./cm^3 and that of G3 granites in South Nyanza exclusively lower than the same value. The measuring result of magnetic susceptibility for the granitoid boulders in a Kavirondian conglomerate is divided into two categories: high and low.

There are three patterns of measuring results of magnetic susceptibility for granitoid rocks in North Nyanza. Magnetic susceptibility of some masses is low and that of other masses is high. In addition, magnetic susceptibility is high and low in the different parts of same mass. It is probable that the multiple intrusion occurred even in a respective intrusion body.

Introduction

Geology of western Kenya in the northeast coast of Lake Victoria is mainly made up of the Precambrian volcanic, sedimentary and granitic rocks as a part of Tanzania craton. Magnetic susceptibility of the granitoid intrusive bodies has been measured in place by using an external flat coil of Bison model 3101A in same method with my measurement of granitoid gneisses in the Mozambique belt of south-central and west Kenya (Shiozaki, 1983).

The first quarter of this century a small gold rush happened in this western Kenya, and some gold mines were operated at Kakamega and Migori. Thereafter, however, the productions of gold from these areas had been deseased. I can not enoughly presume what a prospecting procedure will come to be inevitable. An examination of metallogenic potentiality is considered to be one of the inevitable procedure. Therefore, I would like to make clear the metallogenic province of this area in addition to pure scientific studies.

The Archaean rocks of this area are mainly composed of the Nyanzian and

8th Prelim. Rept. Afr. Studies, Nagoya Univ., 165-180, 1983.

Kavirondian systems and their associated granitoid intrusive bodies. Shackleton (1946) designated two ages of the granitoid plutonic activity in which the older granitoid plutons intruded postkinematically into the Nyanzian System before the Kavirondian sedimentation occurred and thereafter the younger granitoid plutons were emplaced postkinematically into the Kavirondian System. His designation has been appreciated and followed by many geologist such as Huddleston, Saggerson, and others. Pulfrey (1946) suggested that the Maragoli granite is composed of multiple intrusive granites. As a result of my measurement of magnetic susceptibility I became to consider that same possibility with Pulfrey's suggestion is also recog-

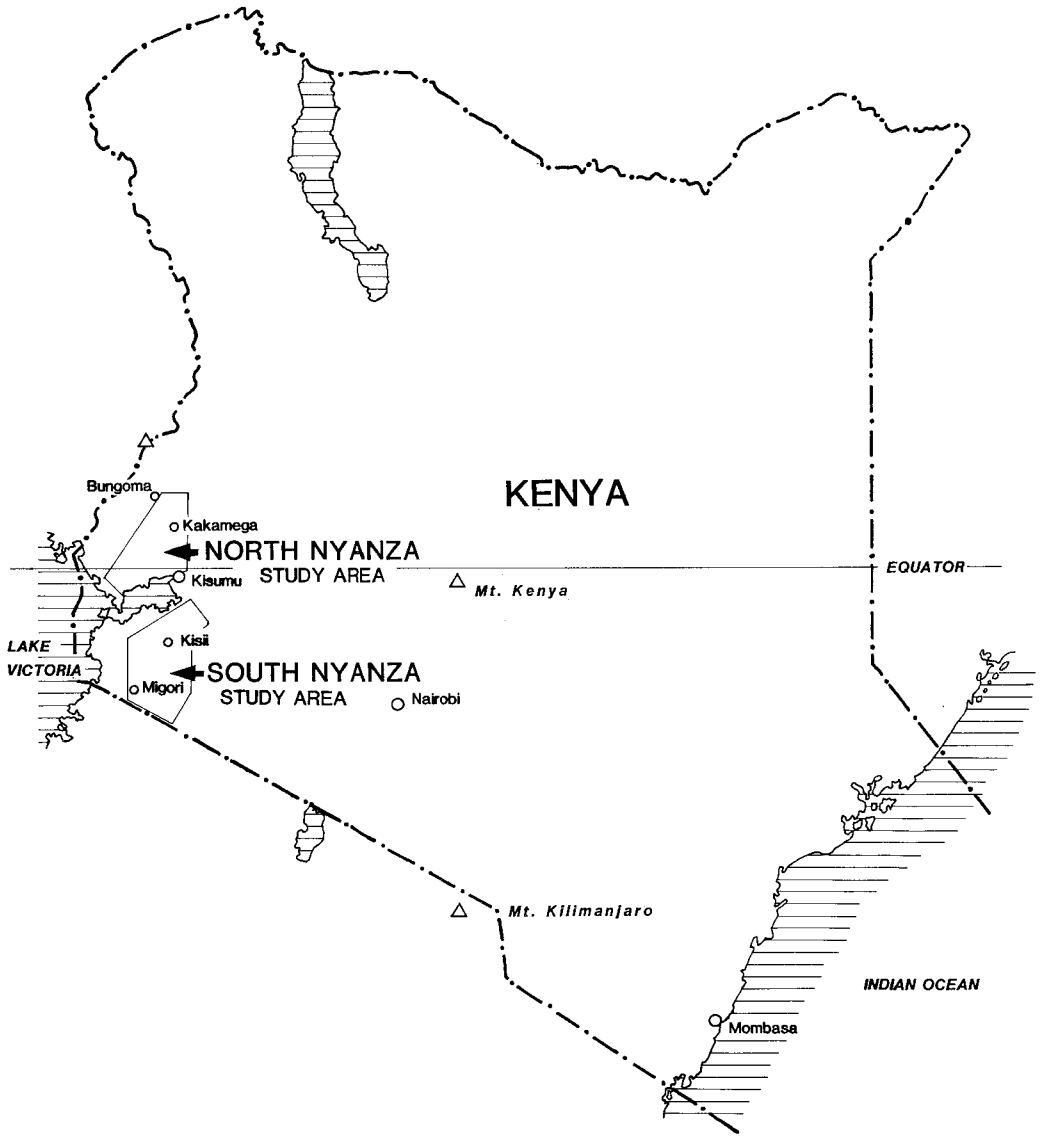

Fig. 1. Map showing the study areas, South Nyanza and North Nyanza.

nized in other plutons as well as the Maragoli granite. In this paper I would like to show the possibility of multiple intrusion even in a respective intrusive body.

Measurements of magnetic susceptibility

1) *Instrument and measuring procedure*

The measurements of magnetic susceptibility of the granitic bodies in the Tanzania craton of west Kenya had been carried out by using the same instrument with that used in the Mozambique belt of south-central and west Kenya, that is, by using an external flat coil of Bison model 3101A. Therefore calibrations and other checks of the instrument were also performed with same method as that in the Mozambique belt (Shiozaki, 1983).

2) *Weathering condition of rocks in this area*

Any examination of weathering conditions is considerably important for measurement of magnetic susceptibility. Climate of Kisumu and adjacent area is different from that of central Kenya (Machakos and its vicinity). Climate of Kisumu is designated as a hot and moist, tropical rain forest climate. Therefore, near the plain surface of this area, lateritic horizons are well developed. Characters of the lateritic horizons are sometimes hard and dark-brown in color being like to a crust of iron pan (cuirass) and some lateritic horizons are not hard and are dark-brown colored and vesicular cuirass. The remained category of the lateritic horizons is loosely gathered aggregates of beans-like (pisolitic) shaped clusters.

Under the such weathering conditions, magnetite crystals and other iron minerals are easily decomposed and removed from the mother rocks. Magnetic susceptibility of the weathered granitic rocks, therefore, has been probably reduced in comparison with that of original fresh rocks.

Measurement of the magnetic susceptibility were performed as possible as on the unweathered fresh rocks, and were not performed as possible as on the weathered rocks and rocks having weathered surfaces.

South Nyanza

1) *Outline of geology*

The Archaean terrain, which surface extends with gentle trend from the southern scarp of the Winam (Kavirondo) rift to the border between Tanzania and Kenya, is made up of the Nyanzian rocks, the small roof-pendants of the Kavirondian conglomerate, and the granitic intrusive bodies. Shackleton (1946) divided the granitic rocks into G2 (post-Nyanzian and pre-Kavirondian) and G3 (post-Kavirondian). Saggerson (1952) designated the Miriu granodiorite from both G2 and G3 granites.

The measurements of magnetic susceptibility were carried out on these three granitic bodies (G2, G3 and GD) and the granitic boulders in the Kavirondian conglomerate.

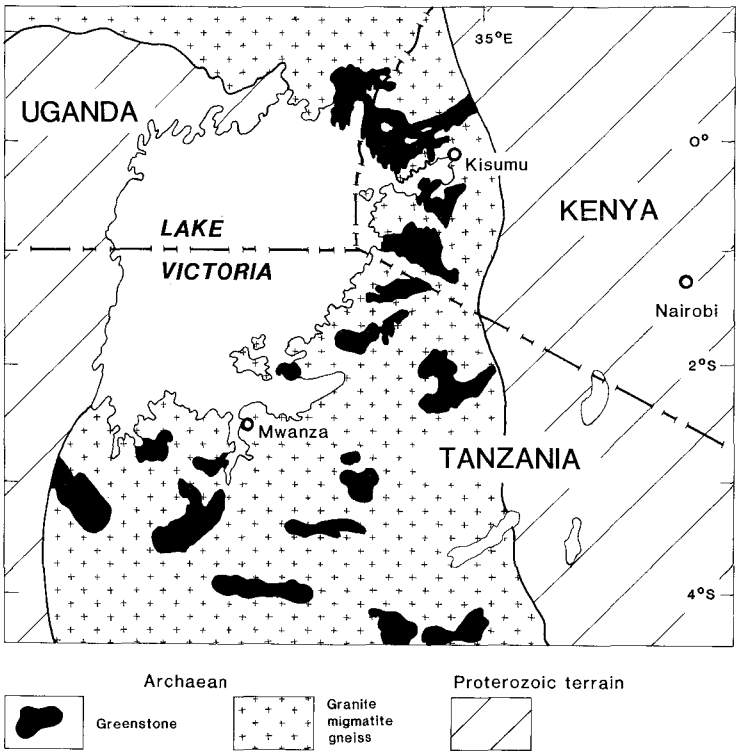

Fig. 2. Geological Sketch map of the northern part of Tanzania (phanerozoic cover removed)
(After Cahen & Snelling, 1966 and Cahen, Delhal & Lavreau, 1976)

2) *Magnetic susceptibility of G2 and G3 granites*

Magnetic susceptibility of G2 granites is exclusively higher than 500×10^{-6} emu. cgs./cm^3 at Nyambija (Rongo gr.), Suna south and Kihancha (Migori gr.). On the other hand, the magnetic susceptibility of G3 granites is exclusively lower than 380×10^{-6} emu.cgs/cm^3 and higher than 135×10^{-6} emu.cgs./cm^3 at Itiero (Itiero gr.), Nabohansi and Tarranganya (Suna gr.).

The classification for G2 and G3 made by shackleton (1964) is coincident with the measuring result of magnetic susceptibility. Granite complex along the border between Kenya and Tanzania is divided into two parallel bodies. The northern, high magnetic susceptibility granite body corresponds to G2 granite and the southern, low magnetic susceptibility granite body to G3 granite.

3) *Magnetic susceptibility of the Miriu Granodiorite*

Magnetic susceptibility of the Miriu granodiorite was measured at north of Sondu. Megascopical feature of granodiorite is migmatitic being mixed with slightly gneissose fine-grained granodioritic palaeozome and massive pink porphyritic medium- and coarse-grained leuco-granitic neozome.

Magnetic susceptibility of the granodiorite palaeozome is high and that of the leuco-granitic neosome is low. The boundary value between high and low values for magnetic susceptibility is 130×10^{-6} emu.cgs./cm^3, which is nearly coincident with that of the granitoid gneisses in the Mozambique belt in Kenya. Granitoid gneisses in the Mozambique belt are divided into two types, domed and undomed, at 130×10^{-6} emu.cgs./cm^3 (Shiozaki, 1983).

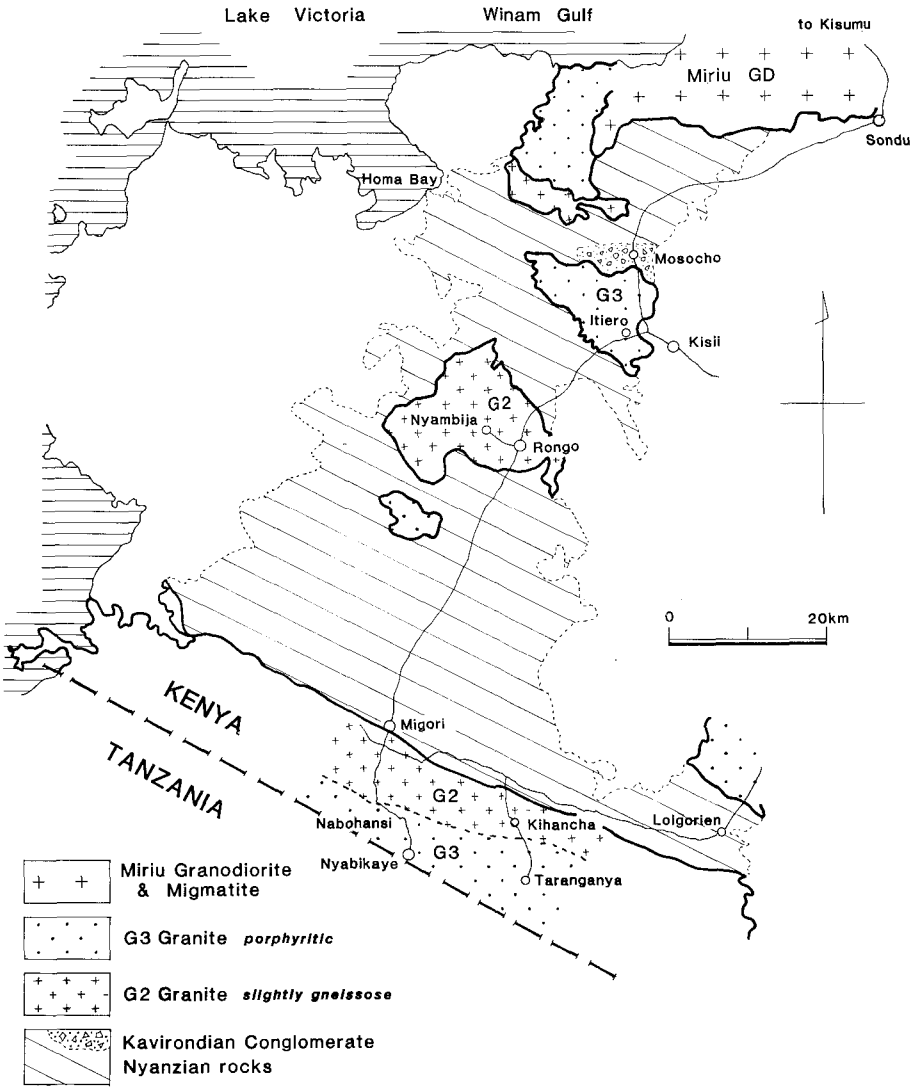

Fig. 3. Index map showing the distributions of G2, G3 and GD bodies in South Nyanza

Table 1. Magnetic susceptibility of granitoid bodies in South Nyanza (volume magnetic susceptibility in $\times 10^{-6}$ emu.cgs./cm^3)

	Locality	Rock	Min.	Max.	Average	Number of Measurings
1.	**Sondu**					
	Miriu grandiorite and migmatite					
		Migmatite (nebulitic)	160	1740	922	5
		Migmatite (nebulitic)	800	1650	1289	5
		Migmatite (nebulitic)	160	2130	1850	5
		Migmatite (schollen & stictolithic)				
		leucozome	25	104	68	6
		melanozome	83	165	116	4
2.	**Itiero air strip**	Po[1]. pink. leuco.	80	520	337	5
3.	**Nyambija**	Rongo Gr.	680	1010	750	8
4.	**Suna south**	G2 Gr.	690	1380	1089	5
		G2 Gr.	570	1550	1084	5
5.	**Nabohansi**	G3 Gr.	70	170	137	5
		G3 Gr. Po. pink. leuco.	120	150	135	2
		G3 Gr.	50	290	192	3
6.	**Kihancha**	G2 Gr.	1125	1935	1483	5
		G2 Gr.	1160	2040	1504	8
		G2 Gr.	1220	1790	1521	6
		G2 Gr.	1280	1700	1496	5
9.	**Taranganya**	G3 Gr.	120	230	177	3
		G3 Gr.	310	410	380	4
10.	**Mosocho**					
	Kavirondian conglomerate		40	60	50	2
	Kavirondian conglomerate		940	950	945	2

[1] Po. = porphyritic

4) *Magnetic susceptibility of the granitoid boulders in a Kavirondian conglomerate.*

Near Mosocho, a Kavirondian conglomerate is exposed as a roof-pendant. The Kavirondian conglomerate contains many rounded boulders, up to 50 cm across, of granitic rocks, volcanic rocks, banded ironstones, chert and other sedimentary rocks.

The granitoids may be apparently designated as G2 granite, post-Nyanzian and pre-Kavirondian, but do not be designated as post-Kavirondian G3 granite. The measuring result of magnetic susceptibility for the granitoid boulders is divided into two categories: high and low.

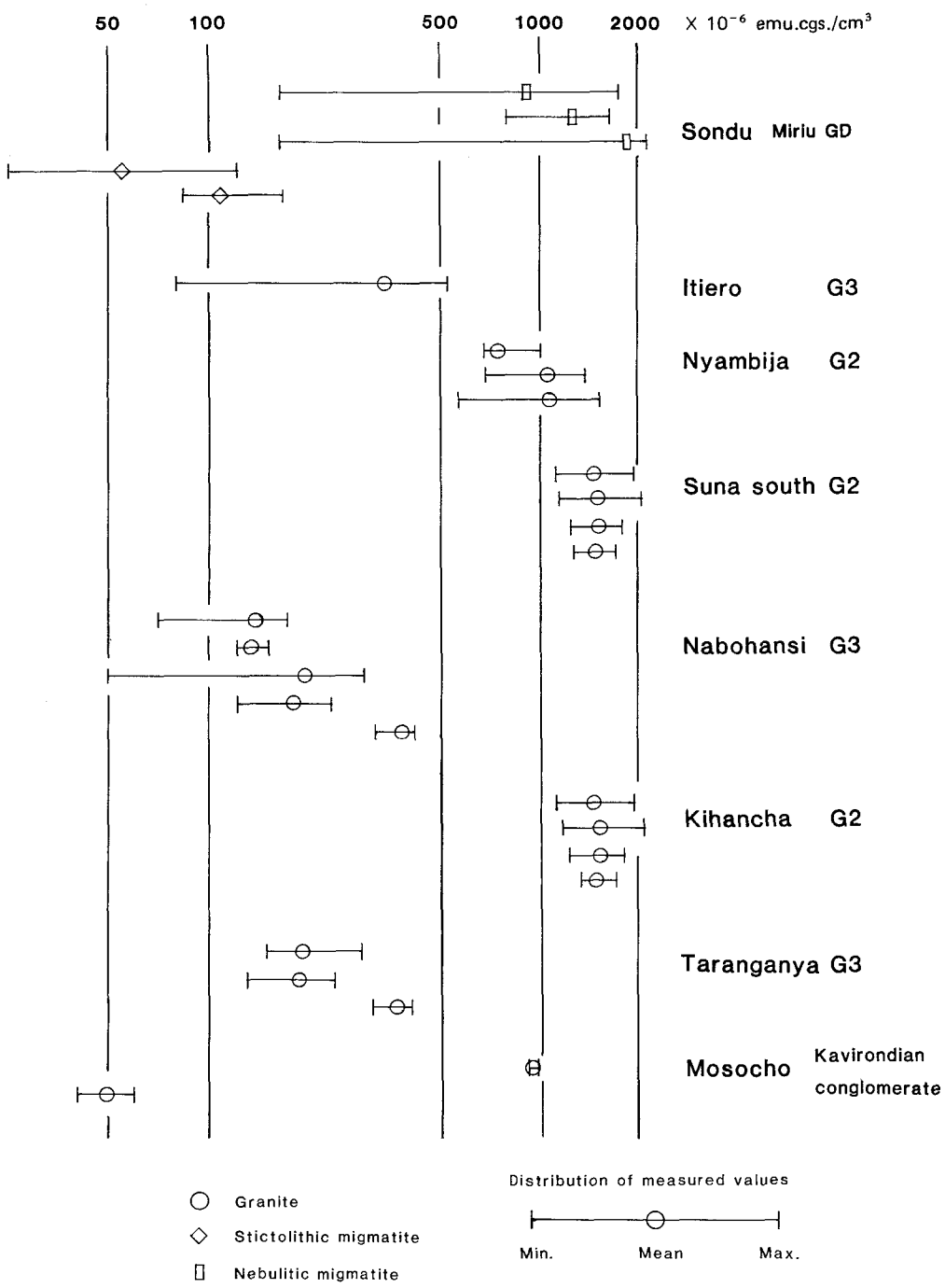

Fig. 4. Magnetic susceptibility of granitoids in the Tanzania craton, South Nyanza, Kenya.
(Volume magnetic susceptibility in $\times 10^{-6}$ emu.cgs./cm^3)

Yanagi and Suwa (1981) made a geochronological study on the granitoid boulder in a Kavirondian conglomerate. The granitoid boulders, however, did not define an isochron. Following possibilities on the granitoid boulders in a Kavirondian conglomerate can be considered: (1) Pre-Nyanzian granite (2) synkinematic Nyanzian granite (3) two granioid rocks of post-Nyanzian and pre-Kavirondian.

North Nyanza

1) *Outline of geology*

Almost all areas of north Nyanza consist of a part of the Tanzanya craton. A very flat surface, which is gently inclined toward the south, is extended from Bungoma to Kakamega. It is named as North Nyanza Plain. In some places, tors and inselbergs are protruded up from the flat surface of the plain. South of Kakamega the surface of the plain becomes undulating land form and ends at the northern scarp of the Winam (Kavirondo) rift.

The rocks of the Tanzania craton are extended with a trend of ENE-WSW, which is also revealed as fold axes and is nearly parallel to the arrangements of rock facies. The rocks of the Kavirondian are distributed near Kakamega and Yala, and the south of Kakamega and Yala is occupied by the Nyanzian system. The northern side of the Kavirondian system is intruded by the Kitoshi Batholith (Sanders, 1965), further northern area of which is covered by vocanics of Mt. Elgon. The Kitoshi Batholith is the most wide-spread granitic body in this area from the west of Nandi scarp to the border between Kenya and Uganda and tnerefore it may not be simple granitoid body.

Other granitic intrusive bodies are distributed at the crest of anticlines of the Nyanzian and Kavirondian systems are elongated along the fold axes. Small bosses, however, are not elongated.

The name of the granitic intrusive bodies, which have been set forth in Fig.5, are shown as follows:

1. Kitoshi Batholith (Mumias Granite)
2. Kakamega Boss (diorite)
3. Yala-Luanda mass
4. Maseno-Maragoli mass
5. Kisian mass
6. Asembo mass
7. Abiero Hill
8. Abom outcrop
9. Ober mass
10. Boro mass

The name, Kitoshi Batholith, was given by Sanders (1965), but another name for same body had been given by Huddleston (1954) as Mumias granite. The name, Kakamega Boss, was given by Huddleston (1954), Kisian granite and Asembo granite given by Saggerson (1952).

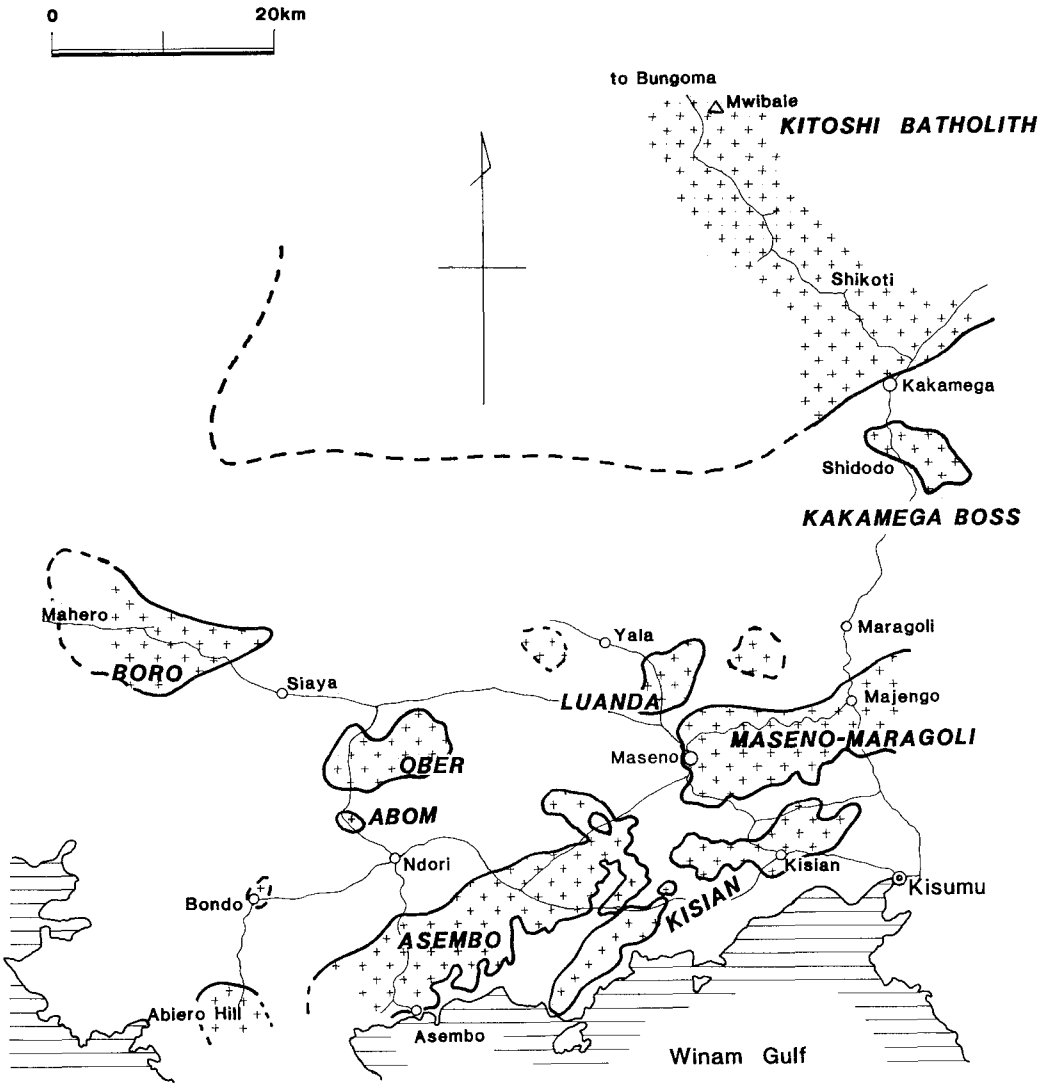

Fig. 5. Distribution of granitoid bodies in North Nyanza

2) *Magnetic susceptibility of the granitic intrusive bodies in North Nyanza*

(i) Kitoshi Batholith: Magnetic susceptibility of the body is not extremely low $100 \sim 500 \times 10^{-6}$ emu.cgs./cm^3 but in some places moderately high near Shikhoti about 1400×10^{-6} emu.cgs./cm^3.

(ii) Kakamega Boss: Magnetic susceptibity of this body is high (about 600×10^{-6} emu.cgs./cm^3).

(iii) Yala-Luanda mass: Magnetic susceptibility of this body is extremely high irrespective of various rock facies (on a out crop at Sibakara 3750×10^{-6} emu.cgs./cm^3 in a mean value averaged and is the highest throughout west Kenya).

Table 2. Magnetic susceptibility of granitoid bodies in North Nyanza (volume magnetic susceptibility in $\times 10^{-6}$ emu.cgs./cm^3)

	Locality	Rock	Min.	Max.	Average	Numbers of Measurings
1.	**Kitoshi Batholith**					
	Mwibale	c. g. leuco. Bi. Gr.	180	490	382	7
	Mwibale	c. g. leuco. Bi. Gr.	250	310	287	2
	Mwibale	c. g. leuco. Bi. Gr.	110	250	163	7
	Shitsukutu	f. g. gn. leuco. Gr.	0	0	0	6
	Iwakhupa	f. g. Po. leuco. Gr.	90	210	162	5
	Shikhoti	Po. Gr.	1300	1540	1395	6
2.	**Kakamega Boss**					
	Shidodo	Po. GD.	550	730	617	7
3.	**Yala-Luanda mass**					
	Sibakara	f. g. GD.	1580	1970	1716	5
	Sibakara	f. g. GD.	3250	4250	3750	5
	Esibila	f. g. GD.	1230	1540	1398	4
	Njisuba	pink. K-f. Po. Gr.	1150	1400	1258	4
		pink. K-f. Po. Gr.	1180	1550	1368	5
	Bunyangu	pink. K-f. Po. Gr.	1230	1540	1398	4
4.	**Maseno-Maragoli mass**					
	Maseno south	K-f. Po. Gr.	980	1300	1168	7
	Maseno north	pink. Gr.	800	900	858	4
	east	pink. Gr.	750	860	798	5
	east	pink. Gr.	570	980	770	3
	Boyani south	K-f. Po. Gr.	440	600	548	5
	Boyani	f. g. Hb. GD.	40	60	50	3
	Boyani	Po. gn. Gr.	520	1120	870	4
	Boyani	Po. gn. Gr.	480	1670	810	4
	Vihyga west	m. g. Hb. Bi. Gr.	150	570	350	5
	Vihyga west	m. g. Hb. Bi. Gr.	385	530	476	5
	Vihyga west	m. g. Hb. Bi. Gr.	430	620	510	3
	Madzuu	m. g. Hb. Bi. Gr.	325	500	350	5
	Kima south	m. g. Hb. Bi. Gr.	320	1180	738	4
	Kima south	m. g. Hb. Bi. Gr.	620	675	621	4
5.	**Kisian mass**					
	Kisian	pink. K-f. Po. Gr.	190	690	514	7
	Kisian	pink. K-f. Po. Gr.	370	1300	855	4
	Kisian	pink. K-f. Po. Gr.	570	1470	1042	6
	Sianda south	pink. K-f. Po. Gr.	2010	2680	2310	6
	Sianda diversion	pink. leuco. Gr.	2420	2615	2493	3
	Sianda diversion	pink. leuco. Gr.	65	320	215	6

	Locality	Rock	Min.	Max.	Average	Numbers of Measurings
	Siand diversion	pink. K-f. Po. Gr.	100	1520	704	5
	Siand diversion	aplite	290	410	313	3
	Sianda weathered	K-f. Po. Gr.	720	1800	1346	7
	Ualo	pink. K-f. Po. Gr.	1050	1900	1450	5
	Ualo	pink. K-f. Po. Gr.	1600	1800	1700	4
	Buoye west	Hb. Bi. Gr.	675	1140	912	3
	Buoye west	Hb. Bi. Gr.	2020	2390	2213	4
	Paw Akche	K-f. Po. Gr.	1660	1950	1805	4
	Kitmikaye	K-f. Po. Gr.	1440	2780	1760	5
	Kitmikaye	K-f. Po. Gr.	1670	2090	1833	6
	Kitmikaye	K-f. Po. Gr.	1460	1570	1515	4
	Kitmikaye	K-f. Po. Gr.	1680	2040	1895	4
6.	**Asembo mass**					
	Awach east	f. g. GD.	1420	2430	1848	5
	Awach east	f. g. GD.	1560	2240	1843	3
	Awach east	f. g. GD.	1340	2060	1667	6
	Awach east	f. g. GD.	700	2760	1666	5
	Awach west	f. g. leuco. Gr.	910	1215	1028	4
	Nyilima	c. g. Bi. Hb. Gr.	340	840	594	5
	Nyilima	c. g. Bi. Hb. Gr.	540	700	640	3
	Nyilima	c. g. Bi. Hb. Gr.	2620	2980	2790	7
	Nyilima	c. g. Bi. Hb. Gr.	2550	2950	2780	3
	Nyilima	c. g. Bi. Hb. Gr.	2080	2780	2554	5
	Nyilima Post Office	c. g. Bi. Hb. Gr.	1060	1380	1273	3
	Kaladini	m. g. Hb. Bi. Gr.	230	350	247	6
	Kaladini	m. g. Hb. Bi. Gr.	220	670	426	6
	Asembo	m. g. Hb. Bi. Gr.	200	450	288	4
7.	**Abiero Hill's outcrop**					
		m. g. leuco. Gr.	820	2980	2145	6
8.	**Abom outcrop**					
		f. g. Hb. Bi. Gr.	480	740	590	4
		m. g. leuco. Gr.	540	560	550	2
9.	**Ober mass**					
	Ober	f. g. GD.	110	210	165	4
	Ober	f. g. GD.	60	100	83	4
	Ober	f. g. GD.	0	200	63	6
	Nyangondo	f. g. GD.	130	240	178	5
	Nyangondo	f. g. GD.	110	400	276	5
	Nyangondo	f. g. GD.	110	400	235	6
	Nyangondo	f. g. GD.	160	300	213	3

	Locality	Rock	Min.	Max.	Average	Numbers of Measurings
10.	**Boro mass**					
	Boro, east	c. g. GD.	200	390	306	5
	Boro, east	c. g. GD.	80	380	296	5
	Boro	Po. GD.	320	390	368	5
	Boro	Po. GD.	220	370	298	5
	Boro, west	Po. GD.	50	270	184	5
	Boro, west	Po. GD.	160	220	198	5
	Boro, farther west	Po. GD.	340	500	410	6
	Boro, farther west	Po. GD.	340	510	470	5
	Mahero	Po. GD.	20	40	28	4

leuco. = leucocratic
c. g. = coarse-grained
m. g. = medium-grained
f. g. = fine-grained
gn. = gneissose

Po. = porphyritic
K-f. = potash-feldspar
Hb. = hornblende
Bi. = biotite

(iv) Maseno-Maragoli mass: As a whole, magnetic susceptibility of the maseno-Pinkish potash-feldspar porphyritic parts show high magnetic susceptibility (ranging from 800 to 1200 $\times 10^{-6}$ emu.cgs./cm^3).

(v) Kisian mass: Magnetic susceptibility of the mass is high irrespective of various rock facies and irrespective of various degree of weathering.

(vi) Asembo mass: Magnetic susceptibility of this body is high in the northern part of the mass and is low in the southern part of the mass. Granitoid rocks occuring in the northern part of the mass contain hornblende and those in the southern part do not contain hornblende.

(vii) Outcrop of Abiero Hill: Magnetic susceptibility is very high (about 2000 $\times 10^{-6}$ emu.cgs./cm^3 in average). Although Hoshino et al (1983) designated this area, Abiero Hill, to be included in the Asembo granite mass owing to the regional trends of the Asembo granite mass. I think it to be not some body compared with the Asembo granite judging from rock facies and magnetic susceptibility.

(viii) Abom out crop: Magnetic susceptibility of this body is low irrespective of various rock facies.

(ix) Ober mass: Magnetic susceptibility of this body is high in the western part of the mass and low in the eastern part of the mass.

(x) Boro mass: Magnetic susceptibility of slightly porphyritic fresh granodiorite body is considerably low.

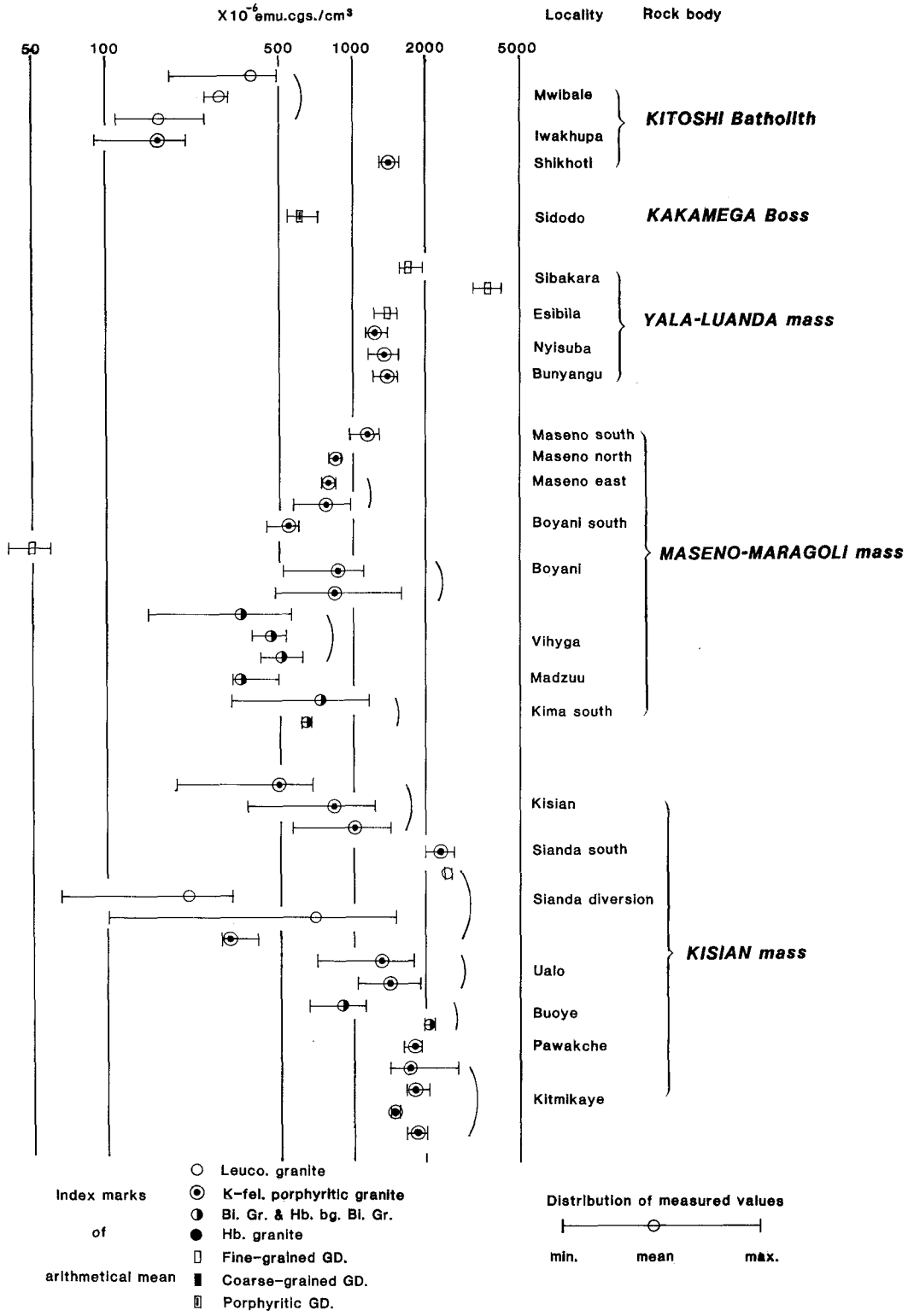

Fig. 6a. Magnetic susceptibility of gronitoid bodies in the Tanzania craton, North Nyanza (eastern region), Kenya.

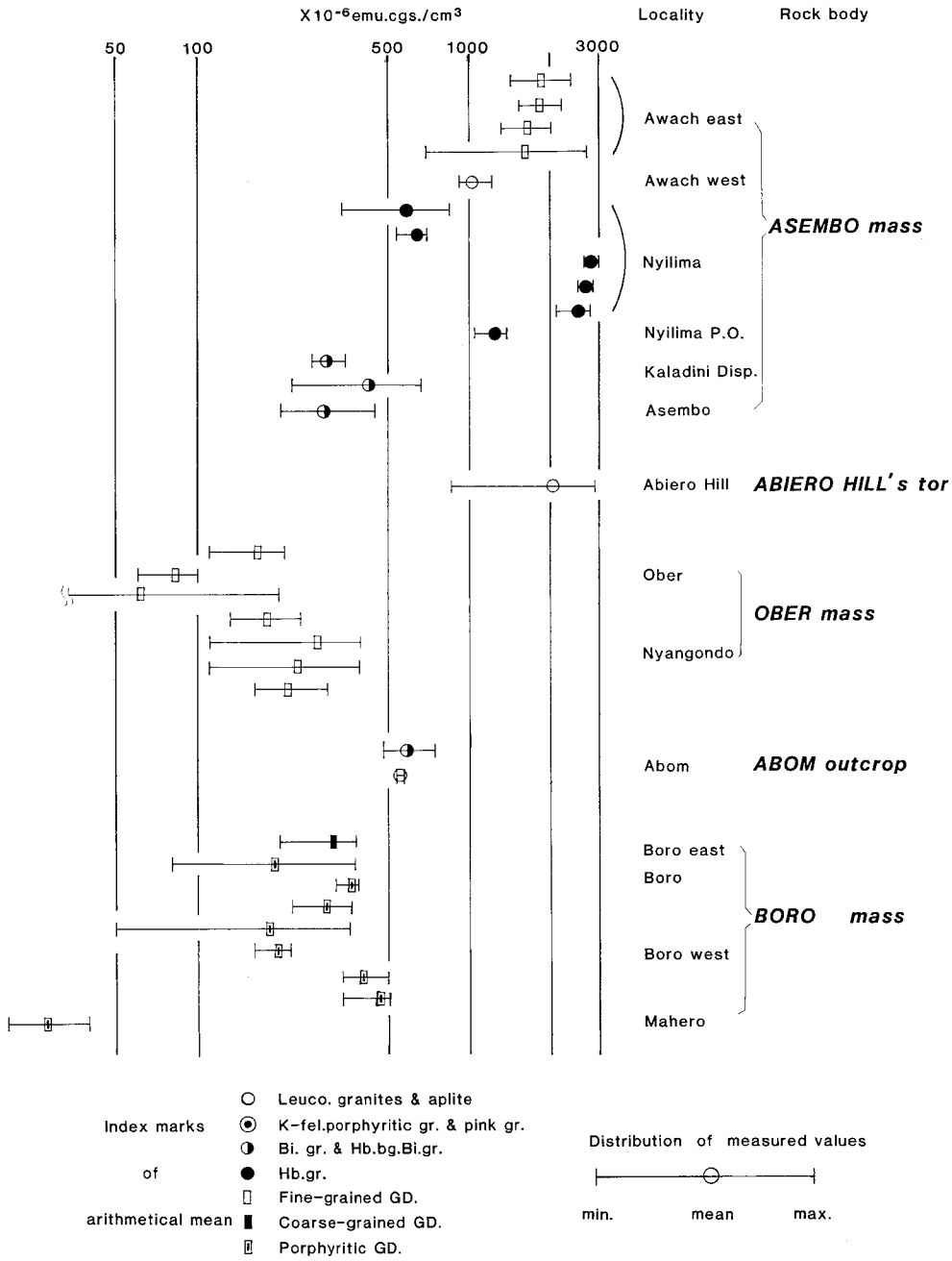

Fig. 6b. Magnetic susceptibility of granitoid bodies in the Tanzania craton, North Nyanza (Western region), Kenya.

Discussion

1. *Comparison between Tanzania craton and Mozambique metamorphic belt.*

Magnetic susceptibility of the granitoids in the Tanzania craton of west Kenya is considerably higher than that of the granitoids and granitoid gneisses in the Mozambique metamorphic belt of south-central and west Kenya. It may be constructive for the future prospecting of xenothermal mineral deposits.

2. *Granitoid rocks in South Nyanza.*

Magnetic susceptibility of G2 granites is exclusively higher than 500×10^{-6} emu. cgs./cm^3 and that of G3 granites is exclusively lower than the same value. Shackleton (1946) considered that the magma that gave rise to the post Nyanzian granites remained as fluid lasting to the post Kavirondian times, indicating a connection between the Nyanzian and Kavirondian orogeneses and that the granites are comagmatic. According to the present data for magnetic susceptibility of these granites, it does not seem that the two granites may be comagmatic.

Magnetic susceptibility of the granodioritic palaeozome in the Miriu granodiorite is high and that of the leuco-granitic neozome is low. The boundary value between high and low values in the Miriu granodiorite is roughly coincident with that of the granitoid gneisses showing domed and undomed structure.

The measuring result of magnetic susceptibility for the granitoid boulders in a Kavirondian conglomerate is divided into two categories: high and low. It may be same cause that the granitoid boulders did not define an isochron (Yanagi and Suwa, 1981).

3. *Granitoid rocks in North Nyanza.*

There are three patterns of measuring results of magnetic susceptibility for granitoid rocks in North Nyanza.

(a) Magnetic susceptibility is low for the Kitoshi, Boro, and Abom masses.
(b) Magnetic susceptibility is high for the Kakamega, Maseno-Maragoli, Yala-Luanda, and Kisian masses.
(c) Magnetic susceptibility is high and low in the different parts of the same mass, e.g., in the Ober and Asembo masses.

Shackleton (1946) designated two ages of the granitoid plutonic activity in which the older granitoid plutons intruded postkinematically into the Nyanzian System before the Kavirondian sedimentation occurred and thereafter the younger granitoid plutons were emplaced postkinematically into the Kavirondian System. His designation has been appreciated and followed by many geologists such as Huddleston (1954), Saggerson (1952), and others. Pulfrey (1946) suggested that the Maragoli granite is composed of multiple intrusion occurered even in a respective intrusion body. From my measuring result, it is probable that the multiple intrusion occurred even in a respective intrusion body.

Acknowledgement — I thank Mr. E.K. Ruchiami, Permanent Secretary of the Office of President of Kenya, for a research permission on my geological studies in Kenya. I thank also Prof. I.S. Loupekine of the University of Nairobi for his kind suggestions and helpful supports and I am very grateful to Mr. L.C. Butaki, Warden of Mines, Mines and Geological Department, Kenya for his warm hospitality upon the export of my rock samples. I express my sincere thanks to Prof. K. Suwa of Nagoya University for his helpful assistances to this study.

This work in Kenya was made possible by the Grant-in-Aid from the Japan Society for Promotion of Science, to which I express my thanks.

REFERENCES

HOSHINO, M., YANAGI, T., SUWA, K., and WINANI, P.L. (1983): Geological structure of the Archaean greenstone belt, northwest of Kisumu, Kenya. *8th Prelim. Rept. Afr. Studies, Nagoya Univ.*, 145-156.

HUDDLESTON, A. (1954): Geology of the Kakamega District. *Rept. Geol. Surv., Kenya*, **28**.

NAKAI, Y. and SUWA, K. (1981): Zircons in the Precambrian granites from the Kisumu area, western Kenya. *6th Prelim. Rept. Afr. Studies, Nagoya Univ.*, 145-150.

PULFREY, W. (1946): Geological survey of Maragoli, North Kavirondo. *Rept. Min. Geol. Dept., Kenya*, **9**.

SAGGERSON, E.P. (1952): Geology of the Kisumu District. *Rept. Geol. Surv., Kenya*, **21**.

SANDERS, L.D. (1965): Geology of the contact between the Nyanzian shield and the Mozambique belt in western Kenya. *Bull. Geol. Surv., Kenya*, **7**.

SHACKLETON, R.M. (1946): Geology of Migori Gold Belt and adjoining area. *Rept. Min. Geol. Dept., Kenya*, **10**.

SHIOZAKI, H. (1983): Magnetic susceptibility of the granitoid gneisses in the Mozambique metamorphic belt of Kenya. *8th Prelim. Rept. Afr. Studies, Nagoya Univ.*, 121-134.

SUWA, K. (1981): Petrochemical and petrographical notes on some Nyanzian volcanic rocks, west Kenya. *6th Prelim. Rept. Afr. Studies, Nagoya Univ.*, 15-32.

YANAGI, T. and SUWA, K. (1981): Rb-Sr radiometric dating on Precambrian rocks in the western part of Kenya. *6th Prelim. Rept. Afr. Studies, Nagoya Univ.*, 163-172.

PLATE I

1. Inselberg consisting of coarse-grained leucocratic biotite granite (Kitoshi Batholith), Mwibale (south of Bungoma), west Kenya (Photo. by H.S., 13 Dec., 1981).

2. Balancing stone, K-feldspar porphyritic hornblende bearing granite, Kitmikaye (North Nyanza) west Kenya (Photo. by H.S., 15 Dec., 1981).

1

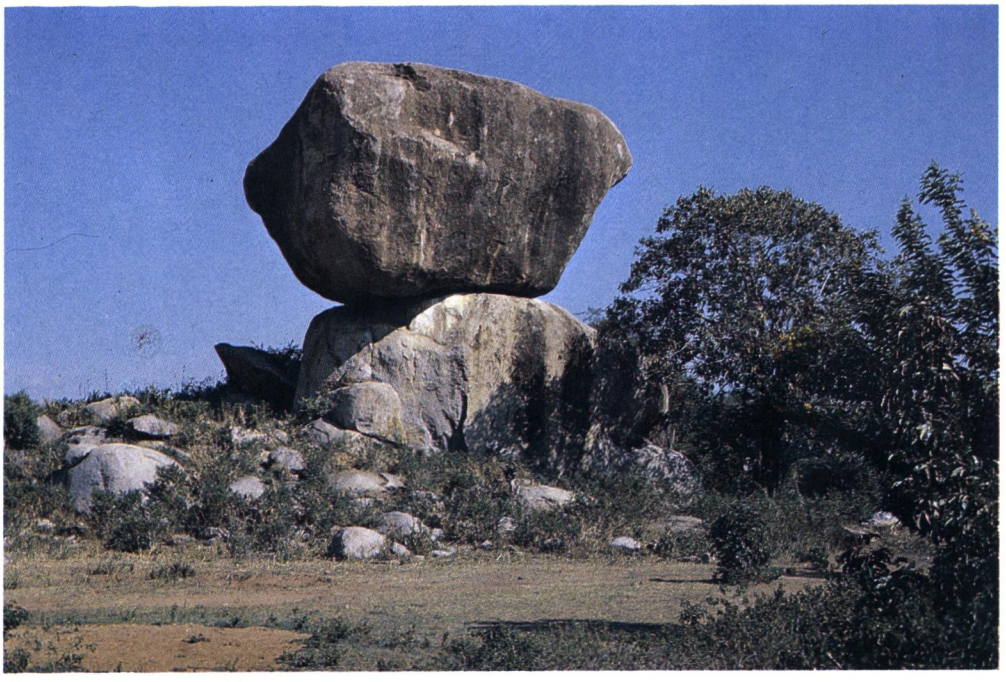

2

Petrographical studies on the YA17-, Y1B3- and UG4-kimberlite-prospecting boring core specimens from Nyanza, western Kenya

Masahiro ITO*, Kanenori SUWA** and A.S. SEGERO***

* Laboratory of Geology, College of General Education, Nagoya University
** Department of Earth Sciences, Faculty of Science, Nagoya University
*** Mines and Geological Department, Kenya

Abstract

Kimberlite-prospecting borings were carried out at three points in western Kenya, based on the airborne survey. Two kimberlite occurrences were newly found from YA17 (34°30.9'E, 0°09.5'N) – and Y1B3 (34°13.9'E, 0°03.0'S) – Holes. UG4-core specimens are composed of Nyanzian volcanic and pyroclastic rocks and mafic igneous rocks. These two kimberlites are "porphyritic" or "crystal tuffaceous" and are intercalated with laminated "tuff", containing many xenoliths of fine-grained altered rocks. YA17-specimens are composed of "phenocrystic" olivine and phlogopite and medium-grained diopside, chromite and other opaque mineral and the matrix of smectite, serpentine, opaque mineral, perovskite, colourless amphibole, titaniferous garnet and apatite. Epidote, tourmaline and ?aegirine are rarely found. Natrolite, cancrinite and sodalite are commonly found in YA17-specimens. Sodalite occurs limitedly in some xenoliths. These minerals may be caused by the contamination of soda-metasomatized volcanic rocks correlated with carbonatite magma during the deuteric stage. Y1B3-specimens are wholly weathered and contain "phenocrystic" phologopite. UG4-specimens are not kimberlite but Nyanzian dacite and dacitic tuff and hornblende dioritic rocks.

Less-than-2μm fractions of YA17- and Y1B3-kimberlites were studied by X-ray diffraction, DTA-TG-DTG, electron microphotography and infrared spectroscopy.

YA17-kimberlites are rich in Al_2O_3, CaO, Na_2O and SiO_2 and poor in MgO. These chemical characteristics may be caused by contamination of soda-metasomatized rocks during the deuteric alteration. The chemical compositions of YA17- and Y1B3-kimberlites from Nyanza, western Kenya are plotted in ($Na_2O + K_2O + Al_2O_3$) - MgO - FeO diagram, together with chemical compositional areas of diamondiferous - nondiamondiferous kimberlites from People's Republic of China.

Introduction

Many points showing high positive geomagnetic intensity were found by airborne survey in Nyanza province, western Kenya, to the northeast of Lake Victoria(Fig. 1). Several kimberlite-prospecting borings conducted by Kenya Mines and Geological Department were carried out, based on the airborne survey, and a few localities of

8th Prelim. Rept. Afr. Studies, Nagoya Univ., 181-196, 1983.

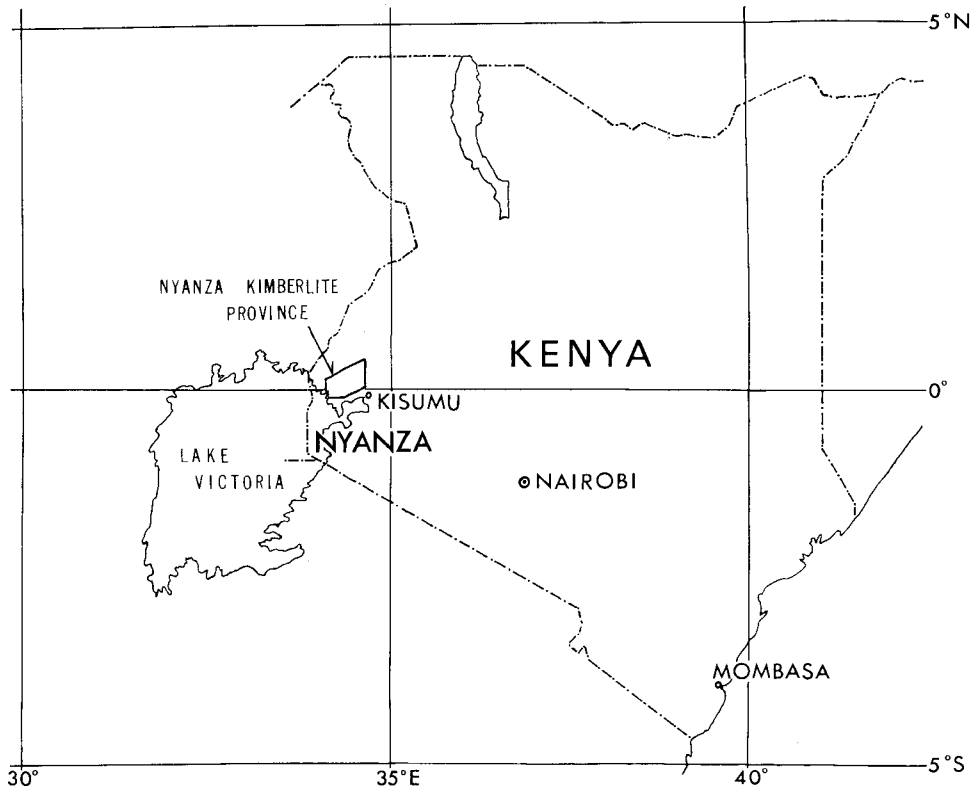

Fig. 1 Locality map of Nyanza kimberlites in Nyanza, western Kenya.

kimberlites were successfully discovered. Kimberlite first found in western Kenya is from Y1B1-borehole "Sakuwa Kapiyo Hole" at Siaya, Nyanza (34° 11.2'E, 0° 04.5'S). Petrographical studies of the Y1B1-kimberlite were already reported (Ito et al., 1981).

In this report petrography of the specimens from YA17-, Y1B3- and UG4-Holes will be described. Situations of these three prospecting boring sites were selected at the points of high positive aeromagnetometric values as shown in Fig. 2. The outward aspects of these boring-core specimens are outlined below;

YA17 Hole:

The coordinates of the borehole site are 34° 30.9'E, 0° 09.5'N, a point 7 km to the north-north-west of Yala. This borehole was drilled about 193 metres deep. Aeromagnetometric pattern around YA17 Hole site is shown in Fig. 2a. Down to about 78 metres from the surface, laminated "tuff" intercalated in weathered crystal tuff- and tuff breccia-like kimberlites is overlain by thin soil layer of light brown colour. These rocks change the colour from greyish yellow through light green to grey with increasing depth. Downward from about 80 metres deep, the matrix of kimberlite becomes hard and greyish green through dark greyish green to

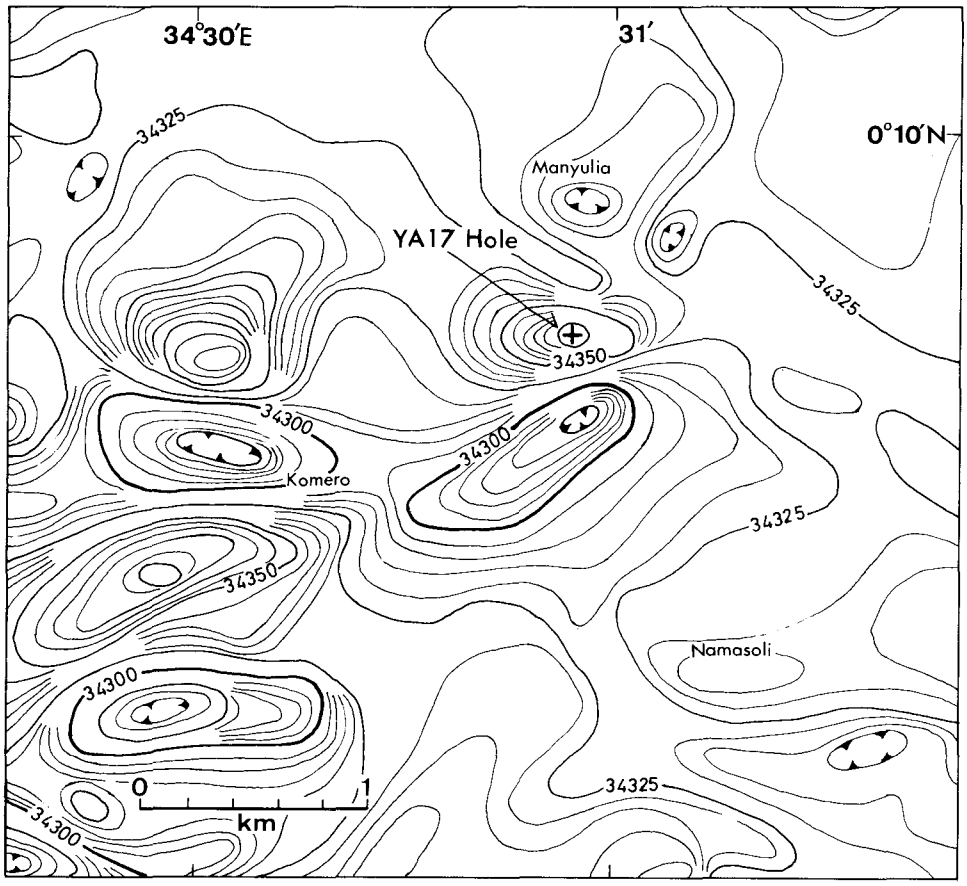

Fig. 2a Aeromagnetometric pattern around YA17-borehole site in Nyanza, western Kenya. Contour interval is 5 gammas.

medium grey in colour. Various contents of xenoliths of ?Nyanzian rhyolitic rocks, basaltic rocks, red chert, gabbroic rock and peridotite are found. "Phenocrystic" olivine and phlogopite are found.

Y1B3 Hole:

The coordinates of the borehole site are 34° 13.9'E, 0° 03'S, a point about 6.4 km east-north-east to Y1B1-borehole site where kimberlite was first found in Kenya. Y1B3 Hole was drilled about 135 metres deep. Aeromagnetometric pattern around Y1B3 Hole site is shown in Fig. 2b. The boring core specimens are composed of tuff- and tuff breccia-like kimberlites interstratified frequently by laminated "tuff" and "tuffaceous sandstone". Weathering is advanced in the whole core specimens, the colour of which is greyish yellow, greyish yellow green and greyish olive green in shallow zone through moderate olive brown and light olive brown to greyish yellow and greyish green in the deep zone.

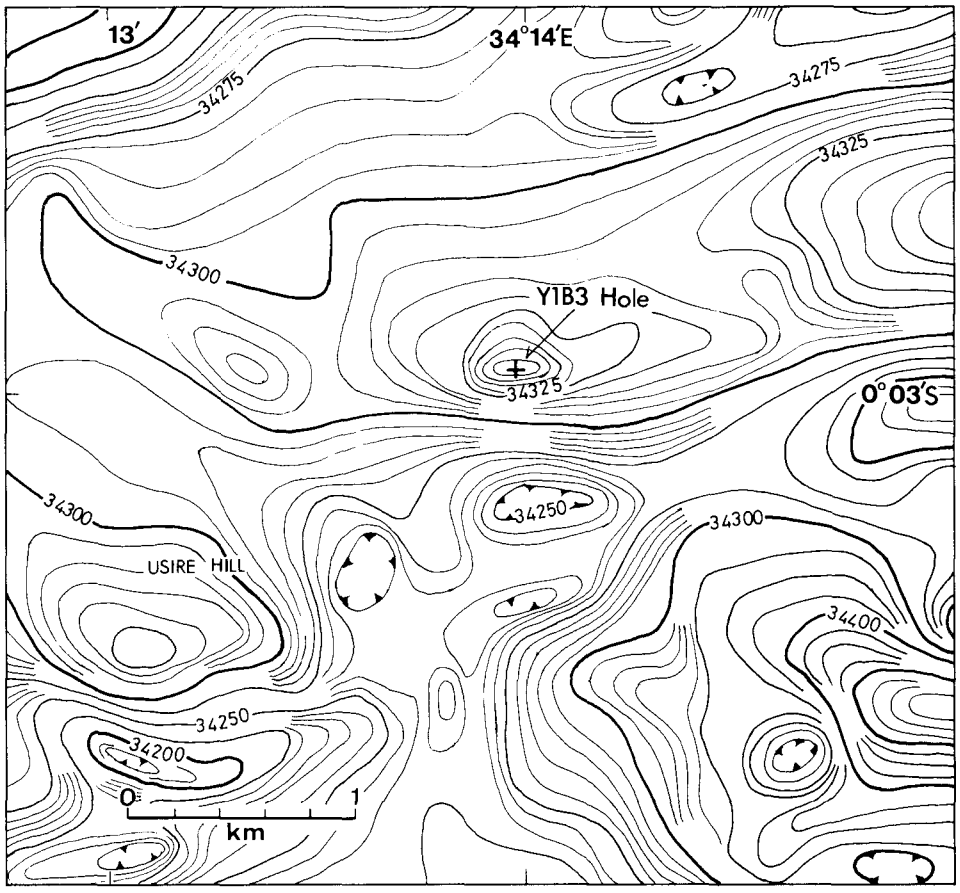

Fig. 2b Aeromagnetometric pattern around Y1B3-borehole site in Nyanza, western Kenya. Contour interval is 5 gammas.

UG4 Hole:

The coordinates of UG4 Hole site are 34° 18.6'E, 0° 02.1'N, a point 4 km south-east to Siaya. Though this point also shows high positive aeromagnetometric value (Fig. 2c), the core specimens picked up by the boring of about 150 metres in depth are not kimberlite but Nyanzian rhyolitic rocks, lamprophyre and gabboric rock. These rocks are overlain by much weathered rocks and soil of about 125 metres in thickness.

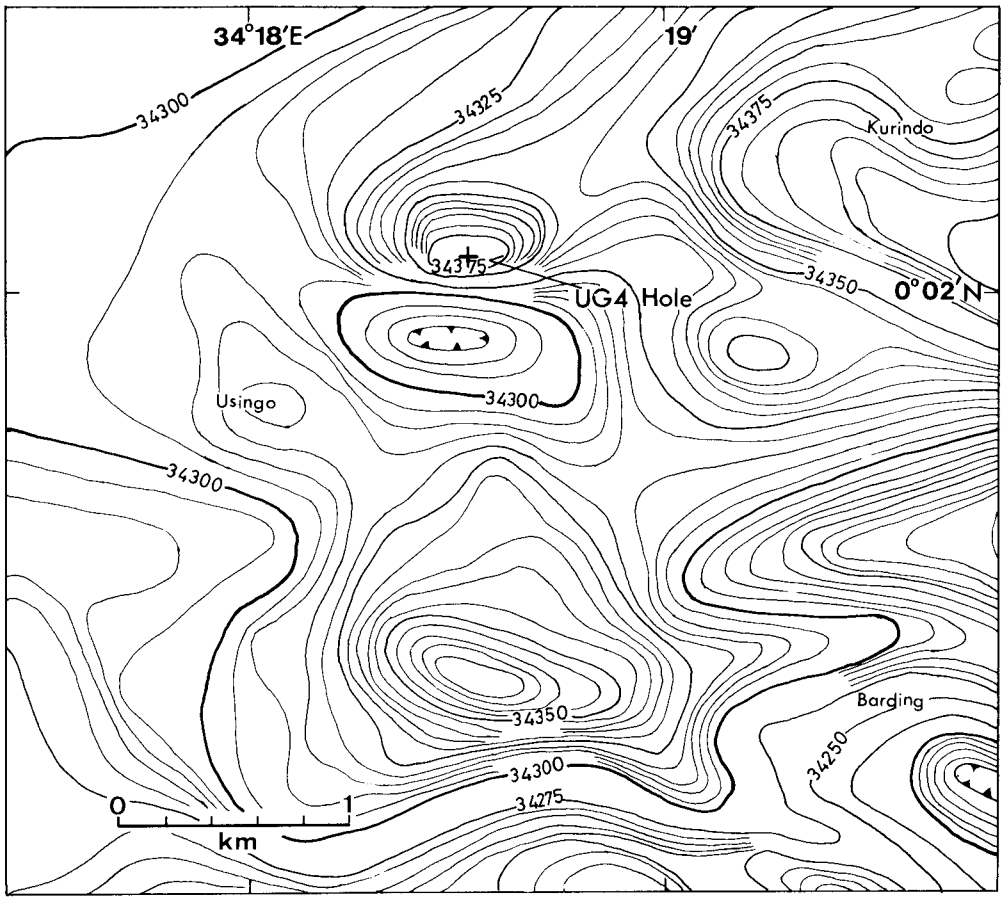

Fig. 2c Aeromagnetometric pattern around UG4-borehole site in Nyanza, western Kenya. Contour interval is 5 gammas.

Petrography

A. YA17- and Y1B3-specimens

Kimberlites from YA17 and Y1B3 boreholes show tuff breccia- or crystal tuff-like texture (Plates I&II). As Y1B3-kimberlites are much weathered, petrography laying stress on YA17-kimberlites will be described.

Olivine is fairly common and is moderately serpentinized and/or carbonatized. Some large "phenocrystic" olivines exhibit corroded form with small patchy inclusions of matrix matter in the rim part. The chemical compositions of "phenocrystic" and moderate-grained olivine grains are shown in Table 1. The rim part of large grain is richer in FeO and poorer in MgO with the composition of $Fo_{85.8}$ than the core part with that of $Fo_{88.7}$. The small olivine grain shows an intermediate composition of $Fo_{87.6}$.

Diopsidic pyroxene is very common in the matrix. It is also found in druse and

Table 1 Electron probe microanalyses of olivine (1&2), diopside (3) and cancrinite (4) in YA17-kimberlite (YA17-21-16) from Nyanza, western Kenya.

	1a (core)	1b (rim)	2 (fine)	3	4
SiO_2	40.61	39.78	39.84	53.33	38.49
TiO_2	0	0	0	1.95	0.02
Al_2O_3	0	0	0	0.41	27.34
Cr_2O_3	0.08	0.07	0.10	0	0.05
FeO*	10.87	13.55	11.93	6.09	0.61
MnO	0.10	0.12	0.16	0.01	0.05
NiO	0.27	0.11	0.26	0	0
MgO	47.71	45.86	47.27	14.04	0.01
CaO	0.10	0.10	0.13	21.93	0.89
Na_2O	0.02	0.03	0.05	1.78	19.12
K_2O	0	0	0	0	0.93
Total	99.76	99.62	99.74	99.54	87.51
Si	1.003 ┐ 1.00	0.997 ┐ 1.00	0.991 ┐ 0.99	1.981 ┐ 2.00	6.587 ┐ 12.00
^{IV}Al	0 ┘	0 ┘	0 ┘	0.018 ┘	5.413 ┘
^{VI}Al	0 ┐	0 ┐	0 ┐	0 ┐	0.102 ┐
Ti	0 |	0 |	0 |	0.054 |	0.003 |
Cr	0.001 |	0.001 |	0.002 |	0 |	0.007 |
Fe^{2+}	0.225 |	0.284 |	0.248 |	0.189 |	0.087 |
Mn	0.002 ├ 1.99	0.002 ├ 2.01	0.003 ├ 2.02	0 ├ 2.02	0.007 ├ 6.92
Ni	0.005 |	0.002 |	0.005 |	0 |	0 |
Mg	1.756 |	1.713 |	1.753 |	0.777 |	0.003 |
Ca	0.003 |	0.003 |	0.003 |	0.873 |	0.164 |
Na	0.001 |	0.001 |	0.003 |	0.128 |	6.345 |
K	0 ┘	0 ┘	0 ┘	0 ┘	0.203 ┘
O	4	4	4	6	25
Mg/(Mg+Fe)	0.886	0.858	0.876		

* Total iron calculated as FeO.

occurs as reaction rim around almost all xenoliths, associated with natrolite, cancrinite, opaque mineral, calcite and rarely apatite(Plate II). The mineral is slightly pleochroic, X = Y = Z = pale yellowish green. The chemical composition is (0.41% Al_2O_3), shown in Table 1.

A small amount of colourless amphibole occurs especially in and around the xenoliths. "Phenocrystic" phlogopite is found as light yellowish brown flakes by naked eyes. It is, however, much altered to calcite and clayey matter. Chromite of light brown to light reddish orange colour in thin section is moderately common. In Plate III X-ray images together with electron figure for one chromite grain rimmed by Ti-Fe opaque mineral are shown.

In YA17-kimberlite natrolite, cancrinite and sodalite are characteristically found. Natrolite occurs ubiquitously in the matrix and also in druse and vein. Sodalite is

only found in fine-grained basic xenoliths. Natrolite is fine-grained prismatic and often occurs as radiated aggregates showing positive elongation (Plate II). This mineral is also found in much weathered Y1B3-kimberlite. Cancrinite occurs as short prismatic crystal or radiated aggregate of negative elongation. It shows weaker birefringence than natrolite.

"Phenocrystic" minerals in Y1B3-kimberlite are olivine and phlogopite and a small amount of pale green hornblende, chromite and opaque mineral. Olivine is almost altered to serpentine and smectite. The pseudomorphs after olivine are surrounded by very fine-grained opaque mineral and perovskite. Phlogopite is also intensely carbonatized and is often deformed.

Matrix is composed of cryptocrystalline layer minerals, serpentine, calcite, opaque mineral, perovskite, titaniferous garnet and a small amount of pectolite, apatite and ?pyrochlore. In Y1B3 epidote, tourmaline and ?aegirine are rarely found.

X-ray diffraction, DTA-TG-DTG and IR analyses were made for the less-than-2 μm fractions of YA17- and Y1B3-kimberlites. Besides layer mineral and serpentine, only a small amount of calcite, opaque mineral and perovskite are found in all fractions. In Table 2, the X-ray data are shown. X-ray diffraction for the specimens heated at various temperatures were made after these cooling down to room temperature. Solvation of the specimens with glycerol spraying was done under heating at 60°C for five hours.

Judging from the X-ray data shown in Table 2, less-than-2 μm fractions of YA17- and Y1B3-kimberlites are considered to be smectite, probably saponite. The mineral of 11Å in YA17-21-16 shows no distinguishable change by heating up to 700°C. It is completely decomposed at 950°C. As any layer minerals can not be now assigned to this mineral, further mineralogical studies will be required.

The electron microphotographs of less-than-2 μm fractions of YA17- and Y1B3-kimberlites are shown in Plates IV & V. Various shapes of clayey matters are observed in YA17-specimen. Spherule is cabbage-like flaky ball with some rough surface just like the crust of bread (Plate IV). Many spherules have commonly kernel coated with curled fibrous bundle (Plate IVB). Fibrous bundle characteristic of saponite is also found (Plate IVA). In Y1B3-1-31 specimen, platy flakes and curled bundles are fairly common. Spherules coated with curled or tangled fibre are characteristically found (Plate V A). Some of spherules are knitting ball-like (Plate V B). Fibrous bundles are curled and distorted. Pseudohexagonal plates of various sizes are ascribed to chrysotile-antigorite.

Simultaneous DTA-TG-DTG patterns for the less-than-2 μm fractions of YA17- and Y1B3-kimberlites are shown in Fig. 3. Rigaku-thermoflex model 8002 was used for the specimens of about 17mg in weight. The experimental conditions are as follows; DTA range: ± 25μV, TG range: 10mg, DTG sensitivity: 0.1 div/min/div, heating rate: 10°C/min. Peak temperatures of endotherms and exotherm for these specimens are shown in Table 3, together with total weight loss percentages at 1000°C. A faint endotherm associated with strong asymmetric endotherm at 92°C can be expected for YA17-21-16 at 148°C, based on the DTG curve. It may corres-

Table 2 Basal spacing (Å) and thermal behaviours of the less-than-2μm fractions of YA17- and Y1B3-kimberlites from Nyanza, western Kenya, treated with various reagents.

YA17 · 21-16 (167.3 m)

	Dry	Wet	EG	GL	300°C	500°C	700°C	(060)
Natural	14.7	15.2	16.4	17.6 + 16.7	14.3	10.0		1.538
	11.3	11.3	11.3	11.3	11.3	11.2		
Mg-form	14.6		16.4		14.3	13.6w		
	11.3		11.3		11.3	11.0	11.0	
K-form	14.6				14.4	13.4	10.2	
	11.1				11.3	11.1	11.1	
NH_4-form	——							

YA17 · 14-35 (119.7 m)

	Dry	Wet	EG	GL	300°C	500°C	700°C	(060)
Natural	14.9	15.0	16.4	17.7	14.9	14.1	15.1w	1.538
						9.72	9.65	
Mg-form	14.6		16.9		14.6	14.4	13.6w	
							9.47	
K-form	14.1sh				14.1	13.6sh	10.4asm	
	12.6				12.1	11.8		
NH_4-form	14.1sh							
	12.6							

Y1B3 · 1-31 (11.7 m)

	Dry	Wet	EG	GL	300°C	500°C	700°C	(060)
Natural	15.8	16.0	16.6	18.1	15.2	12.7	9.77	1.533
Mg-form	15.3		16.8		15.0	9.92	9.57	
K-form	13.1				12.6	12.0	12.0	
MH_4-form	12.7							

w: weak, sh: shoulder, asm: asymmetric.

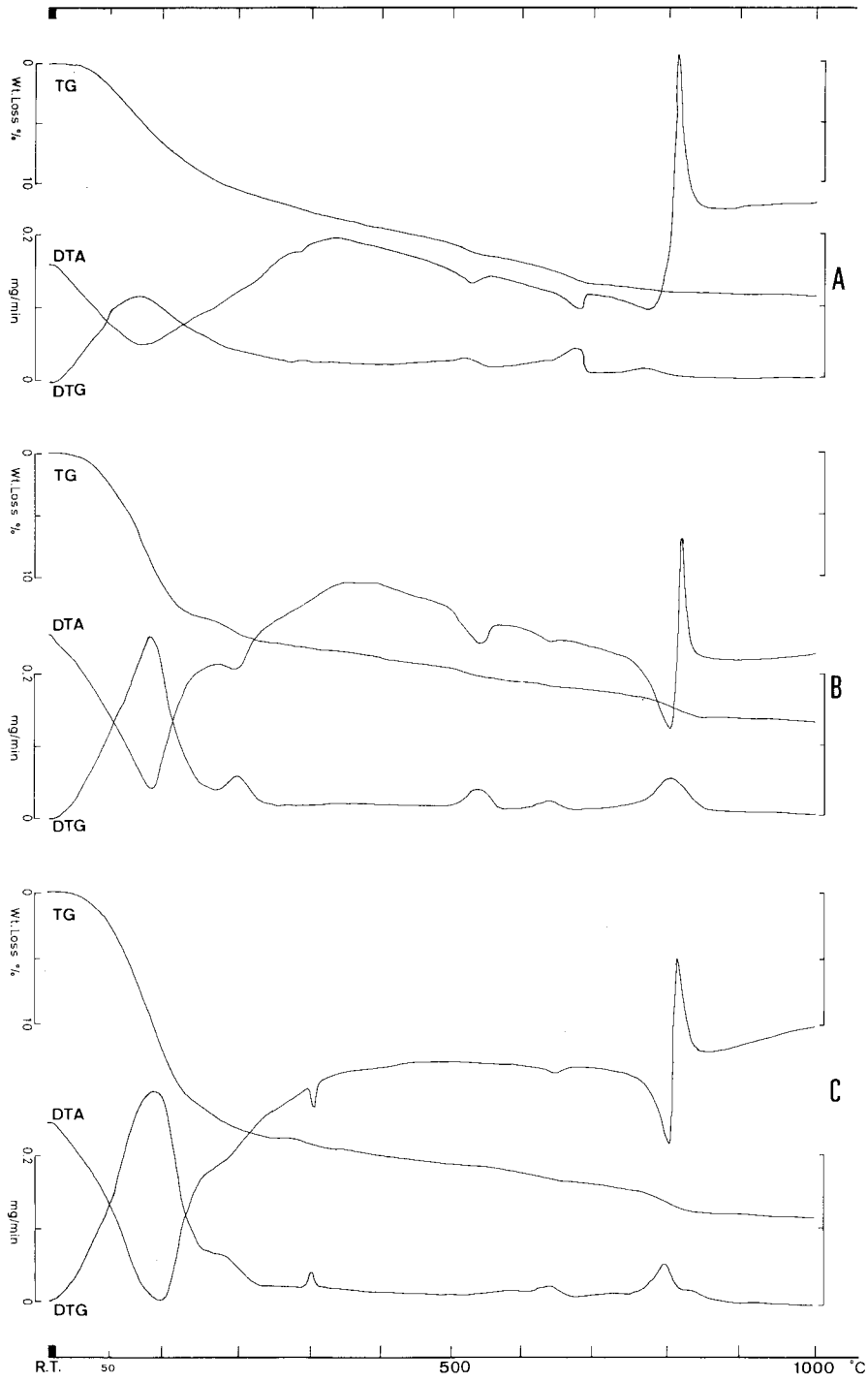

Fig. 3 DTA-TG-DTG patterns for less-than-2 μm fractions of YA17- and Y1B3-kimberlites from Nyanza, western Kenya.
A: Dark grey kimberlite, YA17-21-16 (167.3 m).
B: Light grey kimberlite, YA17-14-35 (119.7 m).
C: Greyish yellow, weathered tuffaceous kimberlite, Y1B3-1-31 (11.7 m).

Table 3 Endothem- and exotherm-peak temperatures (°C), together with total weight loss percentages up to 1000°C, for YA17- and Y1B3-kimberlites from Nyanza, western Kenya.

	peak temperatures (°C)							Total wt. loss %
1	92↓	148↓	293↓	540↓	688↓	778↓	822↑	20.4 (1000°C)
2	94↓	200↓		541↓	647↓	807↓	824↑	21.9 (1000°C)
3	108↓	189↓	308↓		654↓	804↓	818↑	24.9 (1000°C)

↓ : endotherm, ↑ : exotherm.

1. YA17-21-16 (167.3 m), dark grey kimberlite.
2. YA17-14-35 (119.7 m), light grey kimberlite.
3. Y1B3-1-31 (11.7 m), greyish yellow kimberlite.

pond to the endotherm at about 190°C for YA17-14-35 and Y1B3-1-31 specimens. Endotherm at about 300°C for YA17-14-35 and at about 540°C for Y1B3-1-31 can not be found. All specimens examined here indicate a sharp exotherm at about 800°C, successively following an endothem of moderate intensity. Judging from the TG-DTG curve, this exothem exhibits a faint sign of weight loss. Some smectites, montmorillonite and saponite, have an exotherm at about 900°C, which temperature is, however, higher than those for the specimens reported here. The exotherm may be intensified by the recrystallization of decomposition product of admixed serpentine.

Infrared absorption patterns by using KBr disk method for less-than-2 μm fractions of YA17- and Y1B3-kimberlites are shown in Fig. 4. Six main broad bands of various intensity are observed; 3425, 1625 - 1636, 1428 - 1435, 995 - 1010, 655 - 665 and 425 - 450 cm^{-1}, respectively. The band at about 1430 cm^{-1} of various intensity is ascribed to the admixed calcite vibration. A few distinct bands between 3000 cm^{-1} and 4000 cm^{-1} are reported for smectite and serpentine, and the band at about 3600 cm^{-1} is of very strong vibration(Van der Marel and Beutelspacher, 1976). The patterns in Fig. 4 are similar to each other, showing the strong vibrations of 3425 cm^{-1} and 995 - 1010 cm^{-1}. It is noted that these patterns are rather similar to that for vermiculite.

B. UG4-specimens

UG4-core specimens are composed of Nyanzian rocks and melanocratic rocks. The Nyanzian rocks show the pyroclastic texture of rhyolitic or dacitic composition (Plate VI A). This rock consists of plagioclase, quartz, chlorite, opaque mineral, apatite, sphene and calcite. Plagioclase phenocrysts are poor and are altered to calcite and sericite. Groundmass is composed of plagioclase, quartz, chlorite, calcite and a small amount of opaque mineral, sphene and apatite. The melanocratic rocks are dioritic lamprophyre and porphyritic hornblende diorite (Plate VI B), which is composed of plagioclase, hornblende, opaque mineral, apatite, sphene, chlorite, sericite and calcite. Plagioclase is fine- and medium- grained, and is seri-

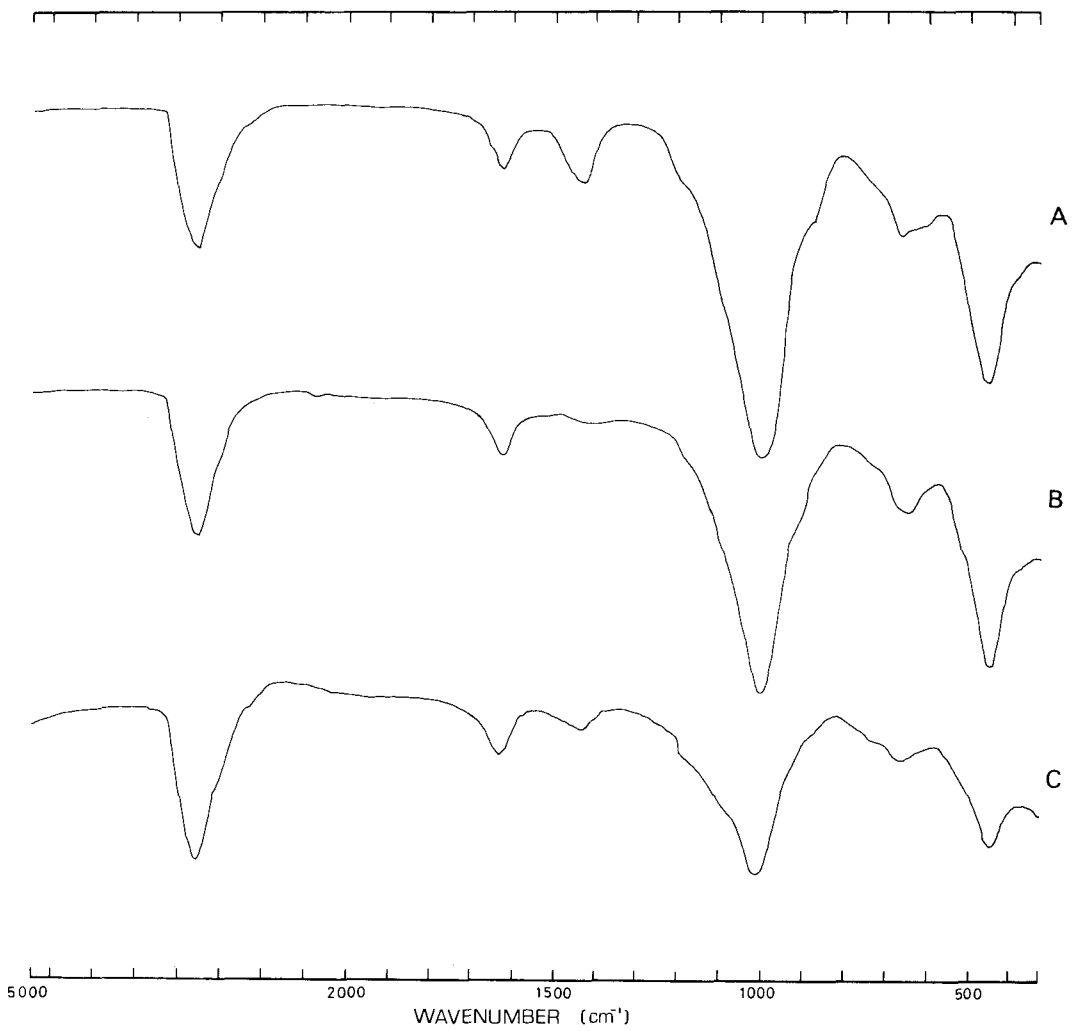

Fig. 4 Infrared absorption spectra for less-than-2 μm fractions of YA17- and Y1B3-kimberlites from Nyanza, western Kenya. A, B and C: the same fractions shown in Fig. 3.

citized and/or carbonatized in various degree. It is twinned without zoning. Hornblende is phenocrystic, showing compositional multi-zoning. The Z-axial colour is dull greenish ochre and dull yellowish green for the core and olive green and pale yellowish green for the rim. Many hornblende crystals are associated with fibrous amphibole which is colourless to very pale yellowish green in colour.

Chemical compositions

Four wholly pulverized samples of YA17-kimberlite and three of UG4-Nyanzian rocks were analysed by X-ray fluorescence spectrometry and titration method. The chemical compositions are shown in Table 4. It is noted that all analysed YA17-

Table 4 Chemical compositions and C.I.P.W. norms of YA17-kimberlites and UG4-Nyanzian rocks from Nyanza, western Kenya.

Analyst: R. Sugisaki

	1	2	3	4	5	6	7
SiO_2	39.90	39.43	38.81	39.20	48.77	60.04	46.46
TiO_2	1.66	1.74	1.80	1.69	0.62	0.82	0.62
Al_2O_3	5.75	5.59	4.77	4.87	11.93	15.53	10.05
Fe_2O_3	7.19	5.76	6.76	6.65	3.39	0.88	1.85
FeO	4.43	6.06	5.61	5.50	5.51	5.65	6.76
MnO	0.20	0.20	0.21	0.20	0.16	0.10	0.19
MgO	16.84	16.93	18.18	18.83	8.30	2.06	9.88
CaO	10.32	12.45	12.52	11.02	10.55	4.17	11.04
Na_2O	3.01	3.90	3.44	3.09	2.17	4.94	1.76
K_2O	0.78	1.17	1.07	0.73	3.14	0.44	0.58
P_2O_5	0.54	0.71	0.75	0.81	0.29	0.18	0.30
$H_2O(+)$	4.78	4.13	3.34	4.48	1.10	1.90	2.59
$H_2O(-)$	4.85	2.25	2.25	3.11	0.21	0.23	0.78
CO_2	0.67	0.54	0.99	0.72	3.01	2.20	7.97
Total	100.92	100.86	100.50	100.90	99.15	99.14	100.83

Norm

		1	2	3	4	5	6	7
Q		0	0	0	0	0	20.27	13.57
C		0	0	0	0	0	4.87	5.64
or		4.61	0	0	3.87	18.56	2.60	3.43
ab		9.61	0	0	0	18.36	41.80	14.89
an		0	0	0	0	13.54	5.60	2.43
lc		0	5.46	4.98	0.35	0	0	0
ne		8.47	12.08	10.09	11.39	0	0	0
ac*		0.21	9.48	9.28	4.55	0	0	0
di	en	15.67	9.75	10.63	15.31	5.19	0	0
	fs	0	1.52	1.12	1.14	1.16	0	0
	wo	18.14	12.62	13.28	18.72	7.46	0	0
hy	en	0	0	0	0	12.91	5.13	24.61
	fs	0	0	0	0	4.12	8.48	10.21
ol	fo	18.42	22.72	24.29	22.15	1.80	0	0
	fa	0	3.90	2.83	1.81	0.63	0	0
	la**	0	7.27	5.93	0	0	0	0
mt		10.12	3.60	5.15	7.36	4.92	1.28	2.68
il		3.15	3.30	3.42	3.21	1.18	1.56	1.18
ap		1.25	1.65	1.74	1.88	0.67	0.42	0.70
cc		1.52	1.23	2.25	1.64	6.85	5.00	18.13

* acmite, ** larnite

1. Dark greenish kimberlite, YA17·15-32 (126.9 m).
2. Dark greyish olive green kimberlite, YA17·18-27 (142.6 m).
3. Dark greyish green kimberlite, YA17·18-24 (146.8 m).
4. Dark greyish green kimberlite, YA17·22-11 (176.8 m).
5. Medium-grained porphyritic hornblende diorite, UG4·15-8 (129.0 m).
6. Nyanzian dacitic tuff, UG4·15-5 (135.6 m).
7. Fine-grained diorite, UG4·16-2 (147.3 m).

kimberlites are rich in Al_2O_3, CaO, Na_2O, TiO_2 and SiO_2 and are poor in MgO in comparison with the chemical compositions of Y1B1-kimberlite (Ito et al., 1981). The small content of MgO may be caused by the scarcity of serpentine in the matrix. Natrolite, cancrinite and pectolite contribute probably to some amounts of Na_2O and CaO of the bulk chemical compositions.

Discussion

Kimberlites and Nyanzian rocks were found by the prospecting-borings based on high positive anomaly of aeromagnetometric pattern. This anomaly is probably caused by the presence of titaniferous magnetite ubiquitously borne in the kimberlite. On the other hand, any amount of magnetite enough to yield a distinguishable anomaly can not be found in the Nyanzian rocks. These anomalies at a few points where only Nyanzian dacitic rocks are picked up by borings may be caused either by hidden kimberlite underlying the Nyanzian rocks or by some basic igneous rocks such as gabbro and diorite of UG4 Hole.

Bulk chemical compositions of YA17-kimberlites, together with Y1B1-kimberlites (Ito et al., 1981), are plotted on $(Na_2O + K_2O + Al_2O_3)$ - MgO - FeO_{total} diagram (Fig. 5). Ruiyuan (1981) indicated a noted relationship between the chemical compositions of host kimberlites and the diamond-bearing contents, as shown in Fig. 5. YA17-kimberlites are all plotted in area III, diamond-absent (very poor) kimberlite field. On the other hand, Y1B1-kimberlites are plotted in area I, diamond-rich kimberlite field, and area II, diamond-poor kimberlite field. It is noted that Y1B1-kimberlite specimens belonging to area II come from shallower part in the prospecting-boring column than those of area I. The situation of YA17-kimberlites in area III may be caused by the presence of smectite of main matrix component in place of serpentine, and the smectite probably shifts the chemical compositions toward the area III. Y1B3-kimberlite is mineralogically similar to Y1B1-kimberlite, though the matrix matter is mainly composed of smectite as a substitute for serpentine. A schematic representation was reported that the alteration process of kimberlites in deuteric condition is divided into three stages; "serpentine stage", "vermiculite stage" and "saponite stage" (Kresten, 1973). Based on this scheme, both YA17- and Y1B3- kimberlites are considered to belong to the "saponite stage".

Natrolite was reported to occur in some xenoliths from Matsoku pipe (Cox et al., 1973). In YA17-kimberlite, natrolite, cancrinite and sodalite also exhibit an intimate genetic relationship to the xenoliths of basic volcanic rocks. Sodalite is especially found only in these xenoliths. These soda-rich minerals may be introduced by the contamination of some metasomatized volcanic rocks genetically correlated with carbonatite magma.

Nyanzian volcanic rocks from the Y1B2- and UR4-boreholes contain sizable amounts of alkalis, especially K_2O, which are different from other Nyanzian rocks collected on the ground (Suwa, 1981). The boring-core specimens from UG4 Hole do not always contain sizable amounts of K_2O. Total contents of alkalis are, how-

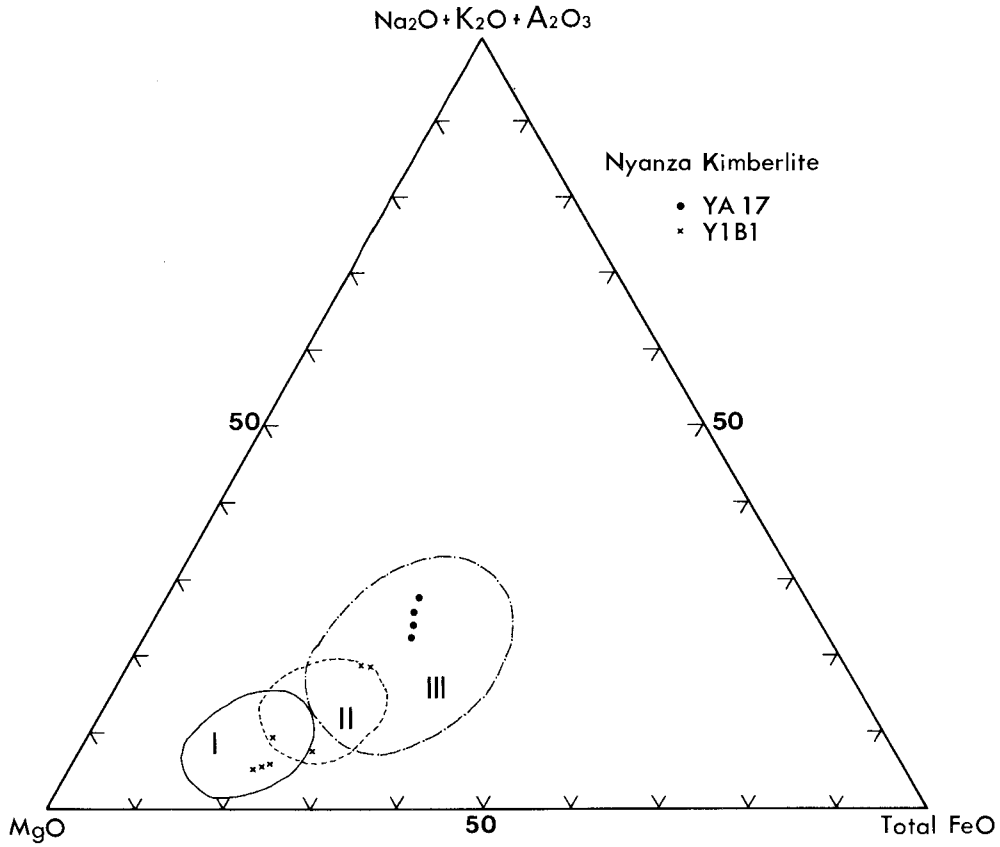

Fig. 5 $(Na_2O + K_2O + Al_2O_3) - MgO - FeO_{total}$ diagram for YA17- and Y1B1-kimberlites from Nyanza, western Kenya, together with compositional fields of diamond occurrences in People's Republic of China advocated by Ruiyuan (1981).
I: Diamond-rich kimberlites area.
II: Diamond-poor kimberlites area.
III: Diamond-absent or very poor kimberlites area.

ever, rather high. Fig. 6 shows a relationship between total FeO/MgO ratio and SiO_2 in weight percentage for UG4-specimens. The UG4 rocks are plotted in tholeiite series field, but the two show small FeO/MgO ratios under the value of two. On the other hand, UR4 specimens are located in the field of calc-alkalic series, though these shows also the ratios under or near the value of two (Suwa 1981). Both calc-alkalic series and tholeiitic series are found for the Nyanzian volcanic rocks.

Acknowledgements – We would like to express our deep gratitude to the Commissioner and Mr. J.K. Wachira, Acting Chief Geologist, of Kenya Mines and Geological Department for their permission of our investigation on many borehole specimens. Our sincere thanks are extended to Professor I.S. Loupekine of the University of Nairobi for kindly affording every facility to our field works and to Dr. K. Motojima

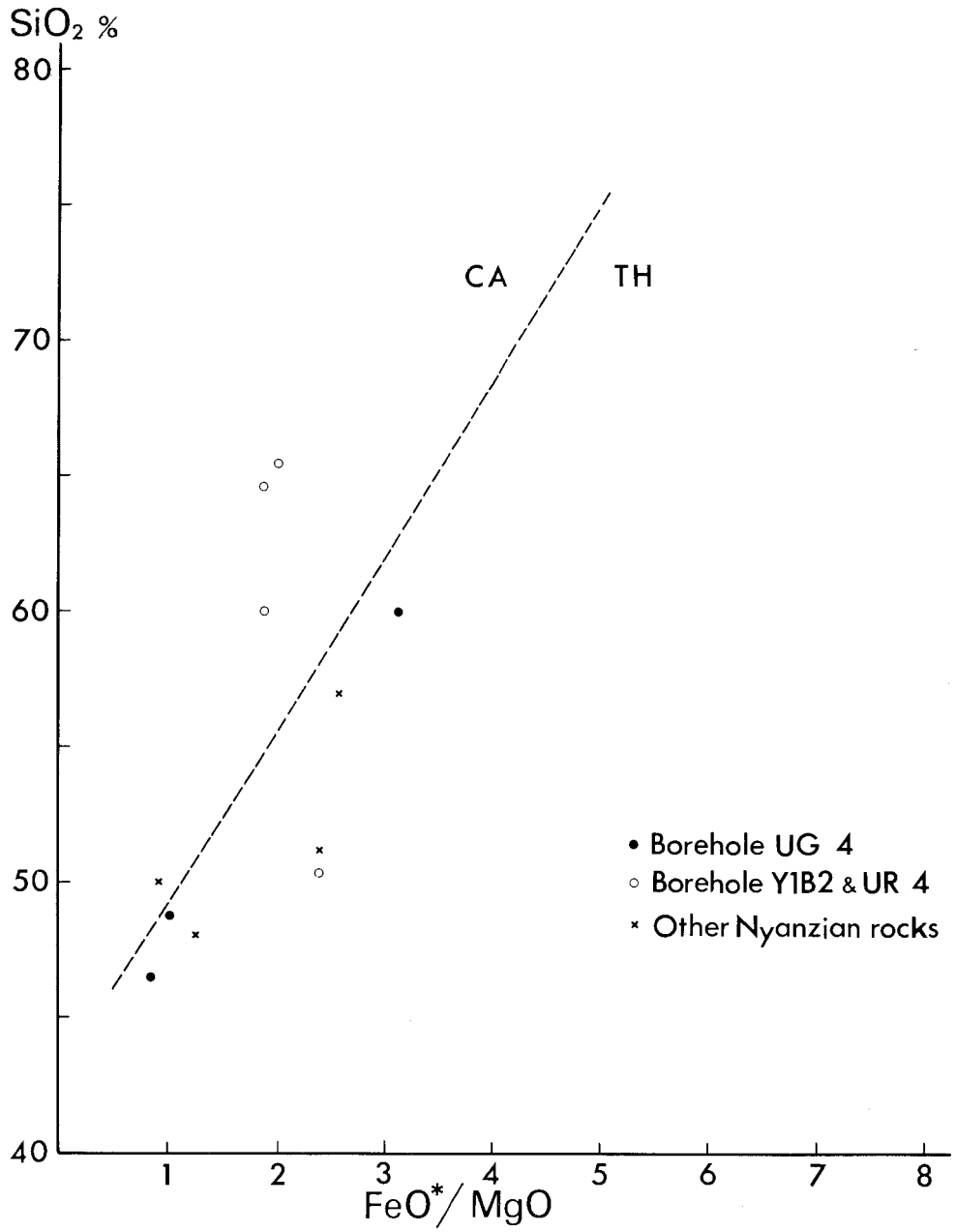

Fig. 6 $FeO_{total}/MgO - SiO_2$ (wt. %) relation for UG4-Nyanzian rocks, together with Y1B2- and UR4-borehole specimens and other Nyanzian volcanic rocks (Suwa, 1981).
CA: Calc-alkalic series field. TH: Tholeiitic series field. (Miyashiro, 1974)

of JICA-Nairobi office for his useful discussions and comments. We are much indebted to Dr. I. Nishida for kindly providing electron microphotographs, and to Mr. H. Noro for his useful suggestions and comments about clay minerals. Our thanks are also due to Dr. T. Yanagi, Mr. K. Tokieda, Dr. H. Umemura, Mr. M. Asami and Mr. M. Hoshino for their laborious collaboration in Kenya in 1981, and due to Dr. R. Sugisaki and Dr. K. Suzuki for their kind assistance in laboratory of Nagoya University.

This work in Kenya was made possible by the Grant-in-Aid for Overseas Scientific Survey from the Ministry of Education, Science and Culture, Japan, to which we express our thanks.

REFERENCES

COX, K.G., GURNEY, J.J. and HARTE, B. (1973): Xenoliths from the Matsoku pipe. In: Nixon, P.H. (ed.), *Lesotho kimberlites.* Lesotho Natl. Dev. Corp., Maseru, Lesotho, 76 - 100.

DANCHIN, R.V., FERGUSON, J., McIVER, J.R. and NIXON, P.H. (1975): The composition of late stage kimberlite liquids as revealed by nucleated autholiths. *Phys. Chem. Earth,* **9**, 235 - 245.

ITO, M., SUWA, K. and WINANI, P. (1981): Kimberlite from Nyanza, western Kenya. *6th Prelim. Rept. Afr. Studies, Nagoya Univ.,* 83 - 99.

KRESTEN, P. (1973): Differential thermal analysis of kimberlites. In: Nixon, P.H. (ed.), *Lesotho kimberlites.* Lesotho Natl. Dev. Corp., Maseru, Lesotho, 269 - 279.

MIYASHIRO, A. (1974): Volcanic rock series in island arcs and active continental margins. *Amer. Jour. Sci.,* **274**, 321 - 355.

RUIYUAN, C. (1981): Petrochemical characteristics of kimberlites and their diamond-bearing degree. *Geochimica,* **4**, 256 - 384. (In Chinese with English abstract).

SUWA, K. (1981): Petrochemical and petrographical notes on some Nyanzian volcanic rocks, west Kenya. *6th Prelim. Rept. Afr. Studies, Nagoya Univ.,* 15 - 32.

VAN DER MAREL, H.W. and BEUTELSPACHER, H. (1979): *Atlas of infrared spectroscopy of clay minerals and their admixtures.* Elsevier.

PLATE I

Microphotographs of Nyanza kimberlites.

A. Dark grey crystal tuffaceous kimberlite. YA17·21·16 (167.3 m). One nicol. Scale bar is 1 mm.
Fine-grained parts of dark colour (centre and upper left) are diopside-natrolite aggregates. Matrix is composed of smectite, serpentine, perovskite, opaque mineral, natrolite and/or cancrinite and calcite. Olivine "phenocryst" (lower left) and medium-grained olivine and diopside are found.

B. Greyish olive green tuffaceous kimberlite. Y1B3·1·31 (11.7 m). One nicol. Scale bar is 0.5 mm.
Much weathered and veined by calcite. "Phenocrysts" are completely altered to smectite and serpentine, surrounded by fine-grained pervoskite and opaque mineral. Matrix is composed of saponite, serpentine, diopside, perovskite, opaque mineral and calcite.

PLATE I

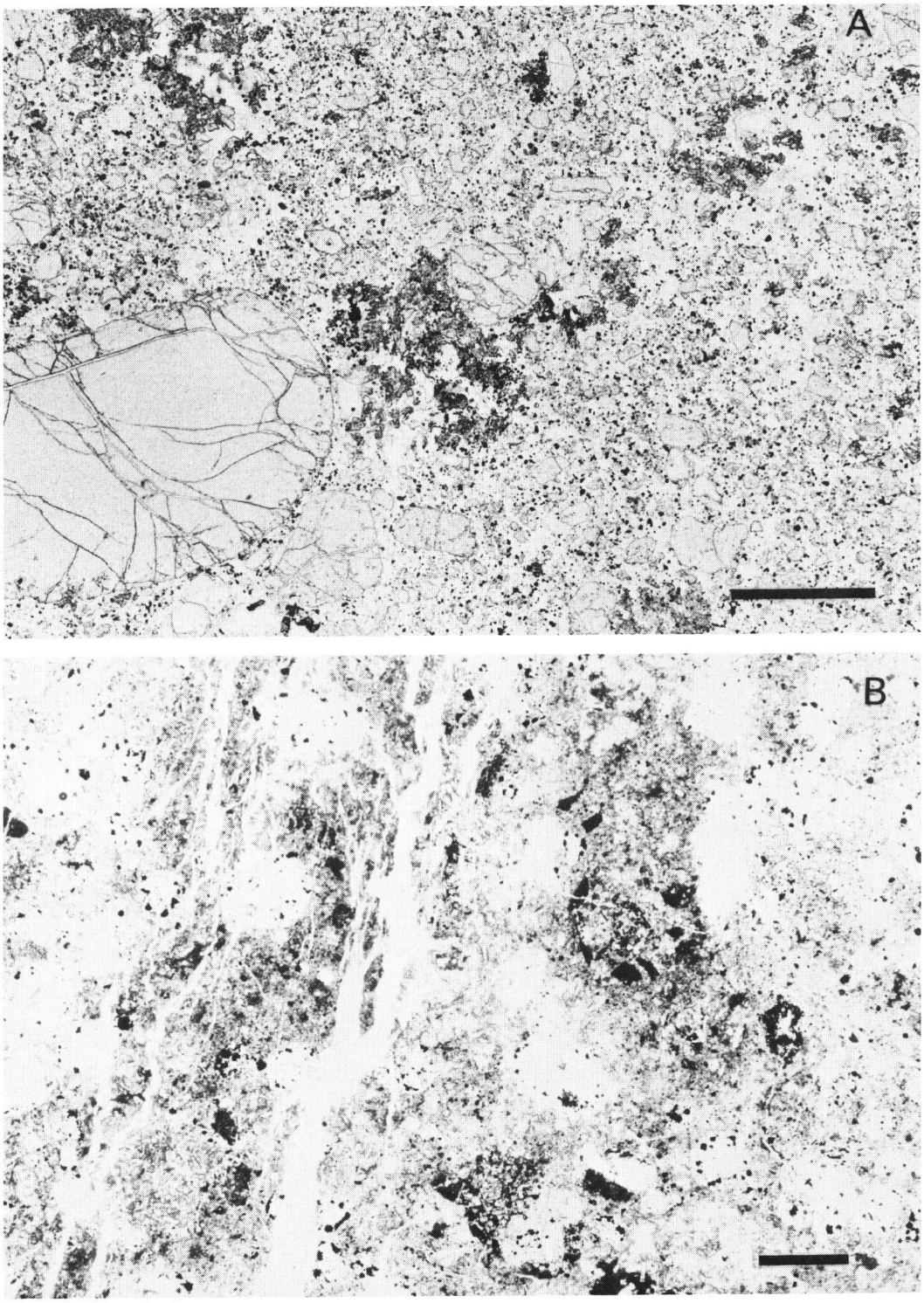

PLATE II

Microphotographs of Nyanza kimberlite.

A. Corroded olivine "phenocryst" (right) and diopside-natrolite druse (left) in YA17-21-16 (167.3 m). One nicol. Scale bar is 0.2 mm.

B. ditto. Crossed nicols.
Natrolite in the druse is fibrous and occurs as radiated aggregates.

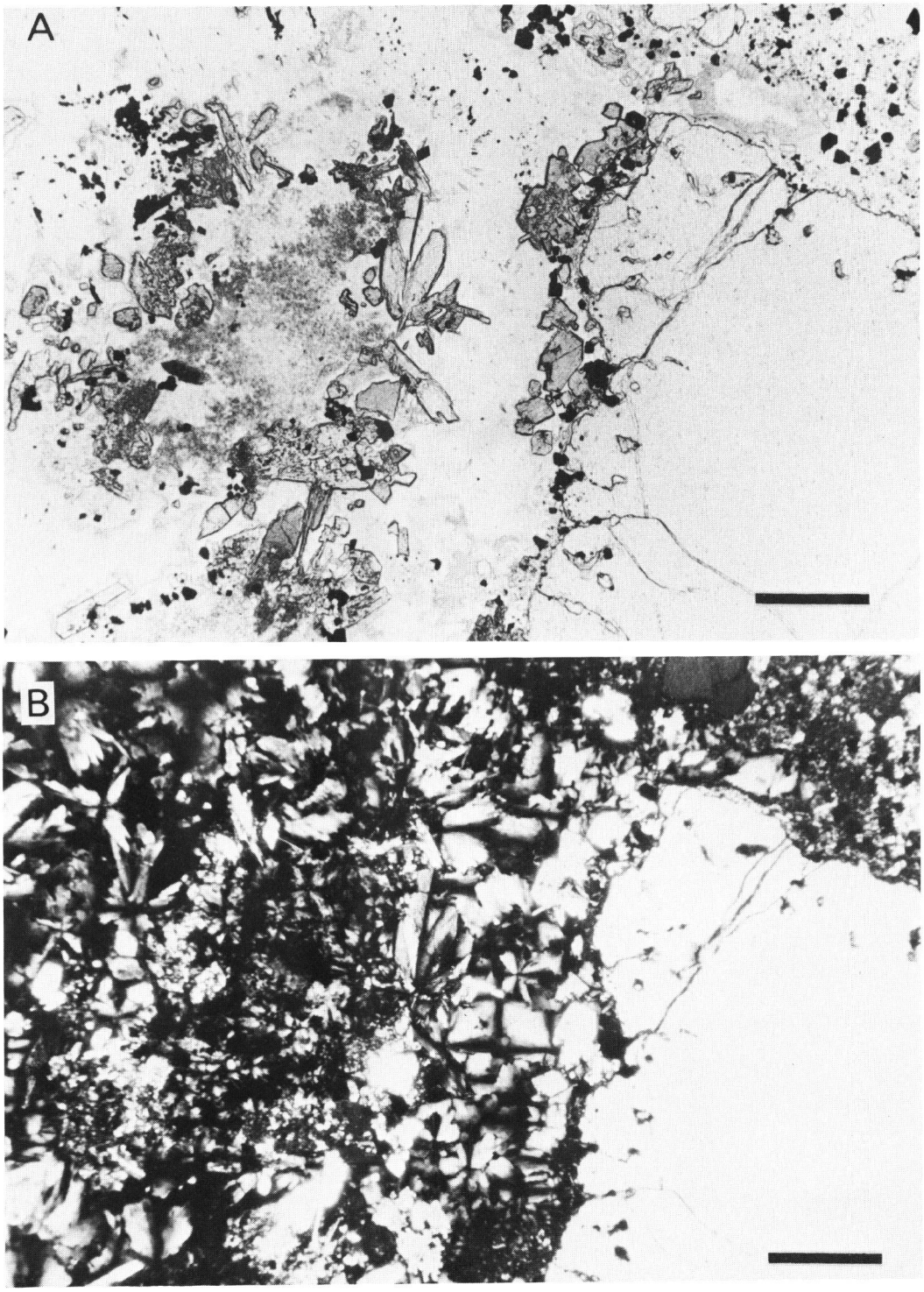
A
B

PLATE III

Electron figure and X-ray images for a chromite grain rimmed by Ti-Fe opaque mineral in Nyanza kimberlite (YA17·21-16, 167.3 m).
Chromite occupies an irregular core part. Several spots showing strong intensity in Ti Kα-image will be assigned to perovskite. Scale bar is 0.02 mm.

PLATE III

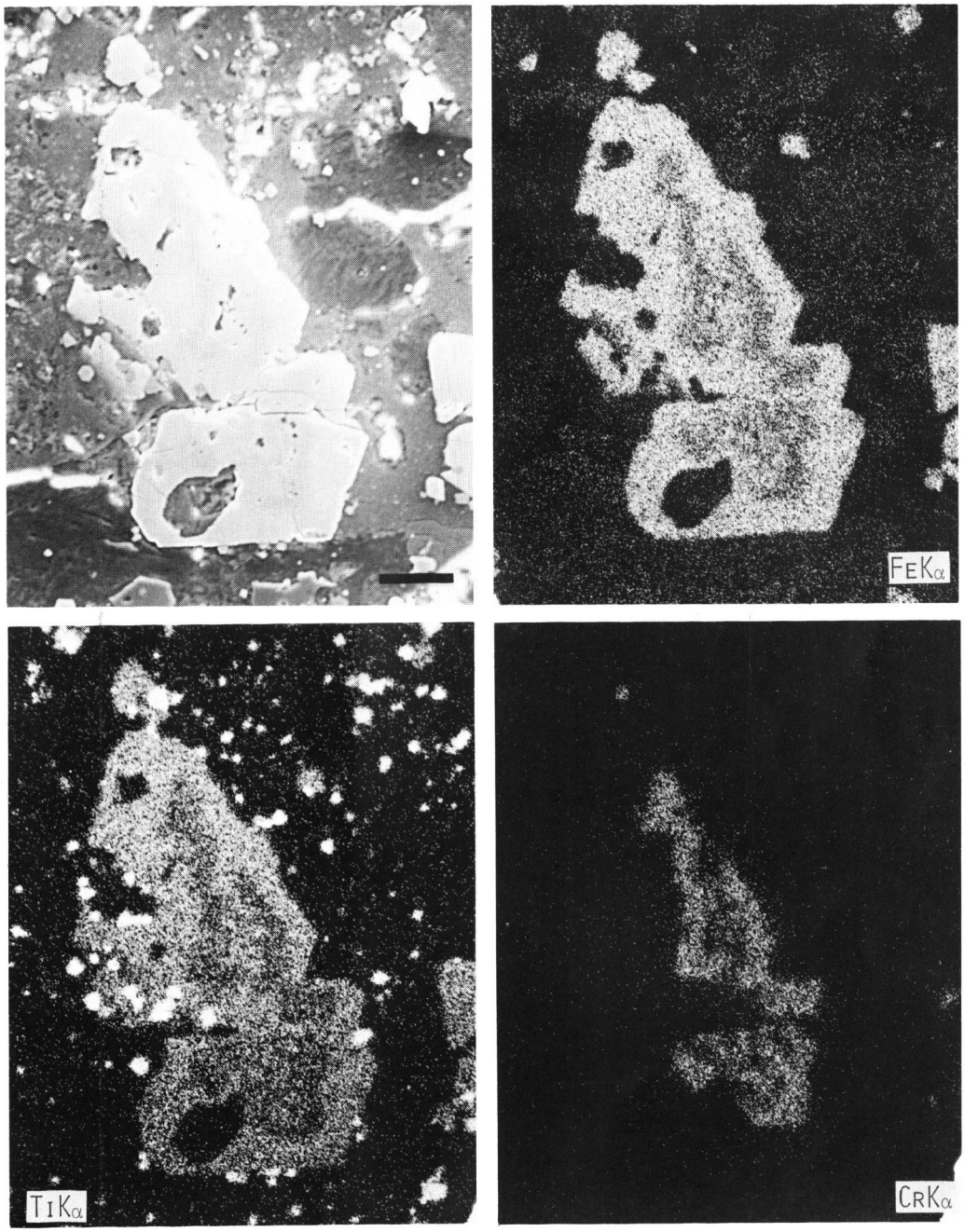

PLATE IV

Electron microphotographs of less-than-2 μm fraction of YA17-kimberlite from Nyanza, western Kenya (photo. by Dr. I. Nishida).

A. YA17-21-16 (167.3 m). Scale bar is 0.2 μm.
Smectite (saponite) and serpentine. Spherulitic aggregates showing the surface just like the crust of bread. Fibrous bundle characteristic of saponite is found at lower right.

B. ditto. Scale bar is 0.1 μm.
Smectite. Spherule twined by fibre and plate.

PLATE IV

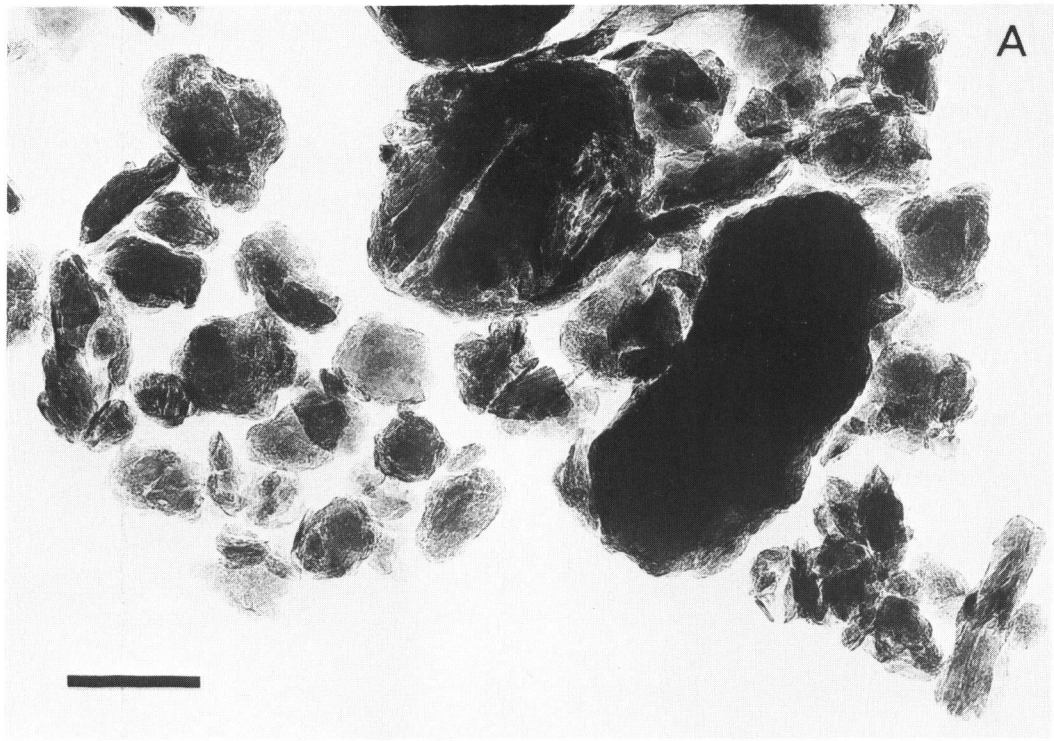

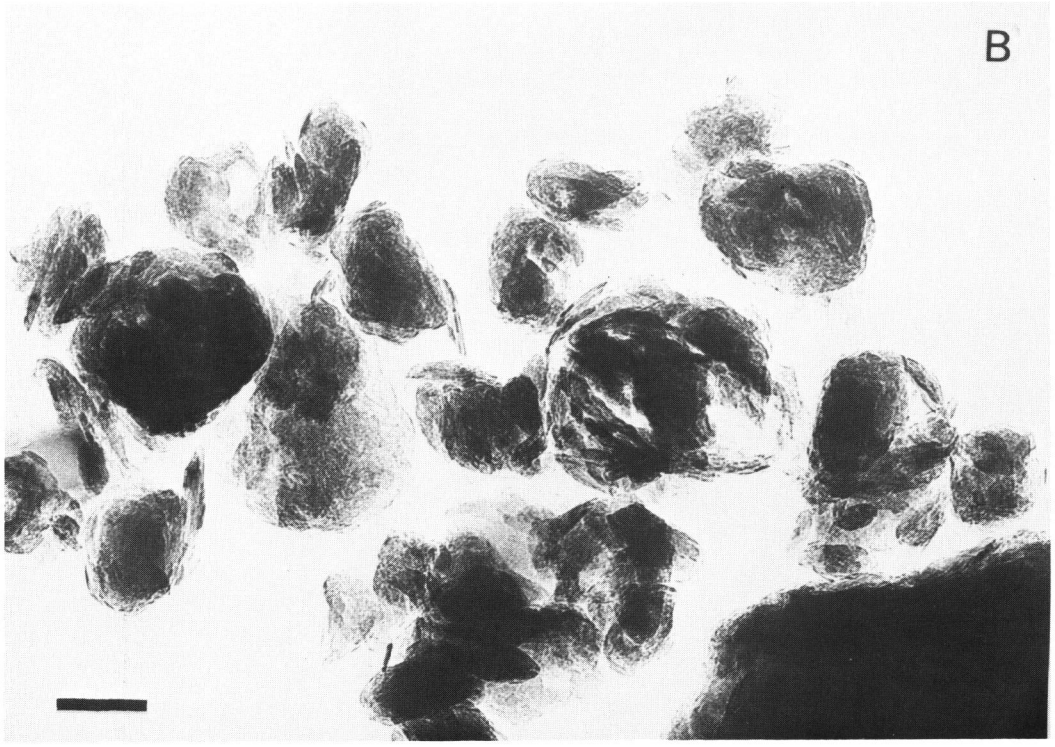

PLATE V

Electron microphotographs of less-than-2 μm fraction of Y1B3-kimberlite from Nyanza, western Kenya (photo. by Dr. I. Nishida).

A. Y1B3-1-31 (11.7m). Scale bar is 0.2 μm.
Smectite (saponite) and serpentine. Irregular platy flake, and curled and distorted fibrous bundle. Tangled fibre (upper left centre) and spherule twined by fibrous bundle (centre).

B. ditto. Scale bar is 0.1 μm.
A knitting ball-like spherule.

PLATE V

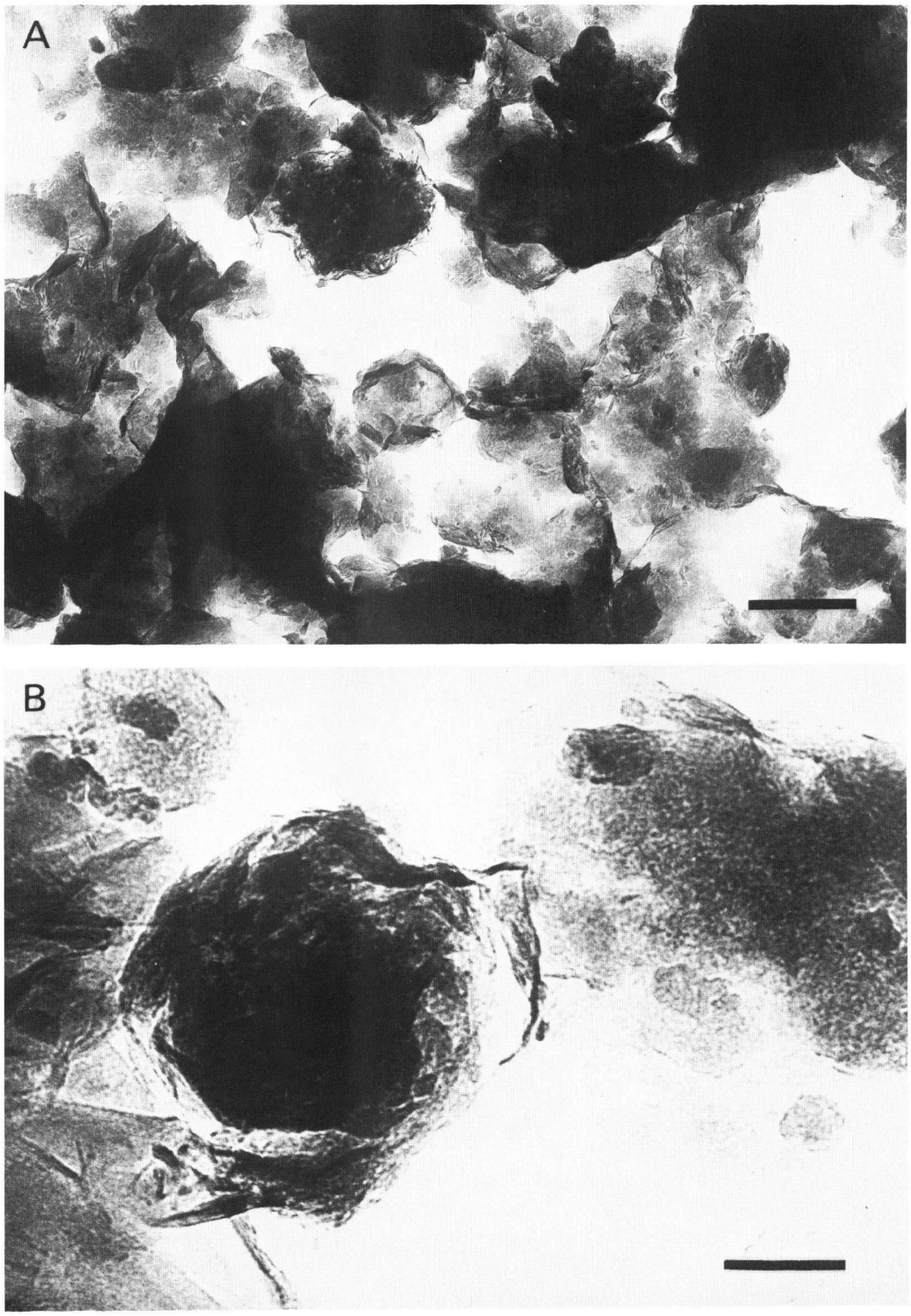

PLATE VI

Microphotographs of UG4-borehole specimens from Nyanza, western Kenya.

A. Dacitic tuff breccia. UG4·16-1 (147.4 m). One nicol. Scale bar is 2 mm. Matrix is holocrystalline-granular and is composed of plagioclase, quartz, calcite, chlorite and opaque mineral.

B. Porphyritic hornblende diorite. UG4·16-4 (144.1 m). One nicol. Scale bar is 2 mm.
Hornblende shows multi-zoning, associated with fibrous amphibole of very pale greenish yellow in colour. Plagioclase is sericitized and/or carbonatized.

PLATE VI

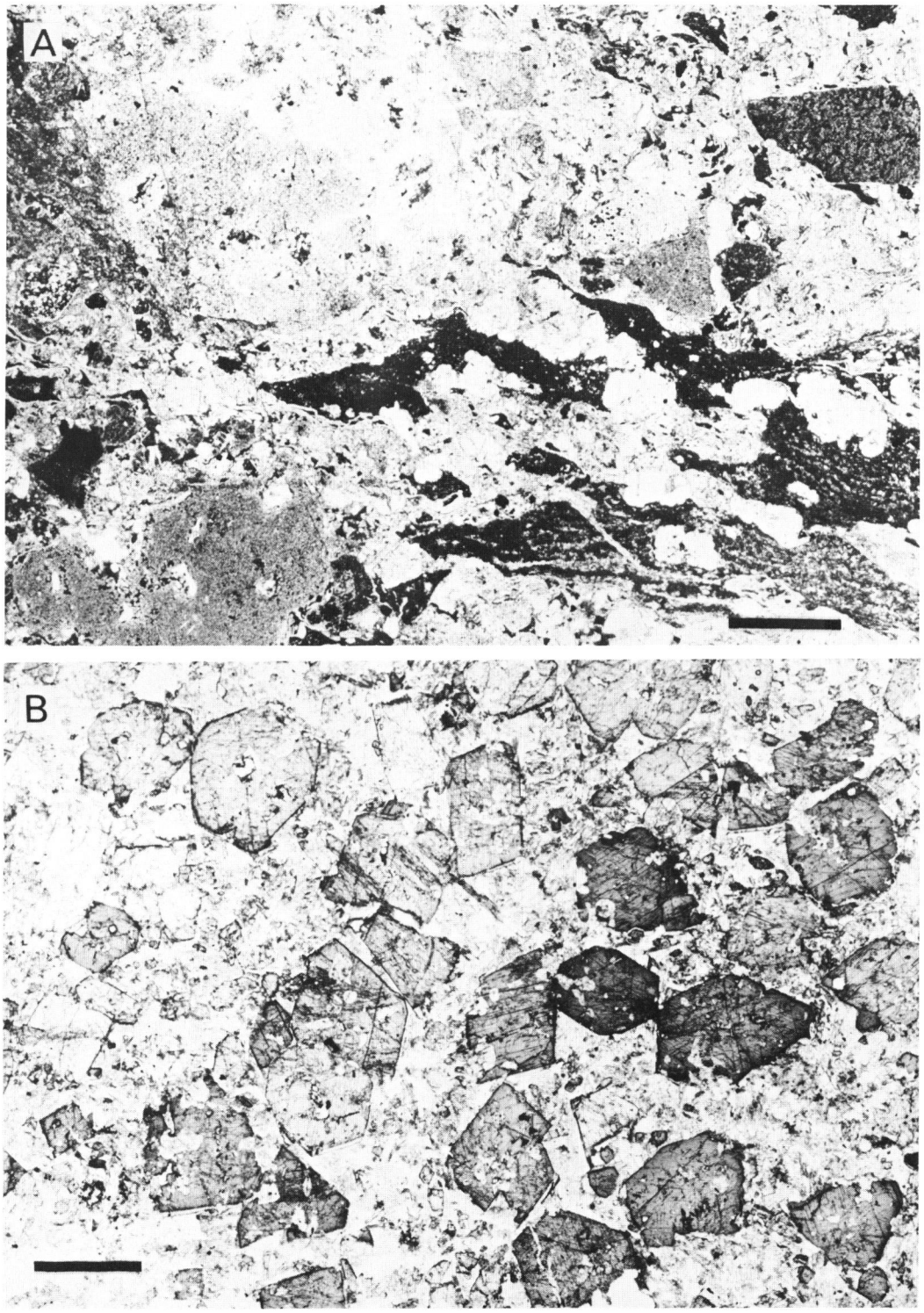

PLATE VII

1. Borehole drilling at the YA17 (34°30.9′ E, 0°09.5′ N), 7 Km to the NNW of Yala, Nyanza province, western Kenya (Photo. by K. S., 29 July, 1981).

2. Borehole core specimens at the YA17, Nyanza province, western Kenya (Photo. by K. S., 29 July, 1981).

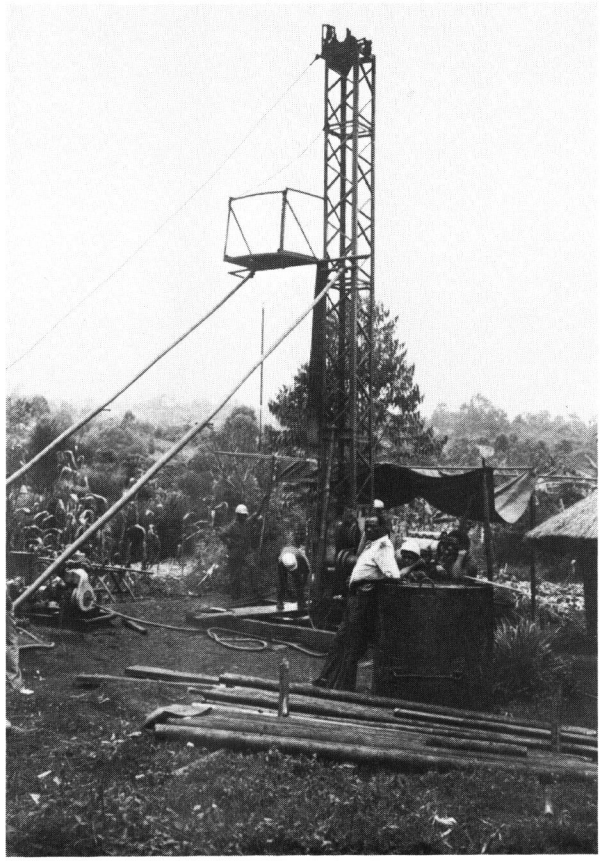

1

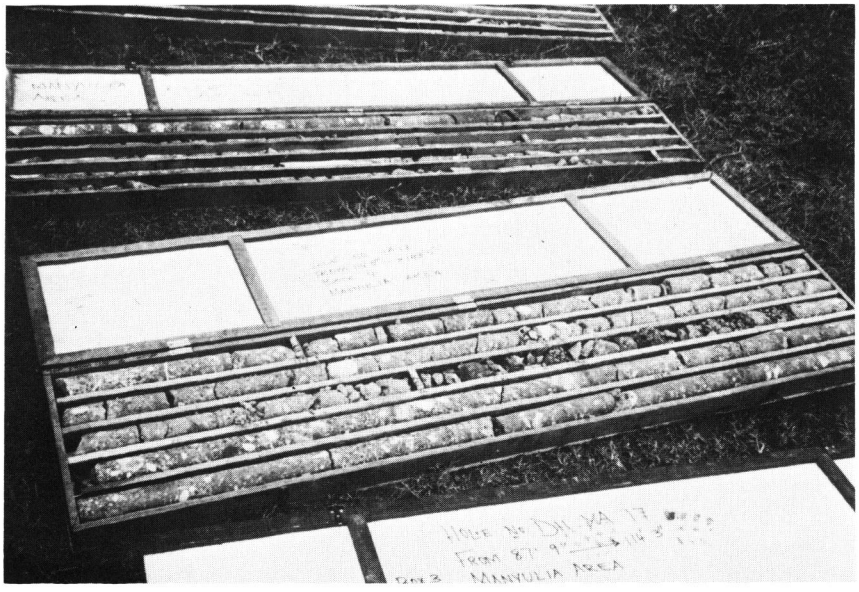

2

PLATE VIII

1. Borehole drilling at the YA17 (34°30.9′ E, 0°09.5′ N), 7 Km to the NNW of Yala, Nyanza province, western Kenya (Photo. by K. S., 29 July, 1981).

2. Borehole core specimens at the YA17, Nyanza province, western Kenya (Photo. by K. S., 29 July, 1981).

1

2

Petrographical note on the xenoliths in YA17-kimberlite from Nyanza, western Kenya

Masahiro ITO*, Kanenori SUWA** and A. S. SEGERO***

* Laboratory of Geology, College of General Education, Nagoya University
** Department of Earth Sciences, Faculty of Science, Nagoya University
*** Mines and Geological Department, Kenya

Abstract

Many fine-grained melanocratic rocks, leucocratic rocks and "gabbroic" rocks of xenoliths together with harzburgite are found in the YA17-kimberlite from Nyanza, western Kenya (34° 30.9'E, 0° 09.5'N). The fine-grained melanocratic rocks exhibit either aphyric texture or arenite-like one and the "gabbroic" rocks exhibit hypabyssal texture. Major constituent minerals of these rocks are similar to each other as follows: natrolite and/or thomsonite, cancrinite, diopside, colourless amphibole, carbonate, pectolite, opaque mineral and clayey matters, together with minor constituents of clinozoisitic epidote, apatite and sphene. Sodalite was found only in a "gabbroic" xenolith. Cancrinite and sodalite were identified by the X-ray powder diffraction. Cancrinite may be carbonate vishnevite or vishnevite based on its low double refraction. These xenoliths except harzburgite in YA17-kimberlite are considered to be derived from some buried Nyanzian rocks which were intensely soda-metasomatized or from hidden alkaline igneous rocks.

Introduction

YA17-kimberlite was taken up by the prospecting boring based on the airborne survey. Coordinates of the locality are 34° 30.9'E, 0° 09.5'N in western Kenya (Fig. 1). The borehole was drilled about 193 metres deep. Down to about 78 metres from the surface, weathered and soft crystal tuffaceous kimberlites are intercalated with laminated "tuff". Downwards from about 80 metres deep, the kimberlites become hard and greyish green through dark greyish green to medium grey in colour. The matrix of YA17-kimberlite is composed of smectite, diopside, colourless amphibole, opaque mineral, natrolite and/or thomsonite and carbonate. Common occurrence of smectite in place of serpentine characterizes the YA17-kimberlite, different from YlBl-kimberlite from Nyanza, western Kenya, already reported by Ito et al. (1981 & 1983).

Various xenoliths of fine-grained melanocratic rock, leucocratic rock, medium-

8th Prelim. Rept. Afr. Studies, Nagoya Univ., 197-204, 1983.

grained "gabbroic" rock and peridotite are distinguished by naked eyes (Plate I). Scarcity of peridotite xenolith is characteristic of YA17-kimberlite.

In this report, petrography of some xenoliths is described.

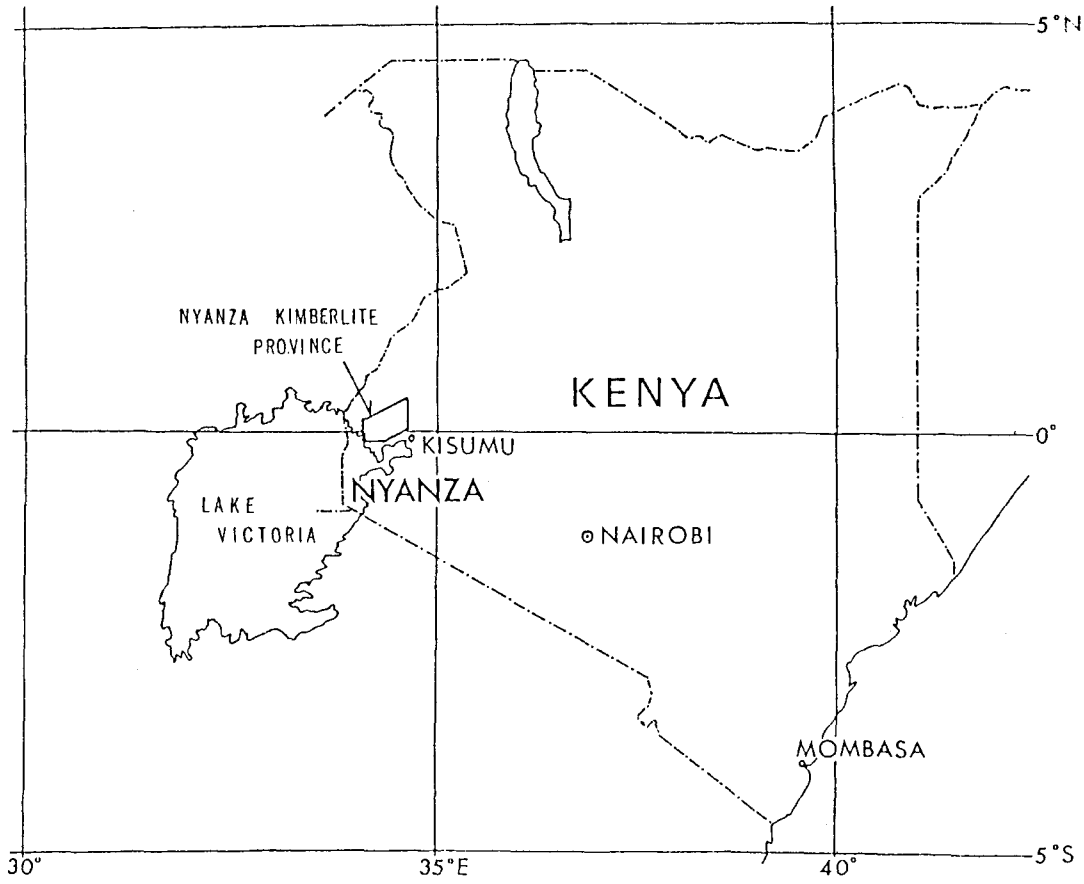

Fig. 1. Kimberlite province in Nyanza, western Kenya.

Peridotite

Peridotite xenoliths are scarcely found in YA17-kimberlite. The xenoliths are not associated with the reaction rim of serpophite different from those in YlBl-kimberlite (Ito et al., 1981). One of them is harzburgite of modal composition as follows: olivine 71.0, orthopyroxene 17.2, diopside 2.0, chromite 0.6, magnetite 0.2, colourless amphibole 0.08 and cryptocrystalline serpentine-natrolite 9.0 volume percentages, respectively. Microphotographs of the harzburgite are shown in Plate II.

Olivine is coarse-grained granular, showing undulose extinction. Along the thin films of cryptocrystalline serpentine in the olivine grains, olivine is often recrystallized to fine granular grains. Chemincal composition of a very coarse-grained olivine

is homogeneous with $Fo_{92.8}Fa_{7.2}$, as shown in Table 1. Orthopyroxene has also the chemical composition of $En_{92.8}Fs_{6.6}Wo_{0.6}$ (2.24% Al_2O_3, in Table 1). Chromian diopside occurs without exception as very fine-grained crystals in veins of cryptocrystalline serpentine and smectite, associated with magnetite, chromite, carbonate and sometimes natrolite (Plate III A). The chemical composition is $En_{53.0}Fs_{3.9}Wo_{43.1}$ (1.66% Al_2O_3 and 2.95% Cr_2O_3), as shown in Table 1. Chromite is light yellowish brown to brownish orange in thin section. It is commonly found as rather small grains in network-veins. The chemical composition of the mineral is shown in Table 1. If iron is supposed to be ferrous in the mineral, the chromite grain analysed

Table 1. Electron probe microanalyses of the minerals from harzburgite xenolith in YA17·18-25 (145.5 m) kimberlite, western Kenya.

	Olivine		Orthopyroxene		Chromian Diopside		Chrompicotite	
SiO_2	41.74		57.15		53.14		0.04	
TiO_2	0		0		0.20		0.04	
Al_2O_3	0		2.24		1.66		23.67	
Cr_2O_3	0		0.56		2.95		45.39	
FeO*	7.09		4.39		2.31		13.19	
MnO	0.10		0.12		0.10		0.20	
MgO	51.30		34.63		17.60		17.07	
NiO	0.30		0.10		0.02		0.14	
CaO	0		0.32		19.92		0	
Na_2O	0.02		0.20		1.33		0	
K_2O	0		0		0.01		0	
Total	100.55		99.71		99.24		99.74	
Si	1.005	1.01	1.960	2.00	1.945	2.00	0.001	
^{IV}Al	0		0.040		0.055			
^{VI}Al	0		0.051		0.017		0.842	1.93
Ti	0		0		0.006		0.001	
Cr	0		0.015		0.085		1.083	
Fe^{2+}	0.143		0.126		0.071		0.333	
Mn	0.002	1.99	0.004	2.00	0.003	2.02	0.005	
Ni	0.006		0.003		0.001		0.003	
Mg	1.840		1.770		0.960		0.767	1.11
Ca	0		0.012		0.781		0	
Na	0.001		0.014		0.094		0	
K	0		0		0		0	
O	4		6		6		4	
Mg/(Mg+Fe)	0.928							

* Total iron calculated as FeO.

is picotite with mole percentages of spinel 30.5, hercynite 13.2, magnesium chromite 39.3 and chromite 17.0, respectively. Thin films of cryptocrystalline serpentine and smectite are found along the grain boundaries between the major constituents of olivine and orthopyroxene. These films are always joined with network-veins which form "pools" everywhere.

Reaction rim around the harzburgite xenolith can not be recognized with naked eyes. Under the microscope, very thin rim of natrolite and/or thomsonite is only found to cover the xenolith. The two minerals occur sporadically as druse associated with carbonate and pectolite in the outer side of the rim. Some olivine grains are granulated, and some orthopyroxenes are recrystallized to fine-grained diopside, actinolitic amphibole and cryptocrystalline serpentine and/or smectite (Plate III B).

Crustal rock-xenoliths

Many xenoliths of fine-grained melanocratic rocks, medium-grained "gabbroic" rocks and leucocratic rocks are ubiquitously found in YA17-boring core specimens, as shown in Plate I. Tow occurrences can be distinguished; one is associated with reaction rim being thick enough to be identified with naked eyes (Plate I A) and the other is without any recognizable rim (Plate 1 B to D). The rim is mainly composed of smectite of greyish yellow brown in colour.

Under the microscope, almost all xenoliths carry commonly thin reaction rim which is composed of fine-grained diopside, opaque mineral, calcite, natrolite and/or thomsonite and pectolite (Plate IV). Opaque mineral is sometimes concentrated in both the rim and the outer part of the xenolith. The grain size of the mineral becomes gradually coarser outwards from the xenolith (Plate V A). In outer part of the rim, diopside becomes everywhere coarse-grained, some of which are zoned (Plates V C&D and VI A&B).

A. Fine-grained melanocratic rocks

Many fine-grained melanocratic rock fragments ubiquitously found in YA17-kimberlite are black, dark green, dark reddish to brownish grey and dark grey in colour. Mineral assemblages are nearly the same in these xenoliths; natrolite and/or thomsonite, pale green to colourless amphibole, diopside, altered biotite, calcite, pectolite, opaque mineral and small amounts of clinozoisitic epidote, apatite, sphene and clayey matter. Under the microscope, some volcanic rock-like and arenaceous rock-like textures are observed as shown in Plates IV, VI C&D and VII A&B.

Long laths of natrolite aggregates derived from ?nepheline and long prismatic or acicular amphibole show aphyric texture. Natrolite in some xenoliths showing arenaceous rock-like texture becomes slightly coarse-grained and is surrounded by interstitial minerals (Plate VII C&D).

B. Medium-grained "gabbroic" rocks

Mineral components of "garbbroic" rock are somewhat different from the fine-grained melanocratic rocks. Mafic minerals which are often "phenocrystic" are colourless to pale yellowish green amphibole, diopside and phlogopite (Plates V B and VII A&B). Almost all amphibole and diopside are products of alteration from brownish green to olive green ?hornblende.

Leucocratic part consists of fine-grained natrolite, cancrinite, apatite and smectite. Sodalite and/or cancrinite are characteristically found in such "gabbroic" xenoliths.

C. Leucocratic rocks and druses

Sizable amounts of leucocratic rocks and druses are found in YA17-kimberlite. Reaction rim of diopside and opaque mineral together with pectolite is commonly accompanied. There are two occurrences as follows; one exhibits the matrix of very fine-grained carbonate, diopside, pectolite and smectite, and the other consists of coarse-grained carbonate, natrolite and/or thomsonite as kernel (Plate IX).

Natrolite, thomsonite, cancrinite and sodalite

Natrolite and/or thomsonite are ubiquitously found in both xenoliths and host kimberlite. Sodalite besides cancrinite occurs especially in "gabbroic" xenoliths (Plate VIII C&D). In Fig. 2, X-ray powder diffraction patterns of these four minerals are shown. Cu Kα radiation was used. These patterns are identified based on ASTM data and on the powder patterns reported by Borg et al. (1969).

Natrolite is distinguished from thomsonite based on splitting of several peaks of the latter mineral. The peaks show d-spacings of 4.64, 4.39, 4.15 and 2.86 Å, respectively, which are found in Fig. 2 at about 19°, 20°, 21° and 31° of 2θ for Cu Kα radiation. Both minerals occur commonly as radiating fibrous aggregates. As thomsonite shows either positive or negative elongation, it is difficult to distinguish under the microscope between natrolite and thomsonite. Optically isotropic fringe is found to occur on the top of the radiating fibrous thomsonite aggregates (Plate IX). Any distinguishable difference in the refractive index is not observed between thomsonite and the associated fringe.

Cancrinite and sodalite are ultimately identified by their X-ray powder diffraction patterns (Fig. 2). Judging from the low double refraction, cancrinite may be rather carbonate vishnevite or vishnevite of cancrinite-vishnevite series.

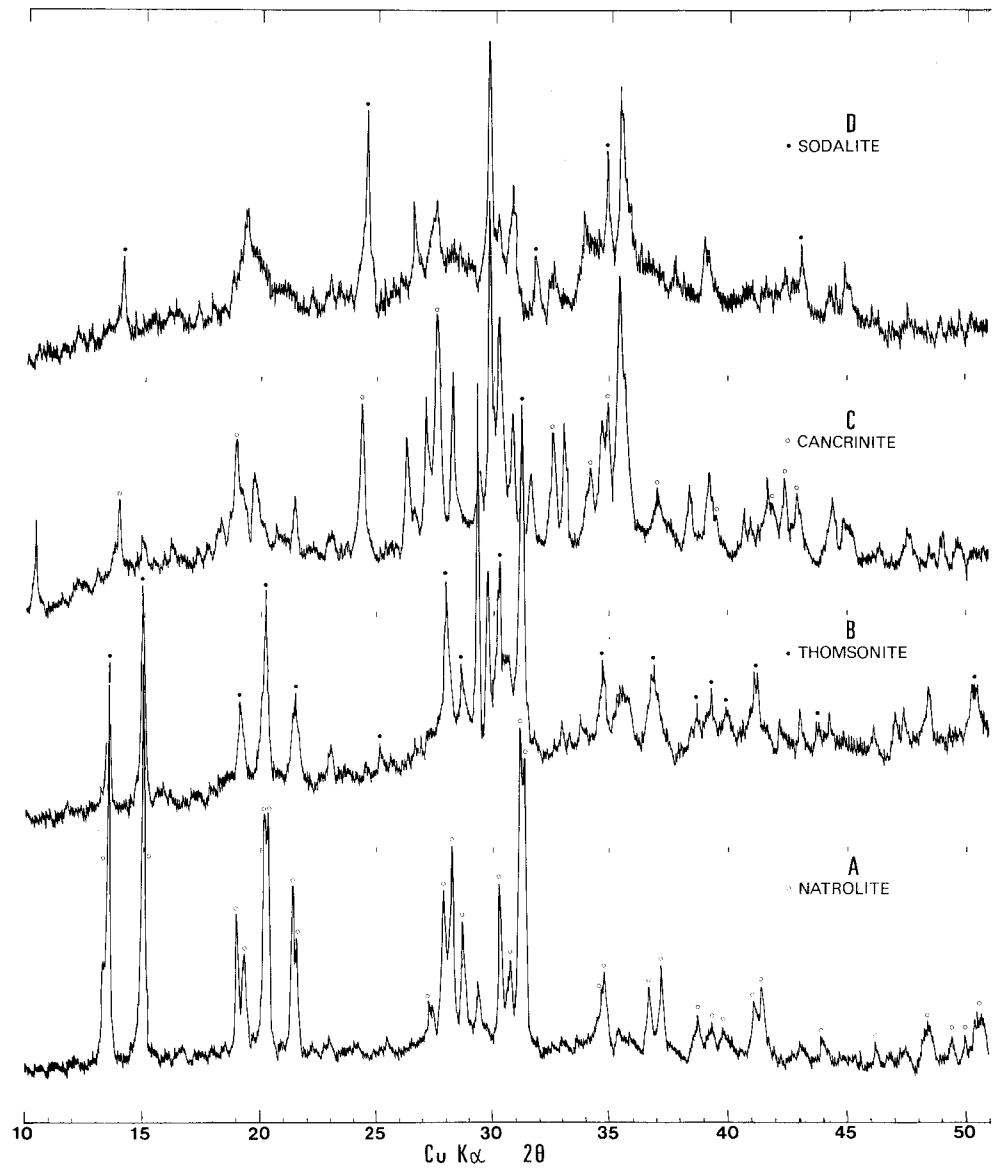

Fig. 2. X-ray powder diffraction patterns for natrolite, thomsonite, cancrinite and sodalite from xenoliths in YA17-kimberlite, Nyanza, western Kanya.

A: Natrolite (open circles) together with admixed calcite and 12Å-layer mineral from a fine-grained melanocratic xenolith. YA17·23-5 (185.8 m)

B: Thomsonite (solid circles) together with admixed calcite, diopside and 15Å layer mineral from a fine-grained melanocratic xenolith. YA17·22-10 (178.5 m)

C: Cancrinite (open circles) together with admixed diopside, amphibole, calcite, natrolite and 13Å-layer mineral from a medium-grained "gabbroic" xenolith. YA17·19-22(153 m)

D: Sodalite (solid circles) together with admixed diopside, mica and 13Å-layer mineral from a medium-grained "gabbroic" xenolith. YA17·20-17(166.5 m)

Discussion

Abundance of fine-grained melanocratic xenoliths and scarcity of peridotite are characteristic of YA17-kimberlite among the Nyanza kimberlites (Ito et al., 1981, 1983). Medium-grained "gabbroic" xenoliths indicate a hypabyssal texture very similar to some basic igneous rocks which were taken up with Nyanzian dacitic rocks by UG4-boring (Ito et al., 1983). Dawson (1980) summarized various occurrences of xenoliths in the kimberlites from five different sources. Diversity in rock species of xenoliths included in the Nyanza kimberlites is significant, because these rocks suggest some schemes on the constitution of crust and upper mantle which are traversed by kimberlite. As the spacial distribution of these xenoliths is probably heterogeneous in the kimberlite diatremes, only one borehole may not indicate the whole internal features of a diatreme.

Though natrolite and related zeolitic minerals together with unidentified minerals were found as secondary products in wide varieties of xenolithic rock; basaltic or doleritic rock, granulite, basic gneiss and so on (Bloomer and Nixon, 1973, Cox et al., 1973, Nixon and Boyd, 1973, Dawson, 1980), any detailed petrographical study of these minerals was not reported. In YA17-kimberlite from western Kenya, natrolite and/or thomsonite occur ubiquitously and the xenoliths except peridotite are completely altered to "natrolite and/or thomsonite rocks". Sodalite besides cancrinite is especially found in "gabbroic" rocks. Le Bas (1977) reported various occurrences of natrolite and cancrinite in alkaline igneous rocks associated with carbonatite from Homa Bay district, western Kenya. Natrolite and cancrinite were described as alteration products of nepheline in nephelinite, phonolite, foyaite, lamprophyre, ijolite and related pyroclastic rocks and as late-stage deuteric minerals. It is significantly noted in relation to the xenoliths in YA17-kimberlite that natrolite was found in fine-grained lavas of basaltic appearance from Homa Bay area. Topography around the location of kimberlite-prospecting borings and occurrence of laminated kimberlitic "tuff" occupying the uppermost part of the boring core indicate weak erosion of the diatreme. Therefore, these xenoliths in YA17-kimberlite are considered not to be derived from the rocks overlying Nyanzian which have subsequently been eroded away after the kimberlite intrusion. However, neither nepheline-bearing rocks nor soda-metasomatized rocks can be found in the kimberlite province of Nyanza, western Kenya.

Skinner and Clement (1979) reported that kimberlite may be altered by deuteric, metasomatic and weathering processes and that metasomatic and/or weathering processes in kimberlites generally produce clay and/or chlorite and/or abundant carbonate minerals. As YA17-kimberlite exhibits the matrix of smectite in place of serpentine and the unaltered "phenocrystic" olivine, alteration and hybridization of this kimberlite may have been taken place due to metasomatic or deuteric process by some possibility. The xenoliths of "basaltic" and "gabbroic" appearances in YA17-kimberlite may be derived from either buried Nyanzian which was variously soda-metasomatized or hidden alkaline igneous rocks.

Acknowledgements — We would like to express our deep gratitude to the Commissioner and Mr. J.K. Wachira, Acting Chief Geologist, of Kenya Mines and Geological Department for their permission of our investigation on many borehole specimens. Our sincere thanks are extended to Professor I.S. Loupekine of the University of Nairobi for kindly affording every facility to our field works and to Dr. K. Motojima of JICA-Nairobi office for his useful discussions and comments. Our thanks are also due to Dr. T. Yanagi, Mr. K. Tokieda, Dr. H. Umemura, Mr. M. Asami and Mr. M. Hoshino for their laborious collaboration in Kenya in 1981, and due to Dr. R. Sugisaki and Dr. K. Suzuki for their kind assistance in laboratory of Nagoya University.

This work in Kenya was made possible by the Grant-in-Aid for Overseas Scientific Survey from the Ministry of Education, Science and Culture, Japan, to which we express our thanks.

REFERENCES

BLOOMER, A.G. and NIXON, P.H. (1973): The geology of Letseng-la-terae kimberlite pipes. In: Nixon, P.H. (ed.), *Lesotho kimberlites.* Lesotho Natl. Dev. Corp., Maseru, Lesotho, 20-32.

BORG, I.Y. and SMITH, D.K. (1969): Calculated X-ray powder patterns for silicate minerals. *Geol. Soc. Amer., Memoir* **122.**

COX, K.G., GURNEY, J.J. and HARTE, B. (1973): Xenoliths from the Matsoku pipe. In: Nixon, P.H. (ed.), *Lesotho kimberlites.* Lesotho Natl. Dev. Corp., Maseru, Lesotho, 76-100.

DAWSON, J.B. (1980): *Kimberlites and their xenoliths.* Springer-Verlag.

ITO, M., SUWA, K. and WINANI, P. (1981): Peridotite xenoliths in kimberlite from Nyanza, western Kenya. *6th Prelim. Rept. Afr. Studies, Nagoya Univ.,* 101-110.

ITO, M., SUWA, K. and SEGERO, A.S. (1983): Petrographical studies on the YA17-, Y1B3- and UG4-kimberlite-prospecting boring core specimens from Nyanza, western Kenya. *8th Prelim. Rept. Afr. Studies, Nagoya Univ.*, 181-196.

Le BAS, M.J. (1977): *Carbonatite-nephelinite volcanism.* John Wiley & Sons.

NIXON, P.H. and BOYD, F.R. (1973): Deep seated nodules. In: Nixon, P.H. (ed.), *Lesotho kimberlites.* Lesotho Natl. Dev. Corp., Maseru, Lesotho, 106-109.

SKINNER, E.M.W. and CLEMENT, C.R. (1979): Mineralogical classification of southern African kimberlites. In: Boyd, F.R. and Meyer, H.O.A. (ed.), *Kimberlites, diatremes, and diamonds: Their geology, petrology and geochemistry. Proc. 2nd Int. Kimb. Conf.*, Amer. Geophys. Union, Vol. **1**, 129-139.

PLATE I.

Boring core specimens of YA17-kimberlite from Nyanza, western Kenya. Coordinates of the locality are 34° 30.9'E, 0° 09.5'N.

A. Light grey kimberlite, YA17-14-35(119.7 m). Scale bar is equal to 1 cm. Many fragments of melanocratic rock are surrounded by yellowish white to grey soft rim which is composed of smectite, calcite, diopside, pectolite and natrolite. Matrix of the host kimberlite is grey to bluish grey in colour and is composed of smectite, diopside, pectolite, calcite, magnetite, serpentine and perovskite.

B. Medium greyish green kimberlite, YA17-21-16(167.3 m). Scale bar is equal to 1 cm.
Medium-grained "gabbroic" xenolith (lower centre) which is accompanied by dark green rim. The "gabbroic" rock is composed of colourless amphibole, diopside, cancrinite, natrolite and/or thomsonite, opaque mineral and smectite.

C. Dark grey kimberlite, YA17-21-16(167.3 m). Scale bar is equal to 1 cm.
Fragments of dark coloured green to greyish rocks with dark grey kernel are observed.

D. Dark greyish green kimberlite, YA17-23-6(184.5 m). Scale bar is equal to 0.5 cm.
Small fragments of white to grey in colour are found everywhere. Glittering matters (left centre) are phlogopite flakes which are altered to calcite, diopside and clay, showing light brown to brownish orange in colour.

PLATE I

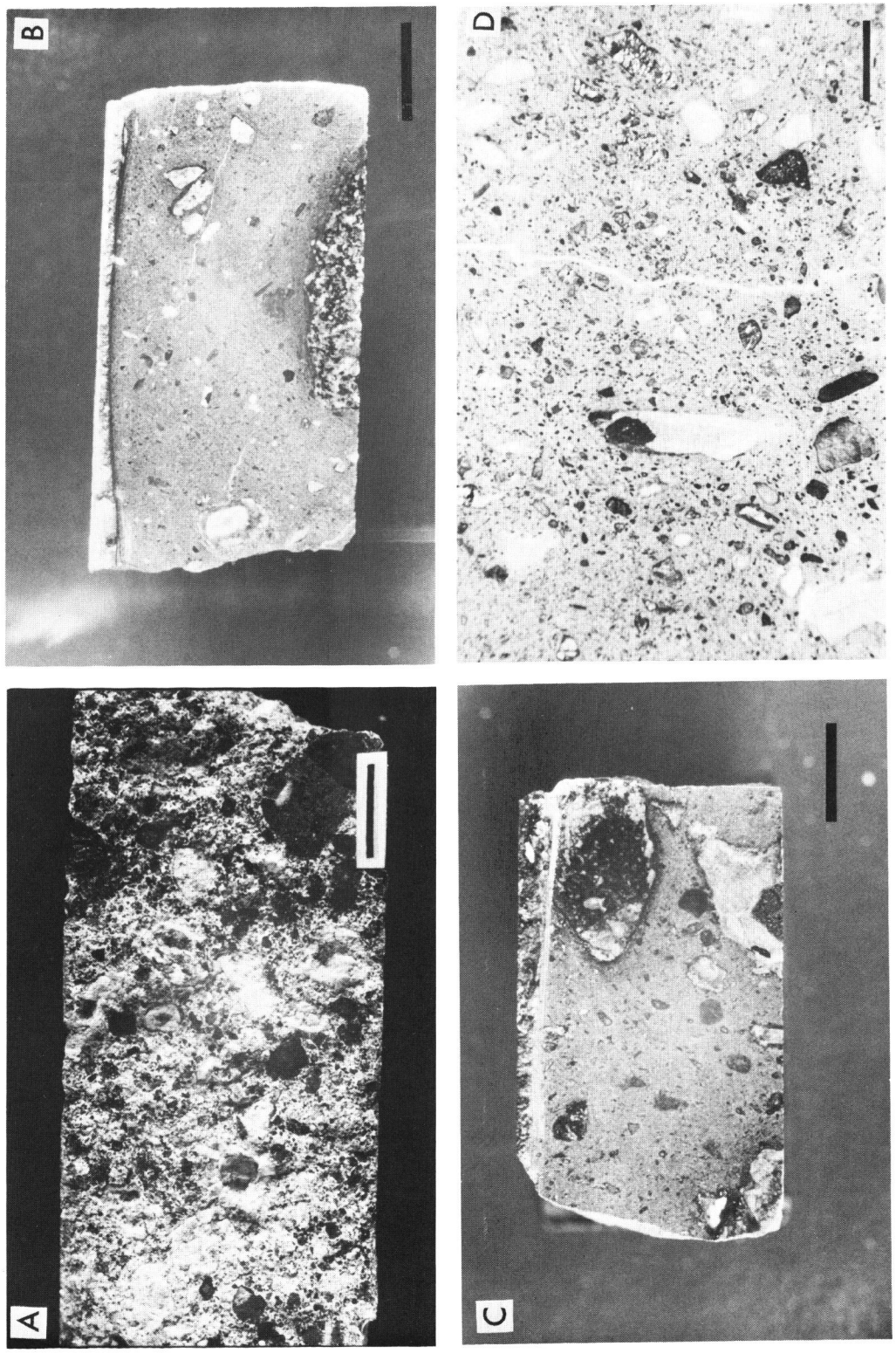

PLATE II.

Microphotographs of harzburgite in YA17-kimberlite from Nyanza, western Kenya. YA17-18-25(145 m).

A. One nicol. Scale bar is equal to 2 mm.
Thin film of cryptocrystalline serpentine and smectite exists along the crystal grain boundaries and in fractures. It enlarges from place to place as "pools", associated with diopside, chromite, magnetite, natrolite and/or cancrinite besides serpentine and smectite. Medium-grained pale grey grains in the photograph are orthopyroxene.

B. ditto. Crossed nicols.
Olivine crystals exhibit undulose extinction.

PLATE II

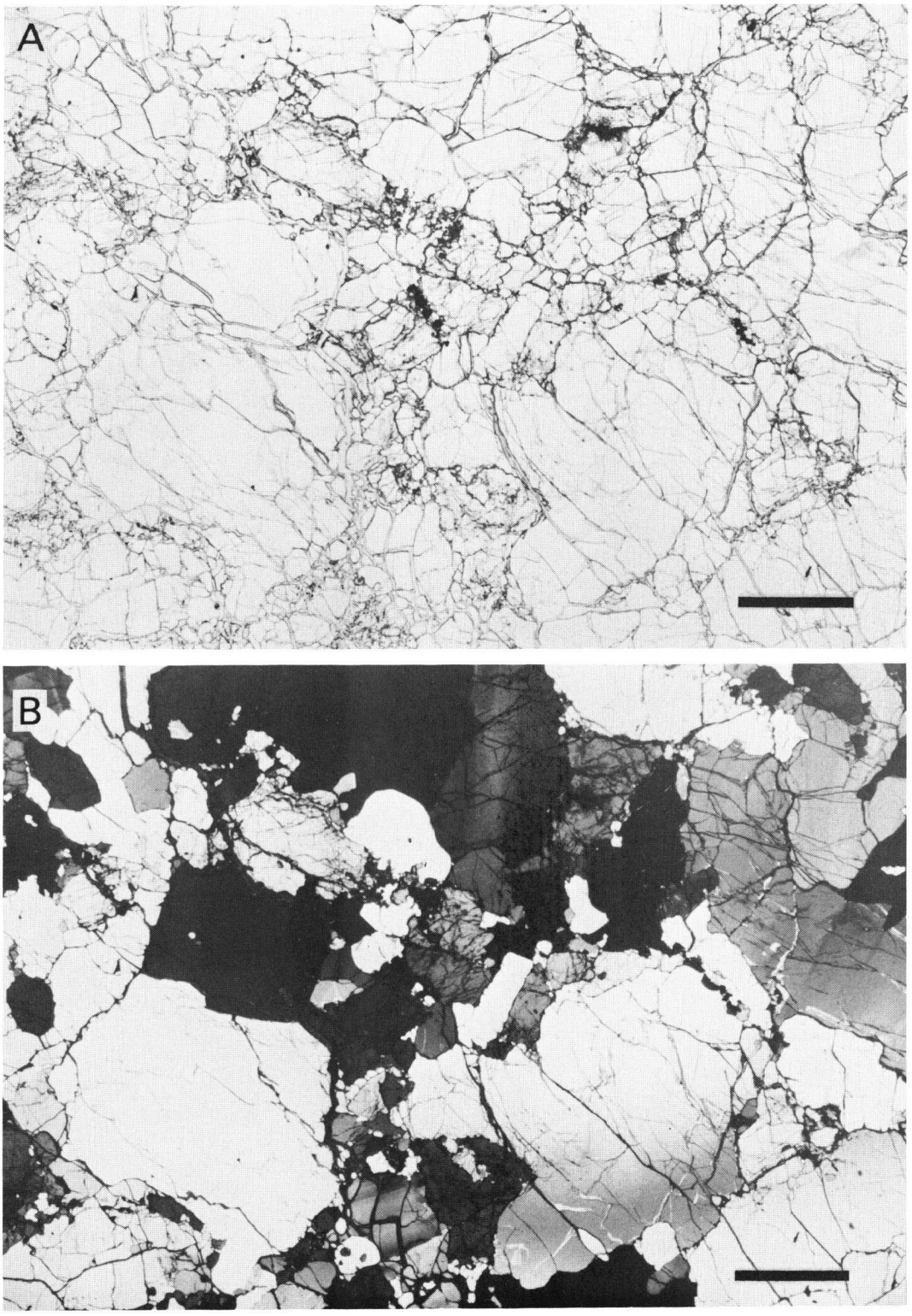

PLATE III.

Microphotographs of harzburgite in YA17-kimberlite from Nyanza, western Kenya. YA17·18-25(145.5 m).

A. A "pool" filled with cryptocrystalline serpentine, fine-grained diopside (stained grey, lower and right centre), opaque mineral (left) and very thin prismatic colourless amphibole (left centre). Large grains (upper and lower) are olivine. One nicol. Scale bar is equal to 0.1 mm.

B. Contact part between xenolithic harzburgite (right) and the host kimberlite (left). One nicol. Scale bar is equal to 0.3 mm.
Olivine is granulated, and pyroxene is completely altered to diopside, actinolitic amphibole and clayey matter (dark, right centre). Reaction rim is thin and is composed of natrolite and/or thomsonite (upper left to lower right), sporadically associated with druse of natrolite and/or thomsonite, carbonate, pectolite (fibrous, grey), opaque mineral and clayey matter.

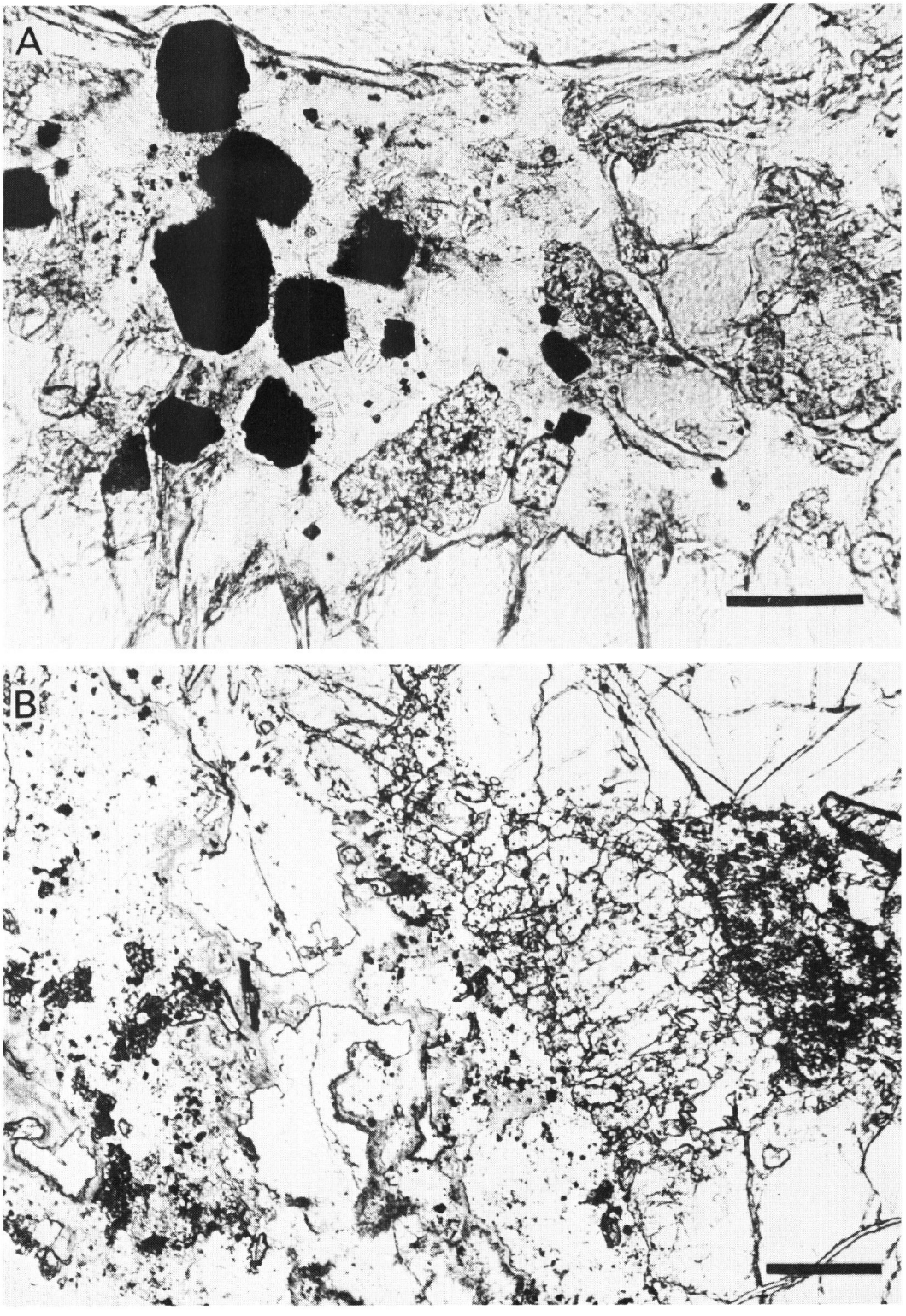
A
B

PLATE IV.

Microphotographs of fine-grained melanocratic xenoliths associated with reaction rim, in YA17-kimberlite from Nyanza, western Kenya. YA17-21-16 (167.3 m). Scale bars are equal to 2 mm.

A. Many melanocratic xenoliths (right and left) show aphyric texture and are, however, composed of natrolite and/or thomsonite, cancrinite, calcite or magnesite, diopside, colourless amphibole, mica, pectolite, opaque mineral and clayey matter.
Small druses of diopside, calcite, colourless amphibole, opaque mineral, natrolite and/or thomsonite are ubiquitously found (lower and upper centre). Large fractured crystals are olivine. One nicol.

B. Crossed nicols.

PLATE IV

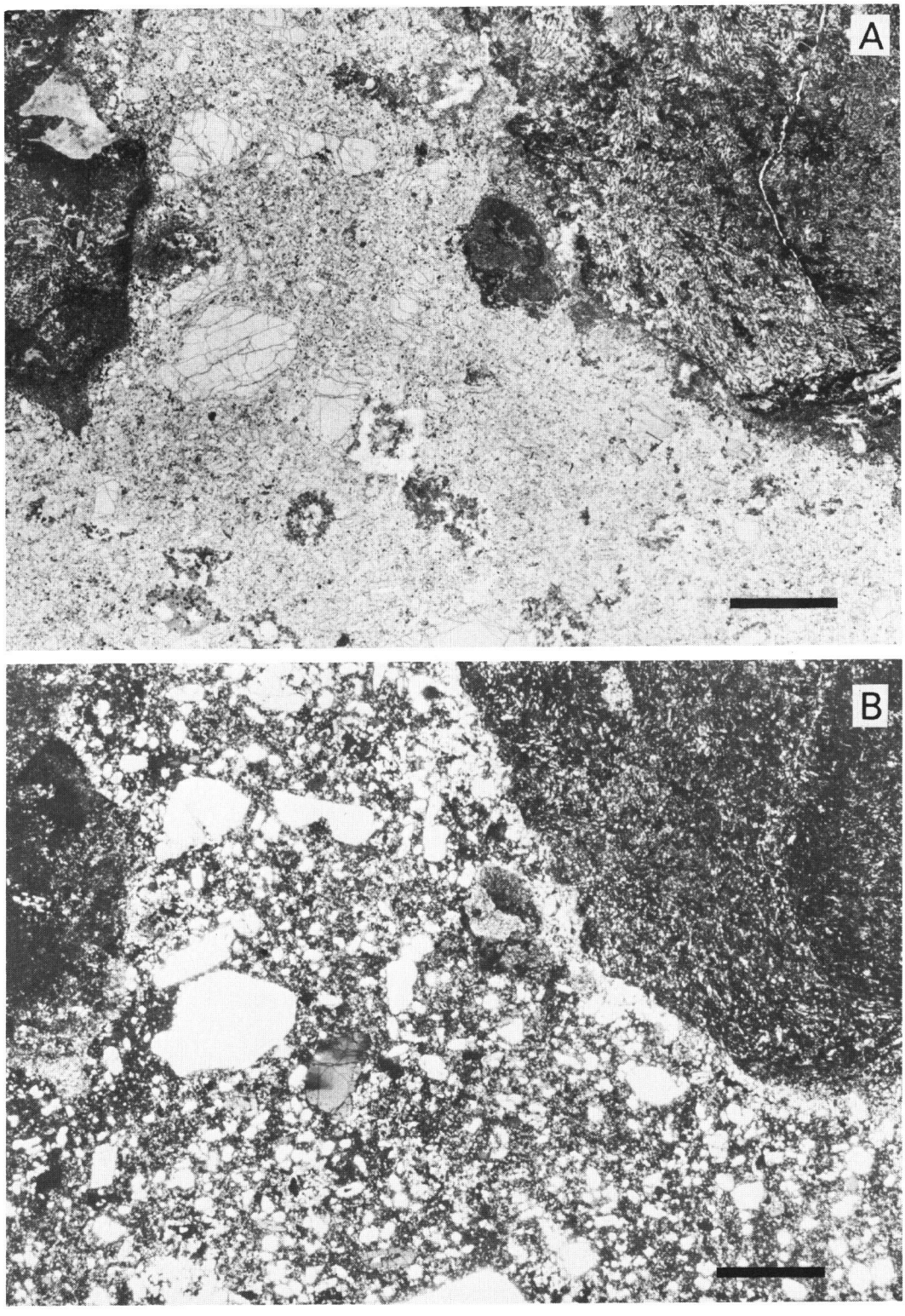

PLATE V.

Microphotographs of reaction zone between xenoliths and the host YA17-kimberlite from Nyanza, western Kenya.

A. Melanocratic xenolith in YA17-21-16(167.3 m). One nicol. Scale bar is equal to 0.5 mm.
Fine-grained euhedral diopside and magnetite occur concentratedly in outer part of the xenolith (right half), followed by coarse-grained diopside-opaque mineral-calcite-natrolite/thomsonite of reaction zone (left half).

B. Reaction zone accompanied with a gabbroic rock-like xenolith. YA17-22-10 (175.8 m). One nicol. Scale bar is equal to 0.5 mm.
Reaction zone of two to four millimetres wide is observed in right two third of the photograph and the host kimberlite is in left side. Natrolite and/or thomsonite (white), calcite (grey), diopside (dark) and small amounts of colourless amphibole, opaque mineral and pectolite occupy the main part of the zone, the outermost part of which is associated with fine-grained diopside.

C. Coarse-grained outer part of the reaction zone around a melanocratic xenolith. YA17-21-16(167.3 m). One nicol. Scale bar is equal to 0.1 mm.
Subhedral and anhedral diopside, natrolite and/or thomsonite and opaque mineral are found. Fine prismatic crystals (left) are also diopside.

D. ditto. Crossed nicols.
Very coarse-grained diopside is slightly zoned (lower right). Natrolite and/or thomsonite occur as radiating fibrous aggregate (lower right).

PLATE V

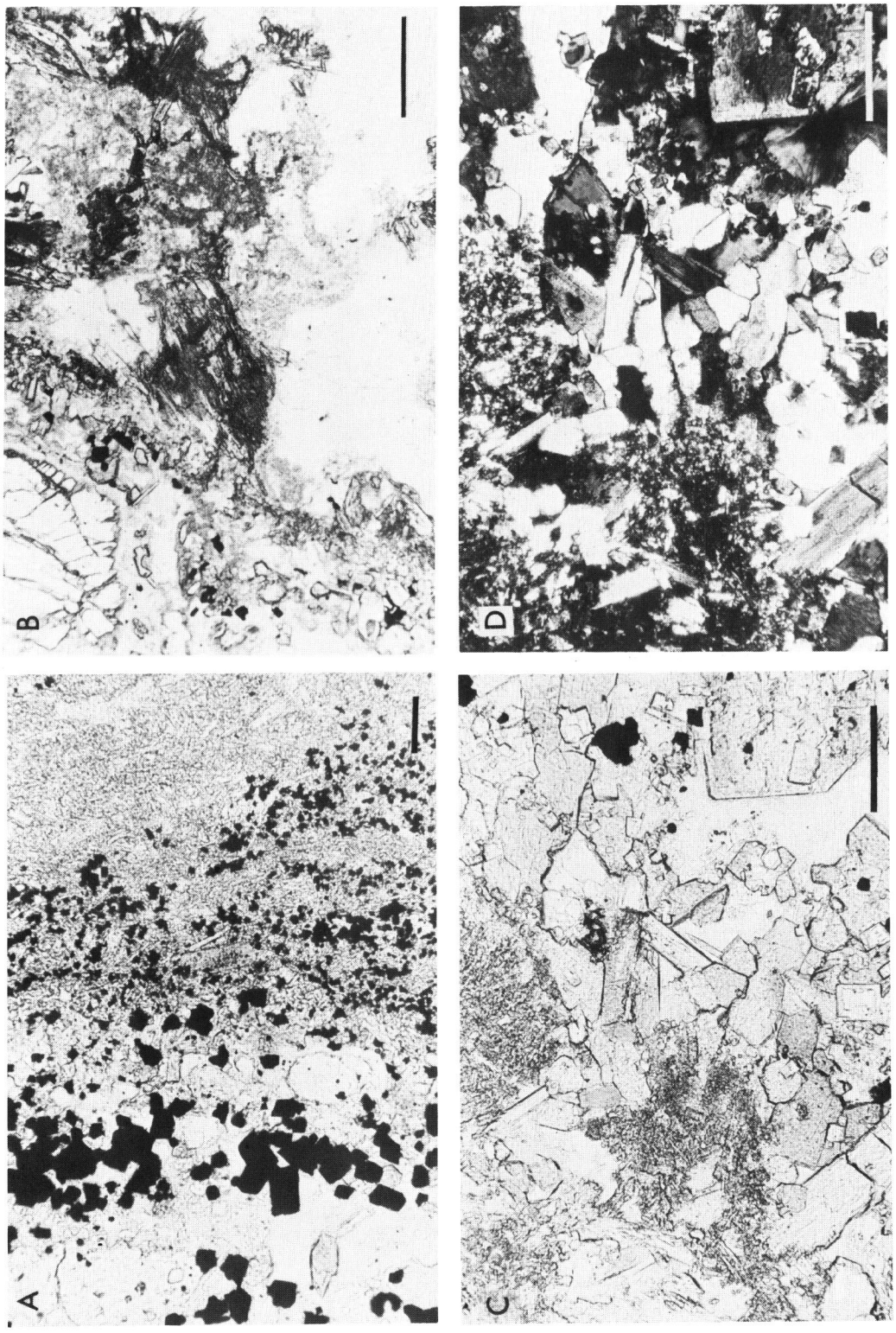

PLATE VI.

Microphotographs of reaction zone and a fine-grained melanocratic xenolith in YA-17-kimberlite from Nyanza, western Kenya.

A. Large radiated aggregate of natrolite in reaction zone of a melanocratic xenolith, YA17-22-10(178.5 m). One nicol. Scale bar is equal to 0.1 mm.
Euhedral to subhedral diopside grains together with prismatic dioside are found. Extremely fine acicular crystals grown on the diopside are pectolite (left lower).

B. ditto. Crossed nicols.

C. Aphyric texture of a fine-grained melanocratic xenolith, YA17-23-3(190.6 m). One nicol. Scale bar is equal to 0.04 mm.
Large prismatic feldspar-like minerals are matted in feathered aggregates of colourless amphibole, associated with micaceous matter, natrolite, carbonate, diopside and opaque mineral.

D. ditto. Crossed nicols.
Long prismatic feldspar-like minerals are composed of finely radiated aggregates of natrolite and/or thomsonite (indicated by two arrows).

PLATE VI

PLATE VII.

Microphotographs of two fine-grained melanocratic xenoliths in YA17-kimberlite from Nyanza, western Kenya.

A. Feldspar-like laths showing aphyric texture. YA17·22-10(178.5 m). One nicol. Scale bar is equal to 0.1 mm. The matrix is composed of natrolite and/or thomsonite, diopside, opaque mineral, pectolite and micaceous mineral. Pectolite is very finely radiated aggregate (right lower and left centre).

B. ditto. Crossed nicols.

C. Arenite-like texture. YA17·23-5(185.8 m). One nicol. Scale bar is equal to 0.1 mm.
Anhedral mineral "grains" of natrolite are surrounded by interstitial brownish micaceous matter, opaque mineral, clinozoisitic epidote, apatite and sphene.

D. ditto. Crossed nicols.
Every "grains" are composed of aggregates of natrolite, associated with small amounts of very pale green amphibole, clinozoisitic epidote and sphene. A large "grain" (centre) shows somewhat different texture from the other "grains".

PLATE VII

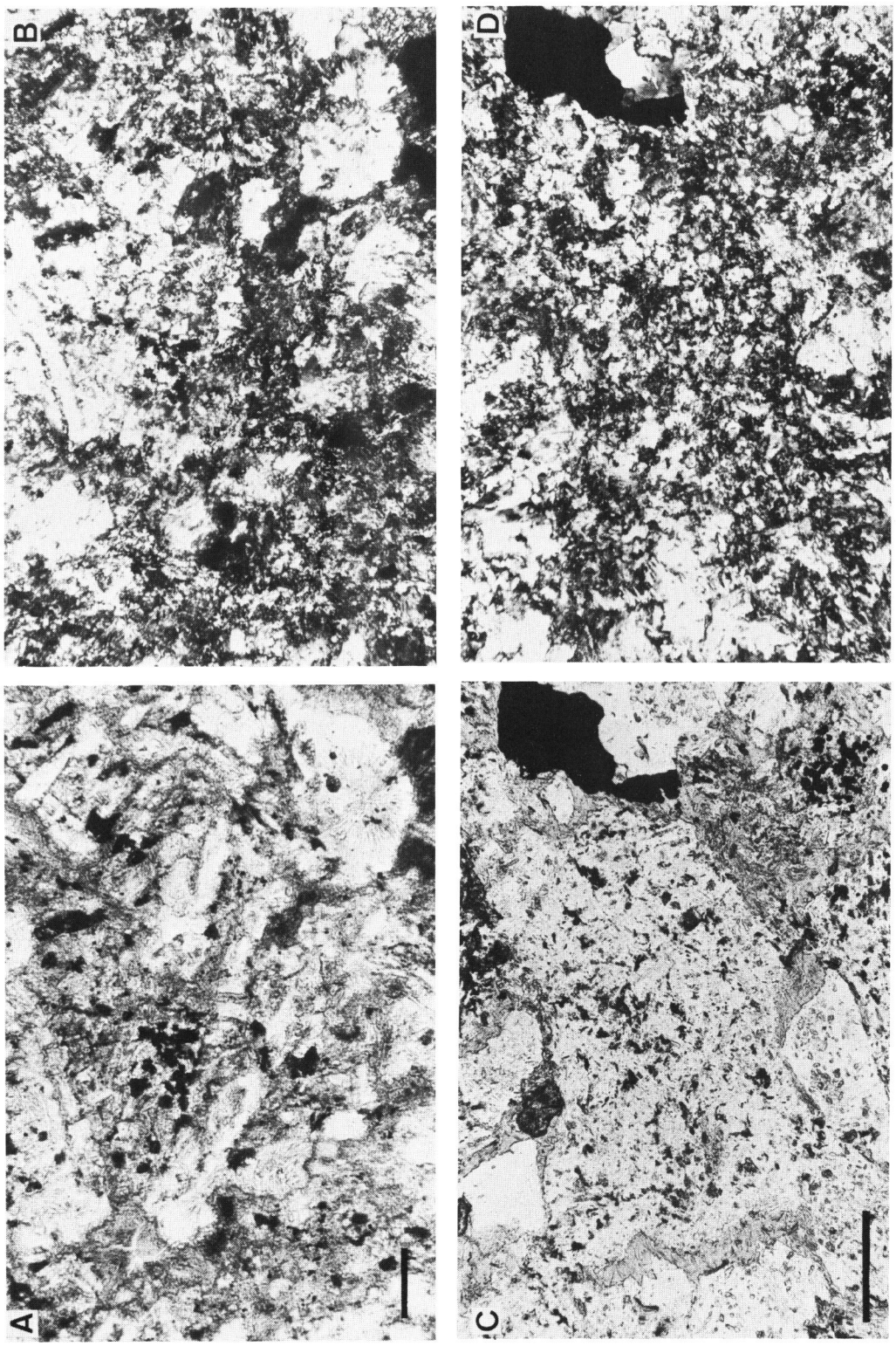

PLATE VIII.

Microphotographs of medium-grained "gabbroic" xenolith and the constituent minerals, in YA17-kimberlite from Nyanza, western Kenya.

A. Hypabyssal rock-like texture. YA17-22-10(178.5 m). One nicol. Scale bar is equal to 0.2 mm.
Phenocrystic amphibole and the matrix of natrolite and/or thomsonite, brownish micaceous mineral, sphene, pectolite, fibrous amphibole and diopside.

B. ditto. Crossed nicols.
All of phenocrystic amphibole are alterd to aggregates of colourless amphibole and diopside, associated with relic cores of dull brownish green hornblende.

C. Cancrinite-rich druse in a fine-grained melanocratic xenolith. YA17-21-16 (167.3 m). One nicol. Scale bar is equal to 0.03 mm.
Cancrinite shows euhedral or subhedral shape, associated with interstitial natrolite and/or thomsonite (centre) and diopside (right centre).

D. Sodalite in a "gabbroic" xenolith. YA17-20-17(166.5 m). One nicol. Scale bar is equal to 0.02 mm.
Sodalite is extremely fine-grained showing very low refractive index (centre). Left side of the photograph is occupied by very fine-grained diopside, natrolite and clayey matter together with sodalite. The right side is mainly occupied by natrolite, colourless mica and clayey matter. Very fine prismatic grains (upper right) are diopside.

PLATE VIII

PLATE IX.

Microphotographs of druse in YA17-kimberlite from Nyanza, western Kenya.

A. YA17-19-22(153.0 m). One nicol. Scale bar is equal to 0.5 mm.
Thomsonite (white)-carbonate (grey) druse rimmed by diopside, opaque mineral and carbonate.

B. ditto. Crossed nicols.
Thomsonite is radiating fibrous aggregate showing negative elongation. It is noted that all aggregates are accompanied by isotropic fringe on their tops.

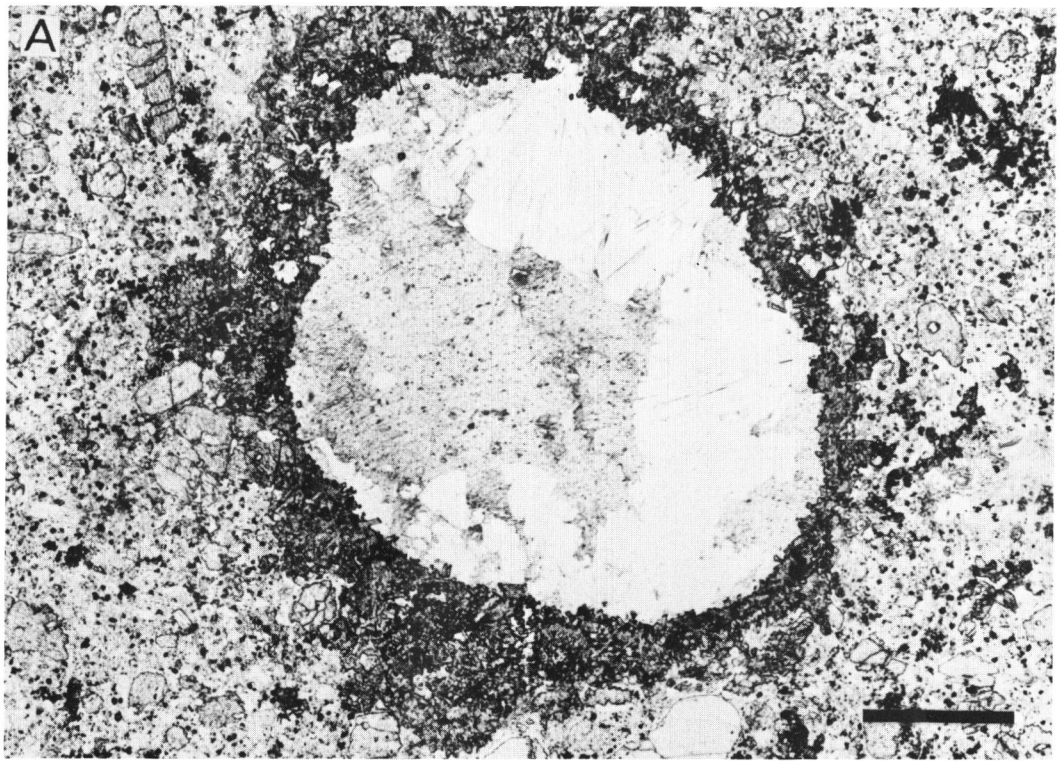
A


B

The origin of pseudoconglomerate in the Rufunsa quartzites of the Kibaran metamorphic belt, Zambia

Hayao UMEMURA* and Kanenori SUWA**

* Department of Geology, Faculty of Science, Kochi University
** Department of Earth Sciences, Faculty of Science, Nagoya University

Abstract

Various types of pseudoconglomerates (all the "pebbles" consist of quartzite) have been observed in a matrix of muscovite-quartz schist around Rufunsa, Zambia. Investigation of these pseudoconglomerates was undertaken from the aspect of their occurrence, the geometrical relationship between the strain properties and some elementary structures and the orientation of c-axes of quartz within the pseudoconglomerates. Investigation results confirmed the involvement of various development stages and deformation styles in the development of pseudoconglomerates and revealed these pseudoconglomerates to be the product of polydeformation phases. Taking all the deformation properties into consideration, the pseudoconglomerates seem to have occurred as a result of various mechanical phenomena such as mainly conspicuous extension (double boudinage) along the bedding, shearing (rodding accompanied with poly-shear planes) and transposition or rotation along the axial plane of folds.

Introduction

Investigation of deformed conglomerates immensely contributes to obtain correct understanding of the transitionary processes of deformation and the strain behaviors or strain intensity during deformation (Whitten, 1966; Ramsay, 1967; Hobbs et al., 1976). In view of this, the origin of pseudoconglomerates frequently seen in a complicated metamorphic belt is regarded as one of the important subjects in geology. It has often been discussed whether they are the deformed morphology of the original conglomerate or resulted from tectonical conglomeration of a stratified layer or rock body.

Rufunsa district where pseudoconglomerates are observed with the presence of complicatedly deformed metamorphic rocks is a region known to have been formed by superimposition of Kibaran orogeny and Lufilian orogeny (Simpson, 1967, Fig. 1).

Pseudoconglomerates which represent a series of rock structures show various aspects by appearance and are developed in the alternation of quartzite and pelitic schists. The origin of these lenticular quartzites has been proposed by two extremely opposed concepts, one regarding the origin as tectonically sheared quartzites and

8th Prelim. Rept. Afr. Studies, Nagoya Univ., 205-215, 1983.

other as deformed pebbles themselves (Simpson, 1967; Mr. J.J. Kaper, personal communication). Both of them, however, failed to provide systematic explication of the multifarious deformation pattern of quartzite in question.

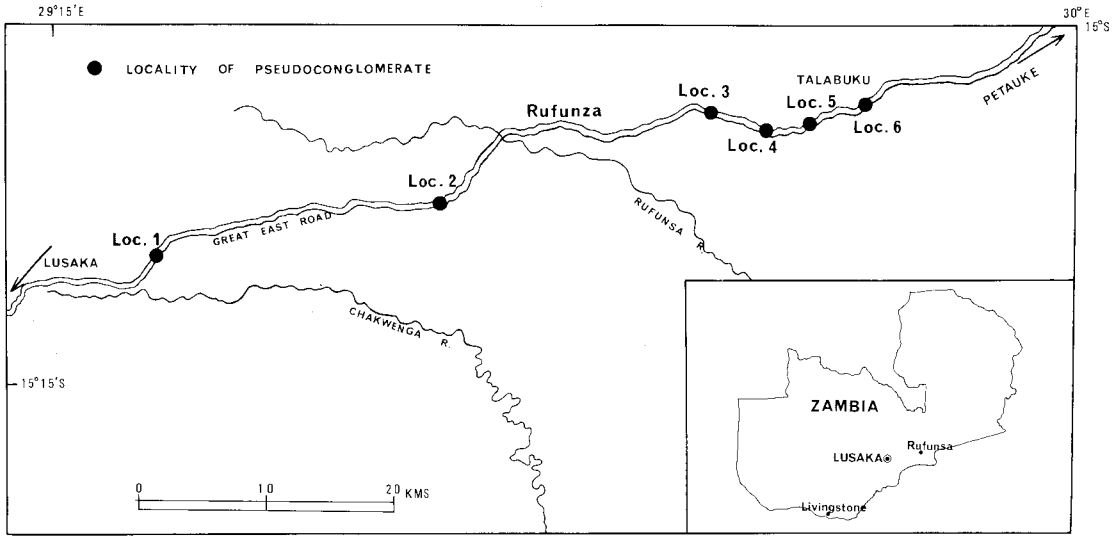

Fig. 1 Localities of pseudoconglomerate in the Rufunsa area.

This paper describes some occurrence (the deformation state of quartzites) of pseudoconglomerates surveyed on the field and the geometrical relation between these pseudoconglomerates and some elementary structures (folds, lineation and foliation), on the basis of which assumption of the genetic factors of pseudoconglomerates is attempted with special reference to double boudinage and rodding. In addition, the measurement results of the c-axes of quarts within the pseudoconglomerate are briefly reported in comparison with the fabric in the c-axes of quartz within the boudinage published elsewhere.

Geological setting

Metamorphic rocks of the Kibaran orogenic belt are exposed along the Great East Road on the site of the survey performed. The metamorphic rocks of Rufunsa area are composed of mainly quartzite and pelitic schist. Representative mineral assemblage in the pelitic schist is quartz-feldspar-muscovite-biotite. Sometimes, muscovite pseudomorph after fibrolite, and chloritized biotite can be observed. Hitherto, it has been accepted that the amphibolite facies metamorphism prevailed at the Kibaran orogenic stage in this area and after that, they were retrogressively metamorphosed, possibly at the Lufilian orogenic stage.

These metamorphic rocks generally run in almost E-W direction (Fig.2). However,

considerably abrupt deviation of their plunge into the northern or southern direction may indicate that the main geologic structure of this area is controlled by complicated folding. Though the stratigraphy of metamorphic rocks is hardly known, it may be roughly estimated that the pseudoconglomerates under study seem to have developed in the same horizon.

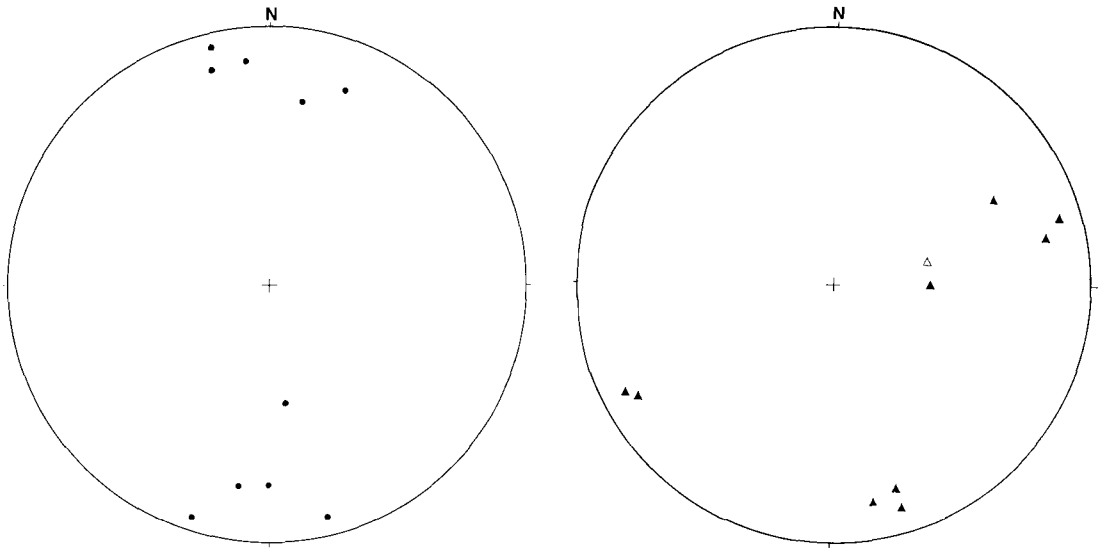

Fig. 2 Diagram showing orientation data of schistosity (●), mineral lineation (▲) and boudin line (△) in the Kibaran metamorphic rocks of the Rufunsa area.

As already described, this area was subjected twice to remarkable orogenic movements, resulting in the penetrative formation of a number of minor structures. On the basis of these geologic features represented by superimposition and oblique intersection, the deformation phase was divided at least into four phases (D_0, D_1, D_2 and D_3).

D_0: the first phase of deformation is characterized by the formation of isoclinal folds (pre-Kibaran orogeny, sedimentary phase?).

D_1: the second phase of deformation is most conspicuous over the whole area, forming folds that plunge by 30°–80° in the E or ESE direction. A marked mineral lineation is noted in the axial trend of folds (Kibaran orogeny).

D_2: the third phase of deformation is characterized by the formation of microfolds with prominent crenulation cleavage. The axes of folds face in approximately N-S direction at the right angle to the trend of D_1-folds (Lufilian orogeny).

D_3: the final phase of deformation is related to fault movement accompanied with the development of brecciation and fragmentation.

Occurrence and deformation properties of pseudoconglomerate

Pseudoconglomerates of various shapes existed in a number of outcrops along the Great East Road, as shown in plates I-VIII. Considerable scattering of deformation intensity was evident at a glance and hence the involvement of multiple deformation mechanisms was suggested, because single phasic deformation can never be expected to cause such diversified deformities. As if supporting the above, a complicated geometrical relationship existed between the morphology of the pseudoconglomerates and mineral lineation of each deformation phase. The authors intend to use the data of strain properties as a clue for explication on the origin of the pseudoconglomerates.

The pseudoconglomerates morphology can be divided mainly into the lenticular type and brecciated type. The strain features are as follows.

(1) Lenticular type

(a) the type which is irregular in size and closely resembles a deformed conglomerate (Plate I-1).

(b) the type that elongates in a rod shape in the direction of D_1-lineation. The profile normal to the elongation is similar to a deformed conglomerate (Plate I-2).

(c) the type that most frequently occurs with a lenticular effect on any profile (Plate II-1). Though very closely resembling a deformed conglomerate in morphology, there is a necking giving an impression as if the quartzite layer could be reconstructed. In this type, D_1-lineation is frequently found to fit in harmony with the morphology of pseudoconglomerate.

(d) the type showing conspicuous elongation in a specific direction (Plate II-2). There is a necking with D_1-lineation parallel to its long axis. Like type (c), the pseudoconglomerate is frequently enclosed by anastomosing shear planes, suggesting the occurrence of transposition during the pseudoconglomerate formation.

(e) this type is basically the same as type (d). However, deformation is mild and a bedding plane is faintly discernible (Plate III-1).

(f) this is a fractured type of type (e). Fragmentation is noted (Plate III-2).

(g) this type is characterized by a boudinage-like pinch-and-swell structure and partial lenticulation. Note perfect preservation, though partly, of the bedding plane.

(h) extremely incomplete pseudoconglomerate with a weak rodding structure. However, the bedding plane is preserved as a whole (Plate IV-2).

As enumerated above, the pseudoconglomerates were divided morphologically into eight types. The relative intensity of deformation appears to grow larger from (a) to (h). Namely, between the two extremities of complete preservation and complete destruction of the bedding plane, there seem to exist the pseudoconglomerates of various phases. This precisely indicates that these pseudoconglomerates are not mere deformed conglomerates. These types seem to be irregularly distributed. Depending on the scale of an outcrop, some of the pseudoconglomerates show gradual shift in type but more frequently incur sudden changes in the deformation in-

tensity. These general structural appearances seem to imply the occurrence of concentrated inhomogeneous stress on the Rufunsa quartzite horizons. The formation stage of these pseudoconglomerates is explained in the next section.

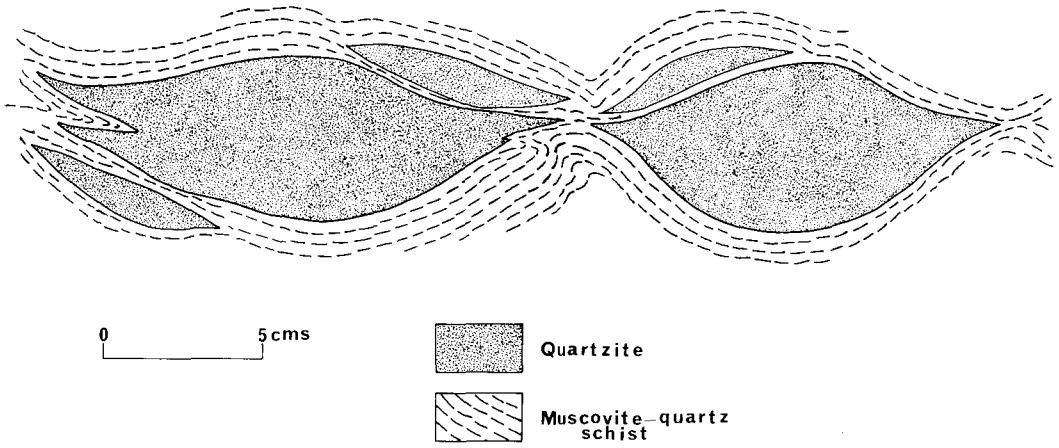

Fig. 3 Sketch of asymmetrical scar fold (resulted from necking) on flanks of boudins. Loc. 2.

(2) Brecciated type

(a) so-called tectonic lens formed by conspicuous shearing (Plate IV-1).

(b) the type that shows both the compression (fracture) and elongation features with an evidence of slight plastic deformation (Plate V-2, VI-1 and VI-2).

(c) the type that closely resembles a fault-induced breccia (Plate VII-1). There is no evidence of plastic deformation.

The pseudoconglomerates of this type are geometrically free from mineral lineations. Generally, mineral lineation is dislocated as a result of brecciation. The shape suggests that these pseudoconglomerates occurred from the deformation process in a relatively low-temperature condition.

Lastly, regardless of the shape of pseudoconglomerates, the most noteworthy finding that demonstrates the origin of pseudoconglomerates is presented. As seen in Plate VIII-1 and 2, the most typical pseudoconglomerates (similar to type (1)-c) are formed by transposition of a quartzite layer along the cleavage parallel to the axial plane of folds and injection of a pelitic schist along the cleavage into a quartzite layer (Fig. 4). This evidence showing the pseudoconglomerate formation by such folding may be decisively important in determining the origin of the pseudoconglomerates of the previously described (1) group.

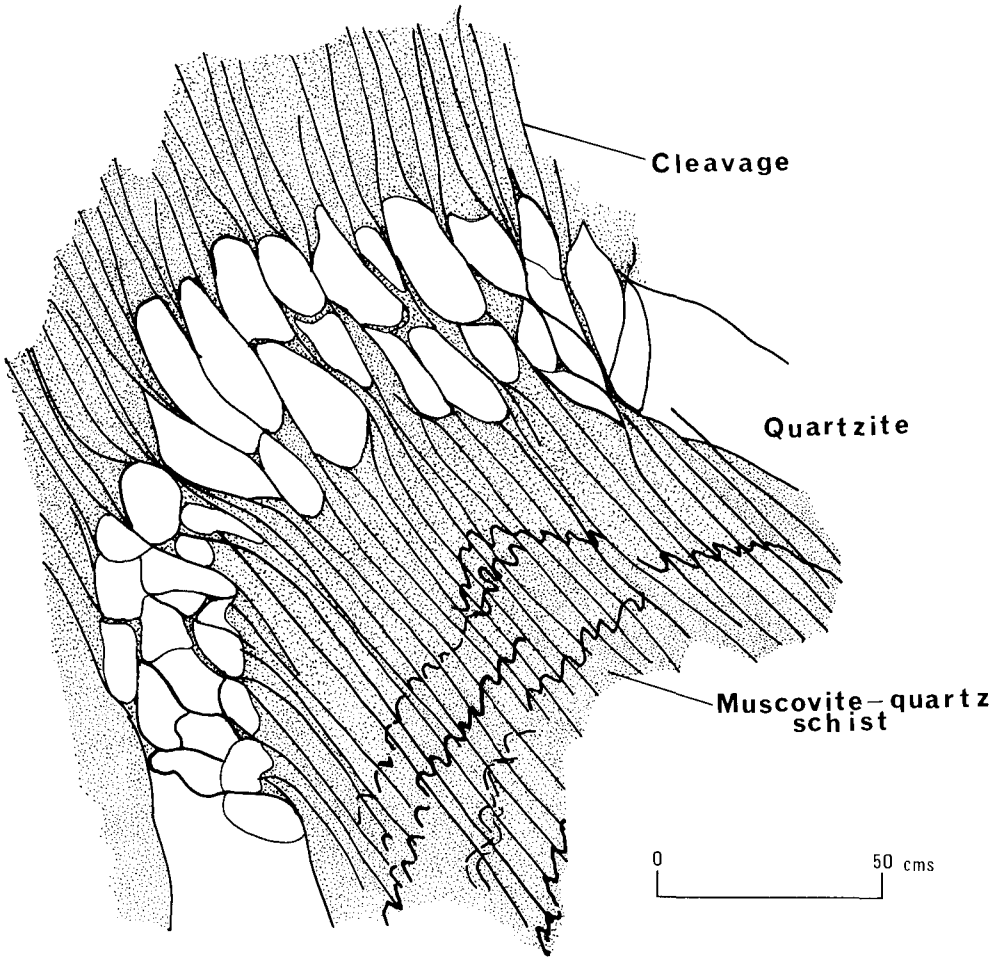

Fig. 4 Displaced, brecciated and fractured quartzite along axial plane cleavage of the D_1-folds. Note the main role of cleavage acting as tectonic knife (Lebedeva, 1979).

Orientation of quartz c-axes in pseudoconglomerates

To assess a part of deformation properties, quartz c-axis orientations were measured optically from thin sections perpendicular to prominent neck line (XZ plane of strain ellipsoid) using a universal stage; 200 grains were measured from different areas of the pseudoconglomerate (Fig. 5). On the occasion of measurement a specimen that closely resembled boudinage because of clear necking was used. The specimen is composed of coarse-grained (0.1 – 0.8 mm) recrystallized quartz with virtually no micas or impurity phases.

In boundinage caused by elongation of a competent layer, the fabrics in quartz c-axes are usually uniform within the boudinage (Sen and Mukherjee, 1975), having the maximum point in the direction of intermediate axis of the strain ellipsoid to

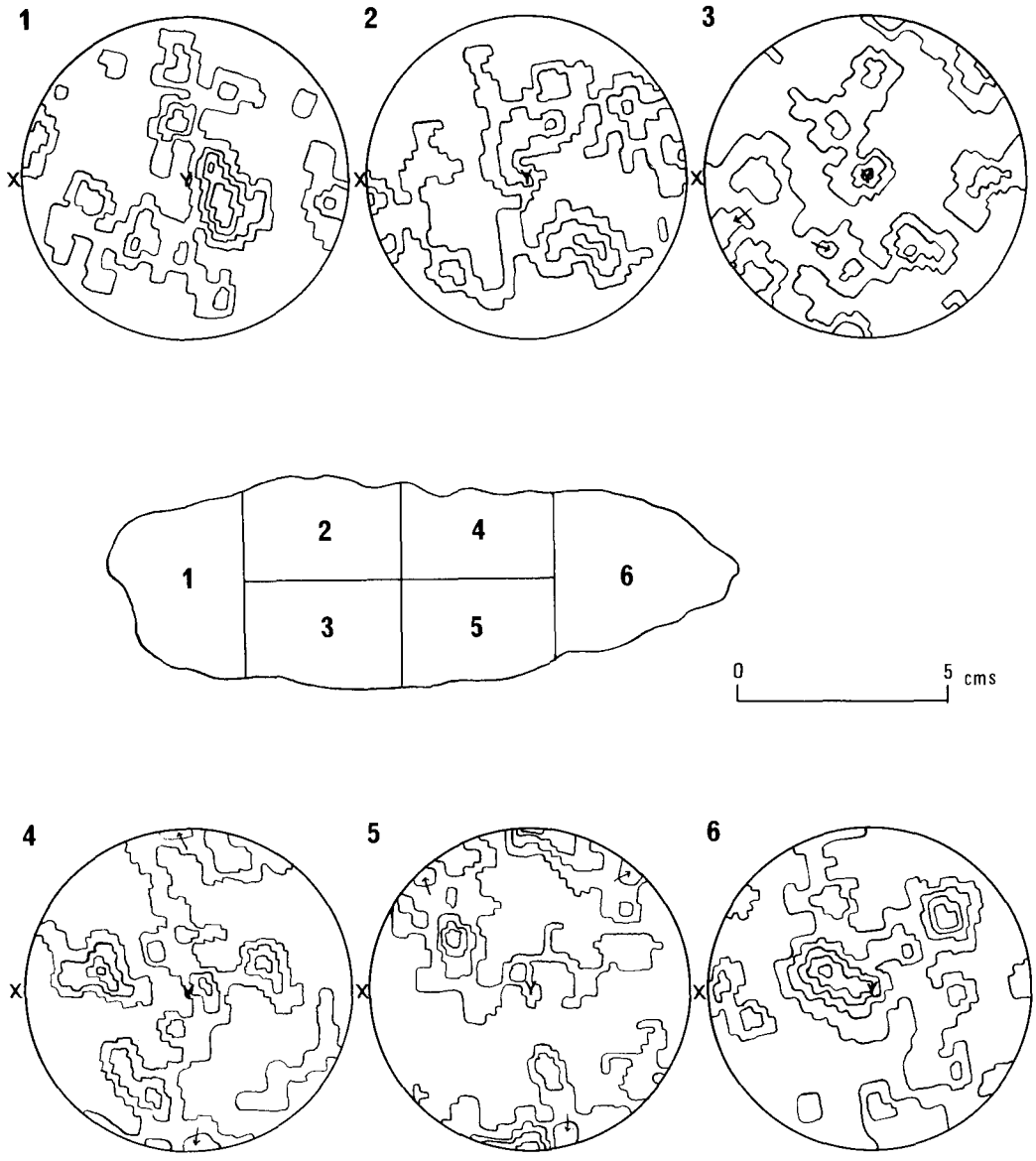

Fig. 5 Petrofabric diagrams from different positions within the lenticular pseudoconglomerate (type 1-c). 200 c-axes of quartz plotted in each case. X (// mineral lineation) and Y (// neck line): the principal axes of strain. Contours (1, 2, 4, 5 and 6): 1–3–5–7%. Contours (3): 1–3–5%.

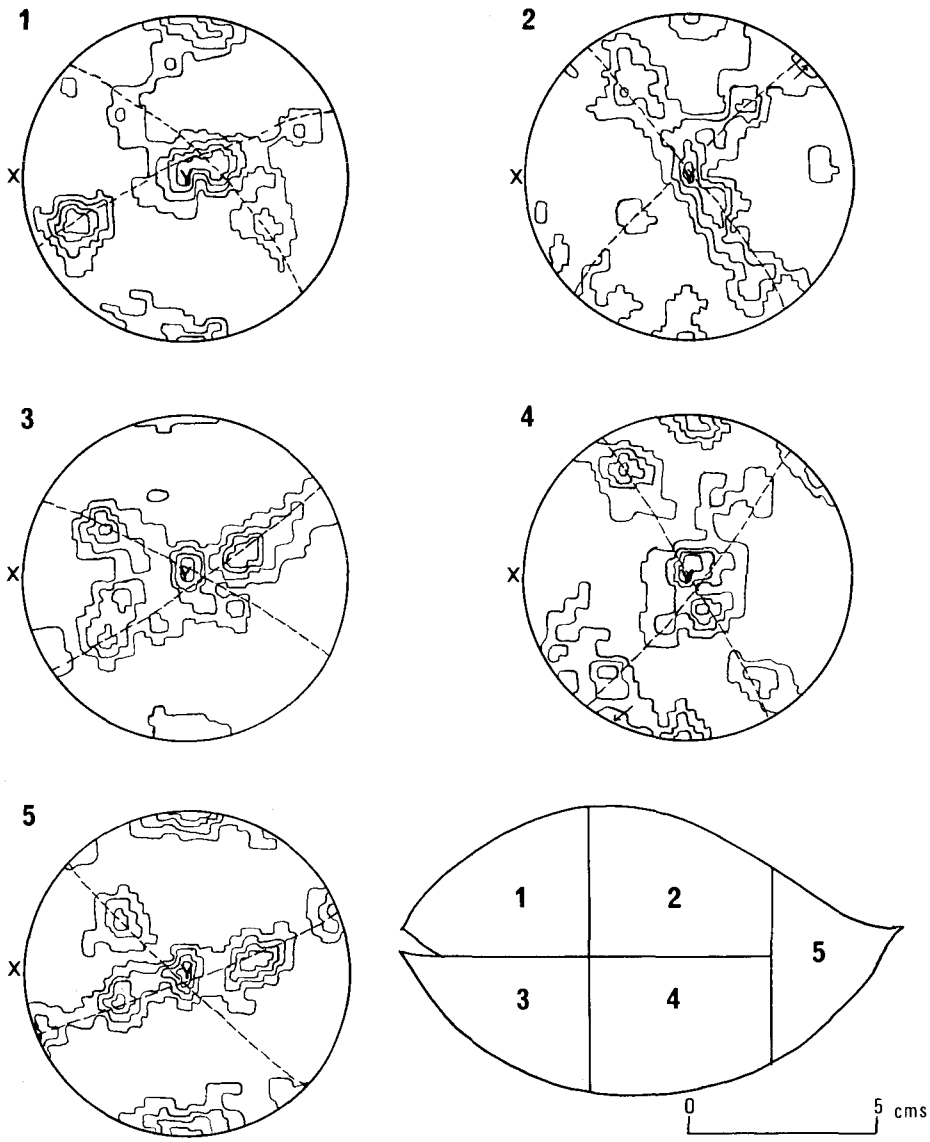

Fig. 6 Petrofabric diagrams from different positions of the boudin in siliceous gneiss of the Takanuki series, Abukuma plateau, northeast Japan. 100 c-axes of quartz plotted in each case. X (// mineral lineation) and Y (// neck line): the principal axes of strain. Contours: 1–3–5–7%.

draw a cross-girdle (Sylvester and Christie, 1968). The similar quartz fabrics were confirmed by the senior author on the boudinage of siliceous gneiss in the Abukuma metamorphic belt, northeast Japan (Fig. 6).

As shown in Fig. 5, the quartz orientation in the pseudoconglomerate gave no evidence of a cross-girdle nor noticeable preferred orientation. Though detailed analysis of a fabric diagram may deviate from the purpose of this paper, intercorrelation is not noted between the strain picture and fabric pattern in the pseudoconglomerate. This seems attributable to complexly deformed double boudinage that characterizes the specimen and the history of deformation that occurred at least four times in this area. At the same time it may as well be presumable that the quartz fabric grown at the time of pseudoconglomeration may have undergone modification or elimination as a result of later deformation and recrystallization. The analysis of c-axes of quartz indispensably need detailed investigations of not only the strain but also c-axes in the host rock as well as surrounding metamorphic rocks containing a fabric of each deformation phase.

Origin of pseudoconglomerate

From the afore-mentioned characteristics of the pseudoconglomerates such as the strain property, structural appearance and c-axis orientation of the quartz in the pseudoconglomerates, it may be self-evident that these pseudoconglomerates were formed at least by deformation of stratified quartzite and by undergoing multiple deformation phases. Emphasis is placed on the following findings to support our concept on the principal mechanism and stage of pseudoconglomerate formation.

(1) The rock type of pebbles is limited to a quartzite.

(2) Co-existence of pseudoconglomerate with various deformation features in the same outcrop.

(3) Transformation of a quartzite preserving the stratified sequence into a highly deformed lenticular quartzite.

(4) Development of double boudinage (Sanderson, 1974)—Necking* in all directions. Some mineral lineations related to the D_1-deformation are morphologically dominated by boudinage, and some of the boudinage are chained together (Plate VII-2). These findings serve as a sufficient evidence of double boudinage.

(5) Prominent elongation and fragmentation resulting from the formation of poly-shear planes—rodding of the quartzite layer.

(6) The formation of pseudoconglomerates by transposition of a quartzite layer along the cleavage parallel to the axial plane of the D_1-folds (Fig. 4).

(7) The pseudoconglomerate strain is most frequently harmonized with the D_1-lineation. The neck line of boudinage developed in the amphibolite of approximate-

*Remarkable quartzite necking reflects conspicuous deformation due to elongation and shearing in a high-temperature metamorphic condition.

ly the same horizon also fits in harmony with the D_1-lineation.

The foregoing may indicate that the skeletal structure formation of pseudoconglomerates resulted from elongation of the bedding in every direction (formation of double boudinage) or strong shearing and rotation along the bedding plane (formation of rodding) due to compressional stress nearly perpendicular to the bedding in a high-temperature condition. In respect to the time of pseudoconglomerate formation, judging from the geometrical relation between the morphology of the pseudoconglomerates and mineral lineation, the D_1-phase might have played a primary role. However, in the presence of superimposition of the D_2-folds on the pseudoconglomerates and brecciated pseudoconglomerates, deformation by compression in the D_2-deformation phase or brecciation in the D_3-deformation phase must have undoubtedly contributed to the development of multi-shaped boudinage. In other words, the Rufunsa area, consistently since the Kibaran orogeny, remained a tectonic and shearing field and incurred a characteristic inhomogeneous strain.

Acknowledgements – The present authors express their sincere thanks to Hon. Mufaya Mumbuna, Minister of Mines, Mr. J.L. Masaninga, Permanent Secretary, Mr. W.C. Fairbairn, Chief Mining Engineer, and Mr. M.D. Kamono of the Ministry of Mines, Zambia; to Mr. N.J. Money, Deputy Director of Zambia Geological Survey Department; to His Excellency the Ambassador E. Seki of the Embassy of Japan in Zambia; to Messrs. T. Ohashi and T. Taguchi of the Marubeni Co. Lusaka office; to Messrs. I. Yamamoto and J. Fujimoto of Power Reactor and Nuclear Fuel Development Corporation (PNC) Lusaka office for the most esteemed and invaluable assistance.

The present authors are very grateful to Dr. T. Yanagi and Messrs. K. Tokieda, M. Asami and M. Hoshino for their laborious collaboration in the field survey in 1981.

The field work was made possible by the Grant-in-Aid for Overseas Scientific Survey from the Ministry of Education, Science and Culture, Japan, to which they express their thanks.

REFERENCES

BORRADAILE, G.J., BAYLY, M.B. and POWELL, C.M.(1982): *Atlas of deformational and metamorphic rock fabrics.* Springer-Verlag, 551 p.

GARRARD, P.(1968): The geology of the Chainama hills area: *Explanation of Degree Sheet 1528, NE. Quarter. Rep. geol. Surv. Zambia,* **24**.

HOBBS, B.E., MEANS, W.D. and WILLIAMS, P.F.(1976): *An outline of structural geology.* John Wiley & Sons, Inc. 571 p.

KRONENBERG, A.(1981): Quartz preferred orientations within a deformed pebble conglomerate from New Hampshire, U.S.A. *Tectonophysics,* **79**, T7-T15.

LEVEDEVA, N.B.(1979): Significance of mechanical hetrogeneities of rocks for formation of flow cleavage. *Tectonophysics,* **54**, 61-79.

MIYATA, T. and SAKA, Y.(1981): Boudinage structures in the Mozambiquian metamorphic

rocks, south of Machakos, Kenya. *6th Prelim. Report Afr. Studies, Nagoya Univ.,* 73-82.

RAMSAY, J.G.(1967): *Folding and fracturing of rocks.* McGraw-Hill, New York, 568 p.

SANDERSON, D.J.(1974): Patterns of boudinage and apparent stretching lineation developed in folded rocks. *Jour. Geol.,* **82**, 651-661.

SEN, R. and MUKHERJEE, A.D. (1975): Comparison of experimental and natural boudinage. *Geol Mag.,* **112** (2), 191-196.

SIMPSON, J.G.(1967): The geology of the Chinyunu area: *Explanation of Degree Sheet 1529, NW. Quarter. Rep. geol. Surv. Zambia,* **19**.

STROMGARD, K.E.(1973): Stress distribution during formation of boudinage and pressure shadows. *Tectonophysics,* **16**, 215-248.

SUWA, K., YANAGI, T., TOKIEDA, K., UMEMURA, H., HOSHINO, M. and ASAMI, M.(1981): Geological research in Zambia, Nagoya University African Geological Research Project (1981). Report to Hon. Mufaya Mumbuna (Minister, Ministry of Mines, Zambia)-MS-

SYLVESTER, A.G. and CHRISTIE, J.M.(1968): The origin of crossed-girdle orientation of optic axes in deformed quartzite. *Jour. Geol.,* **76**, 571-580.

UMEMURA, H.(1973): Origin of the boudin structures in the Gosaisho-Takanuki metamorphic rocks (in Japanese with English abstract). *Res. Rep. Kochi Univ.,* **22**, 209-227.

UMEMURA, H. (1976): Structural level of the Gosaisho-Takanuki metamorphic rocks in the Abukuma plateau (in Japanese). *Jubilee. Publ. Commem. Prof. G. KOJIMA's 60th Birth.,* 172-182.

WEISS, L.E.(1972): *The minor structures of deformed rocks.* Springer-Verlag, 431 p.

WHITTEN, E.H.T.(1966): *Structural geology of folded rocks.* Rand McNally Co., Chicago, 663 p.

WILSON, G.(1953): Mullion and rodding structure in the Moine Series of Scotland. *Proc. Geol. Ass.,* **64**, 118-141.

PLATE I

1. Strongly flattened pseudoconglomerates bear a close resemblance to deformed pebble conglomerate. Loc. 2.

2. Strong elongation (rodding) of quartzite layers observed on exposure surface parallel to a regional lineation. Loc. 2.

PLATE I

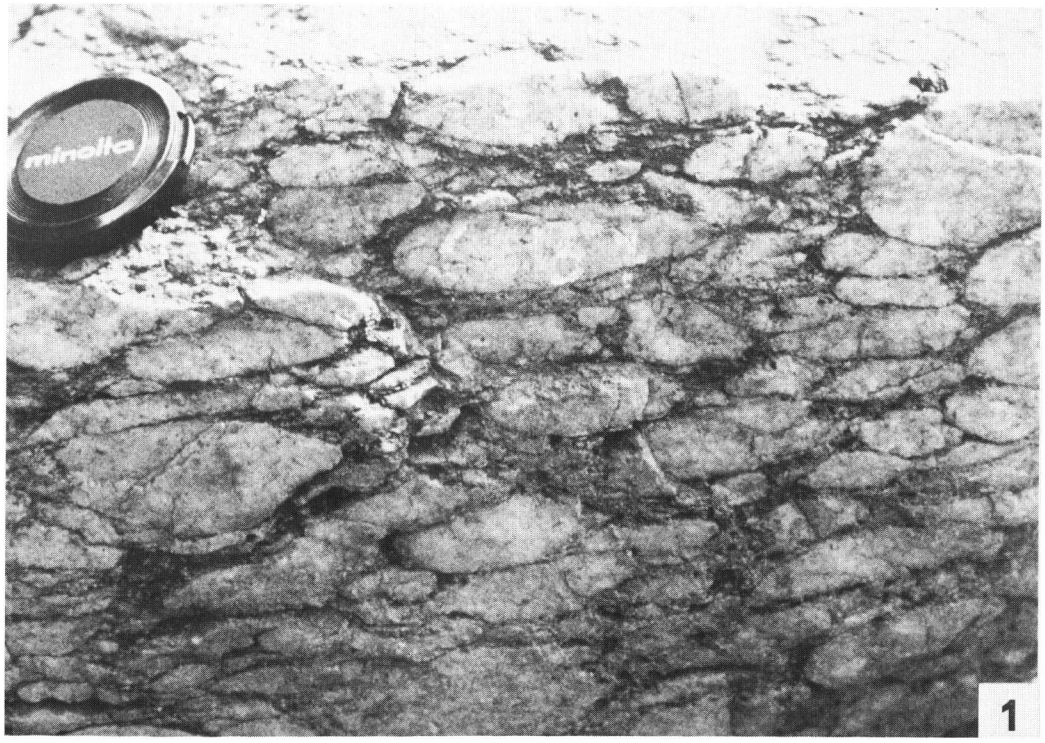

1

2

PLATE II

1. Typical pseudoconglomerates that occur widely and frequently in the Rufunsa area. Muscovite-quartz schist enclosing them is intensely sheared. Loc. 2.

2. Deformed quartzite layers produce rod-shaped or lenticular pseudoconglomerates elongated in the direction of a regional lineation. Loc. 2.

PLATE II

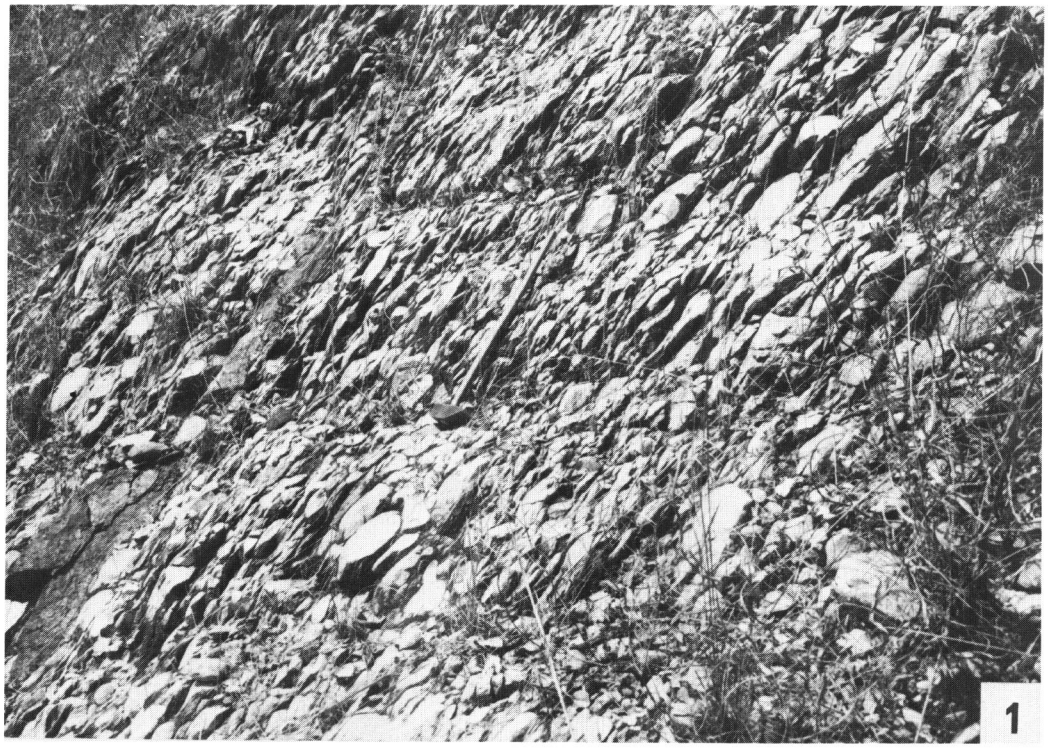

PLATE III

1. Moderately boudinaged and rodded quartzite layers. A later fracture is developed. Loc. 4.

2. Moderately elongated and sheared quartzite layers—typical rod-shaped pseudoconglomerates elongated in the direction of a regional lineation. Note the feeble preservation of their bedding planes. Loc. 4.

PLATE III

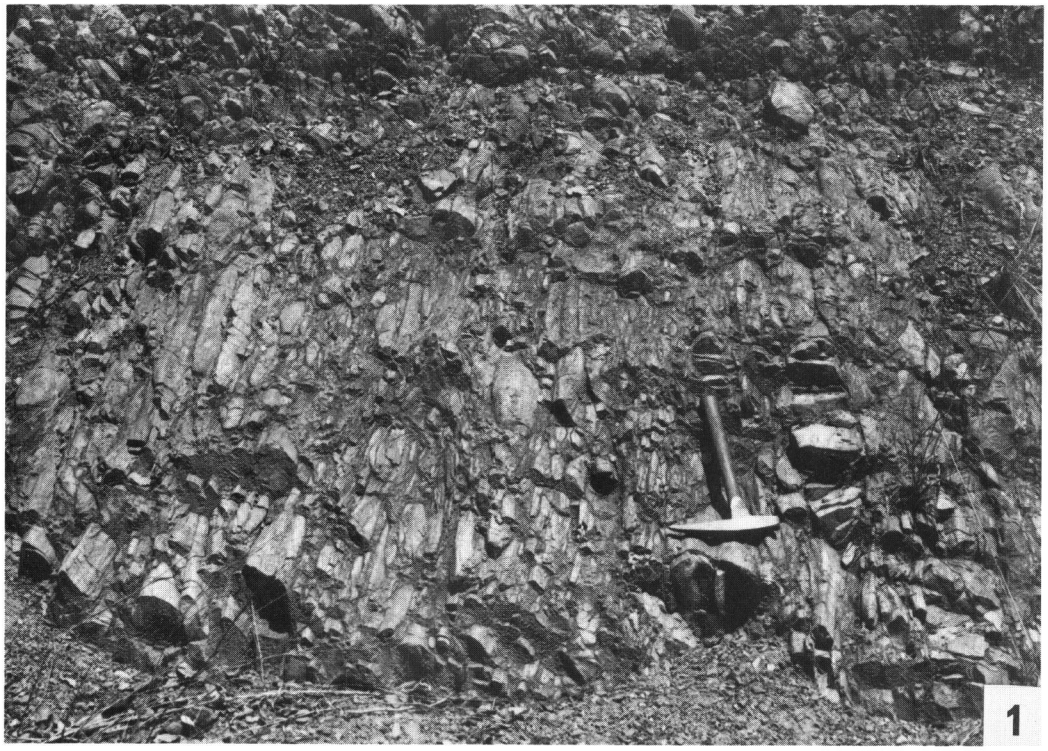

1

2

PLATE IV

1. Slightly elongated and boudinaged quartzite layers. Note that the bedding plane is discernible. Loc. 3.

2. Slightly boudinaged quartzite layers. Note the perfect preservation of the bedding plane in alternating quartzite and muscovite-quartz schist. Loc. 4.

1

2

PLATE V

1. Sheared or boudinaged thin quartzite layers enclosed in thick muscovite-quartz schist. Pseudoconglomerates of this type are closely similar to so-called tectonic lens in their deformation features. Loc. 1.

2. Elongated, brecciated and mylonitized quartzite layer. Loc. 6.

PLATE V

PLATE VI

Brecciated pseudoconglomerates at shear zone. Loc. 6.

1. Note the parallel alignment of their elongation axes.

2. Note the irregular shape of brecciated pseudoconglomerates and slightly fractured feature in them.

PLATE VI

PLATE VII

1. Typically brecciated quartzite presumably resulted from cataclastic (fault) movement. Loc. 6.

2. Pseudoconglomerates resulted from double boudinage. Note that three boudins in the central part are chained together. Loc. 2.

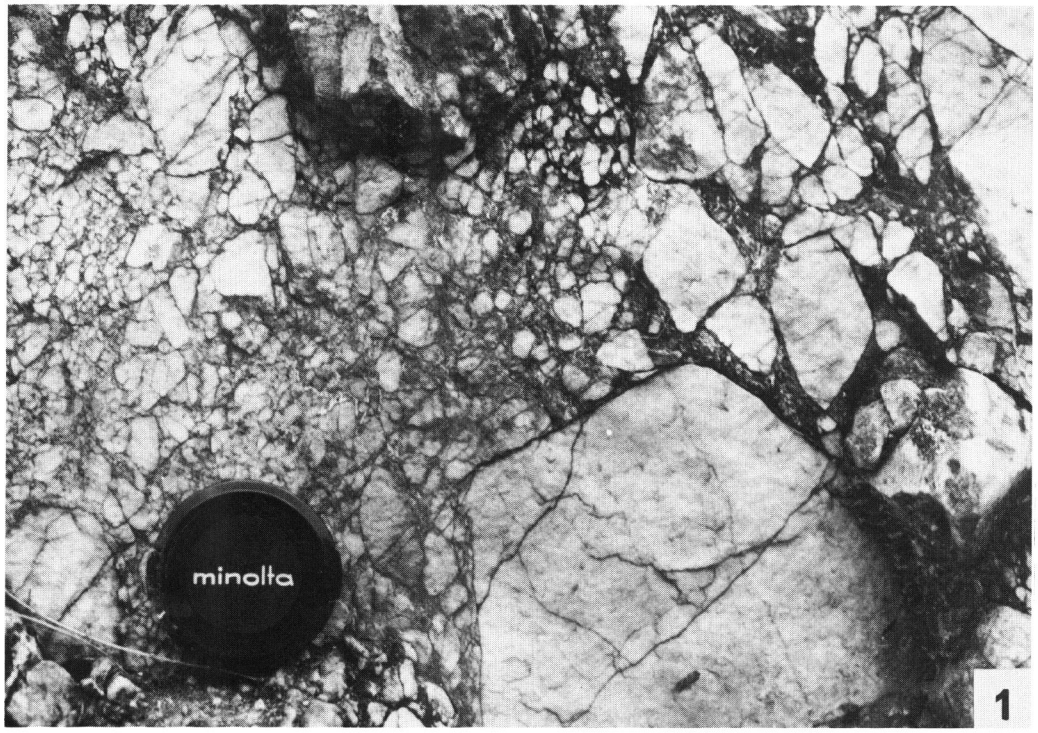
minolta
1


2

PLATE VIII

1. Fold in alternating quartzite and muscovite-quartz schist. Note the development of displaced quartzite along cleavage surface into individual boudins (pseudoconglomerate). See text-figure (Fig. 4). Loc. 5.

2. Detail of plate VIII-1. Note a close similarity in apparent features of pseudoconglomerates with those shown in Plate II-1. Loc. 5.

1

2

Remanent magnetization of the Karroo basalt at the Victoria Falls, Zambia

Katsuyasu TOKIEDA* and Kanenori SUWA**

* Department of Physics, Faculty of Science, Shimane University
** Department of Earth Sciences, Faculty of Science, Nagoya University

Abstract

Eleven specimens for paleomagnetic study were collected from one site in the Jurassic Karroo basalt lavas at the Victoria Falls, Zambia. The stable components of magnetization showed normal polarity with a mean direction of D = 337.6°, I = −53.5°, k = 172, α_{95} = 3.5°, corresponding to a paleomagnetic pole at 64.3°N, 252.6°E.

Introduction

A violent episode of Jurassic volcanism in southeastern Africa is well known as Karroo volcanism. Basaltic outpourings produced vast lava-fields which still remain as isolated patchs over large areas in southeastern Africa. The Karroo volcanism is related to a convective up-welling of the mantle materials responsible for the fragmentation of Gondwanaland (Cox, 1970). The main volcanic activity of the Karroo volcanism extended between 200 and 190 m.y., with acid volcanism continuing until 140 m.y. (Fitch and Miller, 1971). The distribution of the Karroo igneous rocks in southeastern Africa is shown in Fig. 1.

Several paleomagnetic studies have been done on the Karroo lavas and their results were compiled by Irving (1964) and McElhinny (1968, 1972). A huge body of the Karroo lavas is exposed in the Livingstone area as shown by a dashed circle in Fig. 1. The Victoria Falls are formed in the Zambesi Valley which runs through the basalt body from west to east. Nairn (1956) reported a paleomagnetic result of basalt sample taken at one site in this huge body. We collected the Karroo basalt specimens for petrologic and paleomagnetic studies at the Victoria Falls, Zambia.

Samples and measurements

Eleven oriented hand specimens were collected from one site at the top of the Victoria Falls in Zambia (17°55.3'S, 25°51.7'E). The sampling site is shown in Fig. 2. The basalt lava in the Livingstone area is a olivine-poor tholeiite (Cox, 1970). The hand specimens were purple red in colour and full of almond-shaped inclusions of white minerals. A 23mm x 23mm cyrindrical core specimen was drilled from each hand specimen in the laboratory. Measurements of remanent magnetization were made with a Shonstedt SSM-1A spinner magnetometer. All core specimens were subjected to progressive alternating field (AF) demagnetization up to 600 oersted after measurements of natural remanent magnetization (NRM).

8th Prelim. Rept. Afr. Studies, Nagoya Univ., 217-221, 1983.

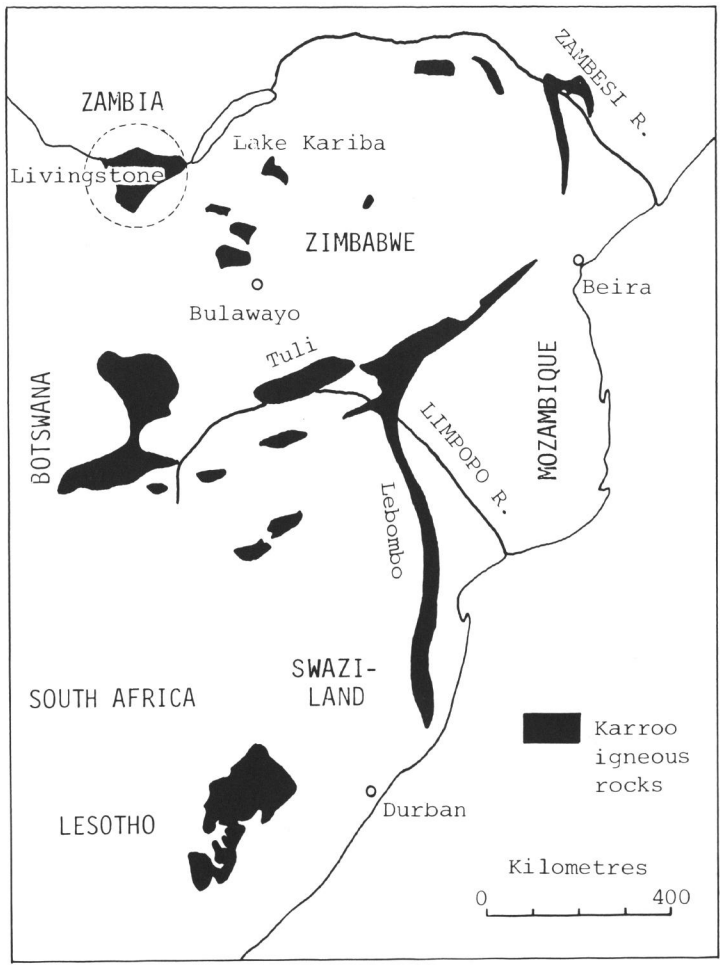

Fig. 1 Simplified geological map showing the distribution of the Mesozoic Karroo igneous rocks in southeastern Africa after Cox (1970).

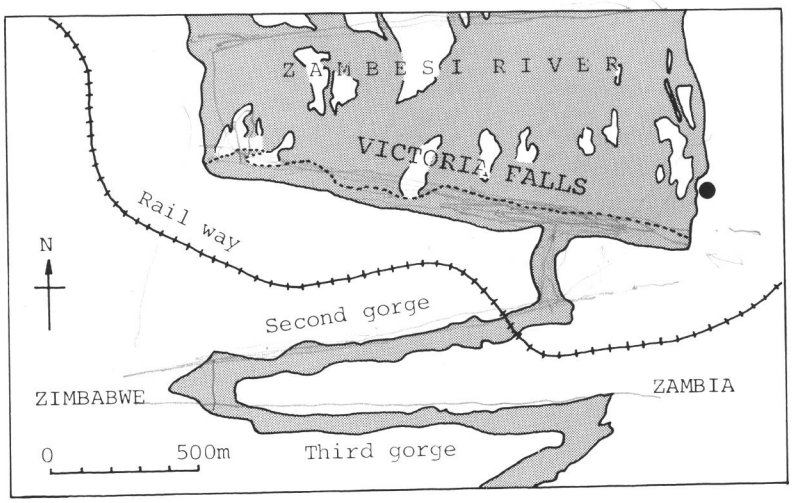

Fig. 2 Map of the Victoria Falls. Closed circle denotes sampling site.

Results

NRM directions of the core specimens are widely scattered before AF cleaning as shown in Fig. 3(a) and NRM intensities range from 1.46 to 5.19 x 10^{-4} emu/gr. After AF demagnetization of 300 oersted, directions of magnetization are observed to be well-grouped (Fig. 3(b)), and the intensities were reduced to about two thirds of the initial values.

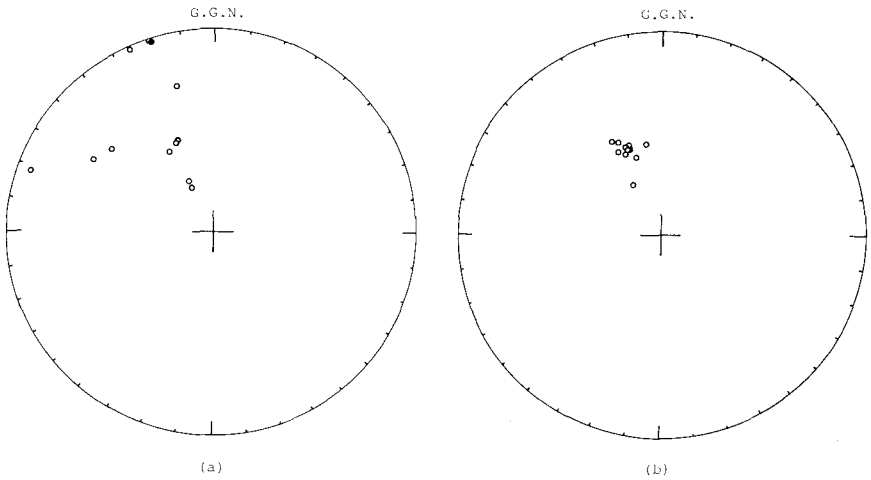

Fig. 3 NRM directions. (a) before cleaning, (b) after cleaning at alternating field of 300 oersted.

Table 1 Paleomagnetic elements derived from the Karroo basalts in southeastern Africa.

Rock unit and location	Age	Direction of magnetization				Si (Sa)	P	Paleomagnetic pole position		Reference
		D	I	k	α_{95}			Lat.	Longi.	
(1) Karroo basalt in the Livingstone area 17°55.3'S, 25°51.7'E	J1	337.6°	−53.5°	172	3.5°	1 (11)	N	64.3°N	252.6°E	This work
(2) Karroo basalt in the Livingstone area 18°S, 26°E	J1	332°	−40°	19	5°	−(−)	N	63°N	281°E	Nairn (1956)
(3) Karroo lavas Central Africa 16-20°S, 26-34°E	J1					9 (−)	M	57°N	264°E	McElhinny (1972)
(4) Karroo dolerite 19.6-29.1°S, 29.1-31.0°E	J1-m (190-154 m.y.)					10 (67)	M	66°N	255°E	McElhinny (1968)
(5) Stromberg lavas 29.5°S, 28.5°E	J1					4 (74)	M	71°N	269°E	Irving (1964)

J1 and Jm denote geological period of lower and middle Jurassic. Polarity (P) is indicated as normal (N) or mixed (M).
The number of sites (Si) and samples (Sa) used in each study are given.

However, the directions of magnetization were not changed to demagnetization of higher fields than 300 oersted. It is, therefore, concluded that the directions of stable magnetization represent a direction of the ambient geomagnetic field at the time the lava cooled. Results of measurements are listed in Table 1, with the data for the same body by Nairn (1956) and the data for the other Karroo basalts compiled by Irving (1946) and McElhinny (1968, 1972). A site mean direction is D = 337.5°, I = -53.5°, k = 172, α_{95} = 3.5°. Fig. 4 shows positions of paleomagnetic south pole obtained by Nairn (1956), Irving (1964), McElhinny (1968, 1972) and this study. The site mean direction at the Victoria Falls is slightly different from that of Nairn's data. The difference in declinations is 5.6° and that in inclinations is 13.5°. This directional discordance between these two sites may result from having sampled different lava flows in the same body. Our specimens were collected from the top suface of the Victoria Falls, whereas Nairn's specimen was taken from the gorge of the Zambesi Valley, being about 20 Km below the Falls on the river. Positions of paleomagnetic south pole for the Karroo basalts, however, are very close to each other as shown in Fig. 4. This suggests that the Karroo lavas in southeastern Africa were emplaced at a relatively short period.

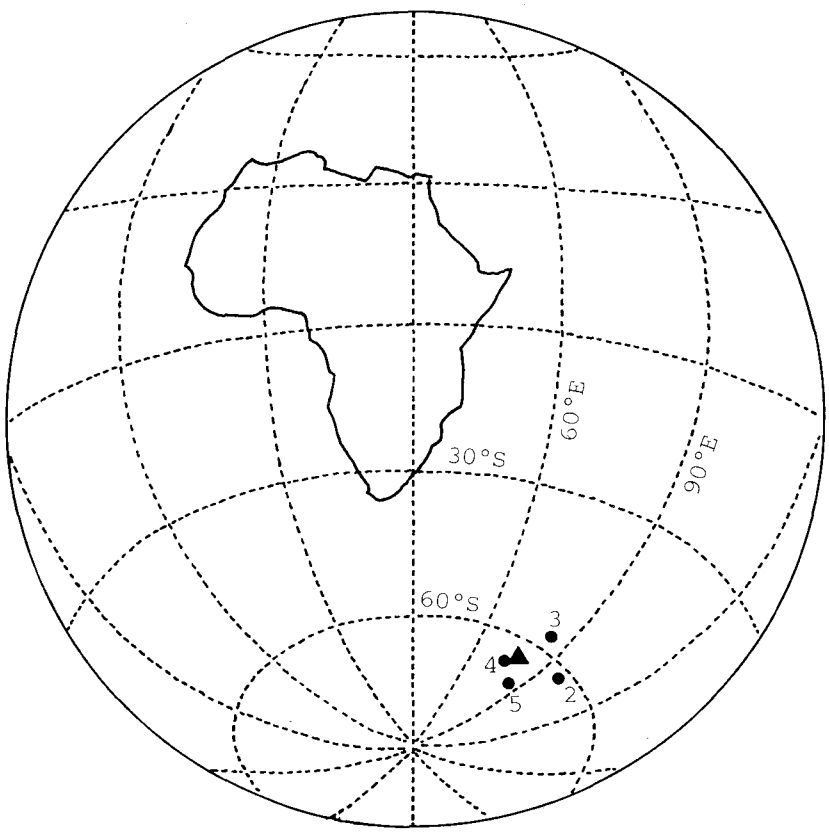

Fig. 4 Paleomagnetic south pole positions for the Karroo basalts in southeastern Africa. Triangle denotes a pole position obtained in this study. Index numbers of the poles refer to Table 1.

Acknowledgements – We express our sincere thanks to Mr. N.J.Money, Deputy Director of Zambia Geological Survey Department; to Mr. M.D.Kamano of the Ministry of Mines, Zambia; to Messrs. T.Ohashi and T.Taguchi of the Marubeni Co. Lusaka office; to Mr. I.Yamamoto of Power Reactor and Nuclear Fuel Development Corporation (PNC) Lusaka office for their most esteemed and invaluable assistance.

We are very grateful to Drs. T.Yanagi and H.Umemura and Messrs. M.Asami and M.Hoshino for their laborious collaboration in the field Survey in 1981.

The field work was made possible by the Grant-in-Aid for Overseas Scientific Survey from the Ministry of Education, Science and Culture, Japan, to which we express our thanks.

References

COX, K.G. (1970): Tectonics and vulcanism of the Karroo Period and their bearing on the postulated fragmentation of Gondwanaland. In: *Clifford,T.N. and Gauss,I.G.(ed.): African magmatism and Tectonics.* Oliver & Boyd, Edinburgh 211-235.

FITCH, F.J. and MILLER, J.A. (1971): Potassium-argon radioages of Karroo rocks from Lesotho. *Bull. Volcanol.* **35**, 64-84.

IRVING, A. (1963): Palaeomagnetic directions and pole positions Part VI. *Geophys. J. Roy. Astr. Soc.* **8**, 249-257.

McELHINNY, M.W. (1968): Palaeomagnetic directions and pole positions Part VIII. *Geophys. J. Roy. Astr. Soc.* **15**, 409-430.

McELHINNY, M.W. (1972): Palaeomagnetic directions and pole positions Part XII. *Geophys, J. Roy. Astr. Soc.* **27**, 237-257.

NAIRN, A.E.M. (1956): Relevance of palaeomagnetic studies of Jurassic rocks to continental drift. *Nature*, **178**, 935-936.

PLATE I

Eastern part of the Victoria Falls (17°55.3'S, 25°51.7'E) with rainbow seen from east (Photo. by K. S., 13 Sep., 1981).

PLATE I

PLATE II

Eastern part of the Victoria Falls (17°55.3'S, 25°51.7'E) seen from south (Photo. by K. S., 12 Sep., 1981).

PLATE II

PLATE III

Stratified lava flows of the Karroo basalt of the Second gorge (17°55.5'S, 25°51.6'E) of the Victoria Falls seen from east (Photo. by K. S., 13 Sep., 1981).

PLATE III

List of publications on African geology

1963 SUWA, K., Geological excursion of north-east Africa. *Monthly Africa,* **3**, Nos.5-10. (*)

SUWA, K., Geology of Ethiopia. *Nagoya Jour. Geol.,* **18**, 13-25. (*)

1964 SUWA, K., Geological excursion of north-east Africa. *Monthly Africa,* **4**, Nos.1 and 3. (*)

SUWA, K., African Rift Valley. *World Geography,* **13**, 320-322. (*)

1965 SUWA, K., Geology of Egypt and Sudan. *Nagoya Jour. Geol.,* **20-21**, 34-48. (*)

1966 MATSUZAWA, I., A study on the formation of the African Rift Valley. *Jour. Earth Sci., Nagoya Univ.,* **14**, 89-115.

MIZUTANI, S. and SUWA, K., Orthoquartzitic sand from the Libyan desert, Egypt. *ibid,* 137-149.

SUWA, K., Maximum microcline in Aswan granitic rocks, Egypt. *ibid,* 116-136.

SUWA, K. and UEMURA, T., Geology of the African Rift Valley and the Olduvai Gorge. *Jour. Afr. Studies,* **3**, 18-48. (**)

SUWA, K., Precambrian of Africa (I). *Earth Science (Chikyu Kagaku),* **84**, 39-48. (*)

1967 MATSUZAWA, I., Some considerations on the formation of the African Rift Valley. *Jour. Afr. Studies,* **4**, 1-24. (**)

SUWA, K., Precambrian of Africa (II). *Earth Science (Chikyu Kagaku),* **21**, 32-44. (*)

1968 SUWA, K., Precambrian of African Continent — Geology and mineral resources. *Jour. Afr. Studies,* **6**, 25-51. (**)

1969 AOKI, H., Gravity measurements of Rift Valleys in Tanzania. *Jour. Earth Sci., Nagoya Univ.,* **17** (special volume), 169-188.

MATSUZAWA, I., Nagoya University African Rift Valley Expedition (NUARVE) in 1968. *ibid,* 1-10.

MATSUZAWA, I., Formation of the African great rift system. *ibid,* 11-70.

MIYAKAWA, K., SUWA, K., and SHIIDA, I., Metamorphic rocks of the North Pare Mountains, Tanzania. *ibid,* 97-106.

MIZUTANI, S. and YAIRI, K., Tectonic sketch of the Mbeya area, southern Tanzania. *ibid,* 107-124.

SUWA, K., OSAKI, S., OANA, S., SHIIDA, I., and MIYAKAWA, K., Isotope geochemistry and petrology of the Mbeya carbonatite, south-western Tanzania, East Africa. *ibid,* 125-168.

YAIRI, K. and MIZUTANI, S., Fault system of the Tanganyika Rift at the Kigoma area, western Tanzania. *ibid,* 71-96.

1970 SUWA, K., Six months of geological studies in Africa during 1969-1970. *Gakujutsu-geppo (Monthly Rept. Sci. Research),* **23**, 46-55. (*)

1971 MATSUZAWA, I., On Africa. *Jour. Afr. Studies,* **11**, 1-8. (*)

MIYAKAWA, K., Recent trends of African studies in Japan — Geology. *ibid,* 9-15. (*)

SUWA, K., Field studies in Africa — Geological researches. *ibid,* 49-58. (*)

SUWA, K., Earth scientific characteristics of African Rift Valley. *World Geography Seminar,* **5**, 73-91. Daimyodo Pub. Co. (*)

1972 SUWA, K., African Rift Valley and volcanism. *Geography,* **17**, 7-14. (*)

SUWA, K. and YAIRI, K., African Rift Valley Research Expedition (2nd). *Gakujutsu-geppo (Monthly Rept. Sci. Research),* **25**, 548-554. (*)

1973 SUWA, K., OANA, S., WADA, H., and OSAKI, S., Isotope geochemistry and petrology of the African carbonatites. *1st International Kimberlite Conference, extended abstract,* 297-300.

SUWA, K., YUSA, Y., and KISHIDA, N., Petrology of peridotite nodules from Ndonyuo Olnchoro, Samburu district, central Kenya. *ibid,* 301-304.

1974 ADACHI, M., The Mesozoic group near Mombasa, Kenya. *Jour. Afr. Studies,* **14**, 14-20. (**)

SHIOZAKI, H., Mineral resources of Africa (1). *Nagoya Jour. Geol.,* **30**, 2-10. (*)

SHIOZAKI, H., Mineral resources and mining affairs of East Africa. *Jour. Afr. Studies,* **14**, 73-81. (**)

YAIRI, K., En echelon pattern of the East African Rift System. *Jour. Afr. Studies,* **14**, 21-46. (**)

1975 SUWA, K., OANA, S., WADA, H., and OSAKI, S., Isotope geochemistry and petrology of African carbonatites. *Phys. Chem. Earth,* **9**, 735-745 (Pergamon Press).

SUWA, K., YUSA, Y., and KISHIDA, N., Petrology of peridotite nodules from Ndonyuo Olnchoro, Samburu district, central Kenya. *ibid,* 273-286 (Pergamon Press).

ADACHI, M. and YAIRI, K., Sedimentological notes on the Bukoban orthoquartzite (late Precambrian) around Kisii, Kenya. *1st Prelim. Rep. Afr. Studies, Nagoya Univ.,* 3-5.

ADACHI, M., Sole markings from the Mazeras sandstones (upper Triassic), northwest of Mombasa, Kenya. *ibid,* 21-25.

ADACHI, M. and YAIRI, K., Preliminary report on the carbonatitic clasts in Tertiary sediments from the eastern Kavirondo Rift Valley, Kenya. *ibid,* 26-28.

BIYAJIMA, K., SUWA, K., and MIYAKAWA, K., Mantled gneiss dome in the Mozambique belt around the Machakos area, Kenya. *ibid,* 6-13.

KAGAMI, H., Maragori granite in Tanganyika craton. *ibid,* 14-16.

KAGAMI, H., ADACHI, M., YAIRI, K., and MATSUZAWA, I., The rocks constituting the Mozambique belt in the northeast district of Lake Victoria. *ibid,* 17-20.

MIYAKAWA, K. and SUWA, K., An occurrence of staurolite from the Kioo pegmatite, Machakos District, Kenya. *ibid,* 52-54.

SHIBATA, K., Preliminary geochronological study on metamorphic rocks from Taita Hills, southern Kenya. *ibid,* 72-75.

SHIOZAKI, H., Fuchsite from Kibingi, Kenya. *ibid,* 70-71.

SUWA, K., Plagioclases in anorthosites. *ibid,* 55-59.

SUWA, K. and AOKI, K., Reverse pleochroism of phlogopites in kimberlites and their related rocks from South Africa. *ibid,* 60-64.

SUWA, K., YUSA, Y., and KISHIDA, N., Petrology of peridotite nodules from Ndonyuo Olnchoro, Samburu District, central Kenya (abstract). *ibid,* 65-69.

SUWA, K., OANA, S., WADA, H., and OSAKI, S., Isotope geochemistry and petrology of African carbonatites (abstract). *ibid,* 81-84.

UEDA, Y., MATSUZAWA, I., and SUWA, K., Potassium-argon age determinations on the Tanzanian igneous and metamorphic rocks. *ibid,* 76-80.

YAIRI, K., Geometry and mechanics of en echelon faulting with applications to the East African Rift System. *ibid,* 29-38.

YAIRI, K., Fault pattern and crustal extension of the Kavirondo Rift Valley in relation to a bifurcating rift model. *ibid,* 39-43.

YAIRI, K. and KATO, Y., Throw variation of normal faults arranged en echelon. *ibid,* 44-51.

1976 GOTO, T., OHNO, I., and SUMINO, Y., The determination of the elastic constants of natural almandine-pyrope garnet by rectangular parallelepiped resonance method. *Jour. Phys. Earth,* **24**, 149-156.

OHNO, I., Free vibration of a rectangular parallelepiped crystal and its application to determination of elastic constants of orthorhombic crystals. *Jour. Phys. Earth,* **24**, 355-379.

SUWA, K., Anorthosites and their plagioclases. *Japan. Assoc. Mineral. Petrol. Econ.*

Geol., Spec. Paper No.1 (Progress in Research on Rock Forming Minerals), 215-242. (*)

SUWA, K., Precambrian anorthosites and their plagioclases. *25th Intern. Geol. Cong., Abstract,* Vol.1, 21.

1977 AOKI, K. and SUWA, K., Major element geochemistry of peridotite nodules from Samburu district, Kenya. *Jour. Japan. Assoc. Mineral. Petrol. Econ. Geol.,***72**, 173-179.

SAKA, Y., Sedimentological notes on the Karroo System in northern Malawi, Africa. *Gakujutsu Kenkyu, School of Education, Waseda Univ., Ser. Biol. & Geol.,* **26**, 35-51.

SUWA, K. and FUJITA, M., Igneous activity of mantle origin and the development of African continental crust, with special reference to the formation of the Yatta plateau. *Gakujutu-geppo (Monthly Rept. Sci. Research),* **30**, 360-367, (*)

ADACHI, K., KATO, Y., and OMI, G., On the palaeolithic stone implements from Rupa, near Moroto. *3rd Prelim. Rep. Afr. Studies, Nagoya Univ. (Archaeology 1),* 51-55.

ITO, A. and ADACHI, K., Kantsyore Island site, East Ankole District, Uganda. *ibid,* 42-44.

KATO, Y. and OMI, G., A geological note on the palaeolithic site of Kilombe, Nakuru District, Kenya. *ibid,* 11-12.

KATO, Y., OMI, G., and ADACHI, K., On the Acheulean site of Mtongwe, Mombasa. *ibid,* 13-17.

KATO, Y. and ADACHI, K., Kainengasi Hill site, East Ankole District, Uganda. *ibid,* 40-41.

KATO, Y., ITO, A., and ADACHI, K., Mweya North Site, Rwenzori District, Uganda. *ibid,* 46-47.

OMI, G. and AGATA, T., Petrological notes on the obsidian mines in Kenya. *ibid,* 18-20.

OMI, G., KATO, Y., and KATO, Y., Preliminary study of the Kafuan culture. *ibid,* 21-39.

AOKI, K. and SUWA, K., Major element geochemistry of peridotite nodules from Samburu District, Kenya (abstract). *2nd Prelim. Rep. Afr. Studies, Nagoya Univ. (Earth Sciences 2),* 161-164.

FUJITA, M., Geology of the Yatta Plateau, Kenya., *ibid,* 165-177.

ITO, H., TOKIEDA, K., SUWA, K., and KUME, S., Palaeomagnetism of South African kimberlites. *ibid,* 194-198.

MIYAKAWA, K. and SUWA, K., A note on the granitoid gneisses from the Machakos area, Kenya. *ibid,* 154-160.

MIYAZAKI, S., Vermiculite-like macroscopic layer silicates from Kenze Forest and Kioo Forest, southern Machakos, Kenya. *ibid,* 184-193.

NUREKI, T., SUWA, K., BIYAJIMA, K., SAKA, Y., and YUSA, Y., Tectonic evolution of the Mozambique belt in area south-east of Machakos, Kenya. *ibid,* 13-38.

SAKA, Y. and YAIRI, K., Karroo System to the west of Karonga, northern Malawi. *ibid,* 70-82.

SAKA, Y., Note on the Karroo System and the probable Dinosaur Beds near the Lion Point, Karonga District, northern Malawi. *ibid,* 83-88.

SAKA, Y. and YAIRI, K., Sedimentary structures of the Karroo System in Livingstonia area, northern Malawi. *ibid,* 89-107.

SHIIDA, I. and HOSHINO, M., Some petrographical notes on phonolite, exposed at the summit of Uhuru Peak, Mt. Kilimanjaro, Tanzania. *ibid,* 178-183.

SUWA, K., Precambrian anorthosites and their plagioclases (abstract). *ibid,* 3-12.

SUWA, K. and SUZUKI, K., Chromian phlogopite in the Bushveld anorthosite, South Africa. *ibid,* 133-138.

SUWA, K. and SUZUKI, K., Contact aureole of the north-eastern part of the Bushveld Igneous Complex, South Africa. *ibid,* 139-153.

YAIRI, K., Fault pattern of the southern part of the Eastern Rift, Tanzania. *ibid,* 39-50.

YAIRI, K., Preliminary account of the lake-floor topography of Lake Malawi in relation to the formation of the Malawi Rift Valley. *ibid,* 51-69.

YAIRI, K. and SAKA, Y., Tectonic notes on the Livingstonia area, northern Malawi, in relation to the post-Karroo rift-faulting. *ibid,* 108-132.

1978 ITO, H., TOKIEDA, K., SUWA, K., and KUME, S., Remanent magnetization of Precambrian and Cretaceous kimberlites in South Africa. *Geophys. Jour. Royal Astr. Soc.,* **55**, 123-130.

SAKA, Y. and MIYATA, T., Sedimentary structures of the Karroo System near Mombasa, Kenya. *Jour. Afr. Studies,* **17**, 58-73. (**)

SUWA, K., Plagioclase twinning in Precambrian anorthosites. *National Geograph. Jour. India,* **24**, 107-120.

1979 SUWA, K., Plagioclase twin laws and fabrics in three specimens of anorthosite. *Lithos,* **12**, 99-107.

SUWA, K., Precambrian of the African continent. *Memoirs Natl. Inst. Polar Res., Special Issue*, **14**, 93-105.

SUWA, K. and YAIRI, K., Geology of Africa. *Iwanami Series on Earth Sciences*, **16** *(Geology of the World)*, 61-98. (*)

INOUE, H. and SUWA, K., Petrographical note on staurolite-kyanite-almandine pelitic gneiss occurring at the western foot of the Mbooni Hills, Machakos area, Kenya — with special reference to the ZnO content in staurolite. *4th Prelim. Rept. Afr. Studies, Nagoya Uni. (Earth Sciences 3),* 97-111.

MIYAKAWA, K. and SUWA, K., The Kalama psammitic gneisses from the Kalama Hills, Machakos area, Kenya. *ibid*, 113-122.

MIYATA, T. and SAKA, K., Deformed cross-lamination in the Karroo System, near Mombasa, Kenya. *ibid*, 63-71.

NUREKI, T. and SUWA, K., Two types of biotite amphibolite in the Linthipe anorthosite body: Examples found in old quarries near Linthipe, central Malawi. *ibid*, 123-132.

OHDE, S., SUWA, K., and KITANO, Y., Trace element geochemistry of carbonatites from Homa Mountain, Kenya. *ibid*, 169-174.

OHDE, S., SUWA, K., YUSA, Y., and KITANO, Y., Rare earth element geochemistry of carbonatites from the Kangankunde mine, Malawi. *ibid*, 175-179.

SAKA, Y. and MIYATA, T., Directional structures and paleocurrent of the Duruma Sandstones (Karroo System) near Mombasa, Kenya. *ibid*, 41-61.

SAKA, Y., RIKITA, M., and MIYATA, T., Grain fabric of the fluvio-lacustrine sandstone (Duruma Sandstones) near Mombasa, Kenya. *ibid*, 73-82.

SHIBATA, K. and SUWA, K., A geochronological study on granitoid gneiss from the Mbooni Hills, Machakos area, Kenya. *ibid*, 163-167.

SUWA, K., NUREKI, T., INOUE, H., BIYAJIMA, K., and MIYAKAWA, K., Geology and petrology of the Machakos area, Kenya. *ibid*, 3-20.

SUWA, K., MIYAKAWA, K., NUREKI, T., SAKA, Y., YUSA, Y., MIYATA, T., and SUZUKI, K., Geological and petrological notes on the Linthipe anorthosite body, Malawi. *ibid,* 21-39.

SUWA, K., SUZUKI, K., MIYAKAWA, K., and AGATA, T., Vanadian and vanadium grossulars from the Mozambique metamorphic rocks, Mgama Ridge, Kenya.

ibid, 87-96.

SUZUKI, K., Pyroxenite and other crustal inclusions from the Kwa Nthuku cinder cone, eastern Emali, Kenya. *ibid*, 133-149.

SUZUKI, K., Hornblendite inclusions from the Ngong Hills in the southern part of the Gregory Rift, Kenya. *ibid*, 151-162.

YAMAGIWA, N., Some interesting corals from the Middle Jurassic Kambe Limestone in Mombasa-Kwale area, Kenya
Part 1. A new coral species, *Thamnasteria (Thamnasteria) mombasensis* found from the Kambe Limestone at southwest of Tsulujimba. *ibid*, 83-85.

1980 KAJITA, S. and KATEEBA, E.R., Geological and geomorphological setting in and around Mweya North Site. *5th Prelim. Rept. Afr. Studies, Nagoya Univ. (Archaeology 2)*, 9-18.

KAJITA, S., Geological and geomorphological setting in and around Rupa Site. *ibid*, 59-65.

SUWA, K., Calcic plagioclase in Yamato meteorite and anorthosite. *Japan. Assoc. Mineral. Petrol. Econ. Geol. Spec. Paper* No.2, 229-234. (**)

SUWA, K., Evolution of late Precambrian Mozambique belt in the Machakos area, Kenya. *26th Intern. Geol. Cong., Abstract*, Vol.**1**, 95.

SUWA, K., Late Precambrian environment controlling the formation of green garnet in southern Kenya and northern Tanzania. *ibid*, Vol.**2**, 616.

SUWA, K., Formation of continental crust. *The Earth Monthly*, 2, 846-854. (*)

1981 SHINNO, I. and SUWA, K., Mössbauer spectra of phlogopites showing reverse pleochroism with special reference to asymmetric quadrupole splitting. *Jour. Japan. Assoc. Mineral. Petrol. Econ. Geol.*, **76**, 122-129. (**)

SUWA, K., Petrology of carbonatite. *Mining Geol.*, **31**, 457-465. (*)

SUWA, K., Petrological studies on the African continent. *Recent Prog. Natural Sci. in Japan*, **6**, 64-71 (Sci. Council Japan).

SUZUKI, K., Grain boundary concentration of rare earth elements in a hornblende cumulate. *Geochem. Jour.*, **15**, 295-303.

HOSHINO, M. and SHIIDA, I., Mineralogy of the Uhuru Peak phonolite from Mt. Kilimanjaro, northern Tanzania. *6th Prelim. Rept. Afr. Studies, Nagoya Univ. (Earth Sciences 4)*, 127-138.

ITO, H., TOKIEDA, K., SUWA, K. and KUME, S., Paleomagnetic results from the Linthipe anorthosite body, Malawi. *ibid*, 189-196.

ITO, M., Chromiferous muscovite in metaquartzite from Mozambique belt, south of Machakos, Kenya. *ibid*, 139-144.

ITO, M., SUWA, K. and WINANI, P., Kimberlite from Nyanza, western Kenya. *ibid*, 83-100.

ITO, M., SUWA, K. and WINANI, P., Peridotite xenoliths in kimberlite from Nyanza, western Kenya. *ibid*, 101-110.

MIYAKE, A. and SUWA, K., Geological structure of the Uvete dome, Kenya. *ibid*, 33-42.

MIYATA, T. and SAKA, Y., Strain distribution around the Uvete dome, Machakos, Kenya: Summary. *ibid*, 67-72.

MIYATA, T. and SAKA, Y., Boudinage structures in the Mozambiquian metamorphic rocks, south of Machakos, Kenya. *ibid*, 73-82.

NAKAI, Y. and SUWA, K., Zircons in the Precambrian granites from the Kisumu area, western Kenya. *ibid*, 145-150.

SAKA, Y. and MIYATA, T., Primary sedimentary structures found in the gneisses of the Mozambique metamorphic belt near Machakos, Kenya. *ibid*, 43-52.

SAKA, Y. and MIYATA, T., Mega- and mesoscopic folds in the Mozambique meta-

morphic belt, south of Machakos, Kenya. *ibid*, 53-66.

SHINNO, I. and Suwa, K., Mössbauer spectrum and polytype of phlogopite with reverse pleochroism. *ibid*, 151-158.

SUWA, K., Petrological studies on the African continent by Nagoya University. *ibid*, 3-14.

SUWA, K., Petrochemical and petrographical notes on some Nyanzian volcanic rocks, west Kenya. *ibid*, 15-32.

SUZUKI, K., Grain boundary concentration of rare earth elements in a hornblendite cumulate from the Ngong Hills, Kenya. *ibid*, 173-180.

SUZUKI, K. and SUWA, K., A layered garnet-pyroxenite nodule from the Kwa Nthuku cinder cone, Kenya. *ibid*, 111-126.

TOKIEDA, K., ITO, H., SUWA, K. and KUME, S., Paleomagnetism of late Precambrian metamorphic rocks from the Machakos area, Kenya. *ibid*, 181-188.

YAMAGIWA, N., Some interesting corals from the middle Jurassic Kambe limestone in Mombasa-Kwale area, Kenya. *ibid*, 159-162.

YANAGI, T. and SUWA, K., Rb-Sr radiometric dating on Precambrian rocks in the western part of Kenya. *ibid*, 163-172.

1982 KATO, Y., A geological note on the Mtongwe site (Kenya). *7th Prelim. Rept. Afr. Studies, Nagoya Univ.*, 9-21.

SHINNO, I., SUWA, K. and TATSUMI, T., Ferriphlogopite associated with carbonatite from Palabora mine, South Africa. *Jour. Mineral. Soc. Japan.*, **15**, 273-282. (**)

SUWA, K., Rock-forming mineral in relation to metamorphism, with special reference to the staurolite as a metamorphic mineral. *Earth Sci.*, **36**, 90-93. (**)

SUZUKI, K. and SUWA, K., A layered garnet-pyroxenite from the Kwa Nthuku cinder cone, Kenya. *Memoirs Geol. Soc. Japan*, **21**, 321-331. (**)

(*) In Japanese

(**) In Japanese with English abstract